\



University of Nottingham
UK | CHINA | MALAYSIA

Electrotherapy for the Treatment of Brain Tumours

Joshua Branter

Supervised by Mr. Stuart Smith, Mr. Surajit Basu and Prof. Richard Grundy

University of Nottingham

Thesis submitted to the University of Nottingham April 2019 for the degree of Doctor of Philosophy

I hereby declare that this dissertation is all my own work, except as indicated in the text

Abstract

Introduction

The scarcity of effective treatment options for high grade brain tumours has led to a wide ranging search for alternative means of therapy for these difficult to treat tumours. Electrical field therapy is one such area that has been considered. The Optune™ system is an FDA approved novel anti-mitotic device that delivers continuous alternating electric fields to the patient for the treatment of primary and recurrent Glioblastoma multiforme (GBM) (TTFields). Alternative electric fields delivery systems are also being investigated for the treatment of various cancers. Here we present our explorative study into the feasibility of repurposing deep brain stimulating (DBS) electric fields for the treatment of brain tumours, as well as our investigations into the effects of TTFields on paediatric brain tumour cell lines.

Methods

A variety of high-grade adult and paediatric brain tumour cell lines were treated with DBS electric fields and TTFields. The effects of electric fields were assessed through a number of avenues including; viability, gene expression, cell cycle, and combinational effects with chemotherapies.

Results

We observed that both DBS electric fields and TTFields affected our brain tumour cell lines with regards to viability, cell cycling, and gene expression. Both of the treatments may be optimised through manipulations of frequency and intensity and may be potentiated with the addition of a variety of chemotherapies.

Conclusions

We have demonstrated efficacy of repurposed DBS electric fields against high-grade brain tumours, as well as TTFields against paediatric high-grade brain tumours. We have also elucidated multiple mechanisms of action while providing avenues for future research.

Acknowledgements

I am a man of few words, therefore, my feelings may not be expressed fully through text. I would like to extend my gratitude to; my supervisors Mr Stuart Smith, Mr Surajit Basu and Professor Richard Grundy for giving me this opportunity, guidance, and helping me to succeed on this journey. To our collaborators, Dr Moshe Giladi, Yaara Porat and the other members of team Novocure, Haifa, for the training, guidance and the opportunity to conduct TTFields research. To Dr Maria Estevez-Cebrero for the constant support and guidance throughout my entire project. And lastly, to all of the other members of the CBTRC – you lot are alright.

Table of Contents

Abstract 2
Introduction 2
Methods 2
Results 2
Conclusions 2
Acknowledgements 3
Chapter 1: Introduction 15
1. Cancer 15
2. Brain Tumours 16
2.1. Incidence 17
2.2. Classification of Brain Tumours 19
2.2.1. Classification: Cell of Origin and Tumour Location 19
2.2.2. Classification: Histology 19
2.2.3. Classification: World Health Organisation (WHO) Classification 20
3. Glioblastoma multiforme 21
3.1. Cell of origin for Glioma 21
3.2. WHO Classification of Glioma 22
3.3. Epidemiology 23
3.4. Biological Behaviour 24
3.5. Morphological Features 24
3.6. Genetic aberrations of GBM 27
3.6.1. Isocitrate dehydrogenase IDH1/2 28
3.6.2. 0(6)-Methylguanine-DNA Methyltransferase (MGMT) 28
3.6.3. Epidermal Growth Factor Receptor (EGFR) 29
3.6.4. Phosphatase and tensin homolog (PTEN) 31
3.6.5. Telomerase Reverse Transcriptase (TERT) 31

3.7. Epigenetic aberrations of GBM 32
3.8. Clinical Signs and Symptoms 34
3.9. Standard of Care for GBM patients 34
4. Paediatric Brain Tumours 37
4.1. Paediatric High-Grade Glioma 37
4.1.2. Current Therapy Strategies 39
4.2. Paediatric Ependymoma 40
4.2.1. Current Therapy Strategies 41
4.3. Paediatric Medulloblastoma 42
4.3.1. Current Therapy Strategies 44
5. Electric Field Technologies for the Treatment of Cancer 45
5.1. Optune™ (Formerly known as NovoTTF-100a) for Adult GBM. 45
5.1.1. Tumour Treating Fields Therapy Indications and Contraindications for GBM Patients 52
5.1.2. Tumour Treating Fields Interactions 53
5.1.3. Anti-mitotic effects of TTFields 54
5.2. Pre-clinical TTFields Studies in Combination with Chemotherapies 58
5.2.1. Tumour Treating Fields in Combination with Alkylating agents 58
5.2.2. Tumour Treating Fields in Combination with Radiation Therapy 59
5.2.3. Tumour Treating Fields in Combination with Anti-angiogenics 60
5.2.4. Tumour Treating Fields in Combination with Mitotic inhibitors 61
5.2.5. Tumour Treating Fields in Combination with Immunotherapy 65
5.2.6. Tumour Treating Fields in Combination with Novel agents 67

5.2.7. Pre-Clinical Conclusions 68
5.3. TTFields Clinical Trials in Glioblastoma multiforme 70
5.3.1. TTFields Pilot Study in Recurrent GBM Patients 70
5.3.2. TTFields Phase III Clinical Trial in Recurrent GBM (EF-11 Trial) 71
5.3.3. TTFields Phase I Clinical Trial in Newly Diagnosed GBM ... 74
5.3.4. TTFields Phase III Clinical Trial in Newly Diagnosed GBM (EF-14 Trial Interim Analysis) 76
5.3.5. TTFields Phase III Clinical Trial in Newly Diagnosed GBM (EF-14 Trial Final Report) 81
5.3.6. TTFields Phase III Clinical Trial in GBM: Scepticism 84
5.4. TTFields Clinical Trials in Other Tumour Types 85
5.4.1. TTFields Clinical Trials in Brain Metastases Secondary to Non-small Cell Lung Carcinoma 85
5.4.2. TTFields Clinical Trials in Non-small Cell Lung Carcinoma 85
5.4.3. TTFields Clinical Trials in Ovarian Carcinoma 86
5.4.4. TTFields Clinical Trials in Pancreatic Adenocarcinoma 86
5.4.5. TTFields Clinical Trials in Mesothelioma 87
5.5. Summary of Tumour Treating Fields Clinical Trials 88
5.6. Nativis Voyager® ulRFE® System for GBM 93
5.6.1. Radio Frequency Energy Interactions 94
5.6.2. Radio Frequency Energy *in vitro* and *in vivo* 95
5.7. Intratumoural Modulation Therapy (IMT) for GBM 97
5.7.1. Intratumoural Modulation Therapy Interactions 98
5.7.2. Intratumoural Modulation Therapy *in vitro* and *in vivo* 98
5.8. TheraBionic P1 Medical Device for Advanced Hepatocellular Carcinoma (HCC) 102
5.8.1. TheraBionic P1 Therapy Interactions 105
5.8.2. TheraBionic P1 Therapy *in vitro* and *in vivo* 105

6. Deep Brain Stimulation System Specifications 108
6.1. Electrical Sources 108
6.2. Unilateral and Bilateral Systems 108
6.3. DBS Electric Fields 109
6.3.1. Electrode Design 109
6.3.2. Polarity 110
6.3.3. Electrical Signal 110
6.3.4. Battery 110
6.3.5. DBS Programmers 111
6.3.6. Interconnectivity 111
6.4. Neurophysiology of Deep Brain Stimulation 111
6.5. Deep Brain Stimulation Mechanisms of Action 113
6.5.1. The Excitation Hypothesis 113
6.5.2. The Inhibition Hypothesis 114
6.5.3. The Disruption Hypothesis 114
6.6. Clinical Applications of Deep Brain Stimulation 115
6.6.1. Deep Brain Stimulation for Parkinson Disease 115
6.6.2. Deep Brain Stimulation for Pain 115
6.6.3. Deep Brain Stimulation for Dystonia 116
6.6.4. Deep Brain Stimulation for Essential Tremor 116
6.7. Deep Brain Stimulation for the Treatment of Brain Tumours .. 116
6.7.1. Membrane Potential (V_m) of Cells 117
6.7.2. Membrane Potential (V_m) and Cancer 118
6.7.3. Membrane Potential (V_m) and Proliferation 119
6.7.4. Clinical Opportunities for Deep Brain Stimulation for the Treatment of Brain Tumours 120
6.8. Concluding Remarks 121

Chapter 2: Deep Brain Stimulation for the Treatment of Brain Tumours 122

1. Introduction 122

1.1. Aims and Objectives 122

2. Deep Brain Stimulation Methods 124

2.1. Cell Culture and Cell Lines 124

2.1.1. Cell Subculture 125

2.1.2. Cell Storage 125

2.1.3. Cell Recovery 126

2.1.4. Neural Stem Cell Culture and Generation of Astrocyte Cell Line 126

2.2. Deep Brain Stimulation Experiments 127

2.2.1. DBS Lead Maintenance 127

2.2.2. Experimental Setup 128

2.2.3. DBS Programming 130

2.2.4. DBS Control Samples 133

2.2.5. Multiple DBS Leads 133

2.2.6. Temperature Measurement 133

2.2.7. Voltage Measurements 133

2.3. Analyses of DBS Treated Cells 133

2.3.1. Cell Storage for Further Analysis 133

2.3.2. Cell Count 144

2.3.3. Cell Viability 144

2.3.4. DBS Intensity Titration 145

2.3.5. DBS Frequency Titration 145

2.3.6. Withdrawal Analysis 146

2.3.7. Flow Cytometry Cell Cycle Analysis 146

2.3.8. DBS in Combination with Chemotherapeutics 148

3. Deep Brain Stimulation Results and Discussion 151

3.1. Electric fields delivered from DBS leads reduce metabolic activity in a voltage dependent manner in GBM cell lines 151

3.1.1. Results 151

3.1.2. Discussion 151

3.2. Electric fields delivered from DBS Leads reduce cell counts in GBM cell lines in a voltage dependent manner 155

3.2.1. Results 155

3.2.2. Discussion 155

3.3. The frequency of electric fields delivered from DBS leads has a profound effect on the metabolic activity of GBM cell lines 158

3.3.1. Results 158

3.3.2. Discussion 158

3.4. Electric fields delivered from DBS Leads demonstrate efficacy against Ependymoma and Medulloblastoma cell lines 162

3.4.1. Results 162

3.4.2. Discussion 162

3.5. Electric fields delivered from DBS Leads has no effect on cell viability of non-dividing H1-hESC-derived Astrocytes 166

3.5.1. Results 166

3.5.2. Conclusion 166

3.6. Efficacy of DBS electric fields treatment may be increased with the addition of multiple DBS Leads 169

3.6.1. Results 169

3.6.2. Discussion 169

3.7. Electric fields delivered from DBS Leads reduce in intensity throughout the cell culture flasks 173

3.7.1. Results and Discussion 173

3.8. Electric fields delivered from DBS Leads have lasting effects on growth rates of GBM cell lines 176
3.8.1. Results 176
3.8.2. Discussion 176
3.9. Electric fields delivered from DBS Leads do not cause temperature increases within cell culture flasks 178
3.9.1. Results and Discussion 178
3.10. Electric fields delivered from DBS Leads have promote G0-phase accumulation of GBM cell lines 179
3.10.1. Results 179
3.10.2. Discussion 179
3.11. The efficacy of electric fields delivered from DBS Leads may be increased with the addition of mitotic inhibitors in GBM cell lines 182
3.11.1. Results and Discussion 182
3.12. The efficacy of electric fields delivered from DBS Leads may be increased with the addition of Temozolomide in GBM cell lines 195
3.12.1. Results and Discussion 195
4. Conclusions 201
4.1. Main Findings 201
4.1.1. DBS Electric fields have anti-proliferative effects on high-grade brain tumour cell lines 201
4.1.2. DBS Electric Fields cause cell cycle arrest of GBM cell lines 201
4.1.3. DBS Electric Fields efficacy may be augmented with the addition of chemotherapies 202
4.2. Future Work 202
4.2.1. DBS Electric Fields and the Brain 202
4.2.2. DBS Electric Fields and the Combination Approach 203
4.2.3. DBS Electric Fields and Frequency 203

Chapter 3: Tumour Treating Fields for the Treatment of Paediatric Brain Tumours 205
1. Introduction 205
1.1. Aims and Objectives 205
2. Tumour Treating Fields Methods 207
2.1. Cell Culture and Cell Lines 207
2.2. Tumour Treating Fields Experiments 207
2.2.1. Base Plate and Dish Maintenance 207
2.2.2. Experimental Setup 207
2.2.3. TTFields Application 208
2.2.4. TTFields Control Samples 209
2.2.5. TTFields Experiment End-point 209
2.3. Analyses of Tumour Treating Fields Treated Cells 210
2.3.1 Cell Storage for Further Analysis 210
2.3.2. Cell Count Measurements 210
2.3.3. Cell Viability Measurements 211
2.3.4. TTFields Frequency Titration 211
2.3.5. Cell Cycle Analysis 211
2.3.6. Withdrawal Analysis 212
2.3.7. TTFields in Combination with Mitotic Inhibitors 213
3. Tumour Treating Fields Results and Discussion 215
3.1. Tumour Treating Fields demonstrate variable efficacy in a frequency dependent manner 215
3.1.1. Results 215
3.1.2. Discussion 216
3.2. Tumour Treating Fields have no effect on the cell viability of non-dividing hiP-derived Astrocytes 219
3.2.1. Results 219

3.2.2. Discussion 219
3.3. Tumour Treating Fields have lasting effects on growth rates of brain tumour cell lines following withdrawal from treatment 223
3.3.1. Results 223
3.3.2. Discussion 223
3.4. Tumour Treating Fields promote G2/M-phase accumulation in paediatric brain tumour cell lines 226
3.4.1. Results 226
3.4.2. Discussion 226
3.5. The efficacy of Tumour Treating Fields may be increased with the addition of mitotic inhibitors in brain tumour cell lines 230
3.5.1. Results and Discussion 230
4. Conclusions 237
4.1. Main Findings 237
4.1.1. TTFields have anti-proliferative effects on high-grade paediatric brain tumour cell lines 237
4.1.2. TTFields cause mitotic arrest at the G2/M checkpoint in paediatric brain tumour cell lines 237
4.1.3. TTFields efficacy may be augmented with the addition of mitotic inhibitors 238
4.2. Future Work 238
4.2.1. TTFields and the Brain 238
4.2.2. TTFields and the Combination Approach 239
4.2.3. TTFields and Paediatric Brain Tumours 239
Chapter 4: Electrogenomics 241
1. Introduction 241
1.1. Aims and Objectives 242
2. Methods 243
2.1. Cell Culture and Cell Lines 243

2.2. Gene Expression Analysis 243
2.2.1. Electric Fields Treated Cell Sample Collection 243
2.2.2. RNA Extraction 243
2.2.3. RNA Amplification 244
2.2.4. Microarray Analysis 246
2.2. Gene Target Analysis 251
2.2.4. Hierarchical Clustering Analysis 251
2.2.5. Volcano Plot Analysis 251
2.2.6. Venn Diagram Analysis 252
2.2.7. Gene Target Identification 252
2.2.8. Gene Ontology Analysis 252
2.2.9. KEGG Pathway Analysis 253
2.2.10. Western Blot for Validation 253
3. Gene Expression Results and Discussion 258
3.1. DBS electric fields and TTFields treatment causes gene expression changes in GBM cell lines 258
3.1.1. Results and Discussion 258
3.2. DBS electric fields and TTFields treatment causes similar genetic aberrations 262
3.2.1. Results and Discussion 262
3.3. Gene Ontology and KEGG Pathway Analyses 271
3.3.1. Results and Discussion 271
4. Conclusions 279
4.1. Main Findings 279
4.1.1. DBS electric fields and TTFields treatments cause similar genetic changes in GBM cell lines 279
4.1.2. Electrical treatment promotes dysregulation of mitochondrial and endoplasmic reticulum processes in GBM cell lines 280

4.1.3. Electrical treatment may potentially target metabolic pathways through interactions with electron transport chain in GBM cell lines 280
4.2. Future Work 280
4.2.1. Electric Fields in a Combinational Approach 281
Chapter 5: Conclusions 284
1. Introduction 284
2. Discussion 284
2.1. Optimisation of Electric Fields 284
2.2. Mitotic Arrest 284
2.3. Combination with Chemotherapy 285
2.4. Gene Expression 286
3. Future Directions 287
3.1. Measuring Ion Flux 287
3.2. Characterising Endoplasmic Reticulum Stress 288
Appendix 291
1. Appendix 1 – Gene Expression Data 291
References 292

Chapter 1: Introduction

1. Cancer

Cancer is currently a worldwide leading cause of death, expected to further grow in line with ageing populations, growing populations, and the increasing prevalence of lifestyles choices correlated with an increased cancer risk (Forouzanfar et al.). This trend is particularly true in developing- and middle-income countries as they economically grow, facilitating the adoption of lifestyle choices which perpetuate cancer in higher-income countries, including; tobacco use, excess bodyweight, and physical inactivity of the population (Torre et al., 2016).

Up to 18.1 million new cancer diagnoses and 9.6 million deaths as a results of cancer are estimated to occur worldwide during 2018 (Bray et al., 2018). Global incidence rates are typically higher in higher-income countries (North America, Europe, and Oceania for example), higher in males than females, and vary greatly depending upon the registry interrogated. Incidence rates across 50 registries compiled here (Torre et al., 2016) estimate 100-400 per 100,000 and 100-300 per 100,000 cases of cancer in males and females, respectively. Mortality rates from this data set approximate 50-200 per 100,000 and 50-100 per 100,000 cancer related deaths in males and females, respectively (Torre et al., 2016). Asia accounts for the highest proportion of cancer cases worldwide with 48.4% of cases, followed by Europe with 23.4%, then the Americas which accounts for 21.0%, then Africa with 7.3% of total cancer incidences worldwide (Bray et al., 2018). However, the overall mortality rates for Europe and for the Americas are lower than their incidences rates, while Asia and Africa mortality rates exceed their incidence rates; with 20.3% for Europe, 14.4% for the Americas, 57.3% for Asia, and 7.3% for Africa (Bray et al., 2018). The discrepancies between the global incidence and mortality rates between regions may be due to differences between the countries socioeconomics, as well as differences between the prevalence and distributions of cancer types between the regions (Bray et al., 2018). Table 1. describes the global incidences of various types of cancers as well as their mortality rates in 2018.

Cancer Type	Number of New Cases	% of New Cases	Number of Deaths	% of Deaths
Lung	2,094,000	11.6	1,761,000	18.4
Breast	2,089,000	11.5	627,000	6.6
Prostate	1,277,000	7.1	359,000	3.8
Colon	1,097,000	6.1	551,000	5.8
Non-Melanoma of the skin	1,042,000	5.8	65,000	0.7
Stomach	1,034,000	5.7	783,000	8.2
Liver	841,000	4.7	782,000	8.2
Rectum	704,000	3.9	310,000	3.2
Oesophagus	572,000	3.2	509,000	5.3
Cervix	570,000	3.2	311,000	3.3
Thyroid	567,000	3.1	41,000	0.4
Bladder	549,000	3.0	200,000	2.1
Non-Hodgkin Lymphoma	510,000	2.8	249,000	2.6
Pancreas	459,000	2.5	432,000	4.5
Leukaemia	437,000	2.4	309,000	3.2
Kidney	403,000	2.2	175,000	1.8
Lip/Oral	355,000	2.0	177,000	1.8
Brain/CNS	297,000	1.6	241,000	2.5
Ovary	295,000	1.6	185,000	1.9
Melanoma of the skin	288,000	1.6	61,000	0.6

Table 1. Global incidence and mortality figures and rates of the top 20 cancer types (Numbers rounded to nearest 1,000). Adapted from (Bray et al., 2018).

2. Brain Tumours

Management of both the disease- and treatment-related symptoms of solid tumours is fundamental for the care of patients, especially those of whom

with advanced disease (Cleeland et al., 2013). Primary brain tumours are associated with significant disease- and treatment-related burden for the patients. Moreover, the symptom burden of the patient upon diagnosis may be predictive of outcome, measured through overall survival (OS) and progression-free survival (PFS) (Armstrong et al., 2013). Overall, brain tumours have significant burden upon the patient, are difficult treat, and frequently cause death. A growing body of research has given insight into the causes, with potential treatment strategies, for these tumours through connections made between cell death, proliferation, and differentiation of tumour cells and normal developing cells. However, much remains unclear and provides an ongoing challenge for cancer research as a whole.

2.1. Incidence

The annual age-standardised incidence of primary malignant brain tumours globally is 3.7 per 100,000 for males and 2.6 per 100,000 for females (Bray et al., 2018, Bondy et al., 2008). Brain and CNS tumours are the most common type of tumours in children between 0-14 years of age, with an annual age-adjusted incidence rate of 5.54 per 100,000 children (Ostrom et al., 2017). Brain and CNS tumours also have age-adjusted incidence rates of 10.94 per 100,000 and 40.82 per 100,000 in people between the ages of 15-39 and 40+, respectively. Brain and CNS tumours have an average age adjusted mortality rate of 0.71 per 100,000, 0.94 per 100,000, and 8.94 per 100,000 for the population between the ages of 0-14, 15-39, and 40+ years, respectively. For the population between 0 and 14 years of age, these tumours rank as the fourth most common cause of death. For the population between 15 and 39 years of age, these tumours are the fifth most common cause of death for this demographic (Ostrom et al., 2017). A breakdown of the incidence of brain and CNS tumours by tumour location is outlined in Figure 1.

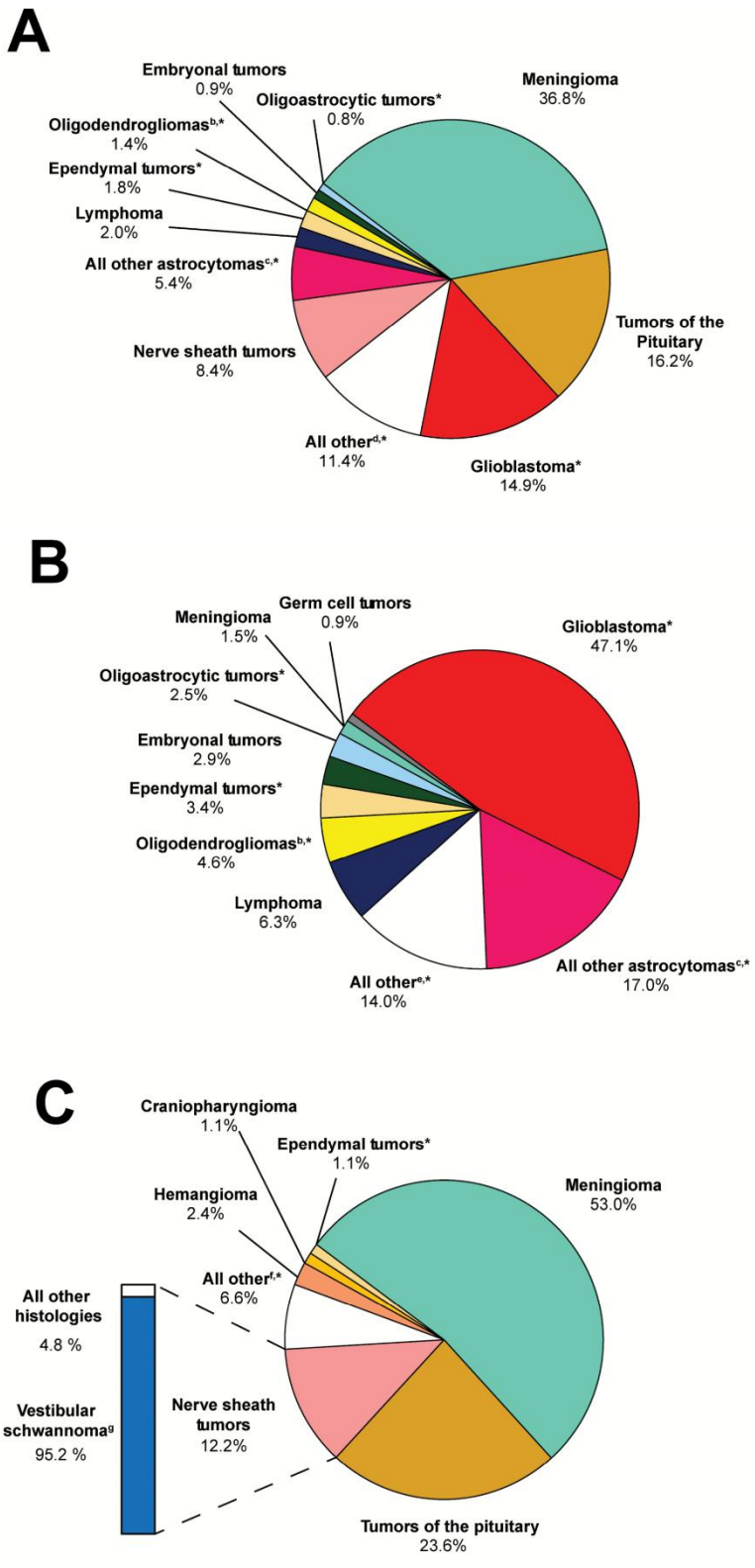


Figure 1. Distribution of; **A**. All Primary Brain and Other CNS Tumours by Site (N=379,848), **B**. Malignant Primary Brain and Other CNS Tumours by Site (N=119,674), and **C**. Non-Malignant Primary Brain and Other CNS Tumours by Site (N=260,174), CBTRUS Statistical Report: NPCR and SEER, 2010-2014. Image adapted from (Ostrom et al., 2017).

2.2. Classification of Brain Tumours

Brain and CNS tumours are classified according to;

1) Cell of origin

2) Location of the tumour within the CNS

3) Histological Grade

4) The World Health Organisation (WHO) Classification

2.2.1. Classification: Cell of Origin and Tumour Location

Brain tumours arising from outside the brain parenchyma are classified as extrinsic brain tumours, while brain tumours arising from within the brain parenchyma are of said to be intrinsic brain tumours as described in table 2.

Relationship to the Brain Parenchyma	Cell Type	Tumour Type
Extrinsic	Meningothelial	Meningioma
	Mesenchymal	Sarcoma
Intrinsic	Glial	Astrocytoma
		Ependymoma
		Oligodendroglioma
	Neural	Medulloblastoma
	Choroid Plexus	Choroid Plexus Carcinoma

Table 2. Table showing tumour type as defined by the cell of origin and the relationship to the brain parenchyma.

2.2.2. Classification: Histology

The histological grade of brain tumours may differ across tumour types (Louis et al., 2007), however, grading in general may be as follows;

> **Grade 1)** Low levels of proliferation of the tumour mass with potential for surgical cure.

Grade 2) Low levels of proliferation of the tumour mass while being infiltrative.

Grade 3) Medium/High levels of proliferation of the tumour mass while having evidence of malignancy.

Grade 4) High levels of proliferation of the tumour mass, malignancy, rapid progression of the disease, and highly lethal tumours.

2.2.3. Classification: World Health Organisation (WHO) Classification

The WHO classification of tumours has previously been based upon tumour grade and tumour histology (Louis et al., 2007), however, the 2016 revision included elements of molecular stratification into their new classification (Louis et al., 2016) as described in Table 3. Further classification of tumours is likely increase with time as greater understanding and evidence of biological differences between the tumours emerges, resulting in revisions of the classifications.



WHO grades of select CNS tumours

Diffuse astrocytic and oligodendroglial tumours	
Diffuse astrocytoma, IDH-mutant	II
Anaplastic astrocytoma, IDH-mutant	III
Glioblastoma, IDH-wildtype	IV
Glioblastoma, IDH-mutant	IV
Diffuse midline glioma, H3 K27M–mutant	IV
Oligodendroglioma, IDH-mutant and 1p/19q-codeleted	II
Anaplastic oligodendroglioma, IDH-mutant and 1p/19q-codeleted	III
Other astrocytic tumours	
Pilocytic astrocytoma	I
Subependymal giant cell astrocytoma	I
Pleomorphic xanthoastrocytoma	II
Anaplastic pleomorphic xanthoastrocytoma	III
Ependymal tumours	
Subependymoma	I
Myxopapillary ependymoma	I
Ependymoma	II
Ependymoma, *RELA* fusion–positive	II or III
Anaplastic ependymoma	III
Other gliomas	
Angiocentric glioma	I
Chordoid glioma of third ventricle	II
Choroid plexus tumours	
Choroid plexus papilloma	I
Atypical choroid plexus papilloma	II
Choroid plexus carcinoma	III
Neuronal and mixed neuronal-glial tumours	
Dysembryoplastic neuroepithelial tumour	I
Gangliocytoma	I
Ganglioglioma	I
Anaplastic ganglioglioma	III
Dysplastic gangliocytoma of cerebellum (Lhermitte–Duclos)	I
Desmoplastic infantile astrocytoma and ganglioglioma	I
Papillary glioneuronal tumour	I
Rosette-forming glioneuronal tumour	I
Central neurocytoma	II
Extraventricular neurocytoma	II
Cerebellar liponeurocytoma	II
Tumours of the pineal region	
Pineocytoma	I
Pineal parenchymal tumour of intermediate differentiation	II or III
Pineoblastoma	IV
Papillary tumour of the pineal region	II or III
Embryonal tumours	
Medulloblastoma (all subtypes)	IV
Embryonal tumour with multilayered rosettes, C19MC-altered	IV
Medulloepithelioma	IV
CNS embryonal tumour, NOS	IV
Atypical teratoid/rhabdoid tumour	IV
CNS embryonal tumour with rhabdoid features	IV
Tumours of the cranial and paraspinal nerves	
Schwannoma	I
Neurofibroma	I
Perineurioma	I
Malignant peripheral nerve sheath tumour (MPNST)	II, III or IV
Meningiomas	
Meningioma	I
Atypical meningioma	II
Anaplastic (malignant) meningioma	III
Mesenchymal, non-meningothelial tumours	
Solitary fibrous tumour / haemangiopericytoma	I, II or III
Haemangioblastoma	I
Tumours of the sellar region	
Craniopharyngioma	I
Granular cell tumour	I
Pituicytoma	I
Spindle cell oncocytoma	I

Table 3. Table showing tumour classifications as per the WHO 2016 revision. Image from (Louis et al., 2016).

3. Glioblastoma multiforme

'Glioma' describes primary brain tumours arising from glial cells. Gliomas include astrocytic tumours, Ependymomas, oligodendrogliomas, and mixed gliomas. Gliomas encompass the most common tumour type of CNS cancers, accounting for approximately 80% of all primary malignant brain tumours. Of these, Glioblastoma multiforme (GBM) is the most common astrocytoma, while being upwards of 60% of all adult brain primary intrinsic tumours (Schwartzbaum et al., 2006). Despite decades of advancement in the laboratory with regards to potential treatments, little progress has been made in the clinic as GBM is still an exceptionally poor prognosis tumour.

3.1. Cell of origin for Glioma

Genome-wide molecular phenotyping has advanced our characterisation of gliomas and produced distinct genetic subtypes. The division of

morphologically indistinguishable tumours into four subtypes – defined by their genetic aberrations and unique gene expression profiles, has suggested potential candidate cells for the cell of origin for GBMs (Verhaak et al., 2010a). However, it has been shown that tumours may be comprised of subpopulations of these distinct subtypes (Patel et al., 2014), and has thus far had limited relevance clinically with regard to guiding trials. The current hypotheses is that the cell of origin may be neural stem cells, glial progenitor cells and/or astrocytes for gliomas, summarised by (Zong et al., 2012). Ultimately, elucidation of the cell of origin may lead to greater understanding of gliomagenesis and provide more effective treatment strategies for this deadly disease.

3.2. WHO Classification of Glioma

Gliomas are classified into WHO Grade I-IV tumours and these classifications are determined via histopathological criteria. Grade I gliomas are lesions with a low invasive and proliferative potential, whereas Grade II-IV gliomas are lesions with a high invasive and proliferative potential. GBM tumours are classified as WHO Grade IV tumours (Louis et al., 2016), due to their highly aggressive and invasive nature. Below are glial tumours and their respective WHO classification (Louis et al., 2016).

Grade I) Pilocytic astrocytoma, Subependymal giant cell Astrocytoma, Subependymoma, Myxopapillary Ependymoma, Ganglioglioma

Grade II) Low-grade diffuse Astrocytoma, Low-grade Oligoastrocytoma, Low-grade Oligodendroglioma, Pleiomorphic xanthoastrocytoma, Low-grade Ependymoma

Grade III) Anaplastic Astrocytoma, Anaplastic Oligoastrocytoma, Anaplastic Oligodendroglioma, Anaplastic pleiomorphic xanthoastrocytoma, Anaplastic Ependymoma, Anaplastic Ganglioglioma

Grade IV) Glioblastoma multiforme, Malignant glio-neuronal tumour

3.3. Epidemiology

GBM tumours account for 50% of gliomas in brain tumour patients of all age groups (Rock et al., 2012). The incidence rate of GBM is currently 2-3 per 100,000 adults in Europe and North America (Thakkar et al., 2014). Incidence rates of GBM in infants is estimated to be 1.1-3.6 cases per 100,000 infants (Winters et al., 2001). GBM tumours are biased towards male patients in adult and paediatric populations, with a ratio of 1.26 per 1 female patient and 3.3 per 1 female patient in adults and paediatric patients, respectively (Winters et al., 2001, Mahvash et al., 2011). The incidence rates of gliomas is outlined in Table 4.

Tumour Type	WHO Classification Grade	Incidence Rate	Male:Female Ratio
Pilocytic Astrocytoma	I	0.23	1.09
Diffuse Astrocytoma	II	0.13	1.46
Oligodendroglioma	II	0.34	0.92
Oligoastrocytoma	II	0.1	1.0
Ependymoma	II/III	0.23	1.29
Anaplastic Astrocytoma	III	0.49	0.77
Anaplastic Oligodendroglioma	III	0.1	1.15
Anaplastic Oligoastrocytoma	III	0.08	0.77
Glioblastoma multiforme	IV	2.96	1.26

Table 4. Table describing a variety of gliomas and their incidence rates (Ostrom et al., 2017). Incidence rates are per 100,000 person per year.

3.4. Biological Behaviour

GBM tumours develop within the brain in the overwhelming majority of patients, and more specifically within the cerebral hemispheres (Krex et al., 2007), the cerebellum (Hur et al., 2008), and more rarely, in the brainstem (Lakhan and Harle, 2009). GBMs are highly infiltrative tumours which pose a significant surgical challenge for surgeons, with the enhancing region of the tumour being typically what can be resected (Smith et al., 2014). As previously mentioned, GBMs are highly infiltrative, but rarely metastatic. However, cases of metastatic disease demonstrate metastases via the cerebrospinal fluid (CFS) (Birbilis et al., 2010) and blood (Lun et al., 2011). These rare GBM metastases have been shown to target the Liver, bones, lymph nodes and lungs (Seo et al., 2012).

3.5. Morphological Features

GBM tumours consist of cells exhibiting anaplasia, polymorphism, necrosis, and anisokaryosis, with regards to morphology (Figure 1) (Aldape et al., 2015). GBMs are infamous for their apparent histological and cytological intratumour heterogeneity, as well as molecular heterogeneity (Sottoriva et al., 2013, Patel et al., 2014). One of the most prevalent features of GBM histology are necrotic foci, with the tumour core exhibiting large amounts of necrosis (Perry and Wesseling, 2016). GBM cells exhibit nuclear atypia – hyperchromatic, and multinucleated, with an increased nucleus to cytoplasm ratio (Urbańska et al., 2014). Other cells present within GBM tumours may also be binucleated cells, lymphocytes, macrophages, neutrophils, and commonly, necrotic cells (Schultz et al., 2005). Multiple histological features and variants of GBM are shown and described in Figure 2 A-J.

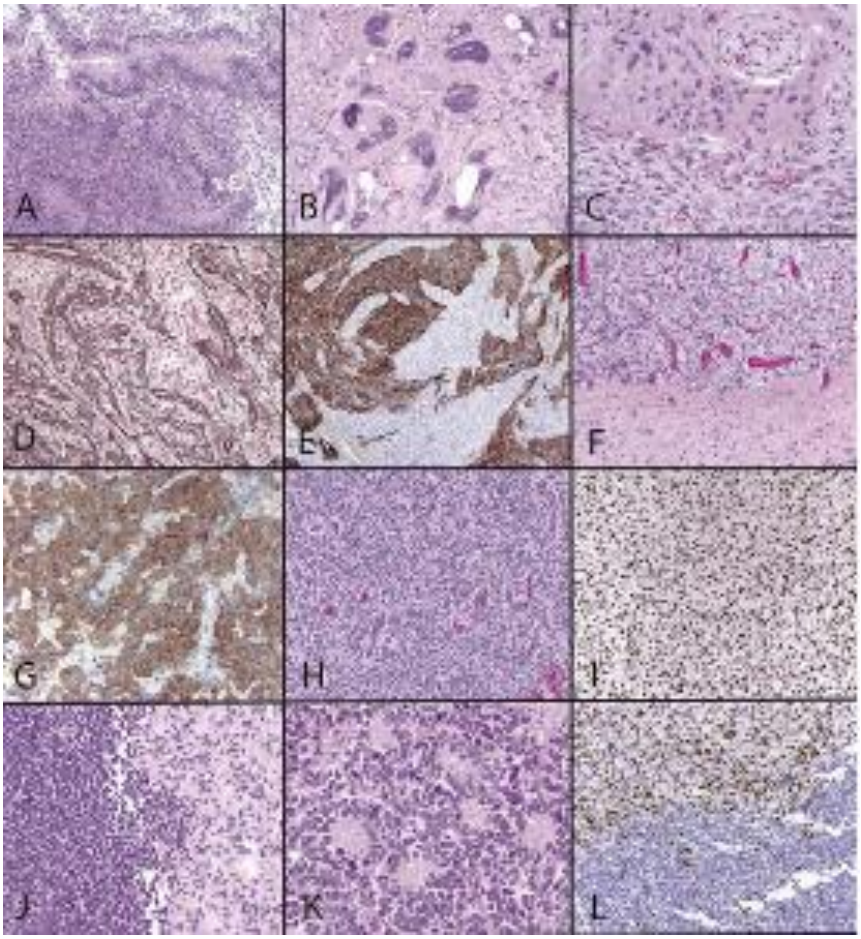


Figure 2. Histology of GBM and its variants - Image adapted from (Perry and Wesseling, 2016); A) GBM histology, characterised by pseudopalisading necrosis histology. B) Giant cell GBM histology, characterised by large, pleomorphic, and multinucleated cells. C) Gliosarcoma histology, characterised by island of fibrillary-appearing glioma and fasicular spindled sarcomatous. D) Gliosarcoma histology, reticulin-rich sarcomatous region. E) Gliosarcoma histology, glial fibrillary acidic protein (GFAP) positive glial region. E) Epithelioid GBM histology, characterised by a resemblance to melanoma. F) Epithelioid GBM, BRAF V600E-mutant positive region. G) Small cell GBM histology, characterised by small mono-nucleated cells. H) Small cell GBM, Ki-67 positive histology. I) GBM with primitive neuronal component histology, characterised by clear differentiation between hypercellular component and 'classic diffuse glioma' component. J) GBM with primitive neuronal component, Homer Wright rosettes positive. K) GBM with primitive neuronal component histology, GFAP and OLIG2 negative.

3.6. Genetic aberrations of GBM

Advancements in genome wide genetic and pathway analysis have yielded a complex heterogeneous landscape of GBM. The genetic alterations of GBM are plentiful and cover the entire genome, while affecting up to 80% of chromosomes (Zhang et al., 2012). The more common genetic aberrations include, but not limited to; epidermal growth factor receptor (EGFR), platelet derived growth factor receptor α (PDGFRα), tumour protein 53 (TP53), p16, isocitrate dehydrogenase (IDH1), chromosome 7 gain, chromosome 10 loss, as well as deletions corresponding to chromosomes 19q and 22q (Parsons et al., 2008, Verhaak et al., 2010b, Zhang et al., 2012, Brennan et al., 2013a). Owing to GBM's heterogeneity, paediatric GBMs have genetic mutations and chromosomal modifications that are distinct from their adult counterparts. It has been observed that very frequent p53 mutations, up to 63% of patients (Suri et al., 2009), and EGFR overexpression in up to approximately 40% of patients (Hatanpaa et al., 2010). Other common paediatric alterations include; mutant PTEN, MDM2 amplification and epigenetic inactivation or deletion of p16 (Sturm et al., 2014).

Genome wide gene expression profiling has been undertaken comparing gene expression patterns of adult versus paediatric GBMs (Faury et al., 2007) and primary versus secondary GBMs (Maher et al., 2006, Tso et al., 2006). More recently, unsupervised clustering of gene expression from large GBM tumour sample cohorts from the Cancer Genome Association (TCGA) expanded upon previous subtype classification (Phillips et al., 2006) and identified four distinct molecular subtypes of GBM; neural, proneural, mesenchymal and proliferative (Brennan et al., 2013a, Verhaak et al., 2010b). The proneural subtype was characterised largely by mutations in IDH1 and PDGFRα, while mutations in EGFR were largely identified in proliferative subtype tumours. Mutations in neurofibromin (NF1) were linked to mesenchymal subtype tumours (Brennan et al., 2013a, Verhaak et al., 2010b).

3.6.1. Isocitrate dehydrogenase IDH1/2

Five genes encode the three human IDH catalytic isozymes; IDH1, IDH2, and IDH3 (Cohen et al., 2013). IDH1 and IDH2 proteins reside within the cytosol and mitochondria, respectively, produce reduced nicotinamide adenine dinucleotide phosphate (NADPH) to NADP+ via oxidative decarboxylation of isocitrate to α-ketoglutarate (α-KG). This process is performed outside of the Kreb cycle, but IDH3 performs this process within the Kreb cycle (Pollard and Ratcliffe, 2009). IDH proteins also protect cells from oxidative stress, where cells with lower levels of IDH are more susceptible to oxidative damage from free radicals and reactive oxygen species (Lee et al., 2002). Overall, IDH is a key enzyme within the citric acid cycle, as well as functioning to maintain the cellular redox state.

Somatic mutations in IDH1/2 are commonly screened to aid in differentiation between primary and secondary GBMs. IDH1 mutations are present in a very high proportion of WHO grade II and III astrocytoma cases (over 80%), while being exceptionally rare (under 5%) in de novo GBM cases (Parker et al., 2015). Therefore, mutations in IDH1 can be used as an indication of secondary GBM as WHO grade II and III astrocytomas are precursors of secondary GBMs (Ohgaki and Kleihues, 2013). The prognostic value of IDH1 mutations is a more favourable outcome for the GBM patients in both low-grade and high-grade astrocytomas (Wick et al., 2009, van den Bent et al., 2013). Functionally, mutant IDH1 and IDH2 alters GBM metabolism to favour the reduction of α-ketoglutarate to 2-hydroxyglutarate (Dang et al., 2010), causing a reduction in rate of glycolysis (Mustafa et al., 2014). The IDH mutant tumours notably have a reduction in both hypoxia-inducible factor (HIF) 1α and lactate dehydrogenase A (LDHA), owing to their less aggressive phenotype (Mustafa et al., 2014).

3.6.2. 0(6)-Methylguanine-DNA Methyltransferase (MGMT)

0(6)-Methylguanine-DNA Methyltransferase (MGMT) is a DNA damage repair protein which prevents cross-linking of double stranded DNA as a response to chemotherapies, specifically alkylating agents. MGMT actively removes methyl-lesions from the 0(6)-guanine position to prevent the

formation of 0(6)-methylguanine and the subsequent cross-linking of DNA (Esteller et al., 1999).

A landmark phase III trial identified MGMT promoter methylation as an independent predictor of patient response to radiotherapy and TMZ chemotherapy (Stupp et al., 2005, Stupp et al., 2009). The chemotherapy Temozolomide (TMZ), an alkylating agent which induces cytotoxic O6-guanine methyl adducts leading to double stranded DNA breaks, is the standard of care chemotherapy used for GBM patients (Stupp et al., 2005). Hypermethylation of the MGMT promoter leads to a reduction in MGMT protein expression. Analysis showed that patients with a hypermethylated MGMT promoter region had an additional 5.4 month survival benefit over patients with a non-methylated MGMT promoter when treated with radiotherapy and TMZ (Hegi et al., 2005). However, the use of MGMT promoter methylation as a prognostic marker for therapeutic response should be used with caution as it has been noted that patients with this CpG-methylated phenotype can be poor-responders while non-methylated MGMT patients may have prolonged survival (Parker et al., 2015).

3.6.3. Epidermal Growth Factor Receptor (EGFR)

Epidermal growth factor receptor (EGFR), also referred to as HER1, belongs to a family of tyrosine kinase receptors including other members; HER2, HER3, and HER4. EGFR is very frequently hyper-activated and/or overexpressed in GBM through both ligand-dependent and ligand-independent mechanisms (Verhaak et al., 2010b, Brennan et al., 2013b). Cancer achieves these mechanisms of over-activity through a number of means; deletion or missense mutations resulting in constitutive activation of EGFR, gene amplification resulting in greater levels of EGFR receptor protein, aberrant EGF ligand production, as well as malfunctioning in the EGFR degradation processes resulting in over-activity of EGFR signalling (Hatanpaa et al., 2010). EGFR over-activity impacts many tumorigenic processes in many cancer types, such as promoting cancer cell proliferation, invasion, and cell survival (Brennan et al., 2013b), and as such, has been a therapeutic target of chemotherapies.

EGFR is overexpressed in approximately 60% of primary GBMs, compared to only approximately 10% in secondary GBMs (Brennan et al., 2013b). The most prominent EGFR mutation in GBM is the EGFRvIII variant, which is a product of a DNA sequence deletion of the sequence encoding the extracellular domain which produces a truncated and constitutively active form of EGFR (Wong et al., 1992). The EGFRvIII variant is a cancer specific mutation, and has yet to be detected in normal tissues, however, only a limited proportion of EGFRvIII positive tumours express the mutant protein (Wong et al., 1992, Hwang et al., 2011, Xu et al., 2017).

EGFR has been successfully targeted in multiple cancer types, predominantly with EGFR-targeted monoclonal antibodies (mABs) and small molecule tyrosine kinase inhibitors (sTKIs) (Sim et al., 2018). EGFR-mABs would compete with EGFR-activating ligands for binding, effectively down-regulating EGFR expression and reducing cell proliferation (Waksal, 1999). The EGFR-mAB, Cetuximab, had shown promising results in pre-clinical cell culture and mouse models in GBM with its anti-tumoural and radiosensitizing effects (Eller et al., 2005). Furthermore, Cetuximab has been shown to interact with EGFRvIII, where Cetuximab-EGFRvIII binding promotes internalisation of the receptor, and thus, a reduction in kinase activation (Patel et al., 2007). However, Phase I/II studies of Cetuximab in recurrent GBM patients has failed to demonstrate any additional efficacy over standard of care chemotherapies (Stragliotto et al., 1996). TKIs target EGFR activity with the approach of competitively binding the EGFR kinase domain adenosine triphosphate binding pocket to target receptor catalytic activity (Baselga et al., 2006). The TKIs; Gefitinib, Erlotinib, and Lapatinib, had previously demonstrated efficacy in breast cancer and NSCLC, but failed to show efficacy in newly-diagnosed or recurrent GBM patients as either monotherapies or in a combinational approach in multiple Phase II trials (Rich et al., 2004, Thiessen et al., 2010). The lack of clinical efficacy of these TKIs was attributed to insufficient inhibitory interactions with AKT, this may be attributed to the non-specific targeting of the TKIs due to homology of EGFR ATP-binding pockets with other tyrosine kinase receptors coupled with general drug penetration issues within the brain (Vivanco et al., 2012, Laquintana et al., 2009).

3.6.4. Phosphatase and tensin homolog (PTEN)

Phosphatase and tensin homolog (PTEN) is observed to be one of the most commonly downregulated or lost genes implicated in tumourigenesis of brain, prostate, and breast cancers (Milella et al., 2015). PTEN functions as a tumour suppressor through its negative regulatory interactions with the phosphoinositide 3-kinase (PI3K) pathway, with activity of the PI3K pathway stimulating cell proliferation (Parsa et al., 2007), invasion (Ströbele et al., 2015), DNA damage repair (Gaspar et al., 2010), as well as cell survival (Gaspar et al., 2010). The loss of heterozygosity at chromosome 10q23 occurs in approximately 70% of GBMs (Bigner et al., 1988), resulting in approximately 40% of GBMs harbouring mutations in PTEN (Wang et al., 1997). PTEN deletions are common among all GBM genetic subgroups, apart from IDH1 mutant GBMs (Guan et al., 2014). However, loss of PTEN is not associated with poorer survival in newly diagnosed GBM patients who are treated with TMZ (Carico et al., 2012), despite PTEN being implicated in malignant progression of GBM (Rasheed et al., 1997).

3.6.5. Telomerase Reverse Transcriptase (TERT)

Telomerase activity as a result of mutations within the promoter region of the telomerase reverse transcriptase (TERT) gene has a significant role in tumourigenesis and has been implicated in the development of brain tumours, including GBM, oligodendrogliomas, and other astrocytomas (Lee et al., 2017, Dubbink et al., 2015). Mutations within the promoter of TERT result in elongation of telomere length due to hyperactivation of TERT, resulting in the propagation of cancer development via maintaining self-renewal of cancer cells (Vinagre et al., 2013, Chiba et al., 2017). TERT mutations occur most commonly with the subset of GBMs harbouring EGFR amplifications as well as being IDH wild-type (Nonoguchi et al., 2013). Patients harbouring TERT mutations alone have been shown to have poor survival (median OS 11.3 months) relative to patients without TERT or IDH1/2 mutations (median OS of 16.6 months), as well as patients with mutant IDH1/2 (median OS 42.3 months) (Killela et al., 2013).

3.7. Epigenetic aberrations of GBM

Epigenetic activation and silencing of oncogenes and tumour suppressor genes may occur aberrations in DNA methylation and histone modifications and regulations. Hypermethylation of cytosine in CpG dinucleotides and CpG islands is a common DNA modification in cancer (Carén et al., 2013). This process occurs when methyl groups are donated by S-adenosyl methionine, with the reaction being catalysed by DNA methyltransferases. Aberrations of histone modifications, altered expression of chromatin regulators, and expression of histone variants prevalent in cancer are responsible for DNA misfolding (Jenuwein and Allis, 2001). Modifications of histone tails include; methylation, phosphorylation, ubiquitination, acetylation, sumoylation, and ADP-ribosylation (Kouzarides, 2007). Common epigenetic aberrations present in GBM include; hypermethylation of tumour suppressors (Herman et al., 1996, Horiguchi et al., 2003, Nakamura et al., 2001), DNA repairs genes (notably MGMT) (Costello et al., 1994), and cell cycle regulators among others (Gonzalez-Gomez et al., 2003, Uhlmann et al., 2003). Distinct subgroups of GBM tumours may be stratified from the large variety of epigenetic modifications found in patients (Sturm et al., 2012), as described in Figure 3.

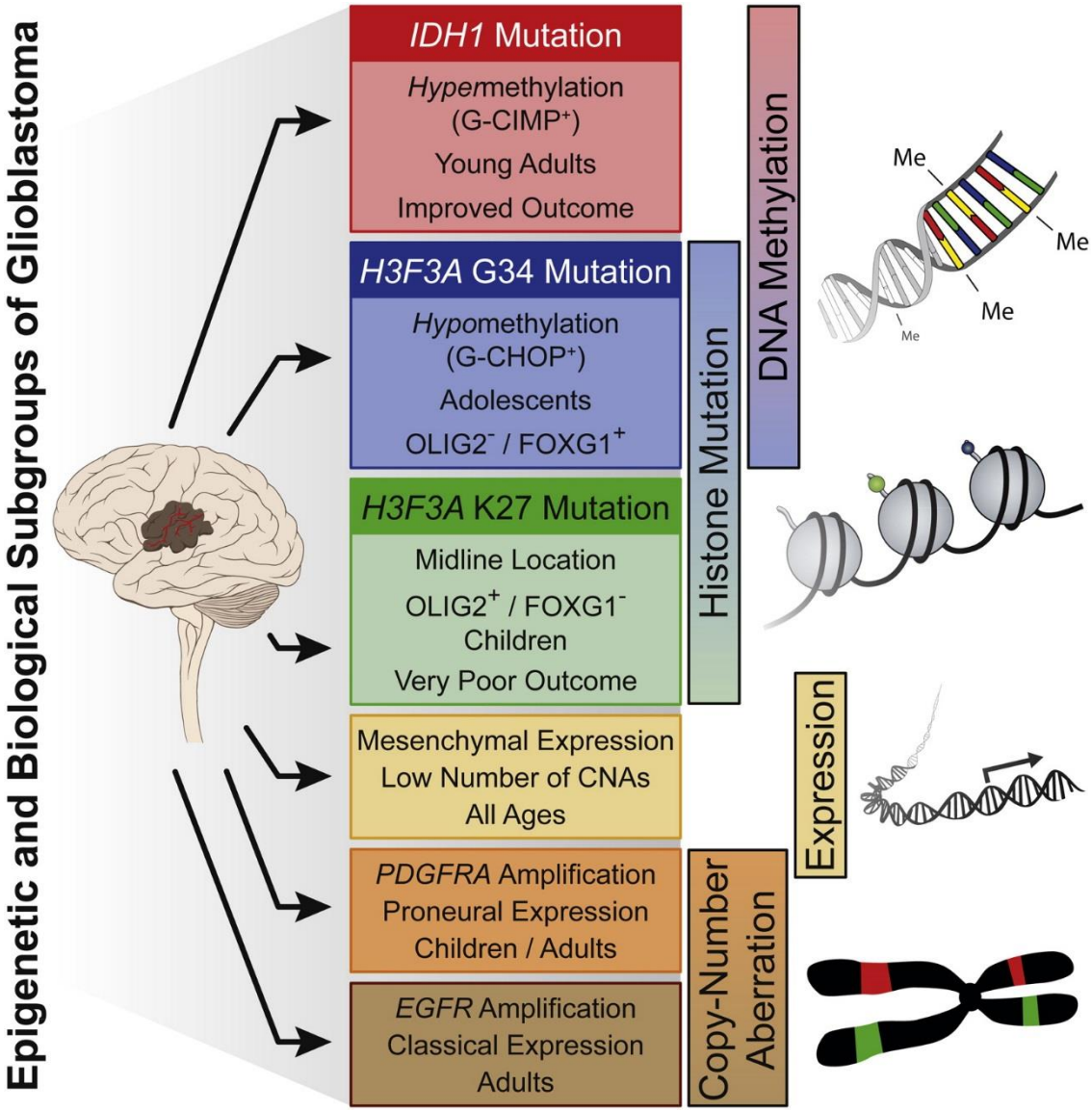


Figure 3. A diagram describing the distinct epigenetic and biological subgroups of GBM. Image from (Sturm et al., 2012).

3.8. Clinical Signs and Symptoms

The clinical manifestation and its subsequent symptoms are dependent upon the tumour location, direct effect of necrosis, and the increasing intracranial pressure (Hanif et al., 2017);

A) Healthy brain tissue destroyed by necrosis may cause focal neural deficit and cognitive impairments in ~40-60% of patients.
B) Intracranial pressure as a result of the increasing tumour mass and oedema surrounding the tumour may cause progressively severe headaches in ~30-50% of patients.
C) The tumour location may account for focal onset seizures in ~20-40% of patients.

The most common symptoms of a GBM are often non-specific and may include; headaches, ataxia, seizures, frequent syncope, and dizziness (Levine et al., 1987). Due to these non-specific symptoms, GBMs as well as other brain tumours may be misdiagnosed as other diseases (Lakhan and Harle, 2009). Primary GBMs typically present with a relatively sort clinical history when compared to secondary GBMs which clinical history may span years (Hanif et al., 2017).

3.9. Standard of Care for GBM patients

GBMs are characterised by their highly invasive nature, with the tumour surrounded by peri-tumoural oedema and inflammation. These factors combined produce unclear tumour margins which ultimately make GBMs less susceptible to complete surgical resection. Regardless, radical surgical resection remains as the first line of treatment for GBM patients. Tumour resection facilitates a conformational pathologic diagnosis of the disease, reduces tumour burden as well as relieving compression of vital brain constituents (Hottinger et al., 2014). The most important independent, treatment-related factor of OS in patients is the extent of surgical resection (Wolbers, 2014, Li et al., 2016). It has been shown that an extent of resection of at least 78% is adequate to have prognostic benefit when the patient receives further treatment with chemoradiation therapy (Sanai et al., 2011). However, more recent reports have implicated the residual tumour volume being the greater predicator of outcome over extent of

resection as a percentage (Chaichana et al., 2014, Grabowski et al., 2014). Surgical resection of GBMs has been augmented with fluorescence in an attempt to improve the efficiency of surgical resection. 5-aminolevulinic acid (5-ALA) is a natural precursor of haemoglobin which elicits the accumulation of fluorescent protoporphyrin IX in malignant tissue (Regula et al., 1995). The accumulation of 5-ALA in malignant glioma tissue facilitates its use in fluorescence-guided surgery of GBM (Pichlmeier et al., 2008, Stummer et al., 2000, Schucht et al., 2012, Stummer et al., 2006). Stummer *at al* demonstrated how fluorescence-guided surgery with 5-ALA enables more complete resections of the contrast-enhancing region of the tumour, resulting in improvements to progression-free survival in patients (Stummer et al., 2006).

As of 2005, the standard of care for adult GBM patients has been surgical resection, radiotherapy, with concomitant and adjuvant Temozolomide (TMZ) as per the Stupp protocol (Stupp et al., 2005). Concomitant TMZ, at a dose of 75mg/m^2, is orally administered daily throughout radiotherapy, with radiotherapy being 60Gy delivered in 30 fractions. Adjuvant TMZ is delivered 4 weeks following radiotherapy at a dose of 150-200mg/m^2 for 5 days every 28 days as maintenance therapy (Stupp et al., 2005). Follow up magnetic resonance imaging (MRI) would be undertaken after every 2-3 TMZ cycles to assess response and stability of the tumour to treatment (Hottinger et al., 2014). The Stupp protocol was proposed following a randomized phase III trial, where median overall survival (mOS) improved from 12.1 to 14.6 months and the 2-year survival rate increased from 10% to 27% in patients received TMZ and radiotherapy (Stupp et al., 2005). Analysis of the trial showed that the addition of TMZ to the treatment regime predominantly benefitted patients who were positive for methylated MGMT (Hegi et al., 2005). Clinicians may also incorporate Gliadel® wafers into their treatment regime. The wafers are a biodegradable polymer containing 3.85% Carmustine which are implanted into the resection cavity to supply a controlled release of Carmustine at the time of surgery (Xing et al., 2015, Fleming and Saltzman, 2002). The safety and efficacy of Gliadel® wafers has been demonstrated in newly diagnosed GBM and recurrent malignant glioma patients (Westphal et al.,

2003, Valtonen et al., 1997, Brem et al., 1995). A meta-analysis reported a significant increase in overall survival for newly diagnosed high-grade glioma, however, this increase was not seen in recurrent disease patients (Hart et al., 2011). Multiple clinical trials and studies have assessed the efficacy of the VEGF-inhibitor, Bevacizumab (Gilbert et al., 2013, Chinot et al., 2011, Vredenburgh et al., 2012, Lai et al., 2011, Hofland et al., 2014). Reports show that Bevacizumab may improve median progression-free survival, but does not improve overall survival in primary GBM patients (Chinot et al., 2011, Gilbert et al., 2013). However, recurrent GBM patients do not receive benefit further from Bevacizumab in a combinational therapy regime as opposed to Bevacizumab as a monotherapy in patients with a KPS of 60 or higher (Friedman et al., 2009a, Verhoeff et al., 2010, Hasselbalch et al., 2010, Kreisl et al., 2009a, Taal et al., 2014).

The standard of care for adult GBM patients differs from that for elderly and paediatric patients. It has been shown that elderly patients benefit from radiotherapy, irrespective of being standard (30 fractions of 2Gy) or hypofractionated (34Gy in 3.4Gy fractions or 40Gy in 2.6Gy fractions) (Roa et al., 2004). Trials have compared standard radiotherapy, hypofractioned radiotherapy and TMZ alone in elderly GBM patients, and have demonstrated no significant difference in outcome for the treatment modalities (Wick et al., 2012, Malmström et al., 2012). Similar to adult GBM patients, positive MGMT-methylated elderly patients benefitted significantly with TMZ monotherapy as opposed to radiotherapy. Whereas elderly patients treated with TMZ alone with unmethylated MGMT fared much worse (Malmström et al., 2012, Wick et al., 2012).

4. Paediatric Brain Tumours

Tumours of the central nervous system (CNS) are the second most common neoplasm in paediatric patients. These tumours are the most common type of solid tumour (Kaatsch, 2010), while accounting for 26% of total cancer incidence in children. The sensitive nature of the developing brain has drastic implications on the care of paediatric brain tumour patients with regards to diagnosis, treatment, and follow up.

4.1. Paediatric High-Grade Glioma

Paediatric high-grade gliomas (pHGG) comprise between 8 to 12% of primary paediatric CNS tumours (Bondy et al., 2008). pHGG's typically are of astrocytic origin and are classified as either Grade III or Grade IV under the WHO classification, characterised by their aggressive and malignant phenotype (Louis et al., 2007). HGG is a blanket term for a variety of heterogeneous tumours, however, the most common histologies are anaplastic astrocytoma (WHO Grade III) and GBM (WHO Grade IV). Subgroups of pHGG are summarised in Figure 4. pHGGs may develop anywhere along the CNS, but disproportionately manifest within the supratentorial (ST) region of the brain (Broniscer and Gajjar, 2004). The Central Brain Tumor Registry of the United States (CBTRUS) reported a pHGG incidence rate of 0.85 per 100,000 children between 0 and 19 years of age (Ostrom et al., 2017). This incidence rate also includes anaplastic, oligodendroglioma, mixed glioma, and malignant glioma in the report. Paediatric patients between the ages of 15 and 19 years old account for the highest incidence of pHGG, and the median age of pHGG patients is 9 years old (Ostrom et al., 2017). Clinical presentation of pHGG may be similar to many newly diagnosed brain tumours. pHGG patients often present with symptoms of persistent headaches, ataxia, and nausea (Fangusaro, 2012). More specific symptoms, such as focal motor deficits, chorea, and dysmetria, may be reflective of the tumour's location within the brain (Fangusaro, 2012).

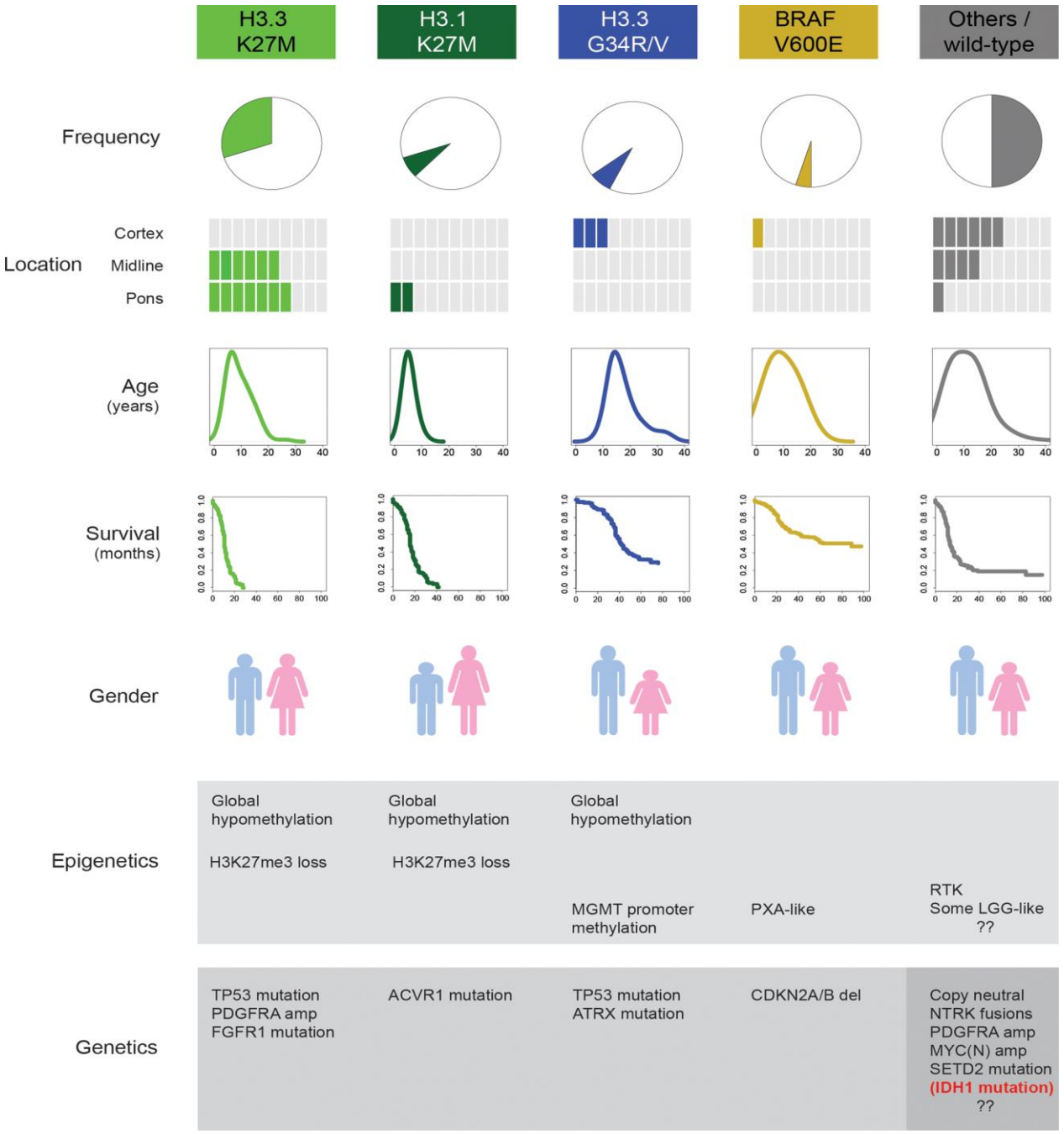


Figure 4. Image showing classifications of pHGG with regards to frequency, location, age, survival, gender, epigenetic and genetic aberrations. Image from (Persson et al., 2016).

4.1.2. Current Therapy Strategies

Diagnosis of pHGG follows clinical presentation, imaging, and histopathological confirmation of the disease. Standard therapies available to pHGG patients are surgical resection of the tumour mass, chemotherapy, and radiotherapy for older patients. The extent of surgical resection, with gross total resection (GTR) being the goal, is a significant prognostic marker for pHGG patient survival (Finlay et al., 1995). As with many tumours, complete radiographic GTR still leaves residual tumour cells that propagate tumour recurrence and invasion, making a GTR without significant morbidity excessively hard (Fangusaro, 2012). Local recurrence from the residual tumour cells is treated with focal radiotherapy around the tumour bed for pHGG patients over 3 years of age (Buckner et al., 2007), as younger patients have a greater susceptibility to the deleterious effects of radiotherapy on the developing brain (Freund et al., 2015, Sanders et al., 2007). Typically, pHGG patients would receive radiotherapy dosed at 50-60Gy in daily fractions of 180-200cGy for a treatment duration of 6 weeks. Chemotherapy for pHGG was first shown to improve patient survival when used in combination with focal radiotherapy compared to radiotherapy alone in the CCG-943 trial. Patients receiving chemotherapy received weekly vincristine during radiotherapy, followed by maintenance chemotherapy cycles of vincristine, lomustine, and prednisone for 8 cycles (Spostol et al., 1989). The 5-year event free survival (EFS) for pHGG patients being treated with chemotherapy and radiotherapy was 46% versus 18% for patients treated with radiotherapy alone (Spostol et al., 1989). However, future post-hoc analysis concluded that many of the patients had low grade gliomas (LGG) which most likely skewed the conclusions of the clinical trial (Finlay and Zacharoulis, 2005). Following the conclusion of this trial, chemotherapy has been adopted for the treatment of pHGG, despite further trials failing to achieve the outcomes of the CCG-943 trial (Finlay et al., 1995, Cohen et al., 2011). Notably, the combination of TMZ with radiotherapy in pHGG patients, as per the Stupp protocol (Stupp et al., 2005), has been shown to have no survival benefit when compared to historical controls (Cohen et al., 2011).

4.2. Paediatric Ependymoma

Ependymoma tumours are the second most common malignant brain tumours in paediatric patients (Peris-Bonet et al., 2006). Paediatric Ependymomas may arise anywhere along the neuroaxis, but most commonly in the Supratentorial (ST) or the Posterior Fossa (PF) regions of the brain (Godfraind et al., 2012). Paediatric Ependymoma accounts for approximately 10% of all paediatric brain tumours. The incidence rates have been presented as 3.7 cases per million in 0-19 year olds, between the years of 2007-2011, within the USA (Howlader et al., 2015), with a disproportionately prevalent in patients of 0-3 years old (Peris-Bonet et al., 2006). Reported survival rates for paediatric Ependymoma patients have been 82.6% (Godfraind et al., 2012) and 81.1% (Massimino et al., 2016) for 5-year survival in a multiple trials with patients having mixed tumour locations. A dominant factor of survival rates is recurrence, with an approximate 50% recurrence rate at 5 years coupled with an approximate 25% of these patients surviving 5 years after first recurrence (Messahel et al., 2009). Extent of surgical resection has been reported to be a significant clinical factor associated with event-free survival (EFS) (Agaoglu et al., 2005, Grill et al., 2001, Jaing et al., 2004, Massimino et al., 2004). However, gross total resection (GTR) is particularly challenging due to the location of the tumour and the surrounding delicate structures, with only approximately 50% of cases attaining GTR (Bouffet et al., 1998, Perilongo et al., 1997). GTR is however, often curative in Ependymoma, while being more effective than any other treatment (Wu et al., 2016, Chai et al., 2017). Therefore, further surgical strategies are employed to achieve GTR for Ependymoma patients such as intraoperative MRI (Gamboa et al., 2018). Advancements in molecular biology techniques have yielded extensive classification of Ependymoma subtypes, described in Figure 5., however, the clinical implications for these subtypes have yet to be conclusive (Hoffman et al., 2014, Pajtler et al., 2015).

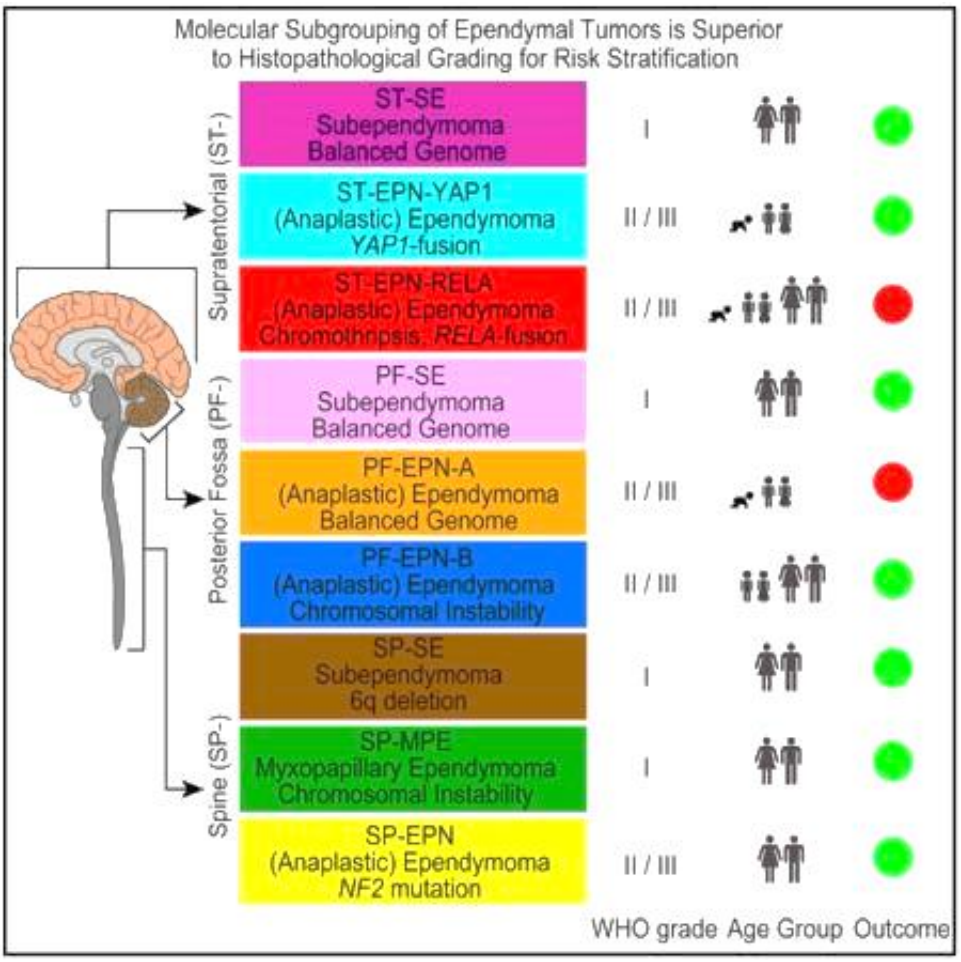


Figure 5. Infographic describing the different Ependymoma subgroups with regards to their tumour locations and genomic characteristics. Image adapted from (Pajtler et al., 2015).

4.2.1. Current Therapy Strategies

Diagnosis of the disease follows clinical presentation, imaging, and histopathology. Commonly presented symptoms of the disease include headaches, ataxia, and nausea/vomiting. The accepted treatment strategies for paediatric Ependymoma include surgery, radiotherapy, and chemotherapy. Treatment via surgery is used in all patients, with the aim of achieving GTR (Jaing et al., 2004, Paulino et al., 2002). Adjuvant radiotherapy is frequently used in older paediatric patients, with radiotherapy being recommended for all patients upon tumour recurrence (Grundy et al., 2007, Messahel et al., 2009). However, patients under three years of age are typically not treated with radiotherapy due to concerns of long-term developmental and neurological concerns (Rudà et al., 2017). The youngest of patients often receive chemotherapy as

opposed to radiotherapy (Rudà et al., 2017, Grundy et al., 2007). Overall, optimal treatment strategies for paediatric are still emerging, with the majority of clinical trials having small cohorts with varied treatment protocols, ultimately producing a very heterogeneous data set for paediatric Ependymoma patients.

4.3. Paediatric Medulloblastoma

Medulloblastoma tumours are the most common malignant paediatric brain tumours (Louis et al., 2007). Medulloblastomas are embryonal tumours which arise in the PF region of the brain, and are classified as WHO Grade IV tumours (Louis et al., 2016). Paediatric Medulloblastoma accounts for approximately 20% of paediatric CNS malignancies and have an incidence of between 2.0 and 5.8 cases per million (Johnson et al., 2014). Medulloblastomas often occur alongside several predisposition disorders, including; Li-Fraumeni Syndrome (Mutations in TP53) (Li and Fraumeni, 1969, Li and Fraumeni Jr, 1969), Gorlin Syndrome (Mutations in SUFU and PTCH1) (Wolter et al., 1997, Taylor et al., 2002), and APC-associated polyposis conditions (Hamilton et al., 1995). The majority of Medulloblastoma cases occur in patients between the ages of 4 and 7, with approximately 70% of cases in patients under the age of 16 (Louis et al., 2007).

Diagnosis of the disease following imaging and histopathology would define the treatment strategy due to Medulloblastomas having multiple, distinct histological variants described in Table 4. (Louis et al., 2016);

Classic – described as having densely packed, small rounded cells surrounded by minimal cytoplasm.

Desmoplastic – described as having regions of differentiated nodules surrounded by regions of highly proliferative cells.

Medulloblastoma with extensive nodularity (MBEN) – described as having a nodular phenotype similar to Desmoplastic but with more-enlarged nodules surrounded by small rounded cells.

Large cell Anaplastic (LCA) – described as having large rounded cells surrounded by an abundance of cytoplasm, accompanied with features of anaplasia.

and molecular subgroups are described in Figure 6.

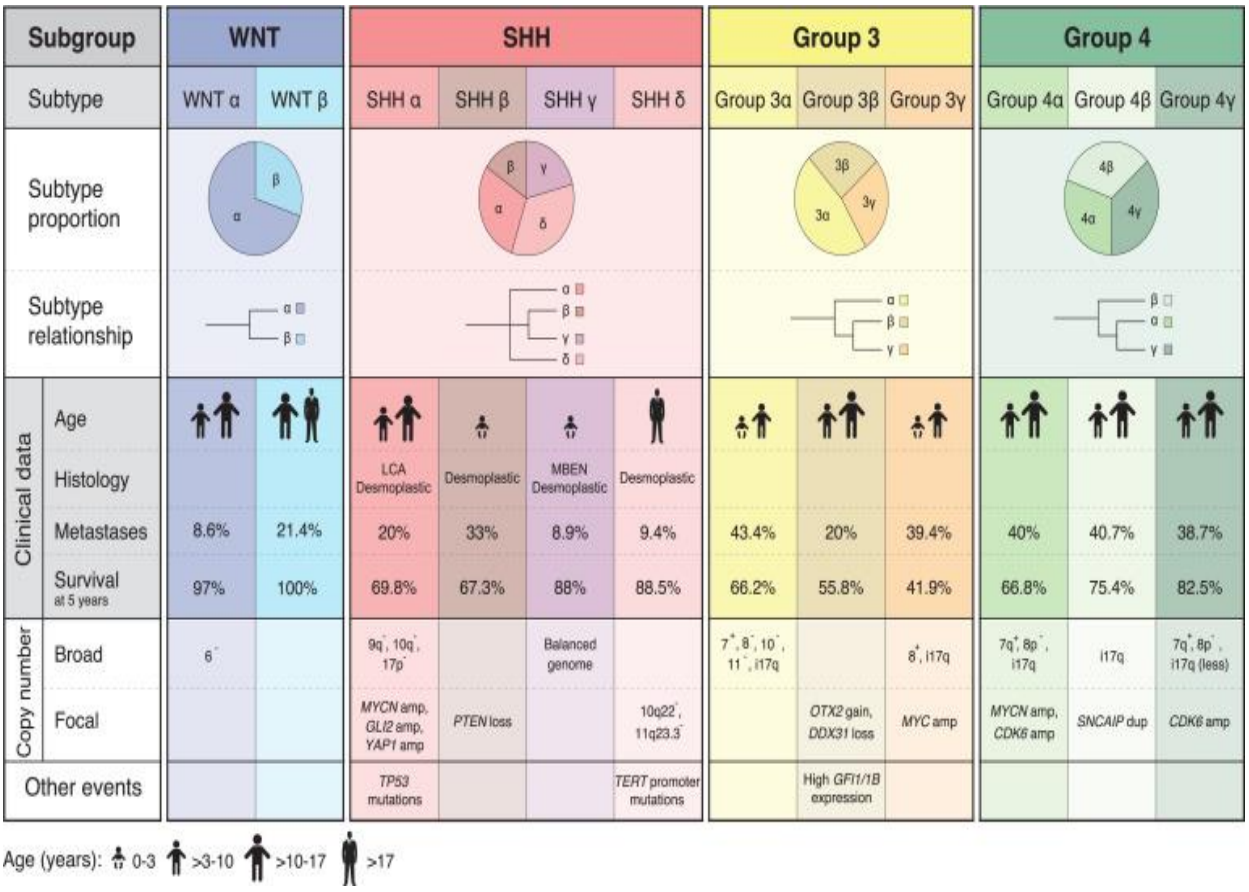


Figure 6. Infographic describing the different Medulloblastoma subgroups with regards to their subgroup, subtype, age, histology, metastasis status, survival, and copy number. Image from (Northcott et al., 2012, Cavalli et al., 2017).

4.3.1. Current Therapy Strategies

Paediatric Medulloblastoma patients are stratified into risk categories based upon their clinicopathological features, including; age of the patient at diagnosis, metastatic status, and the histology. Standard-risk patients are over the age of 3, have a non-metastatic disease, and have a near-total or total resection. High-risk patients are under the age of 3, or have metastatic disease, or have residual disease, or have LCA histology (Kool et al., 2012). Surgical resection remains first-line treatment for Medulloblastoma patients, with the extent of surgical resection being correlated with improved PFS and OS (Massimino et al., 2016). Patients will receive further treatment in the form of adjuvant chemotherapy and radiotherapy, which is specified as per the patients' risk category. Standard-risk patients are typically treated with craniospinal radiotherapy (CSRT), which in itself results in approximately a 60% 5-year OS rate (Packer et al., 1991). Chemotherapy pre- and post-surgery boasts an 80% 5-year OS rate, with the use of concomitant Vincristine with CSRT, followed by a maintenance chemotherapy regime of Cisplatin, Vincristine, and either Cyclophosphamide or Lomustine (Packer Regime) (Packer et al., 2006). High-risk patients may be treated with fractionated radiotherapy or high-dose chemotherapy, a regime including Cyclophosphamide, Vincristine, and Cisplatin (Gajjar et al., 2006), and this has produced 5-year survival rates of up to 70% for high-risk patients (Taylor et al., 2005, von Hoff et al., 2009). However, high-risk patients under 3 years old are rarely treated with radiotherapy in order to preserve neurocognitive faculties in the long-term (Pizer and Clifford, 2009). Infant patients are instead treated with systemic chemotherapy post-surgical resection with Vincristine, Cyclophosphamide, Etoposide, Carboplatin, and Methotrexate. This is then followed by Methotrexate via intrathecal administration, to produce a 5-year OS rate of 77% for these infant Medulloblastoma patients (Rutkowski et al., 2005).

5. Electric Field Technologies for the Treatment of Cancer

5.1. Optune™ (Formerly known as NovoTTF-100a) for Adult GBM

The scarcity of effective treatment for GBM and relapsed paediatric brain tumours has lead to a wide ranging search for other means of therapy for these difficult to treat tumours. Electrical field therapy is one such area that has been considered. The Optune™ system (Novocure) is a US Food and Drug Administration (FDA) approved novel anti-mitotic device that delivers continuous alternating electric fields to the patient for the treatment of primary and recurrent Glioblastoma multiforme (GBM). Optune is indicated for patients which are of at least 22 years of age, with histologically confirmed supratentorial GBM (WHO grade IV astrocytoma (Louis et al., 2007). Optune in combination with Temozolomide (TMZ) has been approved for use in adult patients with newly diagnosed GBM following maximal safe resection, as well as completion of radiation therapy with concomitant TMZ (Stupp et al., 2005).

The Optune™ system is composed of four transducer arrays, a field-generator, and a power source (Figure 7-11.). The field-generator delivers electric fields through the insulated transducer arrays which are applied to the shaved scalp of the patient. The field-generator delivers pre-set electric fields (200kHz for glioma as determined by Kirson et al (Kirson et al., 2004) and with a minimum field intensity of 1.0V/cm (Wenger et al., 2015) – termed tumour treating fields (TTFields) throughout the tumour in a non-invasive manner (Lacouture et al., 2014). Much progress has also been made with optimisation of transducer layout in order to deliver a more efficacious treatment to improve patient outcome. The optimal array placement on the patient's scalp is calculated using NovoTAL™ (Novocure Ltd., Haifa, Israel) simulation software, which will look to optimise field intensity within the tumour with variables such as tumour loci and patient's head measurements (Chaudhry et al., 2015).

A single transducer array is composed of 9 insulated biocompatible ceramic disks. A conductive hydrogel is applied to the patient's shaven scalp to prevent direct contact of the ceramic disks and scalp. Thorough and frequent shaving of the patient's scalp is required for optimal contact

between the transducer arrays and skin. Application of the transducer arrays to the scalp of the patients is not a sterile process, however the prescribed transduced arrays are supplied in individual sterile packages in order to reduce risk of infection. For GBM patient's, Optune TTFields therapy is delivered through two pairs of orthogonally positioned transducer arrays on the patient's scalp. These particular components are secured in place, emphasis on continuous skin contact, by being attached to a hypoallergenic medical adhesive bandage. A single cable connects each transducer array to the portable field generator component of the Optune™ system (Lacouture et al., 2014). A critique of the Optune system is the cumbersome nature of the field-generator, however this has been address by Novocure with production of a second generation design – yielding a reduction in total weight of over 50% (https://www.optune.com/hcp/therapy/system).



Figure 7. The Optune System as worn by GBM patients - The Optune System consisting of a field generator connected to a transducer array, with the included backpack to facilitate portability of the field generator.

	First-generation Optune System	Second-generation Optune
		
Total weight (Device and battery)	6 lbs	2.7 lbs
TTFields generator (The device)	2 lbs	1.5 lbs
Battery Weight	4 lbs	1.2 lbs
Size	Device: 8.3 x 8.3 x 1.75 in Battery: 8.25 x 8.25 x 1.1 in	Device with incorporated battery: 7.1 x 2.3 x 7.6 in
Features	Portability	Easy-grip texture allows for better handling

©Novocure 2017 All rights reserved.

Figure 8. Diagram outlining key design features implemented with the Second-generation Optune System over the First-generation device.

Number	Component
1	Electric Field Generator
2	Portable Batteries
3	Battery Charger
4	Plug-in Power Supply
5	Connection Cable
6	Transducer Arrays
7	Power Cords
8	Shoulder Bag
9	Portable Battery Case

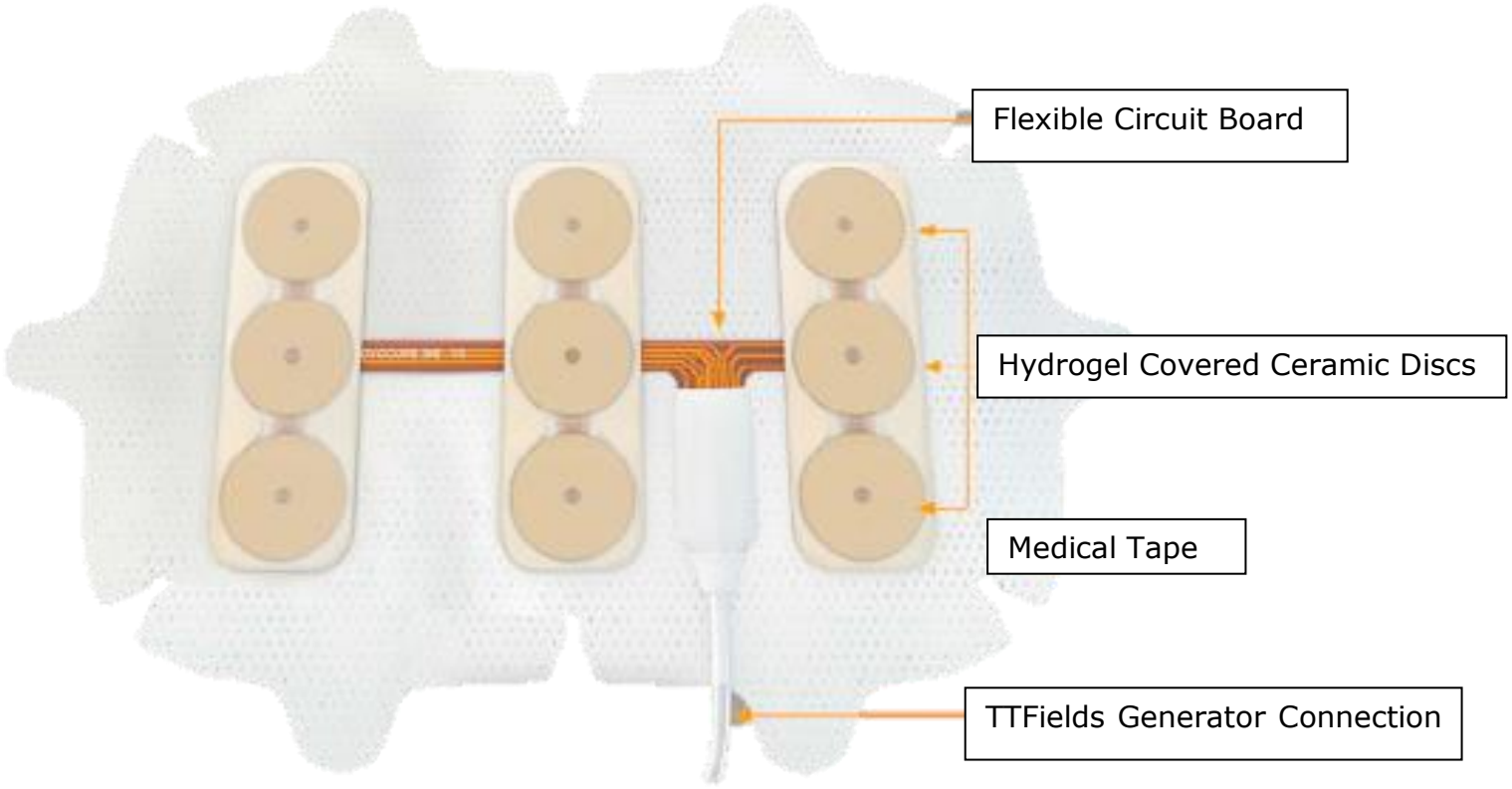


Figure 9. Diagram defining the main components of the Optune System.



Features of the Optune System Electric Fields Generator	
Size	7.1 x 2.3 x 7.6 inches
Weight	2.7lbs (Electric Fields Generator and Battery)
Pre-set Frequency	200kHz
Output Current	Up to 707mA RMS
Power	Can swap batteries without disrupting TTFields delivery
Software	Real-time which applies continuous TTFields treatment while simultaneously monitoring parameters
Safety	Monitored parameters which fall outside of acceptable levels stop TTFields treatment and notifies the patient

Figure 10. Diagram and Table defining the main features of the Optune System Electric Fields Generator.



Features of the Optune System Transducer Arrays
TTFields are applied via Capacitive Coupling
Transducer arrays contain 9 hydrogel covered ceramic disks
Flexible materials/components used allow greater adaption to the patient's head curvature
The TTFields alternatively switch between the two pairs of transducer arrays
Each transducer array contains 8 temperature sensors which alarm if the patient's skin temperature exceeds 41^0C

Figure 11. Diagram and Table defining the main features of the Optune System Transducer Arrays.

5.1.1. Tumour Treating Fields Therapy Indications and Contraindications for GBM Patients

Disease	TTFields Patient Indications
GBM	Age of 22 years or older
GBM	Histologically-confirmed GBM
GBM	Supratentorial located GBM
Newly Diagnosed GBM	In combination with TMZ following maximal debulking surgery, and after completion of concomitant radiochemotherapy
Recurrent GBM	Histologically- or radiologically-confirmed recurrence of GBM in the supratentorial region
Recurrent GBM	Optune is intended to be used as a monotherapy as an alternative to standard GBM therapies

Table 5. A table outlining the indications for newly diagnosed and recurrent GBM patients for TTFields therapy.

TTFields Patient Contraindications
GBM patients under 22 years of age
GBM patients with tumours outside the supratentorial region of the brain
Patients with active implanted medical devices e.g. Deep Brain Stimulators, Vagus Nerve Stimulators, Spinal Cord Stimulators, Pacemakers, Programmable Shunts, and Defibrillators
Patients with skull defects
Patients sensitive to hydrogels
Patients who are pregnant or are trying to get pregnant
Patients who are unable to use the Optune System independently or who are not able to access care

Table 6. A table outlining the contraindications for GBM patients for TTFields therapy.

A number of indications and contraindications are associated with the Optune System for the treatment of newly diagnosed and recurrent GBM (Table 5-6.). Firstly, the effects of TTFields have only been studied with adults, therefore Optune TTFields therapy may only be administered to patients of 22 years or older. Patients are excluded from treatment if they have a skull defect which would restrict attachment of the transducer arrays, and also if they have known sensitivity to conductive hydrogels (http://www.optune.com/Content/pdfs/Optune_IFU_8.5x11.pdf).

Recently, medically implanted devices (such as DBS devices) were removed from the list of official contraindications due to a retrospective analysis of 1,402 patients which revealed no device related safety concerns for the 49 patients with a variety of implanted medical devices (Ashby et al., 2015). Lastly, considerations have to be made regarding patients without access to assistance with the Optune system (either a friend/relative or carer) or do not have sufficient mental competence for personal maintenance of and compliance with the system – patients are expected to comply to the system on average at least 18 hours per day (Wong et al., 2015b).

5.1.2. Tumour Treating Fields Interactions

Understanding the mechanisms of action of TTFields requires familiarity with three electromagnetic concepts. First, an electric field may be uniform, where an electric field is constant at every point in space, or it may be non-uniform, where an electric field varies in direction (convergent or divergent) and/or magnitude at a particular point in space (Gutin and Wong, 2012). Second, electric fields may be constant, where the source charge remains constant such that a test charge will converge, in a single direction, within the constant field towards the opposite polarity source. An electric field may also be a time-varying field – where the charges of the sources do not remain constant and therefore alternate space (Gutin and Wong, 2012). Lastly, the test charge may be a monopole or dipole. An electric monopole will simply travel along the direction of an alternating uniform field, however, an electric dipole will rotate within the alternating uniform field to orientate to the current's direction. Dielectrophoresis is a process where electric monopoles and dipoles migrate towards the point

of greatest electric field intensity within the converging non-uniform electric field (Gutin and Wong, 2012).

The initial theory was that mitosis of actively dividing tumour cells could be perturbed with the application of alternating electrical fields (Kirson et al., 2004). Palti and colleagues tested the hypothesis that alternating electric fields may disrupt mitosis in eleven different cancer cell lines, and demonstrated that the formation of mitotic spindles could be disrupted by alternating electric fields. More specifically, Palti and colleagues showed that alternating electric fields at optimised frequencies (TTFields) interfered with the polymerization process of tubulin subunits during the metaphase of the cell cycle (Kirson et al., 2004). Another conclusion of the study was the significance of optimising the TTFields to a specific cancer cell type to exhibit greatest efficacy. The optimal frequencies determined for glioma cell lines were 200kHz, and with an intensity of 1-3V/cm (Kirson et al., 2004). The considerations of the frequency and intensity parameters is necessary to avoid unwanted stimulation of excitable cells and patient tissue heating (Omar, 2014). Undesirable excitable cell stimulation is unlikely to happen as TTFields use electric fields at frequencies up to 1,000 times larger than electric fields used for neuromodulation therapy, this is because a membrane's excitability response time being too slow to recognise such high frequency electric fields (Omar, 2014, Kirson et al., 2004). Conversely, exceptionally high frequencies, within the MHz range, cause greater integration of the hyperpolarization/depolarization cycles resulting in dielectric losses – electrical heating as a result of rapidly oscillating molecules (Omar, 2014, Kirson et al., 2004).

5.1.3. Anti-mitotic effects of TTFields

Of particular interest is the mechanism and interactions of TTFields with these polar molecules during mitosis, as this is where TTFields may express their anti-tumour effects (Gera et al., 2015, Kirson et al., 2007, Kirson et al., 2004, Giladi et al., 2015c). Certain events during this process are paramount to the understanding of how TTFields function and have therapeutic potential. Before the actualisation of the metaphase-plate, paired centromeres are captured by the ends of microtubules, before becoming orientated towards their respective poles by their opposing

metaphase spindles, during anaphase to become separated via cytokinesis (Kops and Shah, 2012, Gera et al., 2015). Sister chromatid separation through cytokinesis is a consequence of Cyclin B and Securin ubiquitin-mediated degradation by Cdc20 and Anaphase Promoting Complex C (APC/C) (Pines, 2011, Kops and Shah, 2012, Gera et al., 2015). This APC/CCdc20 destruction complex is dependent on proper microtubule localisation and function within the anaphase and metaphase spindles (Pines, 2011, Kops and Shah, 2012, Gera et al., 2015). The key point of this process is that errors that disrupt this intricate process, particularly following commitment to anaphase, are likely to be irrevocable (Huang et al., 2009). This dependency of cancer cells on mitotic competence is the basis for a number of therapies targeting mitosis (Dominguez-Brauer et al., 2015), and is also the basis of TTFields as previously stated, errors committed within anaphase results in a multitude of cell fates and phenotypes including mitotic catastrophe, aberrant mitotic exit, aneuploidy, multi-nucleation, mitotic slippage and apoptosis (Hayashi and Karlseder, 2013, Giladi et al., 2015c, Gera et al., 2015).

One of the processes which TTFields seem to target is tubulin polymerization (Gera et al., 2015, Kirson et al., 2004, Gutin and Wong, 2012, Giladi et al., 2015c). Microtubules consist of polymerized tubulin dimers, arranged around a hollow core in parallel (GM, 2000). The dynamic instability of microtubules is particularly crucial for cytoskeleton remodelling which occurs during mitosis, simply put, tubulin dimers undergo expeditious cycles of polymerisation and depolymerisation. Both α-tubulin and β-tubulin are bound to guanosine triphosphate (GTP) which in turn regulates the polymerization process, and it is the hydrolysis of GTP, bound to β-tubulin, to guanosine diphosphate which favours depolymerisation (Dye and Williams, 1996, GM, 2000). In summary, microtubule formation is determined by the rate of tubulin polymerization relative to the rate of tubulin depolymerisation/GTP hydrolysis. Therefore, TTFields would promote depolymerisation, given that tubulins are among the most polar molecules within cells (Gutin and Wong, 2012, Davies et al., 2013), by causing misalignment of tubulin subunits as they become forced to align with the electric field rather than their respected

microtubule filament axis (Davies et al., 2013, Gutin and Wong, 2012). This in turn promotes hydrolysis of GTP to GDP at the positive end of the microtubule, dissociation of tubulin subunits and overall microtubule disruption (GM, 2000).

Given that TTFields affect mitosis through their effects on proteins that possess a high dipole moment and significance within the mitotic process, it would be reasonable to assume that TTFields would interact with a large number of proteins. Recently, Gera *et al* showed the effects of TTFields on other key mitotic proteins and that TTFields express a more diverse interaction than once thought (Gera et al., 2015)**.** Gera *et al* focussed on the Septin heterotrimer (Referred to as Septin from now on), composed of Septin 2, 6 and 7, due to its large dipole moment of 2711D as well as its interaction with the cytokinetic cleavage furrow (CCF) formation (Gera et al., 2015). Of note is the dipole moment of Septin, which is larger than the dipole moment of tubulin dimers (1660D). Other components of the CCF were excluded from the analysis due to incomplete crystal structure information prohibiting dipole moment calculations, including Anillin and PLK1 (Gera et al., 2015)**.** The significance of Septin resides within the anaphase spindle midline and CCF, where through cooperation with Anillin, stabilisation of microtubule structures and the boundaries of the CCF contractility are distinguished (Field et al., 2005, Frenette et al., 2012, Gera et al., 2015)**.** Anillin functions as an adaptor protein for binding of ECT2 to the Septin/Anillin complex to facilitate both regulation and localisation of the CCF and for stability of anaphase spindle midlines (Gera et al., 2015, Frenette et al., 2012)**.** Septin/Anillin regulation of CCF contraction is through crosslinking actin, myosin II and RhoA (Straight et al., 2005, Piekny and Glotzer, 2008) to facilitate actin-dependent myosin contraction at the CCF (Liu et al., 2012)**.** In a similar fashion as tubulin, TTFields would exert rotational stress on Septin, and most likely many other proteins involved within CCF formation/regulation and progression through anaphase.

Lastly, in combination with previously discussed protein interactions, TTFields also disrupt mitosis through membrane blebbing at times coinciding with the onset of anaphase (Gutin and Wong, 2012, Davies et

al., 2013, Gera et al., 2015). The most probable causes of such violent blebbing observed as a response to TTFields would be; i) aberrant localisation of CCF contractile elements, producing ectopic cleavage furrows (Gera et al., 2015) and ii) dielectrophoretic forces acted upon the CCF (Gera et al., 2015, Gutin and Wong, 2012, Kirson et al., 2004). TTFields in combination with the mitotic cell's morphological changes (a resemblance to an hourglass) during the formation of the two daughter cell produces a non-uniform intracellular electric field, with the highest electric field density at the CCF directly between the dividing cells (Davies et al., 2013). As described previously, sufficiently polar organelles and other macromolecules will gravitate towards the point of the greatest electric field intensity – the CCF, further disrupting the intricate mitotic process. It has been noted that these mechanisms are responsible for membrane disruption analogous to membrane blebbing (Kirson et al., 2004, Gutin and Wong, 2012, Gilden et al., 2012, Gera et al., 2015).

Overall, these results demonstrate how TTFields appear to affect mitotic cells throughout the latter stages of/and subsequent to metaphase (Gera et al., 2015, Lee et al., 2013). Literature has also demonstrated that the anti-mitotic effects of TTFields operates in both a p53-dependent (Gera et al., 2015) and –independent (Schneiderman et al., 2015) manner. Also, this presents TTFields as a 'new wave' mitotic inhibitor due to the metaphase/anaphase specific disruption paradigm, where other mitotic inhibitors and traditional therapies mediate anti-tumour effects by triggering the G1/S or G2/M checkpoints of the cell cycle (Harrison et al., 2009, Fernet et al., 2010, Gera et al., 2015). This could potentiate a synergistic effect of TTFields with other therapies affecting mitosis in combination from a more 'complete' coverage of the mitotic cycle.

5.2. Pre-clinical TTFields Studies in Combination with Chemotherapies

5.2.1. Tumour Treating Fields in Combination with Alkylating agents

In accordance with the current standard of care, TMZ is used in combination with RT for patient benefit (Stupp et al., 2005). Two relevant highlights of this randomized phase III are apparent; firstly, the combinational therapeutic route produced a significant increase to both median OS (12.1 to 14.6 months) and 2-year survival (10% to 27%), secondly, a genetic determinant of benefit from TMZ was present in the form of methylation status of O-6-methyl-guanine-DNA methyltransferase (MGMT) (Stupp et al., 2005). Similarly, phase III studies concerning elderly patients, showed that patients expressing a methylated MGMT status benefitted greatly from TMZ treatment, although not in combination with RT, further emphasises genetic predisposition to therapeutic response (Malmström et al., 2012, Wick et al., 2012). MGMT functions to remove the highly mutagenic and genotoxic O^6-methylgunanine residues caused by TMZ (Kondo et al., 2010). A negative feedback loop occurs upon MGMT-dependent repair of these methyl adducts whereby MGMT becomes irreversibly inactivated. It is in this absence of active MGMT that mismatch occurs during replication between methylgunanine and thymine and causes subsequent double-stranded breaks (DSBs) (Kondo et al., 2010, Margison and Santibáñez-Koref, 2002). Complimentary resistance mechanisms to TMZ, as well as other alkylating agents, are reviewed here (Kondo et al., 2010).

The most recent Phase III TTFields trial, the EF-14 trial, showed a potential additive benefit of combining TTFields with TMZ in primary adult GBM patients (Stupp et al., 2015a, Stupp et al., 2017a). The results of this trial will be discussed more in detail in subsequent sections. Silginer and colleagues investigated TTFields in combination with TMZ in pre-clinical *in vitro* glioma models focussing on MGMT-status and TMZ-resistance (Silginer et al., 2017). The study highlighted that TTFields' efficacy was not dependent on MGMT expression, nor was it diminished within TMZ-resistant cell lines (Silginer et al., 2017). The lack of overlap between the TTFields and TMZ-resistance mechanisms is not wholly unexpected however, as the described mechanisms of action for TTFields has yet to be

shown to interact with MGMT (Hegi et al., 2005){Giladi, 2015 #122. This feature of the study highlights how TTFields may be a therapeutic option for patients whom would not benefit greatly from TMZ treatment i.e. patients with a negative MGMT methylation status (Hegi et al., 2005).

A proposed mechanism of synergism would be that TTFields may potentially influence DNA fragment orientation to perturb DSB-repair mechanisms (Giladi et al., 2014). A common theme will emerge that TTFields in combinational therapeutic routes appear potentially to have positive synergistic effects without any known overlapping toxicities.

5.2.2. Tumour Treating Fields in Combination with Radiation Therapy

Radiation therapy (RT) represents another physical treatment modality for cancer treatment. The high-energy ionizing radiation used for treatment damages the DNA of targeted cancerous cells, as well as normal cells which are adjacent to the targeted cells (Baskar et al., 2012). RT may be delivered to the patient through two different means; external beam radiation or through internal radiation sources, with external radiation being delivered via high-energy protons, photons or particle radiation (Baskar et al., 2012). Adjuvant RT would be utilised to target any residual tumour remaining following the resection albeit following a 4 week post-surgery recovery period (Pirzkall et al., 2009). As with other therapies, RT achieves therapeutic efficacy predominantly through a variety of DNA lesions; notably single- (SSBs) and DSBs (Begg et al., 2011). It is these lesions which induce cell death via apoptosis and mitotic catastrophe {Haas-Kogan, 1996 #80}(Vakifahmetoglu et al., 2008).

Given that TTFields influence polar molecules, TTFields should theoretically interact with the fragmented DNA strands following RT. Similar to how TTFields disrupt microtubule assembly (Kirson et al., 2004, Gutin and Wong, 2012, Gera et al., 2015, Giladi et al., 2015c), TTFields may be able to influence DNA fragment orientation in a fashion to decrease DNA ligation to reduce the effectiveness of DNA repair mechanisms. This phenomenon has been reported on previously (Giladi et al., 2015a, Giladi et al., 2014) with reports of reduced clonogenic survival and cell viability despite the increased number of Rad51 and γ-H2AX foci when TTFields and radiation

treatment were used in combination. This report suggests a reduction in DNA strand break repair competency due to the reduction in cell survival despite the upregulation of DNA repair markers Rad51 (Bindra et al., 2004) and γ-H2AX (Jamal et al., 2010). More recently, the effects of TTFields in combination with radiation treatment were more intently interrogated, with an emphasis on timing TTFields with regards to RT (Ho Kim et al., 2016, Giladi et al., 2017). Kim and colleagues reported on the synergistic properties of TTFields with ionising radiation when TTFields were given prior to radiation treatment (Ho Kim et al., 2016). The combinational therapeutic route resulted in greater amounts of p53-dependent apoptosis, as well as produced mitotic anomalies indicative of TTFields treatment – multi-nucleated phenotype and both mono-polar and multi-polar spindle structures (Ho Kim et al., 2016, Giladi et al., 2017). Giladi and colleagues also investigated this combination but with TTFields following RT (Giladi et al., 2017). Again, it was shown that efficacy of RT may be increased with TTFields when administered following radiation treatment. Taken together, these reports suggest that TTFields may be used as a strategy to sensitise glioma to RT, whether TTFields is administered before or after RT. These interactions pose an interesting synergy paradigm which may be irrespective of established RT resistance and other DNA damage repair mechanisms.

5.2.3. Tumour Treating Fields in Combination with Anti-angiogenics

Bevacizumab is a humanised monoclonal antibody which antagonizes Vascular endothelial growth factor (VEGF) to inhibit binding to VEGF-Receptor (VEGFR) (Chamberlain, 2011). Bevacizumab acquired US Food and Drug Administration (FDA) approval for the treatment of recurrent GBM, following two Phase II studies – (Friedman et al., 2009b) and (Kreisl et al., 2009b) in 2009. In summary, both studies concluded that Bevacizumab use was associated with a higher PFS. However, subsequent studies have shown that Bevacizumab does not significantly increase median OS when administered as a front-line therapy for newly diagnosed GBM patients (Chinot et al., 2014, Gilbert et al., 2014). Furthermore, Bevacizumab has been associated with a number of negative side effects; decline in neurocognitive function, gastrointestinal perforation,

thromboembolic events, renal failure, hypertension, neutropenia and overall decreased quality of life (Chamberlain, 2011, Chinot et al., 2014, Gilbert et al., 2014, Wu et al., 2010). It appears that the majority of the lower-grade adverse effects appear to be indicative of VEGF disruption in non-cancerous cells.

As with other combinational therapeutic routes, TTFields combined with Bevacizumab is intriguing as both have shown an improvement to PFS in GBM patients (Chinot et al., 2011, Gilbert et al., 2013), and may provide additive efficacy. Firstly, TTFields efficacy has been shown in a large phase III trial to be comparable to BPC chemotherapies, including Bevacizumab (31% of patients), but without a diverse and adverse side effects profile akin to conventional chemotherapies (Stupp et al., 2012b). Lastly, there has been evidence to suggest that TTFields may increase the safety profile of Bevacizumab when used in combination for treatment of recurrent gliomas (Elzinga et al., 2013). Although on a small scale, Elzinga *et al* retrospectively analysed patients (n=20) treated with the combination of TTFields with Bevacizumab and found no instances of intracranial haemorrhage or thromboembolic events (Elzinga et al., 2013). These particular events occur in 3% and 2.4-12.5% of patients treated with Bevacizumab respectively (Chamberlain, 2011), although it is worth noting that spontaneous intracranial haemorrhage occurs in roughly 2% of patients without Bevacizumab treatment (Chamberlain, 2011). However, the exact molecular nature, if any, of these synergistic events has yet to be elucidated and should be a topic of future research. Lastly, bevacizumab is known to reduce vasogenic brain oedema, thereby reducing patients' dexamethasone requirements. The significance of reducing a patient's dexamethasone's dosage will be expanded upon in later sections.

5.2.4. Tumour Treating Fields in Combination with Mitotic inhibitors

Given the intricate, yet inherently unstable mitotic process in proliferative cells, many inhibitors have been explored for the treatment of cancers; including anti-microtubular, anti-kinase and other molecular targets. The induction of mitotic cell death (MCD) is the rationale behind targeting mitosis in cancer cells. Dividing cells are highly susceptible to MCD when

exposed to disruptive stresses (Rieder and Maiato, 2004). It is these stresses which have the potential to activate the spindle assembly checkpoint (SAC), leading to a prolonged mitotic arrest where a number of different cell fates are actualised – albeit intra- and inter-line variations in cell fates are expected (Gascoigne and Taylor, 2008).

The anti-microtubular class of mitotic inhibitors can be divided into two distinct sub classes; microtubular-stabilizing (i.e. Taxanes and Epothilones) and microtubular-destabilizing agents (i.e. Vinca alkaloids) (Dumontet and Jordan, 2010). These agents have demonstrated anti-tumour activity in a variety of tumours such as breast, non-small cell lung and ovarian cancer (Chan et al., 2012). The microtubule-stabilizers, such as Paclitaxel, typically bind β-tubulin with high affinity to induce conformational changes which in turn results in stability of tubulin interactions (Jordan and Wilson, 2004, Dumontet and Jordan, 2010). Conversely, the microtubule-destabilizers, such as Vinblastine, target microtubule polymerization through binding the vinca domain of both tubulin monomers and microtubules, causing the necessary conformational changes to reduce microtubule formation (Dumontet and Jordan, 2010, Jordan and Wilson, 2004). Although dissimilar, both subclasses aim to cause MCD in a SAC-dependent manner. However, there has been limited transfer from laboratory to clinical practice for the majority of mitotic inhibitors (Chan et al., 2012). This may in part be due to two main limitations; i) the phenomenon of mitotic slippage to circumvent mitotic arrest/MCD and ii) G2/M selective inhibition. Firstly, the polyploid phenotype typical of cells following mitotic arrest presents a paradigm where multiple cell fates are a result, with cells either succumbing to MCD in the subsequent G1 phase, senescence or existing as viable multiploidal cells (Yamada and Gorbsky, 2006). The latter has the potential to produce cells with increasing degrees of instability from subsequent cell cycles, an overall increase in cellular stress, chemoresistance and is a predictor of intrinsic taxane resistance (Restall et al., 2015). The selective nature of mitotic inhibitors naturally leads to limitations in drug efficacy. Considering drug retention times as well as mitotic-specific drugs targetting mitotic machinery at the G2/M-M-phase,

a large population of G1- and S-phase cells may remain refractory to the cytotoxic treatment (Chan et al., 2012). Compounding this selectivity, the mitotic index of human tumours has been estimated to be less than 1% with mean doubling times of a range of solid tumours ranging from ~100 to ~400 days summarized by Komlodi-Pasztor *et al* (Komlodi-Pasztor et al., 2012). These observations of substantial doubling times and low mitotic indexes of solid tumour emphasise the necessity of chronic treatment over a period of multiple months of mitotic inhibitors. However, significant dose-limiting toxicity has been associated with tubulin-targeting agents – notably neutropenia (Jackson et al., 2007, Chan et al., 2012), which has been a persistent challenge during the drug development process. Therefore, improving drug half-life and/or drug delivery limitations, while simultaneously reducing the dose-limiting toxicities associated with tubulin-targeting agents, may be a promising area of investigation for improving mitotic inhibitory therapy for patients.

Mitotic kinase or associated protein inhibitors may also be a viable option for the treatment of cancer. More selective protein or kinase inhibitors seem to be attractive therapeutic options as they add more options for drug resistant tumours but have also been found to have less associated toxicities than their tubulin-associated counterparts on the whole (Chan et al., 2012, Jackson et al., 2007, Komlodi-Pasztor et al., 2012). Members of the Polo-like kinase (PLK) and Aurora kinase families are of particular interest to anti-mitotic therapies given their relatively restricted expression to M-phase, with minimal to null expression in G0, G1 and S-phases (Jackson et al., 2007). PLK1 and Aurora kinases are involved with multiple mitotic process including spindle assembly, cytokinesis, chromosome segregation and activation of the SAC (Chan et al., 2012, Gautschi et al., 2008, Petronczki et al., 2008). Similar to microtubular associated therapies, inhibition of PLK1 and Aurora Kinase A in GBM cells appears to activate the SAC, cause MCD and mitotic arrest (Tandle et al., 2013, Van Brocklyn et al., 2014). However, given that both PLK1 and Aurora Kinase A expression appears at S-phase and peaks at the G2/M checkpoint (Anger et al., 2003, Tanaka et al., 2002), combining these kinase inhibitors with

the microtubule associated agents may provide greater therapeutic efficacy through a more complete coverage of the cell cycle.

TTFields may be considered as a physical novel mitotic inhibitor, so combining TTFields with biological mitotic inhibitors would appear logical. Firstly, assuming compliance to the Optune TTFields system is in the upper bracket of patient beneficial compliance (18 hours and above) (Kanner et al., 2014), TTFields may overcome the limitations of mitotic inhibitor drug retention. Synergism between TTFields and mitotic inhibitors, particularly microtubule-stabilizers, has been demonstrated and novel mechanisms of increased efficacy have been postulated (Munster et al., 2015, Kirson et al., 2009d). Kirson *et al*, suggested that as paclitaxel promotes microtubule elongation due to greater stability of tubulin dimers, TTFields would demonstrate greater influence over the microtubules due to the now greater dipole moment to increase microtubule misalignment (Kirson et al., 2009d, Tuszynski et al., 2016). This is because the displacement vector of the positive to the negative charge is a function of an electric dipole moment. However, TTFields were shown to disrupt microtubules, through yet to be determined mechanisms, which may decrease paclitaxel efficacy in GBM (Giladi et al., 2015c). More recently, Voloshin and colleagues investigated the potential for synergism of paclitaxel and TTFields in ovarian cancer cell lines (Voloshin et al., 2016). The highlights of this study were the increased efficacy of TTFields when combined with paclitaxel, as well as increased accumulation of cells in the G2/M phase of the cell cycle when analysed with flow cytometry. However, accumulation of Caov-3 and OVCAR-3 cells in the G2/M phase of the cell cycle significantly increased relative to controls following 72 hours of TTFields treatment with A2780 cells fate being accumulation in the G1 phase following extended exposure to TTFields (Voloshin et al., 2016). The differences between cell fates is further highlighted within the combination indexes (CI) of the cells; specifically, the A2780, OVCAR-3 and Caov-3 cell lines had Cis of 1.03, 0.81 and 0.86 respectively (Voloshin et al., 2016). These data indicate a synergistic paradigm for the OVCAR-3 and Caov-3 cell lines but an additive effect for the A2780 cell line, however these observations may be due to differences in the intrinsic sensitivities of the cell lines to mitotic inhibitor

treatment. Ovarian cells treated with TTFields in combination with paclitaxel also demonstrated multipolar spindle formations, which coincides with previous observations of TTFields treated cells (Giladi et al., 2015c).

It is conceivable the TTFields combined with microtubule-destabilizing agents, such as the vinca alkaloids, should produce a similar effect given their similar modes of action. This hypothesis gains credence from evidence of combinational therapy consisting of paclitaxel and vinorelbine, a semi-synthetic vinca alkaloid, significantly improving outcome for breast cancer patients (Romero Acuña et al., 1999). Interestingly, evidence of combining the microtubule associated paradigms has also appeared in nature with both classes being present within the roots and rhizomes of the bat flower, *Tacca sp* (Risinger et al., 2013). Lastly, it has been shown that TTFields do not perturb localisation of PLK1 from its functional location at the anaphase spindle midline (Gera et al., 2015), but data regarding other mitotic associated proteins has yet to be collected. Therefore, there is reasoning behind combining TTFields with a number of mitotic inhibitors regardless of the mitosis stage of their action.

5.2.5. Tumour Treating Fields in Combination with Immunotherapy

Just as the previously detailed therapeutic options available to GBM patients, immunological agents may have the potential for synergism with TTFields, and thus improved efficacy. Although a newly emerging phenomenon, TTFields indeed seem to induce an immune response and its anti-tumour effects may be, at least in part, dependent on the competence of the patient's immune system (Kirson et al., 2009a, Kirson et al., 2009d, Lee et al., 2013, Wong et al., 2015a). Firstly, TTF-induced mitotic exit subjects the affected cells to cellular stress which among others, upregulates cell surface expression of calreticulin – an endoplasmic reticulum chaperone protein (Obeid et al., 2007), a downregulation of anti-phagocytic signalling molecules such as the cell surface CD47 (Henson and Hume, 2006), as well as promotes secretion of HMGB1 in order to produce an immunogenic phenotype (Kepp et al., 2011). This response termed 'Immunogenic cell death' is a documented phenomenon of cancer cells when subjected to TTFields, which is dissimilar to the inherently

immunosuppressive apoptosis (Obeid et al., 2007, Kepp et al., 2011). There is evidence in favour of TTFields promoting anti-tumour immunogenicity *in vitro* and *in vivo* (Wong et al., 2015a, Kirson et al., 2009d, Kirson et al., 2009a). Kirson *et al* demonstrated how TTFields may inhibit metastasis to the lungs of solid tumours but also noted that significantly greater amounts of infiltrative immune cells were found intratumourally in the metastasis (Kirson et al., 2009a). Immune cells bearing the markers CD4, CD8 and CD45 were among the infiltrative cells, inferring a T-cell mediated response, but this was only true for the TTFields treated rabbits as opposed to the TTFields treated mice (Kirson et al., 2009a)**.** A few potential reasons for this discrepancy are apparent; i) species differences ii) cancer cell line differences iii) tumour volume differences iv) TTFields treatment duration differences. Naturally, differences in cell lines used, as well as species would equate to differences in efficacy of treatments and competency of the immune system (Feng et al., 2011). Lastly, significant differences in exposure durations to TTFields (1 week for mice and 5 weeks for rabbits) would account for differences in response, and indeed highlights a potential dose-dependent relationship between TTFields and an effective immune response.

Wong *et al* 2014 had previously observed that patients with previous low-grade glioma histology and low dosing of dexamethasone in the Phase III trial examining response rates of NovoTTF-100A as a monotherapy relative to the best physicians choice (BPC) chemotherapy had a more favourable outcome (Wong et al., 2014). Although, it is well recognised that patients with a secondary-GBM, have a significantly more favourable prognosis and longer survival (Ohgaki and Kleihues, 2013). Neuro-oncologists traditionally use dexamethasone for patients with malignant brain tumours for its anti-oedema effects (Dietrich et al., 2011). However, dexamethasone does exhibit profound immunosuppressive influence over patients (Dietrich et al., 2011), and therefore has the potential to reduce efficacy of TTFields. Wong *et al* 2015 further examined the effect of dexamethasone on patients and determined a threshold of dexamethasone exposure for preferential survival with TTFields treatment (Wong et al., 2015a). Using an unsupervised mathematical algorithm, it was determined

that patients receiving over 4.1mg/day had a 2.3-fold decrease in median OS for the TTFields treated cohort, compared to a 1.5 fold decrease in median OS for the BPC chemotherapy treated cohort (Wong et al., 2015a). A decrease in median OS was also seen with a progressive decrement in both cohorts until about 8.0mg/day was achieved where there was no further significant effect on median OS (Wong et al., 2015a). However, it could also be assumed that patients requiring higher doses of dexamethasone may be stratified as higher-risk patients, so may therefore have a lower expected OS irrespective of TTFields.

Given that TTFields have not been shown to have any consequential effects on immune system competence, unlike traditionally used therapeutics (Sengupta et al., 2012), TTFields combined with immunotherapeutics gain credence for a number of reasons. Firstly, as stated above TTFields do not compromise the immune system as other agents do, potentially reducing the required dose of concurrent therapeutics. This dosage reduction should in turn reduce their inherent immune compromising nature. Secondly, the physical nature of TTFields appears to improve the infiltrative capacity of CD4 and CD8 cells in rabbit models (Kirson et al., 2009a)**,** this should have clear synergistic effects with immunotherapeutics such as dendritic cells (Yang et al., 2015). However, this potential synergism has yet to be studied and may be the key to bring the promising field of immunotherapeutics closer to the clinic for GBM patients (Nieto-Sampedro et al., 2011, Yamanaka et al., 2005).

5.2.6. Tumour Treating Fields in Combination with Novel agents

Undiscovered and potentially confounding synergistic properties may of course be present with a multitude of other novel or repurposed agents. This is evident through preliminary reports of TTFields with Bevacizumab (Elzinga et al., 2013), as well as TTFields combined with Triflouropromazine, an approved antipsychotic drug. Triflouropromazine has been identified to inhibit mitotic slippage and yet did not decrease slippage when used in combination with TTFields (Porat et al., 2014, Riffell et al., 2009). This is particularly interesting as the treatment appeared to decrease cell counts by up to 14% when used in combination, suggesting

an improvement to efficacy independent of mitotic slippage. Cells treated in combination also experienced an increase in cell size of up to 35%, a well-documented phenomenon of TTFields (Schneiderman, 2013), as well as a reduced clonogenic potential of the cells (Porat et al., 2014). These results taken as a whole may encourage further investigation into TTFields in combination with novel and repurposed drugs.

More recently, TTFields were combined with Withaferin A (Chang et al., 2017), a steroidal lactone originating from the winter cherry plant, *Withania somnifera* (Lavie et al., 1965). Withaferin A had been previously shown to have efficacy against glioma cell lines in vitro as well as in murine orthotopic GBM models (Chang et al., 2016). As has been a theme with other combinational therapeutic strategies with TTFields, greater efficacy is achieved when combining TTFields with Withaferin A compared to each treatment alone (Chang et al., 2017). The mechanisms of Withaferin A have yet to be fully described, though reports have identified Withaferin A to affect expression of transcription factors, such as NF-κB (Heyninck et al., 2014). NF-κB affects cytoskeletal assembly/disassembly (Németh et al., 2004), so this most likely one of the reasons why Withaferin A is also implicated in this process (Bargagna-Mohan et al., 2007).

Interestingly, genome-wide expression analytical approaches are emerging for TTFields treated cell lines in order to further describe mechanisms of action, but also to attempt to characterise low-responsive vs high-responsive cell lines (Karanam et al., 2017). Karanam and colleagues provided data showing differential expression of multiple canonical pathways between responsive and low-responsive cell lines (Karanam et al., 2017). Producing similar data within brain tumour cell lines may be able to provide further direction towards more targeted combinations.

5.2.7. Pre-Clinical Conclusions

Given the limited efficacy of TTFields as a monotherapy (Stupp et al., 2012b), a need for a clear mechanism of action is apparent. There already exists ample descriptive preclinical studies at the cellular level for proposed mechanisms of action (Gera et al., 2015, Giladi et al., 2015c), but there is

a lack of mechanistic studies across more complex models with and without a combinational therapeutic approach. TTFields research is still in its relative infancy with ongoing research, endorsed by the success of the EF-14 trial. The main benefit of concurrent TTFields therapy is predominantly focussed on the lack of overlapping toxicities, however, reports of contact dermatitis is frequent and expected. Not to be overlooked is that TTFields does not appear to perpetuate any consequences synonymous with failed therapy i.e. promoting invasion and metastasis, although this has yet to be studied in-depth.

In conclusion, TTFields offers an exciting platform for a combinational therapeutic approach whether it is with novel or standard anti-tumour agents, with hopes that future treatment strategies may utilise these unique effects associated with alternating electric fields.

5.3. TTFields Clinical Trials in Glioblastoma multiforme

5.3.1. TTFields Pilot Study in Recurrent GBM Patients

The first-in-human pilot trial for TTFields was conducted between 2004 and 2007. The study assessed the safety and efficacy of TTFields therapy in 10 patients with recurrent GBM (Kirson et al., 2007). This preliminary single arm trial was performed after approval from the Na Homolce Institutional Review Board and the Czech Ministry of Health, with the trial analysing time to disease progression (TTP), overall survival (OS), and the progression-free survival at 6 months of the trial patients (Kirson et al., 2007). The trial patients were compared to recurrent GBM patients in a literature based historical control group fashion (Rich et al., 2004, Chang et al., 2004, Brada et al., 2001, Yung et al., 2000).

The TTFields used for the trial patients were set at a frequency of 200kHz, as determined to be the optimal frequency for rat glioma cell line, F-98, and human glioma cell lines, U-118 and U-87 (Kirson et al., 2007). The intensity used for the trial was 1-2V/cm which were generated through controlling the current density about the electrode arrays <31 mA/cm^2 RMS. The intensity used was deemed safe as it's less than half of what has been observed to be injurious to skin, which is approximately $100mA/cm^2$ (Moritz and Henriques Jr, 1947). The patient electrode temperatures were constantly monitored and controlled to be 41^0C and below, this was to keep the temperature significantly below a temperature that may cause thermal injury to the patient (Moritz and Henriques Jr, 1947).

TTFields were delivered via the NovoTTF-100a device (Novocure Ltd., Haifa, Israel) through insulated electrode arrays placed onto the patients head. Patients received TTFields through the electrodes between two perpendicular axis, lateral and anterior-posterior, with directions being switched every 1 second, with the therapy being administered for an average of 18 hours per day. The trial patients received continuous TTFields treatment for a maximum of 18 months, or until disease progression was observed (Kirson et al., 2007).

The trial patients had a median TTP of 26.1 weeks (range of 3-124 weeks), a median OS of 62.2 weeks (range of 20.3-124.0 weeks), and the PFS6

was 50% (range of 23-77%), and the one-year survival rate was 67.5% (Kirson et al., 2007). Notably, two of the ten patients were progression free, and three of the ten patients were alive at the time of publication. As well, despite the accumulative 70 months of TTFields treatment at 18 hours per day on average, there were no instances of serious adverse events, but there were instances of contact dermatitis beneath the electrodes on the patients' head (Kirson et al., 2007).

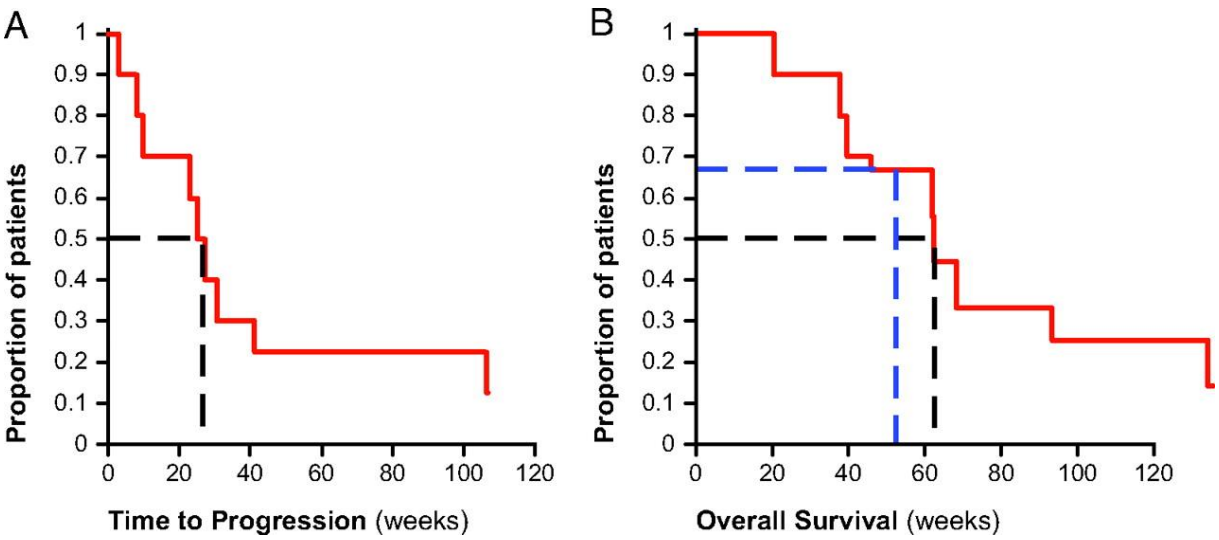


Figure 12. A) Graph showing the TTP of the (Kirson et al., 2007) trial patients (n=10), with a median TTP of 26.1 weeks (black dashed line). B) Kaplan-Meier curve showing the OS of the trial patients (n=10), with a median OS of 62.2 weeks (black dashed line) and a one-year survival rate of 67.5% (blue dashed line). Image from (Kirson et al., 2007).

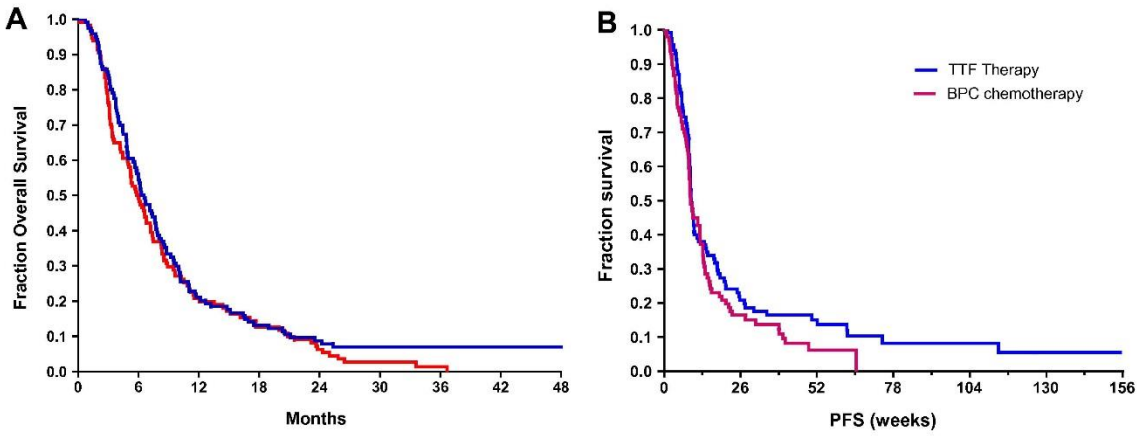
5.3.2. TTFields Phase III Clinical Trial in Recurrent GBM (EF-11 Trial)

Following the trial conducted by Kirson *et al*., (Kirson et al., 2007) the pivotal EF-11 phase III trial was undertaken between 2006 and 2009 (Stupp et al., 2012b). The trial was seeking to assess NovoTTF-100a as a monotherapy in recurrent GBM patients versus treatment with best physician's choice chemotherapy (BPC) within 237 total patients. The trial's primary end-point was OS, with the secondary end-points being PFS, PFS6, one-year survival rate, radiological response, safety and QoL (Stupp

et al., 2012b). The patients of the trial were randomized (1:1) to TTFields 200kHz (n=120) or BPC (n=117) – patients of the BPC arm were administered with either single agent or a combinational therapy regime consisting of; Bevacizumab (31%), Irinotecan (31%), BCNU/CCNU (25%), Carboplatin (13%), TMZ (11%), PCV (9%), other agents (7%) or none received (3%). The patients of the trial were all of 18 years or older with a histologically confirmed GBM, and became eligible following radiological confirmation of disease progression via the Macdonald Criteria. The patients had at least a 70% Karnofsky performance status with adequate haematological, hepatic and renal functioning. The patients had previously undertaken radiotherapy, with and without concomitant and/or adjuvant TMZ, but there were no other limits on the type or number of previous therapies or the number of recurrences. However, participants were excluded from the trial for a number of reasons; for instance, patients with infra-tentorial GBMs, as well as patients with implantable medical devices (Stupp et al., 2012b). However, the use of TTFields on patients with medically implanted devices has been examined more recently and has been removed from the list of TTFields contraindications (Ashby et al., 2015).

The trial concluded that patients treated with NovoTTF-100a therapy experienced very similar efficacy to the patients in the chemotherapy only arm, with the NovoTTF-100a patient arm having a median OS of 6.6 months versus 6.0 months for the BPC patient arm (Hazard ratio (HR) = 0.86 [95% Confidence interval (CI), 0.66 – 1.12]; p = 0.27). The PFS for patients was 2.2 months versus 2.1 months for the NovoTTF-100a patient arm and BPC patient arms (HR 0.81, 95% [CI 0.60–1.09]; p = 0.16). The PFS6 for patients was 21.4% for the NovoTTF-100a patient arm versus 15.1% for the BPC patient arm (HR = 0.81 [95% CI, 0.60 – 1.09]; p = 0.13). The overall response rate was 14.0% and 9.6% (p = 0.19) for the NovoTTF-100a patient and BPC patient arms respectively (Stupp et al., 2012b). The one-year survival rate was 20% for both treatment populations. Interestingly, the main differences between the treatment arms becomes apparent once their respective safety profiles are considered. A reduced frequency of systemic toxicities was observed within

the NovoTTF-100a patient arm. Common toxicities included Grade 3/4 haematological (4% versus 17% of patients), gastrointestinal (3% versus 17% of patients), and infections (4% versus 8% of patients) ($p < 0.05$; Fisher exact test) was observed within the NovoTTF-100a patient arm and in the BPC patient arm, respectively. QOL was also noted to be more favourable in the NovoTTF-100a patient arm with regards to emotional, social, and cognitive functioning. However, patients of the NovoTTF-100a patient arm self-reported slightly less favourable physical functioning than those of the BPC patient arm (Stupp et al., 2012b). The decline of the patients of the NovoTTF-100a patient arm physical functioning may in part be due to the relatively cumbersome nature of the first generation NovoTTF-100a system.



At risk	0 m	6 m	12 m	18 m	24 m	30 m	36 m	42 m	48 m
TTF	120	63	24	15	9	7	4	2	1
BPC	117	56	22	14	6	2	1	0	0

0 m	13 w	26w	39w	52w	65 w	78 w	91 w
120	38	19	14	11	6	4	3
117	34	14	10	3	1	0	0

Figure 13. A) Kaplan-Meier curve showing OS of both (Stupp et al., 2012a) patient arms, with a median OS of 6.6 for NovoTTF-100a patients and 6.0 months for BPC patients. B) Kaplan-Meier curve showing the PFS of both patient arms, with a median PFS of 2.2 months for NovoTTF-100a patients and 2.1 months for BPC patients. Image from (Stupp et al., 2012b).

Following completion of this Phase III trial, post-hoc analyses were performed (Kanner et al., 2014, Vymazal and Wong, 2014) and these gave some further insight into the therapeutic potential of TTFields therapy. Firstly, NovoTTF-100a therapy demonstrated similar efficacy to the best

physician's choice of chemotherapy for patients with recurrent GBM, but was observed to have a more favourable side-effect profile (Stupp et al., 2012b). Secondly, notably, the patient compliance with the NovoTTF-100a system was the main predictor of improvements to OS for patients. Kanner et al reported significantly longer median OS times for patients adhering to the NovoTTF-100a device for 18 or more hours per day. The median OS of patients achieving 18 hours per day or more compliance was 7.7 months compared to 4.5 months for the under 18 hours per day compliant patients ($p = 0.042$). Furthermore, the post-hoc analysis also described a significant 'stepwise correlation' between the median OS and patient compliance, with patient median OS times of 5.8 months, 6.0 months and 7.7 months for <60%, 60%–79%, and 80%–99% compliance with the NovoTTF-100a system, respectively ($p =0.039$) (Kanner et al., 2014).

5.3.3. TTFields Phase I Clinical Trial in Newly Diagnosed GBM

A single-arm, pilot trial was performed to assess the efficacy of TTFields in recurrent and newly-diagnosed GBM patients. The trial included 20 patients, the recurrent GBM patient arm had 10 patients which were treated with TTFields alone as a monotherapy as salvage therapy, with the newly diagnosed GBM patient arm being treated with TTFields in combination with maintenance TMZ following previous chemoradiation therapy. This trial was performed after approval from the Na Homolce Institutional Review Board and the Czech Ministry of Health, with the trial analysing safety, OS, and PFS (Kirson et al., 2009a). The OS of both patient arms was compared to matched historical control patient data with the same age and Karnofsky performance score (Stupp et al., 2005). The PFS of the NovoTTF-100a only patient arm was compared to a matched group of control patients who received salvage chemotherapy upon disease recurrence (n=18). The PFS of the NovoTTF-100a and TMZ patient arm was compared to a matched group of control patients who received TMZ alone (n=32) (Stupp et al., 2005).

The TTFields used for the trial patients were again set at a frequency of 200kHz, as previously used in patients and glioma cell lines (Kirson et al., 2007). The intensity used for the trial was 1-2V/cm which equated to 0.7V/cm (RMS) at the centre of the brain. The intensity used has been

shown previously to be safe on patients' (Kirson et al., 2007). The trial patients received TTFields through the electrode arrays across perpendicular planes to allow greatest coverage of the brain. The TTFields therapy was administered in multiple four-week courses of continuous treatment until disease progression was observed.

The trial's patients with histologically confirmed GBM were treated for an average of one year, with a range of 2.5 months to 24 months. In both patient arms, no NovoTTF-100a device related serious adverse events were observed. The only device related adverse event observed was dermatitis (18 out of 20 patients), which appeared most frequently after the first month of continuous TTFields treatment. The severity of the dermatitis was irrespective of the additional maintenance TMZ for the TTFields with TMZ patient arm, suggesting no overlapping toxicities between TTFields therapy and TMZ. Furthermore, there was no increase in TMZ related adverse events when combined with TMZ either. Overall, the median OS of the TTFields with TMZ patients was over 40 months versus 14.7 months for their matched historical control patients, while the median PFS of the TTFields with TMZ patients was over 35.6 months versus 8.0 months for their matched historical control patients (Kirson et al., 2009a).

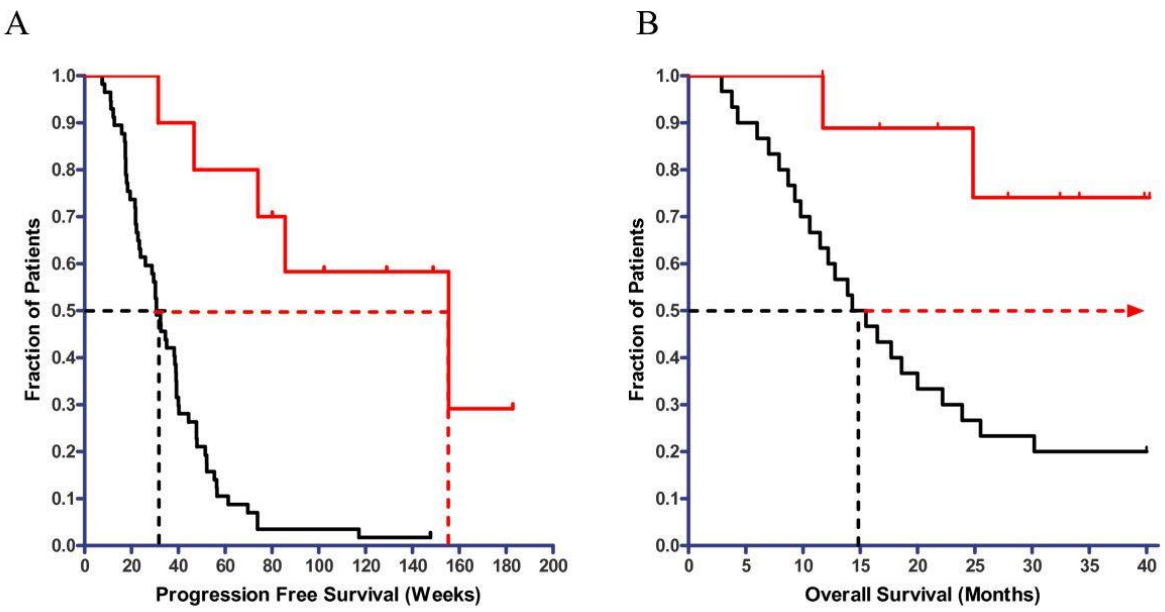


Figure 14. A) Kaplan-Meier curve showing PFS of (Kirson et al., 2009c) newly diagnosed GBM patients receiving either TTFields and TMZ (Red Line) or TMZ alone (Black Line), with a median PFS of 35.6 months for NovoTTF-100a patients and 8.0 months for TMZ control patients. B) Kaplan-Meier curve showing OS of newly diagnosed GBM patients receiving either TTFields and TMZ (Red Line) or TMZ alone (Black Line), with a median OS of over 40 months for NovoTTF-100a patients and 14.7 months for TMZ control patients. Image from (Kirson et al., 2009a).

5.3.4. TTFields Phase III Clinical Trial in Newly Diagnosed GBM (EF-14 Trial Interim Analysis)

An open-label, multicentre, randomised Phase III trial was performed to assess the efficacy and safety of TTFields in combination with maintenance TMZ for the treatment of newly diagnosed adult GBM following initial chemoradiation treatment. Following initial chemoradiation, the trial patients (n=695) were randomised 2:1 to receive maintenance TMZ therapy as per the Stupp protocol in combination with 200kHz TTFields or without (Figure 1.) (Stupp et al., 2015a). The patients eligible for enrolment in this clinical trial were 18 years of age or older, had a histologically confirmed supratentorial GBM, had a KPS score of at least 70%, were progression-free following maximal safe debulking surgery and had completed concomitant chemoradiation therapy with TMZ, as well as

having adequate hepatic, haematological, and renal functioning. Patients who were excluded from the clinical trial (n=324) were excluded for a number of reasons detailed in Figure 15. All clinical trial patients provided written consent before the study commenced, and the study was approved by the various ethics committees and review boards of all the 83 participating centres.

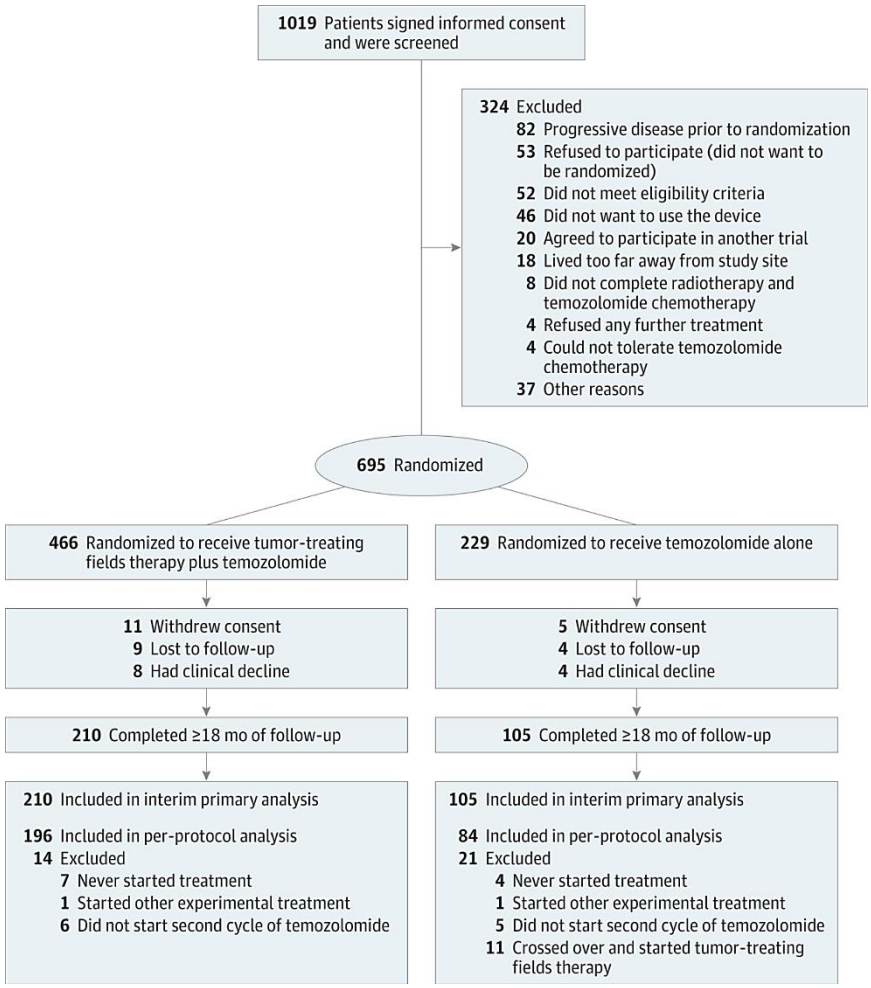


Figure 15. Flow diagram detailing the clinical trial patient randomisation process including the excluded patients. Image from (Stupp et al., 2015a).

Patients in both treatment arms received TTFields via the Optune system. The trial used a similar TTFields delivery protocol to previous trials, as detailed in previous sections, however, differences in the transducer arrays

layout were used. The Optune transducer arrays were optimised to the patients using NovoTAL. Patients who experienced tumour progression were offered second-line chemotherapy, with the TTFields plus TMZ patient arm being offered continuation of TTFields treatment up until second radiological progression for a maximum of 24 months (Stupp et al., 2015a).

The clinical trial's primary end-point was PFS within the intent-to-treat (ITT) population, with the secondary end-point being OS – which would only be tested statistically if the PFS primary end-point was achieved. The clinical trial had a pre-specified interim analysis, which was to be undertaken once the first 315 randomised patients had achieved a minimum of 18 months follow-up. At the interim analysis, the OS would be analysed in an as-treated population, which would exclude patients who violated trial treatment protocols, never received maintenance TMZ, and who had be transferred to a different treatment group. The primary end-point of PFS would be achieved at the interim analysis once the PFS of the ITT population significantly exceeded that of the control group (Stupp et al., 2015a).

The clinical trial patients (n=695) were randomized 2:1 to either the TTFields with adjuvant TMZ or TMZ monotherapy arms, respectively. The primary end-point of the trial was satisfied at the interim of the trial as the PFS of the ITT population was significantly greater for the TTFields plus TMZ arm versus the TMZ only control arm. The secondary end-point of the trial was also satisfied as the OS of the as per-protocol population was significantly higher for the TTFields plus TMZ arm versus the TMZ only control arm (Stupp et al., 2015a).

Analysis of the first cohort of trial patients (n=315) at the pre-specified interim analysis after the minimum of 18 months follow up, showed both significant increases in the median PFS and OS. Of note, the Independent Monitoring Committee for the EF-14 trial recommended that the clinical trial to be terminated at the interim because of the perceived advantageous survival benefits of TTFields combinational therapy with TMZ. This decision caused the patients of the TMZ monotherapy arm to be

provided with access to Optune and TTFields therapy (Stupp et al., 2015a). This decision caused great controversy and drew much criticism to how the clinical trial was conducted (Wick, 2016).

At the interim analysis, the median PFS within the ITT patient population was 7.1 months versus 4.0 months (HR 0.6; log-rank p=0.0014) for the TTFields plus TMZ patient and the TMZ alone patient arms, respectively. Whereas, the median OS for the TTFields plus TMZ patient arm was 19.6 months versus 16.6 months for the TMZ alone patient arm (HR 0.75; log-rank p=0.034) in the ITT patient population. With the OS for the TTFields plus TMZ patient arm at 20.5 months versus 15.5 months (HR 0.67; log-rank p=0.0072) within the as per-protocol patient population (Stupp et al., 2015a).

As with the EF-11 trial, as well as previous reports (Stupp et al., 2012b, Kirson et al., 2007, Kirson et al., 2009a), the addition of TTFields therapy did not yield any significant overlapping toxicities compared to TMZ alone, with the most common TTFields associated side-effect being localised skin toxicities. Up to 43% of the patients receiving TTFields therapy experienced mild to moderate skin toxicities, with 2% of TTFields treated patients experiencing severe skin toxicities (Grade 3) (Stupp et al., 2015a). The majority of these skin toxicities are localised rash/irritation in nature, which can be further described by Lukas et al. (Lukas et al., 2017). The TTFields associated dermatological toxicities can be prophylactically managed, as well as being treated following development. The prophylactic guidelines include; maximising the contact between skin and transducer arrays, taking care with shaving of the scalp, as well as taking care with applying the transducer arrays to surgical scars. Once dermatological toxicities develop, topical antibiotics can be applied to treat infections and corticosteroids should be applied for contact dermatitis and irritation (Lukas et al., 2017). A lot of the dermatological toxicities arise from the application and removal of the transducer arrays, in addition to any

additional inflammation from the applied hydrogel (Lacouture et al., 2014, Lukas et al., 2017).

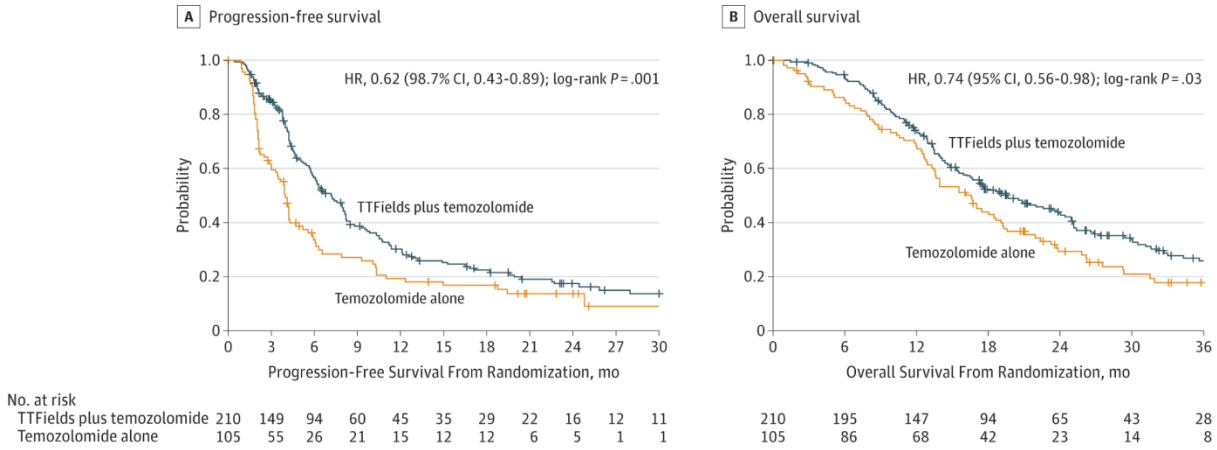


Figure 16. A) Kaplan-Meier curve showing PFS of both (Stupp et al., 2015b) patient arms, with a median PFS of 7.1 for TTFields plus TMZ patients and 4.0 months for TMZ only patients. B) Kaplan-Meier curve showing the OS of both patient arms, with a median OS of 20.5 months for TTFields plus TMZ patients and 15.6 months for TMZ only patients. Image from (Stupp et al., 2015a).

5.3.5. TTFields Phase III Clinical Trial in Newly Diagnosed GBM (EF-14 Trial Final Report)

Patients in the EF-14 trial were randomised to receive TTFields in combination with TMZ or TMZ alone between July 2009 and December 2014, with the dataset for analysis of the trial being completed in December 2016. A greater interrogation of the combination of TTFields in with TMZ can be undertaken with the data set of all 695 patients. The primary end-point of PFS was 6.7 months for TTFields plus TMZ patient arm versus 4.0 months for the TMZ alone patient arm (HR 0.63; log-rank p=<0.001). The secondary end-point of OS was 20.9 months for TTFields plus TMZ patient arm versus 16.0 months for the TMZ alone patient arm (HR 0.63; log-rank p=<0.001) (Figure 6.). Survival benefits were also seen across the 2-, 3-, and 4-year survival rates with the addition of TTFields to TMZ. The survival rates for the 2-, 3-, and 4-year points were 43% and 31%, 26% and 16%, and 13% and 5% (p=<0.05 for all time points), for the TTFields plus TMZ patient arm and the TMZ only patient arms, respectively. The PFS6 of the TTFields plus TMZ patient arm was 56% (range of 51% to 61%) and 37% (range of 30% to 44%) for the TMZ only patient arm (p=<0.001) (Stupp et al., 2017a). With the mature data, further analyses were performed in order to stratify patients to elucidate the characteristics of the patients who performed better in the study, as outlined in Figure 18.

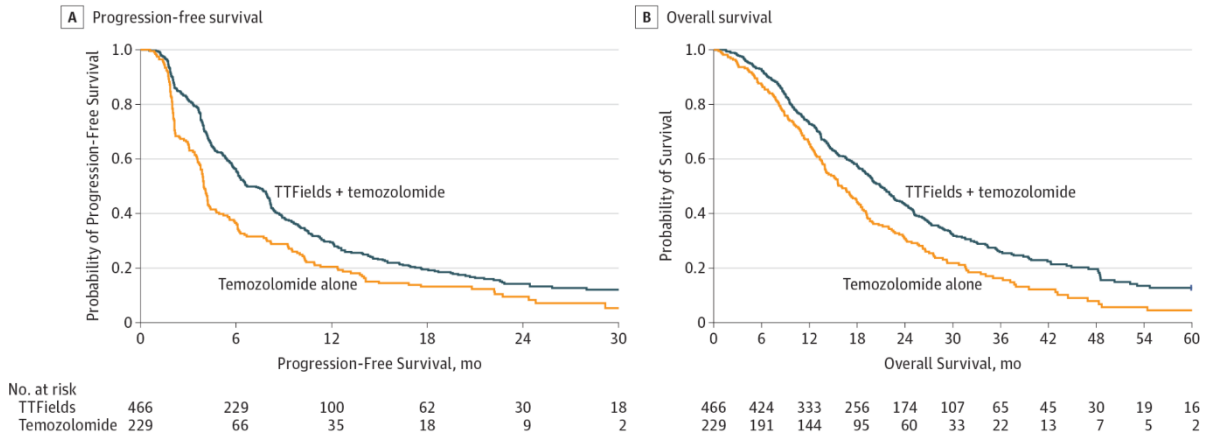


Figure 17. A) Kaplan-Meier curve showing PFS of both (Silginer et al., 2017) patient arms, with a median PFS of 6.7 for TTFields plus TMZ patients and 4.0 months for TMZ only patients. B) Kaplan-Meier curve showing the OS of both patient arms, with a median OS of 20.9 months for TTFields plus TMZ patients and 16.0 months for TMZ only patients. Image from (Stupp et al., 2017a).

Subgroup	TTFields + Temozolomide		Temozolomide Alone		Median Survival (IQR), mo		Hazard Ratio (95% CI)
	No. of Patients	No. (%) Alive at End of Study	No. of Patients	No. (%) Alive at End of Study	TTFields + Temozolomide	Temozolomide Alone	
MGMT promoter region methylation status							
Unmethylated	209	18 (9)	95	3 (3)	16.9 (9.7-28.2)	14.7 (9.8-24.8)	0.66 (0.49-0.85)
Methylated	137	26 (19)	77	9 (12)	31.6 (21.1-48.5)	21.2 (12.3-37.9)	0.62 (0.44-0.88)
Resection							
Biopsy	60	5 (8)	29	0 (0)	16.5 (9.0-24.7)	11.6 (7.1-18.1)	0.50 (0.30-0.84)
Partial	157	20 (13)	77	3 (4)	21.4 (9.9-37.6)	15.1 (7.8-23.3)	0.56 (0.41-0.77)
Gross total	249	32 (13)	123	13 (11)	22.6 (13.4-39.8)	18.5 (12.1-31.6)	0.70 (0.54-0.91)
Region							
Outside United States	245	32 (13)	111	9 (8)	20.1 (11.3-32.2)	15.5 (9.3-25.6)	0.66 (0.51-0.85)
United States	221	25 (11)	118	7 (6)	22.0 (11.3-48.2)	17.1 (9.8-29.2)	0.63 (0.49-0.82)
Age, y							
<65	377	47 (12)	184	14 (8)	21.6 (12.0-39.4)	17.3 (10.6-29.3)	0.69 (0.57-0.85)
≥65	89	10 (11)	45	2 (4)	17.4 (9.0-31.5)	13.7 (7.6-24.8)	0.51 (0.33-0.77)
Karnofsky performance score							
90-100	308	39 (13)	149	11 (7)	23.3 (13.5-41.9)	17.8 (11.9-29.3)	0.70 (0.56-0.87)
≤80	154	16 (10)	74	5 (7)	14.9 (8.4-29.8)	11.0 (5.7-23.3)	0.58 (0.45-0.88)
Sex							
Women	150	21 (14)	72	6 (8)	24.6 (14.4-48.2)	18.5 (11.3-27.6)	0.64 (0.56-0.87)
Men	316	36 (11)	157	10 (6)	19.1 (10.0-34.1)	15.5 (8.4-26.5)	0.63 (0.45-0.88)
Overall	466	57 (12)	229	16 (7)	20.9 (11.3-37.6)	16.0 (9.3-27.5)	0.63 (0.53-0.76)

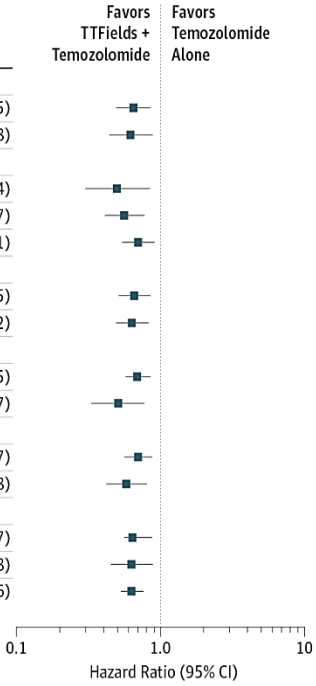


Figure 18. A) A table outlining the median OS of patients stratified by; MGMT status, resection status, region, age, Karnofsky performance score, and sex. The factors associated with greater OS in the trial were; TTFields plus TMZ treatment (HR 0.63, log-rank p=<0.001), MGMT methylated status (HR 0.5, log-rank p=<0.001), age under 65 years old (HR 0.978 per year, log-rank p=<0.001), Karnofsky performance score (p=<0.001), and female gender patients (HR 0.76, log-rank p=0.005). Image from (Stupp et al., 2017a).

5.3.6. TTFields Phase III Clinical Trial in GBM: Scepticism

Despite the promising results of these TTFields trials, numerous limitations of the trials have prompted scepticism among the neuro-oncological community. Firstly, the EF-14 trial (Stupp et al., 2017b) was initiated based off the results of the EF-11 trial (Stupp et al., 2012a) despite the lack of clear benefit of TTFields therapy over the standard of care therapy regime. Secondly, the trials were both run as open-label, non-sham-controlled trials and this may have biased the outcome of the TTFields patients via greater interactions with healthcare professionals. Thirdly, the EF-14 trial was terminated at the interim (Stupp et al., 2015a) and all patients were then given access to TTFields therapy, and thus eliminating the potential for a more 'mature' data set where TTFields with TMZ and radiotherapy may be compared to TMZ and radiotherapy alone in the long-term. Lastly, current pre-clinical TTFields data is very descriptive of the effects of TTFields *in vitro* (Giladi et al., 2015b, Gera et al., 2015), and have yet to be described in more representative models *in vivo*; inclusion of complex and varied tissues at multiple interfaces, and in combination with chemotherapy and radiotherapy – given the limited efficacy of TTFields as a monotherapy (Stupp et al., 2012a). More relevant *in vivo* data, as well as unbiased long-term follow-ups of patients may better represent the effects of TTFields, and would ultimately give credence to the therapy. Lastly, a major concern of the therapy is the very significant cost associated – with an approximate €550,000 per life year gained (Bernard-Arnoux et al., 2016). This cost, particularly as a first-line treatment, far exceeds conventional thresholds of costing for treatments, a significant reduction in cost may allow greater uptake of the therapy within the sceptic neuro-oncological community.

5.4. TTFields Clinical Trials in Other Tumour Types

5.4.1. TTFields Clinical Trials in Brain Metastases Secondary to Non-small Cell Lung Carcinoma

The METIS clinical trial (Table 10.) is an ongoing study of the efficacy of TTFields in NSCLC patients with brain metastases. This randomised clinical trial seeks to test the efficacy, patient safety and tolerability, and the neurocognitive outcomes of TTFields therapy on patients with up to 10 brain metastases following surgery. The study is testing TTFields (150kHz) with supportive therapy against supportive therapy alone, with the primary outcome is time to cerebral progression and the secondary outcome includes OS, QoL, toxicity and safety, and time to neurocognitive failure (NCT02831959).

5.4.2. TTFields Clinical Trials in Non-small Cell Lung Carcinoma

The pilot clinical trial for inoperable Stage IIIB and IV squamous and non-squamous NSCLC patients tested TTFields (150kHz) in combination with concurrent Pemetrexed (Pless et al., 2013). The results of the single-arm Phase I/II clinical trial demonstrated safety and tolerability when combining TTFields with pemetrexed in NSCLC patients. The efficacy of the combinational approach also exceeded that of historical controls (REFERENCE). The median PFS and median OS of patients was 28 weeks and 13.8 months for the TTFields with pemetrexed patient arm versus 12 weeks and 8.2 months for the pemetrexed only historical control patients (Pless et al., 2013).

The LUNAR clinical trial (Table 10.) is an ongoing Phase III clinical trial for squamous and non-squamous NSCLC patients testing TTFields (150kHz) in combination with either Docetaxel or PD-1 Inhibitors (Nivolumab or Pembrolizumab). The primary end-point is greater survival in the TTFields in combination with either Docetaxel or PD-1 Inhibitors treated patient arm versus the Docetaxel or PD-1 Inhibitor treated patient arm. The secondary end-points PFS, QoL, and the frequency of TTFields related adverse events (NCT02973789).

5.4.3. TTFields Clinical Trials in Ovarian Carcinoma

The INNOVATE clinical trial (Table 10.) was a Phase II clinical trial for platinum-resistant, recurrent ovarian cancer patients testing TTFields (200kHz) in combination with Paclitaxel. The primary end-point was treatment-emergent adverse events, and the secondary end-points included PFS and OS. However, the trial's median OS target was not reached, however, this study may warrant a more extensive Phase III trial for the treatment of platinum-resistant ovarian cancer with TTFields due to the lack of efficacious treatments available for platinum-resistant ovarian cancer patients (NCT02244502).

5.4.4. TTFields Clinical Trials in Pancreatic Adenocarcinoma

The PANOVA clinical trial (Table 10.) is an ongoing Phase II clinical trial for advanced pancreatic cancer patients testing TTFields (150kHz) in combination with concomitant Gemcitabine or nab-Paclitaxel. The primary end-point is patient compliance with TTFields delivered through the NovoTTF-100L and the severity and frequency of adverse events. The secondary end-points are PFS, OS and one-year survival rate (NCT02973789).

As per the primary end-points, the median compliance with TTFields therapy was 78% at 14 hours/day for a median of 5 months treatment duration, and the frequency of serious adverse events was 70%. The PFS and OS was 10.3 months and 14.9 months for patients with locally advanced disease and was 5.7 months and 8.3 months for patients with metastatic disease. The one-year survival rate was 86% in patients with locally advanced disease and 40% in metastatic disease. The combination with TTFields with gemcitabine appears to improve PFS and OS for both local and metastatic pancreatic cancer when compared to historical gemcitabine-treated control patients. The observations of greater improvements for locally advanced disease patients may be in part due to preferential targetting of the tumour with TTFields relative to metastases which may evade TTFields treatment.

5.4.5. TTFields Clinical Trials in Mesothelioma

The STELLAR clinical trial (Table 10.) is an ongoing Phase II clinical trial for malignant pleural mesothelioma patients testing TTFields (150kHz) in combination with concomitant Pemetrexed and Cisplatin or Carboplatin. The study enrolled 80 patients for the single-arm clinical trial which are still currently undergoing follow-up. The primary outcome was OS for patients and the secondary outcomes were PFS and patient toxicity and adverse event frequency. The interim analysis of this clinical trial for 42 patients post-follow-up showed a 12-month survival rate of 79.7%, a median PFS of 7.3 months, and no NovoTTF-100L device-related serious adverse events. However, at the interim of the clinical trial, the primary outcome of OS had not been met (NCT02397928).

5.5. Summary of Tumour Treating Fields Clinical Trials

Recurrent GBM		
Study	Trial Design	Notable outcomes
Kirson et al. (Kirson et al., 2007)	(Phase I) - Pilot TTFields clinical trial for recurrent GBM patients	• The median time to disease progression was 26.1 weeks • The median progression-free survival time was 6 months • The median overall survival was 62.2 weeks • 280 weeks of accumulative TTFields treatment without a serious treatment-related event across the 10 trial patients
Stupp et al. (Stupp et al., 2012b)	(Open-label, Phase III) – Clinical trial comparing TTFields as a monotherapy versus chemotherapy in recurrent GBM patients	• The median survival was 6.6 months versus 6.0 months • The progression-free survival rate at 6 months was 21.4% and 15.1% • Common mild to moderate dermatological adverse events related to TTFields therapy become apparent • No other significant overlapping toxicities were observed with TTFields therapy

Table 7. Summary of the development of TTFields clinical trials for recurrent GBM.

Newly Diagnosed GBM		
Study	Trial Design	Notable outcomes
Kirson et al. (Kirson et al., 2009d)	(Phase I) – Pilot TTFields clinical trial for recurrent and newly diagnosed GBM patients	• The progression-free survival time was 155 weeks • The overall survival reached over 40 months for some patients
Stupp et al. (Stupp et al., 2015a)	(Open-label, Phase III) – Interim analysis of trial of TTFields in combination with TMZ versus TMZ only, following initial chemoradiation treatment	• The median progression-free survival of the intent-to-treat population was 7.1 months versus 4.0 months • The median overall survival of the per-protocol patients was 20.5 months versus 15.6 months • No significant overlapping toxicities were observed from combining TTFields to TMZ
Stupp et al. (Stupp et al., 2017a)	(Open-label, Phase III) – Analysis of full patient set of trial of TTFields in combination with TMZ versus TMZ only, following initial chemoradiation treatment	• The median progression-free survival of the intent-to-treat population was 6.7 months versus 4.0 months • The median overall survival of the per-protocol patients was 20.9 months versus 6.0 months • No significant overlapping toxicities were observed from combining TTFields to TMZ

Table 8. Summary of the development of TTFields clinical trials for newly diagnosed GBM.

Ongoing GBM Trials	
Trial ID	Study Title
NCT01954576	A Phase II Study of the Optune System, Enhanced by Genomic Analysis to Identify the Genetic Signature of Response in the Treatment of Recurrent Glioblastoma Multiforme
NCT02441322	High Resolution MRI and MRS to Evaluate Therapeutic Response to Novo-TTF in Newly and Recurrent Glioblastomas
NCT02893137	Enhancing Optune Therapy of Recurrent Glioblastoma Multiforme Using Targeted Surgical Skull Remodeling
NCT02663271	A Phase 2, Multi-center, Single Arm, Histologically Controlled Study Testing the Combination of TTFields and Pulsed Bevacizumab Treatment in Patients With Bevacizumab-refractory Recurrent Glioblastoma
NCT01925573	Proposed Pilot Study of Combined Optune+ Bevacizumab, and Hypofractionated Stereotactic Irradiation for Bevacizumab-Naive Recurrent Glioblastoma
NCT02343549	A Phase II Study of Optune (NovoTTF) in Combination With Bevacizumab (BEV) and Temozolomide (TMZ) in Patients With Newly Diagnosed Unresectable Glioblastoma (GBM)

Table 9. Summary of the ongoing clinical trials for TTFields in newly diagnosed and recurrent GBM.

Other Tumour Targets			
Study Name	Study Title	Trial ID	Tumour Type
COMET	Effect of TTFields (150kHz) in Non-small Cell Lung Cancer (NSCLC) Patients With 1-5 Brain Metastases Following Optimal Standard Local Treatment	NCT01755624	Brain metastases secondary to NSCLC
METIS	Pivotal, Open-label, Randomized Study of Radiosurgery With or Without Tumor Treating Fields (TTFields) (150kHz) for 1-10 Brain Metastases From Non-small Cell Lung Cancer (NSCLC)	NCT02831959	Brain metastases secondary to NSCLC
LUNAR	Pivotal, Randomized, Open-label Study of Tumor Treating Fields (TTFields) Concurrent With Standard of Care Therapies for Treatment of Stage 4 Non-small Cell Lung Cancer (NSCLC) Following Platinum Failure	NCT02973789	NSCLC
INNOVATE	An Open Label Pilot Study of the NovoTTF-100L(O) System (NovoTTF Therapy) (200 kHz) Concomitant With	NCT02244502	Ovarian carcinoma

	Weekly Paclitaxel for Recurrent Ovarian Carcinoma		
PANOVA	A Phase II Study of TTFields (150 kHz) Concomitant With Gemcitabine and TTFields Concomitant With Gemcitabine Plus Nab-paclitaxel for Front-line Therapy of Advanced Pancreatic Adenocarcinoma	NCT01971281	Pancreatic adenocarcinoma
STELLAR	A Phase II Trial of Pemetrexed and Cisplatin or Carboplatin in Combination With TTFields (150 kHz) as First-line Treatment in Malignant Pleural Mesothelioma	NCT02397928	Mesothelioma

Table 10. Summary of the development of TTFields clinical trials for tumour types outside of brain tumours.

5.6. Nativis Voyager® ulRFE® System for GBM

Nativis in a now clinical-stage medical device company founded in 2002 and based out of Seattle, WA. The Nativis Voyager® ulRFE® System (Figure 19.) is a non-invasive medical device for the treatment of brain tumours utilising targeted, ultra-low (0-22kHz) radio frequency energy (ulRFE) to therapeutically regulate cancer cell signalling and metabolic pathways (Barkhoudarian, 2017, Ulasov et al., 2017). The Nativis Voyager delivers ulRFEs throughout the patient to interfere with tumour cells on both molecular and genetic levels. The Nativis system differs from other electro-based systems, notably Optune, through utilisation of dissimilar frequencies on the electromagnetic spectrum.



Figure 19. The Nativis Voyager® ulRFE® System as used in the clinic.

"The company's goal is to transform disease treatment on a global scale with ulRFE®. The proprietary technology has the potential to be applied to a wide range of conditions as well as veterinary medicine and non-medical applications.

Nativis' initial focus is on the treatment of patients with brain cancer who are not well served by conventional standard of care therapies, which often result in poor outcomes and devastating side effects. Additional pre-clinical work is focused on exploring new applications in oncology and pain treatment."

- Nativis statement (http://nativis.com/) – 20/11/2018

5.6.1. Radio Frequency Energy Interactions

The use of non-thermal, electric fields for the treatment of cancer is a continuously developing idea and area of research. Radio frequency energy (RFE) refers to alternating fields within the electromagnetic spectrum between 3kHz-3000GHz (Butters et al., 2014). The reasoning behind using RFEs for the treatment of brain tumours is multifaceted;

1. To overcome the BBB.
2. To overcome drug perfusion limitations within the brain.
3. To overcome therapy-induced resistances associated with chemotherapies.
4. To address treatment-related toxicities.

Firstly, electric fields penetrance has yet to be shown to be affected by the BBB, conversely, electric fields have been used to disrupt the BBB, a technique referred to as electrochemotherapy, to enhance chemotherapy penetrance through the BBB via irreversible electroporation (Garcia et al., 2010). Low frequency RFEs have been shown to have good tissue penetrance, facilitation treatment within areas of the brain that may be poorly perfused, thus addressing drug perfusion limitations within heterogeneous brain tumour masses (Barkhoudarian, 2017). The ability for cancer cells to overcome therapy and develop resistance mechanisms is well documented, and to date, no literature has implicated a resistance mechanism to RFEs within cancer cells. However, Shteingauz and colleagues demonstrated how TTFields treated cell lines may develop resistance to treatment through induction of autophagy in an AMPK-dependent manner (Shteingauz et al., 2018). There have been no reports of treatment related toxicities with RFEs, with the preliminary Phase I trial of Nativis Voyager in recurrent GBM patients reporting no treatment related toxicities (Barkhoudarian, 2017) (NCT02296580). This has been counter to reports from previous TTFields trials in both recurrent and newly-diagnosed GBM patients, where the majority of patients exhibited mild-moderate skin-related toxicities (Stupp et al., 2012b, Stupp et al., 2017a). However, these trials reported no overlapping toxicities with TTFields treatment, giving validity to the use of electric fields technology in a combinational fashion.

It was hypothesized that electrostatic charges of molecules and magnetic fields are essential for many biological processes (Ulasov et al., 2017). Nativis Voyager seeks to transmit RFEs at optimised settings to mimic electromagnetic modulations of recorded interactions, in order to illicit a response without the physical molecule/agonist being used (Ulasov et al., 2017). These electromagnetic modulations were detected with a field sensing system - Superconducting quantum interference device (SQUID). Using SQUID technology, dynamic magnetic fields and their oscillations may be recorded into current sequences, a more in-depth description of SQUID technology may be found here (Butters et al., 2014). And it is with these optimised RFEs that the effects of chemotherapies may potentially be recapitulated without the use of the active agent (Ulasov et al., 2017).

5.6.2. Radio Frequency Energy *in vitro* and *in vivo*

ulRFEs have shown to potentially regulate and affect multiple protein and gene targets (Ulasov et al., 2017, Ulasov et al., 2016). The current theory surrounding the mechanism of action is that RFEs at specific frequencies and currents may redistribute charges within the electron transport chain underlying biological processes via the magnetic field of the RPE (Butters 2014). An RFE signal delivered at 25milliamps and 22kHz was optimised to potentially stabilize tubulin subunits via perturbation of charge within the proteins in a similar fashion to how taxane molecules induce tubulin stabilization and lead to mitotic arrest (Jordan and Wilson, 2004). It is hypothesized that the RFEs used ultimately induce conformational changes within the tubulin subunits, as it has been demonstrated that interfering with electron transport chains may induce receptor responses and conformational changes independent of a physical agonist (Ulasov et al., 2017).

Using this technology, RFEs have also been optimised and validated to target specific gene targets. PLK1 was potentially targeted on the gene and protein level by RFEs in U87 and primary GBM cell lines, resulting in up to 70% reduction of PLK1 mRNA expression and approximately 40% reduction in protein expression (Ulasov et al., 2016). These gene knockdown observations where validated and comparable to PLK1 siRNAs as controls in both 4 hour and 12 hour exposures (Ulasov et al., 2016).

Similar observations have been made for EGFR mRNA expression and protein levels following RFE exposure (Ulasov et al., 2016, Ulasov et al., 2017). RFEs were optimised to mimic EGFR siRNA for U87 cells, 4 hour and 12 hour exposures to both produced an average of 72% and 63% reduction in mRNA levels, respectively. Reductions in EGFR protein levels were observed at the 48 hour and 72 hour post treatment marks, with reductions of 27% and 73%, respectively, for RFE treated cells (Ulasov et al., 2017). This data suggests that RFEs may potentially be optimised to knockdown EGFR at the gene expression and protein levels. More functional analyses of this approach has demonstrated how these RFEs may reduce cell viability via apoptosis, as well as a reducing neurosphere formation of primary GBM cells following exposure of up to 72 hours with RFEs (Ulasov et al., 2017). Lastly, the effects of RFEs on tumour growth in an intracranial xenograft mouse model was assessed. Mice were implanted with U87 cells and were treated with RFEs targeted to EGFR 11 days after implantation against control mice, with mice treated with RFEs demonstrating a prolonged survival of 20% ($p = <0.05$) (Ulasov et al., 2017). Histological assessment of the brain tumour sections revealed a decrease in both EGFR and Ki67 levels in the RFE treated mice. Taken together, these studies have shown that RFEs may be possibly optimised to specific targets, and that targeting EGFR reduces proliferation and cell viability in primary and established adult GBM cell lines (Ulasov et al., 2017). These observations reflect upon the biological significance of EGFR in glioma pathobiology (Hatanpaa et al., 2010).

In conclusion, Nativis Voyager RFEs have shown potential efficacy in vitro and in pre-clinical mouse models when targeting EGFR (Ulasov et al., 2016, Ulasov et al., 2017), as well as demonstrating safety in adult patients with recurrent GBM (Barkhoudarian, 2017) (NCT02296580). However, the specific targeted nature of RFEs may not translate to the clinic as GBMs are classically very heterogeneous (Parker et al., 2015), and in the case of EGFR – only 60% of patients express amplified EGFR levels (Brennan et al., 2013a). Nativis Voyager safety is currently being tested in newly-diagnosed GBM patients in combination with TMZ and radiotherapy, which will be reported on at the end of 2019 (NCT03276286).

5.7. Intratumoural Modulation Therapy (IMT) for GBM

Intratumoural modulation therapy (IMT) refers to the use of MRI-compatible implantable bioelectrodes to deliver low intensity electric fields to diseased areas of the brain (Sebastiano et al., 2018). IMT also addresses the points raised regarding the treatment of brain tumours. However, IMT seeks to repurpose existing implantable electrode technology from the well-characterised DBS therapy. The internalised electrode approach does offer some key advantages over the external Optune system;

1. Implantable electrodes would eliminate the potential adherence issues associated with wearing Optune for over 18 hours a day (Stupp et al., 2017a). This may potentially improve patient's QoL.
2. Skin toxicities would be eliminated due to a lack of a need for scalp shaving, chronic electrode irritation of the scalp (Lacouture et al., 2014).
3. A comparative therapy, such as DBS therapy, is much more economical treatment option, with Optune therapy's cost effectiveness being heavily scrutinised (Wick, 2016).
4. Implantable electrodes offer the opportunity to strategically position electrodes to focus therapy directly to the diseased location, specifically the residual tumour cells beyond the resection bed would be an advantageous target for GBM patients.
5. Implantable electrodes also theoretically allow targeted therapy within regions of the CNS outside of the supratentorial brain regions, where Optune therapy is currently only indicated for tumours arising within the these regions (Stupp et al., 2017a).

IMT studies have utilised low frequency electric fields similar frequencies used in DBS therapy for its neuromodulation effects (Xu et al., 2016), as well using intermediate frequency electric fields (Sebastiano et al., 2018) in pre-clinical models, using established frequencies as those used in TTFields therapy (Stupp et al., 2017a).

5.7.1. Intratumoural Modulation Therapy Interactions

Electrical activity is inherent within cells with implications in many biological processes. The electrical properties of a cell is highly dependent upon the cell membrane and cell composition (Heilman et al, 2013). Therefore, it is logical that cancer cells have distinct electrical properties relative to normal cells (Pollak et al., 2017). Cancer cells in particular have reduced transmembrane potentials as a result of increased extracellular surface negative, which correlates very strongly with high mitotic activity (Yang and Brackenbury, 2013) Dysregulation of the electron transport chain and ion flux processes impacts a cancer cell's ability to maintain homeostasis, which in particular may be a result of high level of dysregulation of ion channels in GBM (Pollak et al., 2017). Furthermore, a disrupted membrane permeability is present in cancer cells, which results in an aberrant intracellular ionic composition relative to normal cells – in particular, cancer cells typically have lower intracellular concentrations of potassium and calcium ions, with an increased concentration of sodium and chloride ions (Steve Haltiwanger). Lastly, ion flux and interactions may be perturbed by distinct pH difference in cancer cells, with tumours typically have an acidic extracellular environment, while having a more alkaline intracellular environment (Honasoge and Sontheimer, 2013).

5.7.2. Intratumoural Modulation Therapy *in vitro* and *in vivo*

Xu and colleagues first undertook IMT *in vitro* studies in GBM patient derived cell lines and commercial GBM cell lines using repurposed Medtronic stimulating electrodes, delivering electromagnetic fields at 130Hz, 4V, and 90μs (Xu et al., 2016), referred to as IMT-130. IMT-130 was used to treat GBM cells and rat post-mitotic neurons for up to 96 hours, and demonstrated up to a 55% reduction in metabolic activity of the GBM cells while having no notable effects on the viability of the neurons (Xu et al., 2016). Notably, IMT-130 treatment did not produce overt morphological changes in treated cells unlike how TTFields treated cells become significantly altered through continuous treatment (Gera et al., 2015). IMT-130 was also used in combination with TMZ in GBM cells to enhance efficacy. The combinational approach of IMT-130 and TMZ produced a significant increase in apoptotic cells compared to SHAM

control and IMT-130-/TMZ-only treated GBM cells, with a ~12% increase compared to the sum of the mono-treatments (Xu et al., 2016). Of note, IMT-130 produced a more significant effect on the reduction of viability of the GBM cells than TMZ-alone (Xu et al., 2016), however, the MGMT-status of the patient-derived cell lines was not provided and GBM cell lines have multiple resistance mechanisms against TMZ. Lastly, IMT-130 was tested in combination with siRNA to assess the potential for IMT-130 treatment to enhance uptake and/or bioavailability of siRNA in GBM cells. Xu and colleagues used HSP27-siRNA to target the heat-shock protein as it has been implicated in cancer cell proliferation, drug-resistance, and migration (van Ommeren et al., 2016). Concomitant IMT treatment with HSP27-siRNA produced a significant increase in the knockdown of HSP27 followed by an increase in GBM cell death (Xu et al., 2016). Taken together, it appears that IMT-130 treatment may improve uptake and bioavailability of drugs, and may explain the observed synergy between IMT-130 and TMZ (Xu et al., 2016).

IMT was later tested in pre-clinical models but with significantly higher frequencies than previously utilised (130Hz) – IMT was tested with 200kHz electric fields (Sebastiano et al., 2018). Referred to as IMT-200. The frequency chosen was that of which is used in clinical TTFields frequency (Stupp et al., 2017a), but the IMT system tests the effects of these fields in an internalised manner with the hopes of producing a higher field intensity within the vicinity of the tumour. Firstly, IMT-200 efficacy was tested in combination with and comparatively to TMZ-only in patient derived GBM cell lines over a 72 hour treatment. A treatment time of 72 hours has been shown in TTFields studies to be sufficient time to cause noticeable effects within GBM cells at these frequencies (Porat et al., 2017). Similar to previous reports; TMZ-alone had modest efficacy against the patient derived GBM cell lines (~17% reduction in viability), IMT-200-alone had a significantly greater efficacy than TMZ-alone (~35% reduction in viability), IMT-200 in combination with TMZ had a profound accumulative effect on the viability of the GBM cells compared to each treatment alone (~55% reduction in viability), and IMT-200 did not have any significant effects on the cell viability or morphology of primary

neurons (Sebastiano et al., 2018). Flow cytometry was performed to assess the percentage of live vs apoptotic/dead cells following the different treatments and combinations over a 72 hour treatment; TMZ-alone (~72% of cells alive), IMT-200-alone (~62% of cells alive), and IMT-200-TMZ (~27% of cells alive). Lastly, IMT-200 was tested in an *in vivo* rodent GBM model with 15 rats. Rats had bilateral tumours grown and each tumour was treated with SHAMT-IMT and IMT-200, randomised to left and right tumours (Sebastiano et al., 2018). Rats treated with IMT-200 had an average reduction of 19.5% of tumour volume compared to the SHAM-IMT treated tumour, the reduction in tumour volume was 14.5% when the significant statistical outlier was excluded, results shown in figure 20. Also, the IMT-200 treated tumours were observed to be typically more compact and rounded in shape, while the SHAM-IMT treated tumours were more irregular in nature (Sebastiano et al., 2018). In conclusion, the current data has provided a proof-of-concept for an internalised system for the treatment of GBM, however, further development of the technology to improve tumour location coverage as well as greater characterisation of the mechanisms of action is warranted before it may be translated to the clinic.

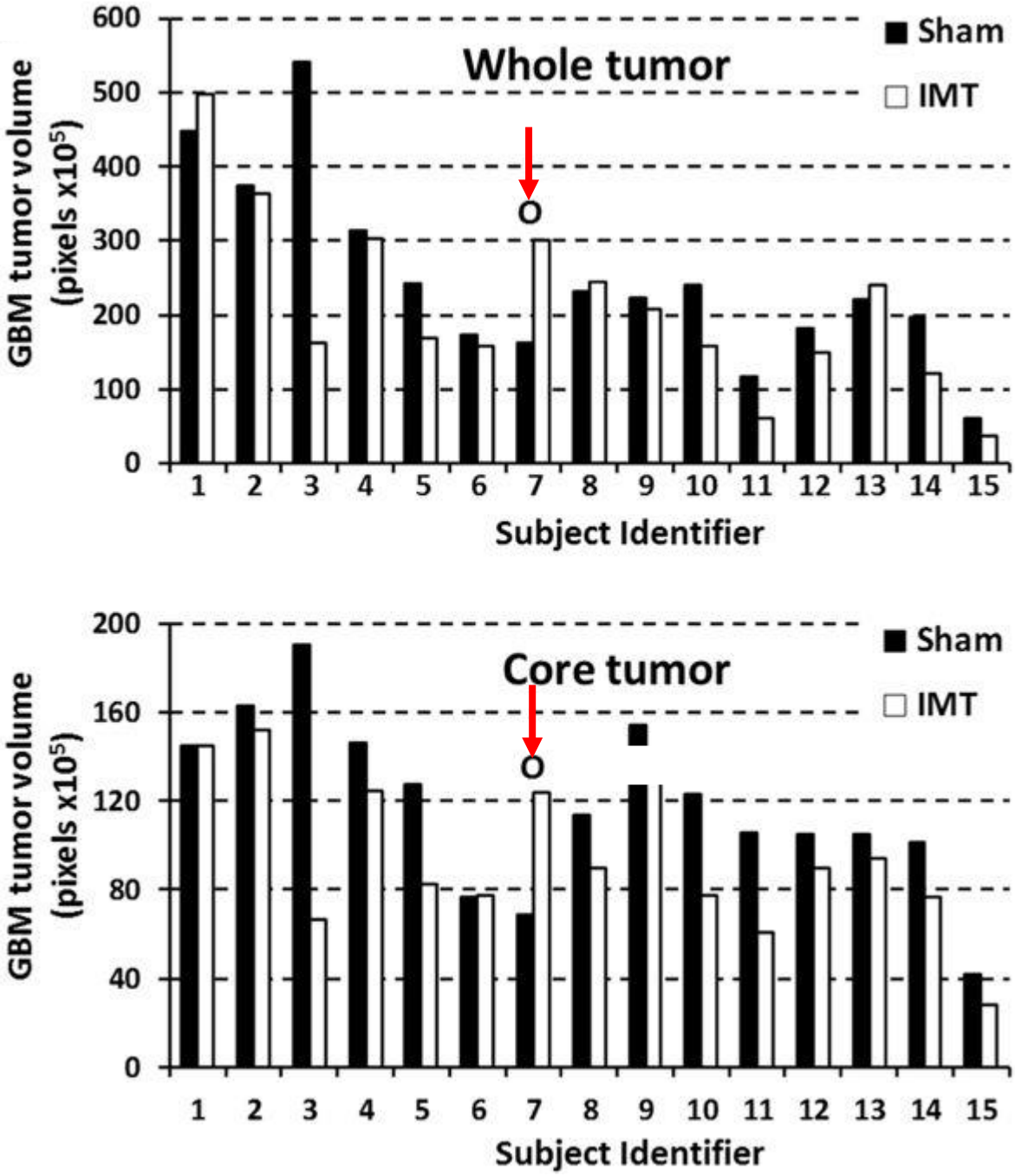


Figure 20. Graphs showing GBM whole and core tumour volumes post IMT-200 and SHAM-IMT treatments in rodents. The red arrows highlight the significant outlier of the cohort. Figure adapted from (Sebastiano et al., 2018).

5.8. TheraBionic P1 Medical Device for Advanced Hepatocellular Carcinoma (HCC)

"Our vision,

Boris Pasche and Alexandre Barbault, coinventors of the TheraBionic technology and cofounders of TheraBionic Inc., formerly TheraBionic LLC, and TheraBionic GmbH, had one goal in mind since the beginning of their research: developing better and safer therapies for cancer."

TheraBionic Inc. statement (https://www.therabionic.com/) – 22/11/2018

The TheraBionic P1 medical device, as described in Figure 20. produces RFEs at amplitudes and frequencies optimised to be tumour-specific. The TheraBionic P1 administers these RFEs to the patient via an antenna, which is placed onto the anterior portion of the patient's tongue. The antenna transmits RFEs throughout the patient's body when placed upon the tongue, as shown in Figure 21. Therapeutic delivery of RFEs consists of three sixty-minute sessions per day (Costa et al., 2011).



Figure 4 Legend;

1. TheraBionic device carrying case
2. TheraBionic P1 therapeutic device
3. TheraBionic docking station for recharging
4. Coaxial cable (1.2m) with patient spoon
5. Power supply for docking station
6. Activation card

Figure 21. The TheraBionic P1 medical device and its components. Image from https://www.therabionic.com/use-of-the-therabionic-p1/



Figure 22. (Left) The TheraBionic P1 medical device administering RFEs into the patient via the mouth. (Right) A schematic showing a representation of the distribution of RFEs within the body – yellow represents regions of highest RFE intensity.

5.8.1. TheraBionic P1 Therapy Interactions

Intrabuccal administration of RFEs was described for its sleep-inducing effects in the 1990s. It was shown that intrabuccal administration of RFEs at a frequency of 27.12MHz, amplitude-modulated at 42.7Hz, produced a significant sleep-inducing effects in healthy patients but not with insomnia diagnosed patients (Reite et al., 1994). However, this RFE amplitude-modulated over four insomnia-specific frequencies; 2.7Hz, 21.9Hz, 42.7Hz, and 48.9Hz, improved insomnia patients' total sleep time, shorter sleep latency, and an increase in the number of sleep cycles when compared to control insomnia patients (Pasche et al., 1996).

RFEs were hypothesised to be able to be optimised to express anti-cancer effects at specific tumour-specific frequencies and amplitude-modulations. Buckner and colleagues demonstrated how amplitude-modulated, optimised RFEs could inhibit the growth of malignant cells through manipulation of Ca^{2+} through T-type voltage-gated calcium channels (VGCC) (Buckner et al., 2015). The RFE signal used was originally designed to regulate epileptic seizure-related membrane activity via manipulation of ion flux (Buckner et al., 2015). These RFEs were shown to inhibit the proliferation of a selection of malignant cells, but interestingly, proliferation was unaffected in their panel of non-malignant cell lines. It was also noted that the malignant cells used had an increased Ca^{2+} influx, specifically through T-type VGCCs, while this CA^{2+} influx was not observed in the non-malignant cell lines. Furthermore, Ca^{2+} influx through inhibition of T-type VGCC blockers effectively negated the anti-proliferative effects of the RFEs. Lastly, RFE treatment of the malignant cell lines altered Cyclin A, B, and D expression, suggesting mitotic arrest at the G2/M-phase checkpoint (Buckner et al., 2015). Overall, the reports from Buckner and colleagues (Buckner et al., 2015) pertaining to electrical treatments and ion flux provides validity to RFEs as therapeutic systems to treat cancer through perturbation of cellular processes via ion manipulation.

5.8.2. TheraBionic P1 Therapy *in vitro* and *in vivo*

Barbault and colleagues reported the occurrence of tumour-specific frequencies when cancer patients were exposed to RFEs at specific

frequencies (Barbault et al., 2009). Using RFEs delivering carrier frequencies of either 433MHz or 27MHz, amplitude-modulated over the range of 0.1Hz-114KHz, 163 cancer patients were treated (Barbault et al., 2009). The study reported perturbations in pulse amplitude and skin electrical resistance following RFE exposure at specific frequencies, however, this was only observed in cancer patients and not healthy patients. Moreover, the RFE effects were apparent at the same frequency modulations within patients with the same tumour type, a tumour-specific frequency. Furthermore, while the majority of the frequencies were tumour-specific, there were 4 frequencies which did overlap in hepatocellular carcinoma (HCC), breast, prostate and pancreatic cancer – 1873.5Hz, 2221.3Hz, 6350.3Hz, and 10,456.4Hz (Barbault et al., 2009). These tumour-specific frequencies were then used on sixteen cancer patients as compassionate treatment who were evaluable for response; two hormone-refractory metastatic breast cancer patients had a complete response lasting 11 months and 13.5 months, a metastatic thyroid cancer patient had stable disease for 7 years, a NSLCC cancer patient had stable disease for 5.1 months, a metastatic pancreatic cancer patient had stable disease for 4.1 months, a metastatic leiomyosracoma cancer patient had stable disease for 4.0 months (Barbault et al., 2009, Zimmerman et al., 2013). Overall, this study demonstrated how tumour-specific RFEs may impact both the primary tumour, as well as the metastases of the disease, this implies that RFE treatment may be systemic.

Following the successful response assessment of RFEs in multiple cancer types in patients with limited treatment options (Barbault et al., 2009), a single-group, single-centre, open-label, Phase I/II trial was undertaken in patients with advanced HCC (Costa et al., 2011). The patients enrolled in the trial had radiological evidence of disease progression, with ~50% of the patients having poor liver function, and therefore, limited treatment options. Of the 267 patients initially assessed, 43 patients were allocated to intervention but only 41 patients received the allocated RFEs. The RFE treatment consisted of 27.12MHz fields, amplitude-modulated over HCC specific frequencies for 60 minutes, three times per day. The patients were compared to control patients from Phase III trials with similar patient

diagnostic criteria receiving Sorafenib (Llovet et al., 2008, Cheng et al., 2009). The median PFS was 4.4 months (95% CI: 2.1-5.3) vs 4.9 months (96% CI: 0.6-10.8), the OS was 6.7 months (95% CI: 3.0-10.2) vs 10.8 months (95% CI: 2.1-34.0) for RFE and Sorafenib treated patients, respectively (Llovet et al., 2008, Cheng et al., 2009, Costa et al., 2011). Of note, RFE treatment was well tolerated and there no NCI grade 2, 3, or 4 toxicities (Costa et al., 2011).

Zimmerman and colleagues performed in vitro studies to elucidate and characterise the mechanisms of action of RFE treatment (Zimmerman et al., 2013). HCC cell lines (HepG2 and Huh-7) and breast cancer cells (MCF-7), as well as corresponding non-malignant cell lines THLE-2 (representative of normal liver cells) and MCF-10A (representative of normal breast cells) were exposed to their tumour-specific frequencies described in the clinical setting (Barbault et al., 2009). The tumour-specific frequencies reduced proliferation in the cancer cell lines, but did not in the control representative normal cell lines. The tumour-specific frequencies were validated in each tumour type – the HCC-specific frequencies did not inhibit proliferation in the breast cancer cell line, and visa-versa (Zimmerman et al., 2013). The response of the HCC cell line, HepG2, to tumour-specific RFEs with regards to gene expression was interrogated via RNA-seq. RFE treatment resulted in significant downregulation of PLP2 – a gene which encodes an integral membrane protein which localises within the ER and has been implicated in migration and invasion of cancer (Lee et al., 2004, Sonoda et al., 2010), as well as significant downregulation of XCL2 – a gene which encodes a protein which enhances chemotaxis and downregulation has been shown to be associated with more-favourable prognosis in breast cancer patients (Teschendorff and Caldas, 2008). Furthermore, HepG2 cells that were exposed to HCC-specific frequencies for 3 hours per day for a one week treatment demonstrated pronounced disruption of the mitotic spindle in approximately 60% of cells, leading to improper chromosomal separation during anaphase, but not in the non-malignant control cells (Zimmerman et al., 2013).

6. Deep Brain Stimulation System Specifications

A typical Deep Brain Stimulation (DBS) system typically consists of an implantable pulse generator (IPG), an electrode that is implanted into the structure of therapeutic interest, and the extension which connects the two. The IPG's is mainly comprised of the power source, a battery, and the electric circuitry required to generate the electrical signal for DBS therapy. A desired therapeutic effect is achieved through a well-optimised electrical stimulatory field, which is calibrated through the DBS system and its technical features.

6.1. Electrical Sources

Electrical sources of a DBS system is either a voltage (V) or a current (C) source. Ohm's Law states that the current is directly proportional to the voltage, and inversely proportional to the resistance (R).

$$\text{Ohm's Law} >>> \text{Voltage (V)} = \text{Current (C)} \times \text{Resistance (R)}$$

Therefore, the current or the voltage may be manipulated through the electrical source. The desired voltage level may be adjusted while using a voltage source. However, the resistance present dictates a certain current value, which influences the desired therapeutic effect. Where resistance depends upon the implanted electrode-tissue interface, as well as the electrical characteristics of the brain tissue. Interestingly, it has been observed that resistance may vary over time, making anticipating the impedance behaviour of the stimulation troublesome (Hartmann et al., 2015). Ergo, the resistance may be subjected to fluctuations, however, these fluctuations may be alleviated through using a current source, as the current can be adjusted directly (Bronstein et al., 2015).

6.2. Unilateral and Bilateral Systems

A DBS system can perform either unilateral or bilateral stimulation, determined by the number of connectors on the IPG, as shown in Figure

22. A functional neurosurgeon can use either two unilateral IPGs or a single bilateral IPG to stimulate multiple brain regions.



Figure 22. Image showing examples of unilateral and bilateral DBS devices. (Left) Medtronic ACTIVA RC (Bilateral) and (Right) Medtronic ACTIVA SC (Unilateral).

6.3. DBS Electric Fields

A DBS electric field must be precisely configured to produce a localised neuronal response, therefore, this configuration has a very high impact on the efficacy of the treatment. A large proportion of the efficacy may be attributed to good position of the electrode and its contact with the neural target of interest (Perlmutter and Mink, 2006). The stimulating electric field itself, is dependent upon the stimulation rate, the pulse width, and the distribution of the current within the targeted neural structure. Furthermore, the current distribution may be altered through optimisation of the polarity, amplitude, the current output from each contact of the electrode, and through electrode design (Amon and Alesch, 2017).

6.3.1. Electrode Design

The contact location within the targeted neural structure is critical for delivering a high efficacy treatment while minimizing side-effects of the treatment (Herzog et al., 2004). The manufacturer produces a fixed design and number of contacts on the electrodes, with more recent designs facilitating directional stimulation options to improve a more targeted neuronal response (Steigerwald et al., 2016).

6.3.2. Polarity

As well as the contacts on the electrode, the IPG case can be programmed as an anode (+), a cathode (-), or off (neutral). A current flows between the anodes and cathodes, and the polarity configuration affects the current. Depending upon the desired configuration, a monopolar, bipolar, or multipolar configuration may be achieved through programming. A monopolar configuration may be achieved through programming a contact on the electrode as cathode, while the IPG case may act as the anode. A bipolar stimulation is achieved through programming an electrode contact as cathode, and another electrode contact as anode, while the IPG case acts as neutral in the circuit. In a multipolar configuration, one or multiple electrode contacts are programmed to be cathode while one or multiple electrode contacts are simultaneously programmed to be anode.

6.3.3. Electrical Signal

The DBS electrical signal is comprised of the signal amplitude, the stimulation rate, and the pulse width. The amplitude dictates the strength of the electrical signal, the amplitude is given as voltage (V) when a voltage source is used, and is given in milliamperes (mA) when a current source is used. Where the stimulation rate defines the number of pulses given per second, and the pulse rate describes the lengths of these pulses – which range anywhere from 10 to 510μs (Amon and Alesch, 2017). Out of these three, it's been observed that the stimulation and amplitude and the rate are most attributed to the efficacy and side-effects of the treatment (Kuncel et al., 2006). When optimising the electrical signal, the pulse width and the stimulation rate may be programmed to the desired rates, as well as varying stimulation amplitudes being programmed to independent electrode contacts.

6.3.4. Battery

DBS systems have both rechargeable and non-rechargeable battery systems. The non-rechargeable systems store enough energy for the entire battery's lifetime, where rechargeable systems must be regularly recharged with an external battery charging system. The battery life firstly depends upon the battery's capacity, and then depends upon the

stimulation parameters; stimulation amplitude, pulse width, stimulation rate, as well as the number of active electrode contacts being used. The battery's longevity is also influenced by the impedances of the electrode (Fakhar et al., 2013).

6.3.5. DBS Programmers

The DBS stimulation field is configured and adjusted using a DBS programmer. The DBS therapeutic parameters are defined on the DBS programmer by either physicians or the patients, and these are then transmitted to the IPG by wireless radio frequencies.

6.3.6. Interconnectivity

DBS systems may be manufactured by multiple companies, in our work we've used Medtronic® components. Different manufacturers may produce their own electrodes and IPGs, but combinations of these from different manufacturers may be possible with adaptors, for example; electrodes from Medtronic® may be connected to Boston Scientific and Saint Jude's IPGs (Amon and Alesch, 2017).

6.4. Neurophysiology of Deep Brain Stimulation

Neuronal function and signalling has been shown to be influenced by electrical stimulation. Neural structures are differentially sensitive to a wide variety of influences, such as; electrical stimulations of varying amplitudes, the geometry of the electric field, the geometry of the targeted elements, as well as the electrophysiological properties of the targeted structures (Perlmutter and Mink, 2006). Despite the well documented clinical benefits of DBS, the mechanisms underlying the therapy are not fully conclusive within the functional neurosurgical community with some remaining ambiguity (Chiken and Nambu, 2016). DBS was initially accepted to inhibit local neuronal elements through observations of reductions in the firing rates of neurons neighbouring the Subthalamic Nucleus (STN) and Globus Pallidus (GPi) upon STN-DBS and GPi-DBS in Parkinson's patients (Chiken and Nambu, 2016). The reduced firing in these regions ameliorates Parkinsonian motor symptoms but does not account for how GPi-DBS for the treatment of dystonia, given that GPi has

minimal neuronal activity during dystonic symptoms (Chiken and Nambu, 2016). However, excitation and excitation-inhibition of target nuclei by DBS may be achieved through signals traversing along efferent neural pathways and/or antidromically activation of the target region along afferent neural pathways (Chiken and Nambu, 2016). Overall, these excitatory and excitation-inhibition may have the potential to normalise or suppress abnormal activities of the target nuclei, but this mechanism has yet to be elucidated as well (Chiken and Nambu, 2016).

However, general principles may be applied from animal work to humans in order to understand which neural elements are affected by electrical stimulation (Ranck Jr, 1975). A key principal is the relationship between the duration and the stimulation amplitude, where current amplitude decreases, the duration must increase in order to produce the desired effect. Where conversely, an increase of stimulation amplitude must occur if the duration decreases to produce a similar effect. The amplitude-duration curve exponentially decays within most neural elements (Perlmutter and Mink, 2006). The 'rheobase' is a measure of membrane potential (the amplitude asymptote threshold). The relationship of the current amplitude and the pulse width is described in the equation below;

$$I_{th} = I_{rh} (1 + T_{ad} / PW)$$

Threshold Current = rheobase (1 + chronaxie / Pulse-width)

So this equation dictates that the larger the chronaxie, the larger the required current or pulse-width needed to activate the neural elements.

The chronaxie distinguishes between the different neural structures/elements of interest. The chronaxie value varies highly between targets, for example, the chronaxie of myelinated axons range between 30-200μs, while the chronaxies of dendrite cells falls between the 1-10ms ranges (Ranck Jr, 1975). Therefore, observations of calculated chronaxies may predict mechanisms of DBS. Holsheimer and colleagues performed a study to calculate the chronaxies of ventral intermediate nucleus of the thalamus (VIM) and GPi-DBS, where they deduced that stimulation of these structures most likely expressed their effects through afferent and

efferent axon-mediated mechanisms as opposed to stimulation of cell bodies (Holsheimer et al., 2000). Responsiveness to electrical stimulation is of course influenced by the distance of the neural element from the DBS electrode (Holsheimer et al., 2000). As per the above equation, the rheobase and chronaxie proportionally rises with the distance of the neural elements from the electrode, so a larger current is required. Lastly, the orientation of the neural element relative to the directional flow of the current determines responsiveness to the electric field (Ranck Jr, 1975). So given the diverse composition of neural structures, the response to DBS in a nucleus is complex due to the varying geometries of the neural elements and the DBS electrode (Perlmutter and Mink, 2006).

6.5. Deep Brain Stimulation Mechanisms of Action

Despite the extensive research and clinical acceptance of DBS therapy, the mechanism of action remains ambiguous. For DBS treatment, three hypotheses have arisen from observations; the excitation, the inhibition, and the disruption hypothesis.

6.5.1. The Excitation Hypothesis

The excitation hypothesis suggests that DBS functions through excitation of local neural elements within the targeted structure (Chiken and Nambu, 2016). Modelling has suggested that subthreshold DBS may suppress intrinsic activity of the cell bodies, while surpassing this threshold may induce activity within the axons (McIntyre et al., 2004b). Therefore, when stimulation fails to overcome GABAergic inhibition of cell bodies, the stimulatory field may still excite efferent axons to provide stimulation to the target nucleus. DBS also excites afferent axons through an antidromic fashion, as it has been observed that thalamic neurons were stimulated antidromically by GPi-DBS most likely from stimulation of thalamic axons close to the GPi-DBS electrode location (Montgomery Jr, 2006), as an example. Overall, DBS excitation may stimulate the target nucleus through efferent pathways or through antidromic activation of afferent pathways in order to either normalise or suppress abnormal neural activity, or to alter the firing rates and patterns of the target nucleus (Chiken and Nambu, 2016).

6.5.2. The Inhibition Hypothesis

The inhibition hypothesis arose from observations of the similarities on the motor signs of Parkinsons disease with STN-DBS (Benabid et al., 1994), STN-blockade (Luo et al., 2002), or STN-lesion (Bergman et al., 1990). This is in spite of neighbouring neurons to the STN and GPi being suppressed during DBS (Filali et al., 2004, Wu et al., 2001). A few potential mechanisms may account for the inhibitory responses seen during DBS. Firstly, DBS may block depolarization and synaptic inhibition, however, there's a possibility of independent activation of efferent neurons of projection neurons (McIntyre et al., 2004a). Secondly, DBS may potentially inactivate intrinsic voltage-gated currents, as seen in as a dramatic reduction of Na^{+} and Ca^{2+} voltage-gated currents as a response to high-frequency stimulation of STN neurons (Beurrier et al., 2001). Lastly, DBS has been shown to activate inhibitory afferents, as seen from inhibitory inputs to GPi neurons in a $GABA_A$ receptor-mediated fashion (Chiken and Nambu, 2013).

6.5.3. The Disruption Hypothesis

The disruption hypothesis describes how DBS may 'disrupt' information flow through structures. It's been shown how cortical stimulation may induce a response consisting of; early excitation, inhibition and then excitation of the GPi. These responses were mediated by the *hyperdirect, direct,* and then *indirect* pathways, respectively (Nambu et al., 2002, Nambu et al., 2000). For example, axon terminals activated by DBS in the target nucleus may induce release of neurotransmitters while dissociating inputs and outputs within the stimulated nucleus (Chiken and Nambu, 2016).

6.6. Clinical Applications of Deep Brain Stimulation

Ever since 1970s DBS has developed to treat multiple neurological disorders including; Parkinson disease, Tourettes syndrome, Essential Tremor, dystonia, as well as a variety of intractable pain syndromes. These disorders may be treated with effective programming and optimised implantation of DBS electrodes.

6.6.1. Deep Brain Stimulation for Parkinson Disease

Stimulation of different neural structures may provide varying clinical effects in Parkinson disease (PD) patients. Stimulation of the Globus pallidus internus (GPi) may reduce the predominant motor manifestations of the disease (Anderson et al., 2005). However, electrical stimulation of the Subthalamic nucleus (STN) addresses these issues. STN stimulation provides comparable reduction in PD motor symptoms as GPi stimulation as facilitating reductions in medication for PD patients (Anderson et al., 2005). Studies have also shown that bilateral STN stimulation may improve tremor, bradykinesia, and tremor, while further reducing the dosage requirements of dopaminergic medications resulting in fewer drug-associated toxicities (Pollak et al., 2002).

Overall, the treatment benefit of STN and GPi stimulation does not typically exceed the therapeutic effects of levodopa, the main benefits of DBS therapy is towards the reductions of medication-induced events (Pahwa et al., 2005), as well as an improved quality of life for PD patients undergoing STN DBS therapy (Diamond and Jankovic, 2005, Lyons and Pahwa, 2005). However, STN stimulation may negatively affect cognitive processes of the patient including; response inhibition (Hershey et al., 2004), untoward emotional responses (Herzog et al., 2003), and mood depression (Berney et al., 2002) to name a few. The main indications for DBS treatment is PD patients who do not respond well to levopoda and patients whose treatment may be limited by dopa-induced side effects (Perlmutter and Mink, 2006).

6.6.2. Deep Brain Stimulation for Pain

DBS has been used as treatment for multiple pain syndromes, including neuropathic pain, lower back pain, as well as cluster-headache pain. The

therapeutic site of stimulation for pain has varied from the sensory thalamus to the posterior hypothalamus, periventricular gray, periaqueductal gray, and the motor cortex (Franzini et al., 2003, Tirakotai et al., 2004). The plethora of stimulation targets is proportional to the variety of pain syndrome aetiologies. For example, DBS treatment of the thalamus has been shown to reduce pain symptoms in phantom-limb syndrome patients (Katayama et al., 2001), while DBS treatment of higher regions, such as cortical targets, has been targeted to reduce symptoms in post-stroke pain syndromes (Katayama et al., 2001). Nociceptive cells within the brain could potentially be identified as suitable DBS targets through mapping the evoked responses to pain stimuli – this may produce a more personalised therapy for a specific type of pain (Hanajima et al., 2004, Pralong et al., 2004).

6.6.3. Deep Brain Stimulation for Dystonia

Initially, medically refractory generalised dystonia was treated with stereotaxic ablations of the GPi or thalamus (Perlmutter and Mink, 2006). This treatment strategy was then used with DBS of the GPi (Kumar et al., 1999) and thalamus (Sellal et al., 1993) targets, however, the GPi is the primary target for primary dystonia (Yoshor et al., 2001, Eltahawy et al., 2004). More recent controlled and uncontrolled trials have also shown how pallidal DBS may improve dystonia symptoms by 30-50% within primary generalised dystonia patients (Coubes et al., 2004, Vidailhet et al., 2005).

6.6.4. Deep Brain Stimulation for Essential Tremor

DBS therapy was first widely used for the treatment of Parkinsonian tremor and for essential tremor. Further single- and multi-centre clinical trials reported significant efficacy in the majority of essential tremor patients with VIM stimulation, with reports of an average tremor reduction of over 80% (Koller et al., 1999, Rehncrona et al., 2003).

6.7. Deep Brain Stimulation for the Treatment of Brain Tumours

Given the already described effects of IMT in GBM cells *in vitro* and *in vivo*, compounded with the observations upon the uncommon occurrence of developing a brain tumour while having an implantable neuromodulation

device, DBS technology may already prophylactically be having anti-tumoural effects. DBS functions to modulate electrical activity of excitable cells, however, non-excitable cells exhibit significant electrical activity as a result of multiple cellular process, such as proliferation (Yang and Brackenbury, 2013). Therefore, electric fields may have potential to take advantage of altered ion flux, membrane potential, and overall bioelectrical properties of cancer cells (Yang and Brackenbury, 2013).

6.7.1. Membrane Potential (V_m) of Cells

The flow of Na^+, K^+, Ca^{2+}, and Cl^- ions is tightly regulated by multiple distinct ion channels and transporters at the plasma membrane. It is the unequal distribution of these ions between the intracellular- and the extracellular-environment which describes the membrane potential (V_m). A cell is in a depolarised state when the V_m is less negative, while a cell is in a hyperpolarised state when the V_m is relatively more negative. V_m is described by Goldman-Hodgkin-Katz equation (Goldman, 1943, Hodgkin and Katz, 1949) which shows the relationship between V_m and the intracellular and extracellular concentration of ions;

$$V_m = \frac{RT}{F} \ln\left(\frac{P_{Na}+[Na^+]_o+P_K+[K^+]_o+P_{Cl}-[Cl-]_o}{P_{Na}+[Na^+]_i+P_K+[K^+]_I+P_{Cl}-[Cl-]_i}\right)$$

Where R=the ideal gas constant, T=temperature, and F=Faraday Constant. Fluctuations in the V_m underlie action potentials (AP) in excitable cells. Aps are a result of sufficient depolarisation, where sufficient polarisation is relative to the AP threshold value. The Aps and their respective threshold values are regulated by key transporters and voltage-gated ion channels, such as Na^+/K^+-ATPase transporter, voltage-gated Na^+ channels (VGSCs), and voltage-gated K^+ channels (K_v) (Yang and Brackenbury, 2013).

6.7.2. Membrane Potential (V_m) and Cancer

It was shown by Cone, 1969 that V_m, depolarisation, and hyperpolarisation is intertwined with the mitotic process and cell cycle progression (Cone, 1969, Cone Jr, 1970), and later, V_m underlining the level of differentiation of a cell (Cone Jr, 1971) among other processes which are described as hallmarks of cancer. Already discussed, the determinants of a cell's V_m are largely disrupted and dysregulated in cancer cells (Pollak et al., 2017), potentially presenting a novel therapeutic avenue for cancer. Interestingly, a body of research has shown clear patterns between the normal cell-V_m and cancer cell-V_m and their respective proliferation profiles. Plainly, rapidly proliferative cancer cells are characterised by a more depolarised V_m, contrary to neurons – terminally differentiated and non-proliferative cells, which are characterised by a more hyperpolarised V_m (Levin, 2007, Binggeli and Weinstein, 1986, Fraser et al., 2005, Mycielska et al., 2005, Yang et al., 2012, Yang and Brackenbury, 2013) (Figure 22).

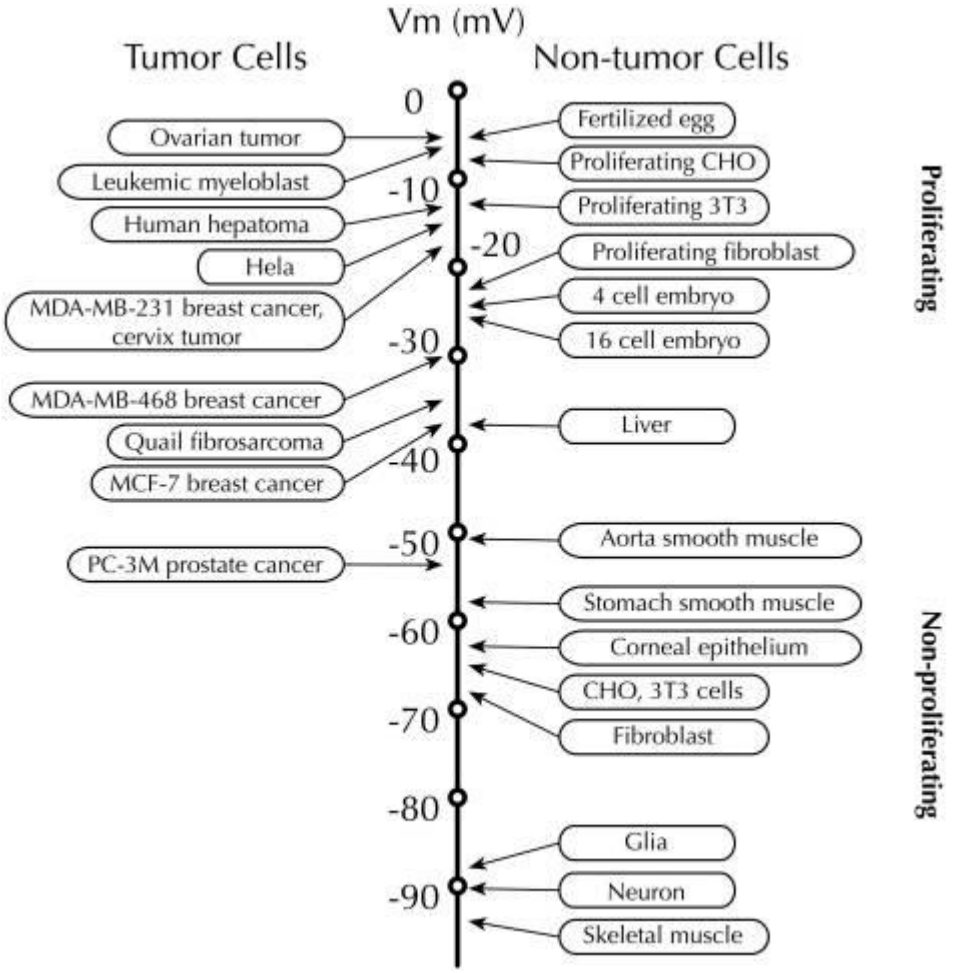


Figure 22. A scale describing V_m values for a range of proliferative and non-proliferative tumour and normal cells. Rapidly proliferating cells possess a more depolarised V_m, while non-proliferative cells have a more hyperpolarised V_m. Image from (Yang and Brackenbury, 2013).

6.7.3. Membrane Potential (V_m) and Proliferation

Fluctuations in V_m has been implicated in the mitotic cycle, in general, the V_m in cells fluctuates between a depolarised and hyperpolarised state (Orr et al., 1972, Binggeli and Weinstein, 1986). Mitosis of CHO (Chinese hamster ovary) cells and mature chick spinal cord neurons have been artificially altered with manipulations in V_m, specifically, hyperpolarisation of each of the cell lines induced mitotic arrest while depolarisation caused proliferation (Cone 1971, Cone 1976). Contrary to observations of mitotic arrest be a consequence of hyperpolarisation, hyperpolarisation occurs at

the G1/S checkpoint to facilitate S-phase initiation in many cell types (Canady et al., 1990, Wonderlin et al., 1995). Hyperpolarisation is subsequently followed by depolarisation upon the cell reaching the G2/M checkpoint of the cell cycle (Blackiston et al., 2009). Although these fluctuations appear to contradict the observations of hyperpolarisation inducing mitotic arrest, the average V_m of actively dividing cells, especially cancer cells, is more depolarised relative to the V_m of most somatic cell types (Figure 22.) (Yang and Brackenbury, 2013). A representation of the fluctuations and their respective cell cycle phase is outlined in Figure 23.

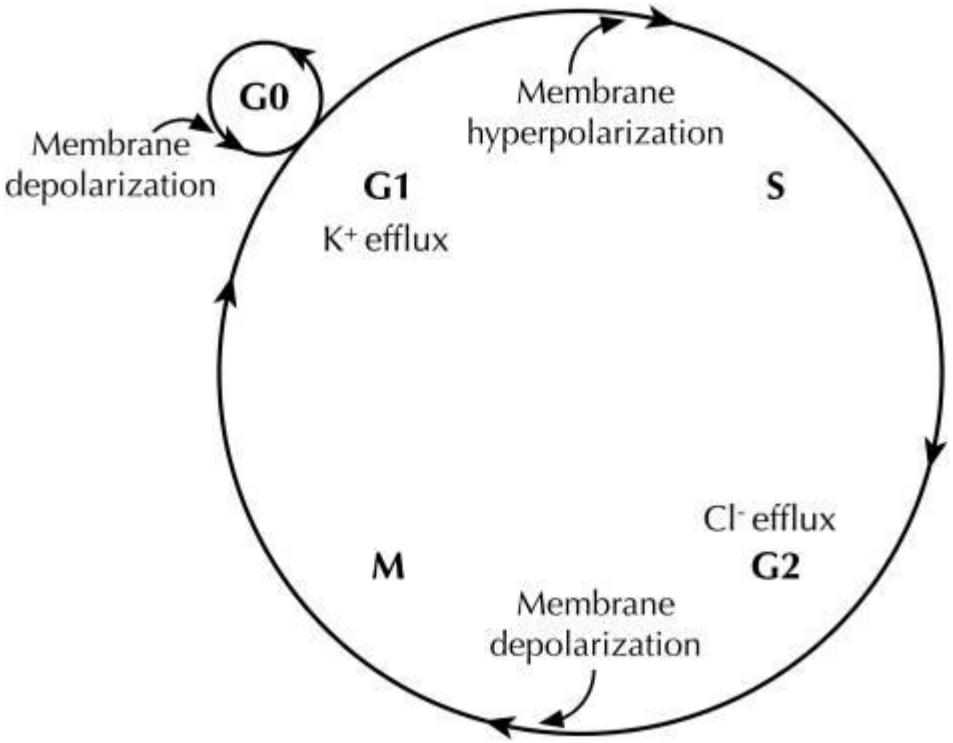


Figure 23. Diagram illustrating V_m fluctuations throughout the cell cycle. A cell's V_m undergoes hyperpolarisation to enter the S-phase through K^+ efflux. At the G2/M checkpoint, depolarisation via Cl^- efflux causes the cells to enter M-phase. Image from (Yang and Brackenbury, 2013).

6.7.4. Clinical Opportunities for Deep Brain Stimulation for the Treatment of Brain Tumours

The observations of the influence of V_m on the cell cycle and the depolarised V_m of cancer cells, suggests that cancer cells utilise their relatively depolarised phenotype to maintain sustained proliferation.

Therefore, modulation of V_m through chronic electrical modulation may provide a clinically relevant approach to treatment of high-grade brain tumours where treatment options are limited by both efficacy and toxicity.

6.8. Concluding Remarks

The treatment of cancer with electrical fields is a promising prospect, particularly with brain tumours where diagnosis may be poor and treatment options may be limited. Therefore, innovations within this field should not only seek to improve OS and PFS, but also improve QoL for patients. The Optune system is currently the only FDA approved electric fields based treatment system for GBM patients which has improved QoL for patients but also notably, improved OS in newly-diagnosed patients in combination with TMZ (Stupp et al., 2017a). A theme of a lack of toxicities associated with electric field treatments is apparent with all the treatments described – Optune (Stupp et al., 2017a), Nativis Voyager (Barkhoudarian, 2017), and TheraBionic P1 (Costa et al., 2011), which should translate to an improvement in or no detriment to QoL with the potential for survival benefit. While all these treatments utilise different fields on the electromagnetic spectrum, the treatments do share striking similarities in their mechanisms of action which may be due to overlooked, or currently non-described mechanisms. Future research into electric fields for the treatment of cancer may elucidate and more thoroughly characterise the mechanisms of action which may be able to be translated into a more efficacious treatment in the clinic.

Chapter 2: Deep Brain Stimulation for the Treatment of Brain Tumours

1. Introduction

Since the start of this project, Xu and collages published on the effects of repurposed Medtronic DBS electrodes on GBM cell lines in a preliminary report (Xu et al., 2016). The key findings of this exploratory study were; DBS electric fields delivered at 130Hz, 4V, and 90μs had an apoptotic effect on GBM cells, and this effect may be increased with the addition of TMZ. This report validated previous observations of 130Hz electric fields having an anti-proliferative effect on GBM cell lines, though Cucullo and colleagues (Cucullo et al., 2005a) described the effects via interactions with ion flux through inwards-rectifying potassium channels. These demonstrated that low frequency electric fields, similar to those used in DBS treatment, may provide a novel therapeutic route for brain tumours.

However, the effects of these low intensity electric fields on brain tumour cell lines have not been characterised further to a large extent. This study sought to provide a greater characterisation of the effects of DBS electric fields on brain tumour cell lines in a bid to provide validity to an internalised electric field delivery system for the treatment of brain tumours.

1.2. Hypotheses

Electric fields delivered from DBS generators have an anti-proliferative effect on brain tumour cell lines and this effect may be augmented with the addition of chemotherapies.

1.3. Aims and Objectives

This chapter presents the preliminary investigations into the anti-cancer effects of electric fields delivered from Medtronic™ DBS electrodes on GBM, Medulloblastoma, and Ependymoma cell lines. The aims of this chapter were to;

1) Characterise the effect of manipulations in frequency and intensity of DBS electric fields on brain tumour cell lines;

2) Investigate the effect of DBS electric fields on human neural stem cells and astrocytes;
3) Investigate the efficacy of DBS electric fields in combination with chemotherapies on GBM cell lines,

The objectives for this study were;

1) Assess how DBS electric fields influence the metabolic activity, cell count, and the cell cycle of treated brain tumour cell lines;
2) Assess how, and to what extent, DBS electric fields influence the metabolic activity and cell count of the treated human normal brain cell lines;
3) Assess how the efficacy of DBS electric fields may be improved with the addition of TMZ and the mitotic inhibitors – Paclitaxel and Mebendazole, and how these may influence metabolic activity, cell count, and the cell cycle of GBM cell lines.

2. Deep Brain Stimulation Methods

2.2. Cell Culture and Cell Lines

The cell lines used and cultured for DBS experiments and their growth medium requirements are detailed in Table 1.. All cell lines were cultured at 37^0C, in a 5% CO_2 incubator in a humid atmosphere.

Cell Type	Cell Line	Growth Medium
Glioblastoma multiforme	U87-MG GIN-5 GIN-8 GIN-28 GIN-31 GCE-77	- Dulbecco's Modified Eagle Medium (DMEM; Gibco™) - 10% Foetal Bovine Serum (FBS; HyClone™) - 1% Penicillin/Streptomycin (Pen./Strep.; Simgma-Aldrich)
	KNS42 SF188	- Dulbecco's Modified Eagle Medium/F-12 (DMEM/F-12; Gibco™) - 10% Foetal Bovine Serum (FBS; HyClone™) - 1% L-Glutamine (L-Glu; Sigma-Aldrich) - 1% Penicillin/Streptomycin (Pen./Strep.; Simgma-Aldrich)
Ependymoma	DKFZ-EPN1 BXD-1245-EPN	- Dulbecco's Modified Eagle Medium (DMEM; Gibco™) - 10% Foetal Bovine Serum (FBS; HyClone™) - 1% Penicillin/Streptomycin (Pen./Strep.; Simgma-Aldrich)
Medulloblastoma	DAOY	- Minimum Essential Media with Earle's salts (MEM; Sigma-Aldrich) - 10% Foetal Bovine Serum (FBS; HyClone™) - 1% L-Glutamine (L-Glu; Sigma-Aldrich) - 1% Sodium Pyruvate (Simgma-Aldrich) - 1% Penicillin/Streptomycin (Pen./Strep.; Simgma-Aldrich)
	UW228-3	- Dulbecco's Modified Eagle Medium/F-12 (DMEM/F-12; Gibco™) - 15% Foetal Bovine Serum (FBS; HyClone™)

		- 1% L-Glutamine (L-Glu; Sigma-Aldrich) - 1% Penicillin/Streptomycin (Pen./Strep.; Simgma-Aldrich)

Cell Type	Cell Line	Growth Medium
Human Induced Pluripotent Stem Cells	hiPSC	- Knockout™ DMEM/F12 (KO DMEM/F12; Gibco™) - StemPro® Neural Supplemement (Gibco™) - 5µg/L Fibroblast Growth Factor-basic (AA 10–105) Recombinant Human (FGF-basic; Gibco™) - 5µg/L Epidermal Growth Factor Recombinant Human (EGF; Gibco™) - 1% Penicillin/Streptomycin (Pen./Strep.; Sigma-Aldrich)
Astrocytes	hiPSC-derived Astrocytes	- Astrocyte Medium (AM; ScienCell™) - 5% Foetal Bovine Serum (FBS; ScienCell™) - 1% Astrocyte Growth Supplement (AGS; ScienCell™) - 1% Penicillin/Streptomycin (Pen./Strep.; ScienCell™)

Table 1. Table describing the cell lines and their growth medium compositions.

2.2.1. Cell Subculture

Flasks had their growth medium removed, cells were washed with HBSS, and 3ml of 1X Trypsin-EDTA (Tryspin; Thermo Fisher) was added to each flask. Trypsinised cells were incubated in a CO_2 incubator and incubated for 5-10 minutes at 37^0C to allow the cells to detach. The Trypsin was neutralised with at least 3ml of growth medium, and then the cells were transferred to new flasks at appropriate split ratios to allow extended growth of cells. Experiments were undertaken with cells within 10 passages of each other.

2.2.2. Cell Storage

Cells were frozen for long term storage upon reaching at least 70% confluency to allow future use of lower passage cell lines. Flasks had their

growth medium removed, cells were washed with HBSS, and 3ml of Trypsin was added to each flask. Trypsinised cells were incubated in a CO_2 incubator and incubated for 5-10 minutes at 37^0C to allow the cells to detach. The Trypsin was neutralised with 3ml of growth medium. The cells were then centrifuged at 120 x g for 5 minutes to pellet the cells. The supernatant was removed and the pellet was suspended in 1ml of 10% DMSO diluted in FBS before being transferred to Cryovials. Cryovials are incubated for 24 hours in a Mr. Frosty™ freezing container (Thermo Fisher) at -80^0C before being transferred for short term storage at -80^0C. Cells are stored at -80^0C for no longer than 6 months and then moved to liquid nitrogen for long term storage.

2.2.3. Cell Recovery

Cells were retrieved from storage and kept on ice. A flask with warm media was prepared, cells were thawed by partial 37^0C water submersion and then transferred into the new flask. Cells are then incubated at 37^0C for 24 hours. The next day, a media changed is performed to eliminate any traces of DMSO.

2.2.4. Neural Stem Cell Culture and Generation of Astrocyte Cell Line

Astrocytes used in experiments were differentiated from human induced pluripotent stem cells. Cell culture flasks used for stem cell and astrocyte culture were coated before use. Geltrex® matrix was diluted 1:100 in warm KnockOut™ DMEM/F-12 medium (Gibco™), and 3ml of the matrix was added to each T25 flask and were incubated for 1 hour at 37^0C. Following incubation, the matrix was removed and the flasks were washed twice with PBS. Neural stem cells were seeded onto the Geltrex® matrix coated flasks at a seeding density of 5 x $10^4/cm^2$ in Neural Stem Cell (NSC) medium. NSCs are maintained in Geltrex® matrix coated flasks, with complete medium changes every 2 days, and NSCs were subcultured to the initial seeding density of 5.0 x $10^4/cm^2$ upon reaching a confluency of 90%.

NSCs were detached from flasks with StemPro™ Accutase™ (Gibco™), growth medium was removed and calls were washed with PBS, Accutase™ was added to the cells for 30 seconds to allow the cells to detach, fresh

medium was added to the cells to neutralise the Accutase™ and to collect the cells. NSCs were then seeded onto Geltrex® matrix coated flasks at a seeding density of 1.5 x $10^4/cm^2$ and incubated overnight at 37^0C in an incubator. The following day, the medium was changed to Astrocyte medium, and the medium was changed every 2 days. The cells were subcultured to the initial seeding density of 1.5 x $10^4/cm^2$ upon reaching 90% confluency. A successful differentiation of Astrocytes from human induced pluripotent stem cells takes 30 days of being cultured in Astrocyte medium.

At day 0, NPC medium was switched to astrocyte medium (ScienCell™). From day 2, cells were fed every 48 hours for 20-30 days. When the cells reached 90- 95% confluency (approximately every 6-7 days), they were split to the initial seeding density (15,000 cells/cm2) as single cells in astrocyte medium, and cultured on matrigel, following 5-10 min incubation with accutase, pipetting, and washing with DMEM (Gibco™). After 30 days of differentiation, astrocytes could be split 1:3 every week with accutase and expanded up to 120 days (15-17 passages) in astrocyte medium containing 2% FBS. Following the initial 30-day differentiation period, astrocytes survive and expand for up to 30 days without FBS.

2.3. Deep Brain Stimulation Experiments

2.3.1. DBS Lead Maintenance

1 x 8 low impedance compact leads (Medtronic™), herein referred to as 'Leads', were used in the DBS experiments. The Leads were soaked in light detergent for 30 minutes before being transferred into 70% ethanol for a further 30 minutes. The Leads were then rinsed thoroughly under running tap water to remove any residual ethanol/detergent. The Leads were then air-dried before being sealed in autoclave bags. The bags were then autoclaved for 60 minutes at no more than 120^0C. The bags were then removed from the autoclave and dried for 30 minutes before subsequent use.

2.3.2. Experimental Setup

DBS electric field treatment was achieved through delivering electric fields from Neurostimulators (Medtronic™), via 1 x 8 low impedance compact leads (Medtronic™) and programmed with the N'Vision™ programmer (Medtronic™) with a bipolar configuration with one anode contact.

The Leads were sterilized as described in 'DBS Lead Maintenance' and then transferred to the incubator. The Leads were returned to the incubator wrapped in ethanol-soaked paper towels to ameliorate this process due to contamination risks.

A cell suspension was prepared in appropriate growth medium, and at an appropriate seeding density as detailed in Table 2.. These cell densities were selected to allow control cells to achieve no more than ~90% confluency after 7 days of growth. A volume of 5ml of the cell suspension was pipetted into a T25 flask, and then were incubated overnight at 37^0C in an incubator to allow the cells to adhere to the flasks. The flasks were then 'topped-up' to 20ml of media per flask to allow an inserted Lead to be fully submerged.

The Leads were again washed with ethanol and then wiped down to remove any excess ethanol before being inserted into a culture flask. The Leads were inserted into the flasks directly through the filter paper in the lid, as shown in Figure 1. And Figure 2.. The neurostimulators were then programmed as detailed within the 'DBS Programming' section, to deliver the desired electric fields with regards to intensity, frequency and pulse width. Upon appropriate programming, the neurostimulators would be 'turned-on' in order to deliver the electric fields throughout the flasks. The electric fields were delivered continuously throughout the experiments until a 'Mid-point' or 'End-point' was reached. Upon reaching an end-point, the Leads were removed from the flasks and then sterilised as described in 'DBS Lead Maintenance' section.

CELL LINE	SEEDING DENSITY
SF188	4,000/ml
KNS42	8,000/ml
GIN28	9,000/ml
GIN31	9,000/ml
U87	8,000/ml
DKFZ-EPN1	6,000/ml
BXD-1245E	6,000/ml
DAOY	8,000/ml
UW228-3	4,000/ml
ASTROCYTES	40,000/ml
Neural Stem Cells	8,000/ml

Table 2. Table outlining the seeding densities of cells used for 7 days DBS treated experiments.



Figure 1. Lead was inserted through the filter paper and angled slightly towards the corner of the flask to allow full submersion as well as facilitating reproducibility by reducing variation in lead placement.



Figure 2. Lead was fully submerged while not physically interacting with the adherent cells.

2.3.3. DBS Programming

Before programming of the pulse generators could begin, contact between the stimulator and the programmer must be established. The programmer head was connected to the back of the pulse generator. A green light illuminated to confirm a connection, and now the programmer is communicating with the pulse generator (Figure 3.). First, the parameters of the treatment were set by clicking on 'Program myStim' (Figure 4.). The home screen will also display the current battery life of the pulse generator

and the programmer. From this interface the parameters of each Lead were programmed independently. The parameters which were adjusted were the intensity (Voltage), frequency (Hertz), Pulse width (μseconds), as well as the Anode and Cathode configuration (Figure 5.). The Lead configuration must contain at least one cathode and anode contact. Electrode impedance is a measure of resistance in the circuit i.e. the medium. Electrode impedance was checked every day and after re-insertion of Leads following readings. Following measurement of electrode impedance, values will be displayed corresponding to the lead and contacts selected; values <500 are considered acceptable and values >10,000 indicate a broken contact or contact not being fully submerged in the medium (Figure 6.).



Figure 3. The programmer head is connected to the pulse generator to establish a connection.

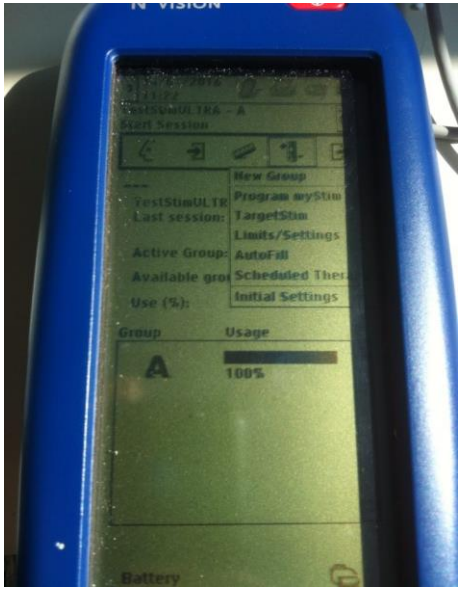


Figure 4. The pulse generator is programmed through the interface 'Program myStim'.

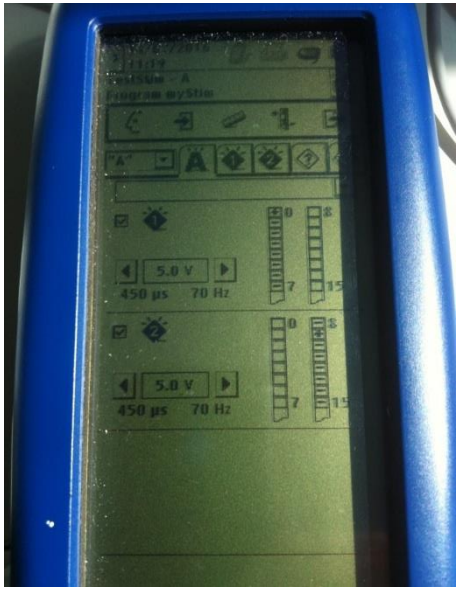


Figure 5. Through this interface, all the parameters were set; intensity, frequency, pulse width, and the anode and cathode configuration.

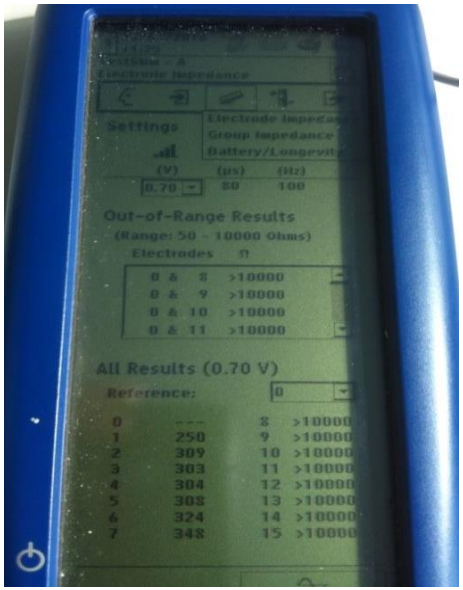


Figure 6. Impedance was measured every day to assess resistance/faulty connections with the Lead to ensure reproducible conditions.

2.3.4. DBS Control Samples

Control cells (the same cell line used in the parallel DBS experiment) were seeded Into T25 flasks. The cells were then incubated overnight at 37^0C in an incubator to allow the cells to adhere to the flasks. The control flasks also had 20ml of medium per flask to replicate the DBS treated flask conditions. The control flasks were then placed into a CO_2 incubator at 37^0C. The flasks also had a Lead inserted as a sham-treatment to confirm bio-compatibility of the Leads being used.

2.3.5. Multiple DBS Leads

Two Leads were inserted into the same T25 flask on lateral sides and the Leads were programmed independently with two distinct approaches, as shown in Figure 7., in an attempt to improve efficacy between the approaches, as well as comparatively to a single Lead approach.

2.3.6. Temperature Measurement

A temperature probe was inserted into the T25 flasks, with measurements taken no shorter than 24 hours following continuous electromagnetic treatment. Triplicate measurements were taken for each flask.

2.3.7. Voltage Measurements

A Lead was submerged in media within a standard 100mm petri dish. A digital Multimeter, MS8233D (HYLEC) was used to measure differences in electromagnetic field intensities within the petri dish. Differences in voltages throughout the dish were measured by inserting one test lead from the Multimeter into the media with the other one in contact with the work surface (Earth). The test lead was positioned next to the anode contact for the reference reading and then measurements were taken every 1cm away from the cathode contact (Centre of the petri dish). Percentage intensity was calculated by normalising measurements to the reading at the anode contact.

2.4. Analyses of DBS Treated Cells

2.4.1. Cell Storage for Further Analysis

Flasks had their growth medium removed, cells were washed with HBSS, and 3ml of Trypsin was added to each flask. Trypsinised cells were

incubated in a CO_2 incubator and incubated for 5-10 minutes at 37^0C to allow the cells to detach. The Trypsin was neutralised with 3ml of growth medium and the cells were transferred to a falcon tube. The cells were then centrifuged at 120g for 5 minutes to pellet the cells. The cell pellet was washed with PBS and then re-centrifuged at 120 x g for 5 minutes to re-pellet the cells. The cells were 'flash-frozen' in liquid nitrogen before being stored at -80^0C for future analyses.

2.4.2. Cell Count

Cells treated with DBS were counted manually with a haemocytometer. Flasks had their growth medium removed, cells were washed with HBSS, and 3ml of Trypsin was added to each flask. Trypsinised cells were incubated in a CO_2 incubator and incubated for 5-10 minutes at 37^0C to allow the cells to detach. The Trypsin was neutralised with 3ml of growth medium and the cells were transferred to a falcon tube. The cells were then centrifuged at 120 x g for 5 minutes to pellet the cells. The supernatant was removed and the pellet was suspended in minimal fresh growth medium (up to 3ml), and then cells were transferred onto a haemocytometer to be counted under a microscope.

Cells from 4 quadrants of the haemocytometer were counted and an average taken. The total amount of cells was calculated using the following calculation;

$$\textbf{Cells/ml} = \frac{\textbf{Average number of cells counted X } 10^4}{\textbf{Initial volume of cells/ml}}$$

2.4.3. Cell Viability

Cells treated with DBS had their cell viability assessed with Presto Blue. Flasks had their growth medium removed, cells were washed with HBSS, and then 1ml of Presto Blue diluted 1:10 with growth medium was added to the flasks. The flasks were then transferred to a CO_2 incubator and incubated for 30 minutes at 37^0C. Following incubation, 100µL of Presto Blue was transferred to a black-bottom 96 well plate in preparation to be analysed via UV/Vis Spectroscopy with the FLUOstar Omega (BMG

Labtech). When a reading was taken at a mid-point, excess Presto Blue was removed, the flask was washed with HBSS, and then fresh growth medium was added before resuming DBS electrical treatment.

2.4.4. DBS Intensity Titration

Cell lines were treated as described in 'Experimental Setup' with being programmed over a range of intensities to determine the most efficacious intensity for each cell line. The intensities programmed for the Leads in each experiment were 0V (Sham), 0.5V, 1.0V, 2.5V, 5.0V, and 10.0V. The intensity titration had multiple mid-points where cell viability readings were taken as detailed in 'Cell Viability', before reaching an end-point. The mid-points where viability measurements were taken was day 0, 1, 2, 5, and 7. Upon reaching the end-point of the experiment, cell viability was assessed with Presto Blue as described in 'Cell Viability' and a cell count was taken as detailed in 'Cell Count'. The most efficacious intensity was determined by comparing the viabilities of the treated cells across all the intensities to the non-treated control cells, with the lowest viability being associated with the most efficacious intensity. The frequency used for experiments using 10.0V intensities had a frequency of 130Hz and a pulse-width of 450µs.

2.4.5. DBS Frequency Titration

Cell lines were treated as described in 'Experimental Setup' with being programmed over a range of frequencies to determine the most efficacious frequency for each cell line. The frequencies programmed for the Leads in each experiment were 60Hz, 90Hz, 130Hz, 160Hz, 190Hz, 500Hz, and 1000Hz. Upon reaching the end-point of the experiment, cell viability was assessed with Presto Blue as described in 'Cell Viability' and a cell count was taken as detailed in 'Cell Count'. The most efficacious frequency was determined by comparing the viabilities of the treated cells across all the frequencies to the non-treated control cells, with the lowest viability being associated with the most efficacious frequency. The intensities used for experiments using 60-190Hz was 5.0V, and the intensity used for experiments with 500Hz and 1000Hz was 1.0V. These intensities were

selected as they were the highest intensities possible at these frequencies with our pulse generators.

2.4.6. Withdrawal Analysis

Cells treated with DBS were counted manually with a haemocytometer. Flasks had their growth medium removed, cells were washed with HBSS, and 3ml of Trypsin was added to each flask. Trypsinised cells were incubated in a CO_2 incubator and incubated for 5-10 minutes at 37^0C to allow the cells to detach. The Trypsin was neutralised with 3ml of growth medium and the cells were transferred to a falcon tube. The cells were counted as described in 'Cell Count' to quantify the cells and then the cells were then reseeded into T25 flasks in 5ml growth medium at the appropriate seeding density, as outlined in Table 3.. Untreated cells were also similarly seeded in T25 flasks in 5ml to be grown alongside treated cells. Both the treated and untreated cells were then grown for 7 days without any further electrical treatments. Following 7 days of growth the flasks had their viability measured, as described in 'Cell Viability', as well performing cell counts, as described in 'Cell Count'.

CELL LINE	SEEDING DENSITY
U87	7,000/ml
KNS42	6,000/ml
SF188	5,000/ml
GIN31	8,000/ml

Table 3. Table outlining the seeding densities of cells used in Withdrawal of TTFields experiments.

2.4.7. Flow Cytometry Cell Cycle Analysis

Cell cycle analysis was performed using flow cytometry, and Weasel V.3.1. was used to analyse the data. Cells treated with DBS were counted manually with a haemocytometer. Flasks had their growth medium removed, cells were washed with HBSS, and 3ml of Trypsin was added to each flask. Trypsinised cells were incubated in a CO_2 incubator and incubated for 5-10 minutes at 37^0C to allow the cells to detach. The Trypsin was neutralised

with 3ml of growth medium and the cells were transferred to a falcon tube. The cells were then centrifuged at 120 x g for 5 minutes to pellet the cells. The supernatant was removed and the pellet was suspended in cold PBS. The cells were then fixed with cold 70% ethanol and incubated overnight at 4°C. The fixed cells were then pelleted via centrifugation at 300 x g for 5 minutes, and the ethanol supernatant was discarded. The pellet was again, resuspended in cold PBS and repelleted via centrifugation at 300 x g for 5 minutes. The supernatant was thoroughly removed and the cell pellet was then resuspended in Propidium Iodide (PI) solution (0.1% Triton X-100, 10µg/ml PI (Molecular Probes, Inc.) and 100µg/ml DNase-free RNase A in cold PBS. The cells were then incubated at room temperature in a dark room for 30 minutes before being transferred to flow cytometry. The PI stained cells were analysed with the FC500 Flow Cytometer (Beckman Coulter) and the data was then processed with Weasel V.3.1. software.

The flow cytometry data file was opened in Weasel. A histogram was produced with the 'Histogram' feature, and a 'Cell Cycle Fit' curve was applied to the data. The percentage of the cells under the curve are used to calculate the percentage of cells in their corresponding cell cycle phase; SubG0 (Apoptotic cells), G0 (Quiescence), S (Synthesis), G2/M (Mitosis), and SuperG2 (Artefactual - where DNA content is measured above n=2).

2.4.8. DBS in Combination with Chemotherapeutics

Before treatment, an IC50 was determined for Paclitaxel, Mebendazole, and TMZ for the cell lines; SF188, KNS42, GIN28, GIN31, and U87. A cell suspension was prepared at an appropriate cell concentration as detailed in Table 4.

CELL LINE	SEEDING DENSITY
SF188	10,000/ml
KNS42	20,000/ml
GIN28	20,000/ml
GIN31	10,000/ml
U87	30,000/ml

Table 4. Table showing the seeding densities used for 48 hours IC50 experiments using 96-well plates.

These cell concentrations were selected as to allow control cells to achieve no more than ~90% confluency after 48 hours of growth. A volume of 100µL of cell suspension was pipetted into each well, and then were incubated overnight at 37^0C in an incubator to allow the cells to adhere to the plate. Following 24 hours, the growth medium was removed and replaced with growth medium and the appropriate drug concentration as described in Table 5.

DRUG	CONDITION					
PACLITAXEL	MEDIUM + DMSO	MEDIUM + 100.0nM	MEDIUM + 10.0nM	MEDIUM + 1.0nM	MEDIUM + 0.1nM	MEDIUM + 0.01nM
MEBENDAZOLE	MEDIUM + DMSO	MEDIUM + 10.0μM	MEDIUM + 1.0μM	MEDIUM + 0.5μM	MEDIUM + 0.1μM	MEDIUM + 0.01μM
TEMOZOLOMIDE	MEDIUM + DMSO	MEDIUM + 2.0μM	MEDIUM + 1.0μM	MEDIUM + 0.5μM	MEDIUM + 0.25μM	MEDIUM + 0.1μM

Table 5. Table showing the drug concentrations used to produce a dose-response curve used for 48 hours IC50 experiments using 96-well plates.

The cells were incubated for 48 hours at 37^0C in an incubator. Cell viability was measured via Presto Blue following 48 hours of treatment. Growth medium was removed from each of the wells and then Presto Blue diluted 1:10 with growth medium was added to the wells. The 6-well plates were then transferred to a CO_2 incubator and incubated for 30 minutes at 37^0C. Following incubation, the 100μL Presto Blue was transferred to a black-bottom 96 well plate in preparation to be analysed via UV/Vis Spectroscopy. The cell viability values obtained from the spectroscopy was used to produce a dose-response curve with Graphpad Prism V.7. in order to calculate an IC50.

DBS experiments were run as described in the section 'Experimental Setup' but with alterations to the growth medium used. All of the flasks were run at 10V, 130Hz and 450μs pulse width for a 5 day treatment. The 6 conditions used were; DBS treated without drug, DBS treated with high dose drug, DBS treated with low dose drug, no DBS without drug, no DBS with high dose drug, and no DBS with low dose drug. Cell viability was then assessed, as described in 'Cell Viability', and then the efficacy of the

DBS with/without the additional drug additions was compared to the non-DBS treated cells with/without the additional drug additions.

3. Deep Brain Stimulation Results and Discussion

3.2. Electric fields delivered from DBS leads reduce metabolic activity in a voltage dependent manner in GBM cell lines

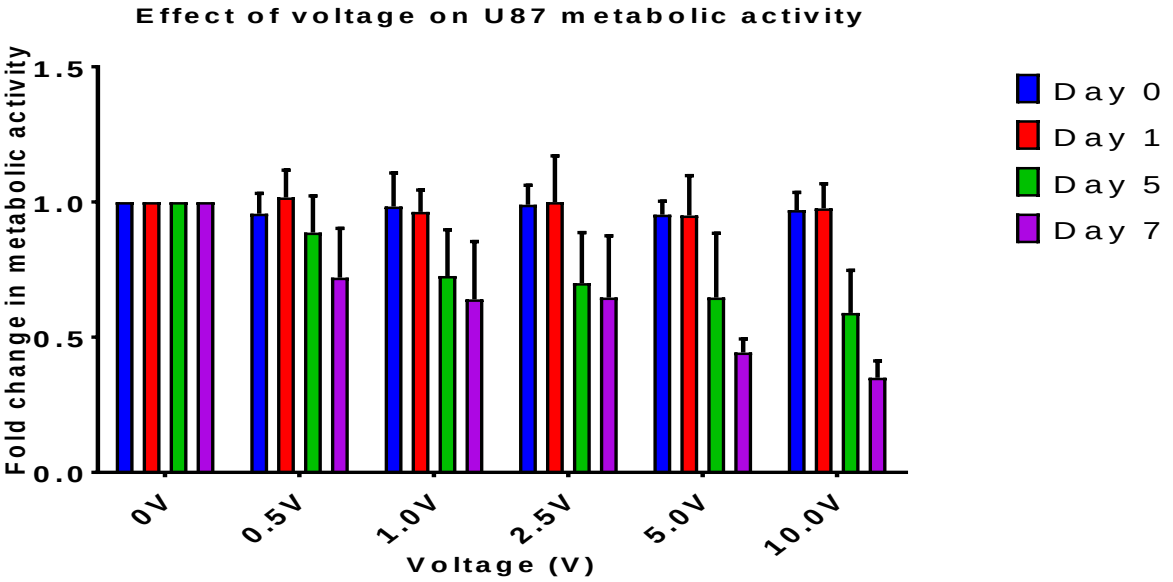
3.2.1. Results

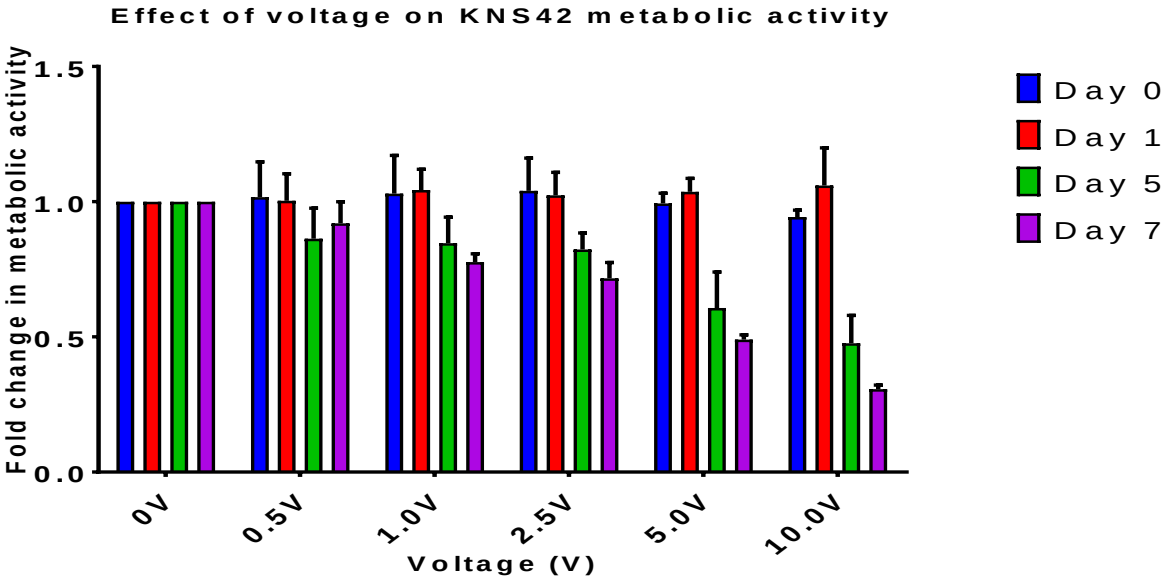
First, we had to determine the optimum parameters for DBS electric fields treatment. We ran a panel of voltages; 0V, 0.5V, 1.0V, 2.5V, 5.0V and 10.0V, against a representative cohort of GBM cell lines; U87, GIN-5, GIN-31, KNS42 and SF188. These voltages covered the range of intensities which could be delivered from the Medtronic pulse generators at a frequency of 130Hz and a pulse-width of 450μs – a frequency chosen as to its clinical relevance with neuromodulation therapy. GBM cell lines were treated with DBS electric fields for 7 days with their metabolic activity being measured intermittently at day 0, 1, 5, and 7 in order to determine the field intensity which had the greatest effect on the cell lines, as well as addressing the effect of treatment duration on the efficacy of DBS electric fields. Higher intensities, as well as a longer duration of treatment, were correlated with the greatest reduction in metabolic activity at the end-point across all cell lines. The reductions in viability following a 7 day treatment at 10.0V/130Hz/450μS were; 65% ($p=<0.0001$; two-way ANOVA) for U87 cells, 69% ($p=<0.0001$; two-way ANOVA) for KNS42 cells, 65% ($p=<0.0001$; two-way ANOVA) for SF188 cells, 39% ($p=<0.0001$; two-way ANOVA) for GIN-5 cells, and 30% ($p=<0.0001$; two-way ANOVA) for GIN-31 cells (Figure 7.).

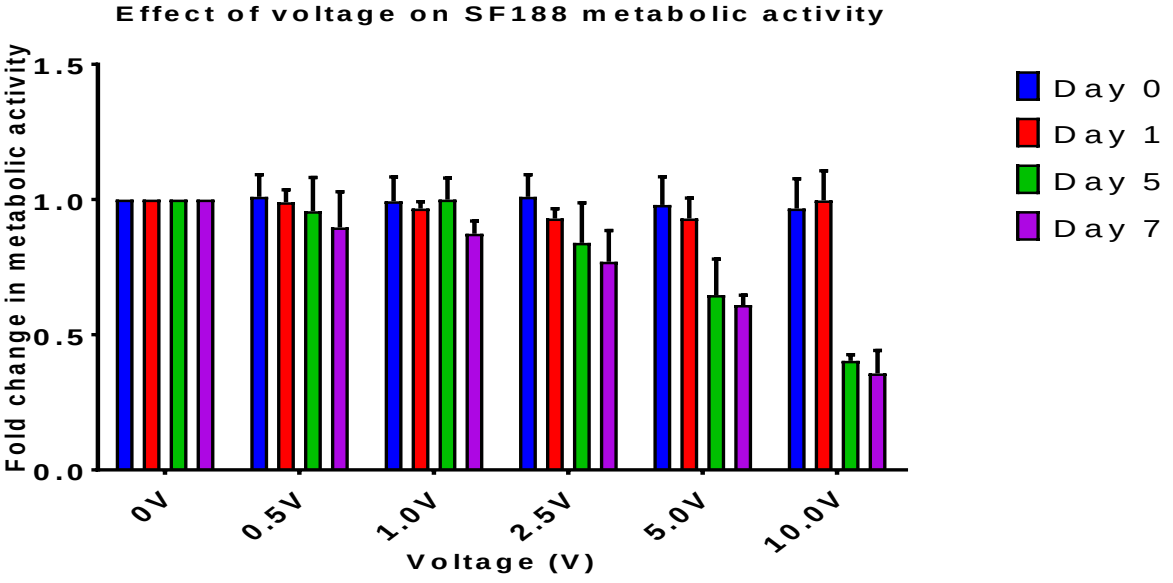
3.2.2. Discussion

We found that DBS electric fields demonstrated efficacy across all of our GBM cell lines, however, the major difference between our work and the previous IMT-130 study is the length of the experiments and the range of intensities used. IMT-30 was reported to have significant efficacy at the 24 hour and then 96 hour treatment while using electric fields at a 4.0V intensity (Xu et al., 2016). None of our cell lines tested showed any significant effect after 24 hours of treatment regardless of intensity. This

may in part be due to differences in initial seeding densities, as our experiments were run over 7 days – the initial seeding density had to be lower than that used by Xu and colleagues. The differences in seeding densities may produce differences in mitotic activity, particularly at the start-point of the experiments. This gives validity to the hypothesis that electric fields perpetuate their effects on actively dividing cells. It's also noteworthy that both the GIN-5 and GIN-31 primary cell lines did not become significantly affected by the DBS electric fields until day 7, this may be a consequence of a relatively much slower doubling time compared to the other cell lines tested and potentially being more representative of patient tumours. This was also contrary to IMT-130 treatment of patient derived cell lines, which were affected at all time points, however, profiles of the primary cell lines in the study were not provided so they may be significant different from our invasive margin derived GIN cell lines. Interestingly, there appears to be no significant difference between a 5.0V treatment and a 10.0V treatment over a 7 day treatment for our commercial lines, however, a significant difference arises within our primary GIN-5 and GIN-31 cell lines, 27% and 19% ($p=<0.0001$ and $p=0.0041$, Ordinary two-way ANOVA) respectively. This may be a consequence of the limited volume of cell culture flasks used, higher intensity electric fields may still be more clinically relevant.


Effect of voltage on U87 metabolic activity
Fold change in metabolic activity
1.5
1.0
0.5
0.0
0V
0.5V
1.0V
2.5V
5.0V
10.0V
Voltage (V)
Day 0
Day 1
Day 5
Day 7


Effect of voltage on KNS42 metabolic activity
Fold change in metabolic activity
1.5
1.0
0.5
0.0
0V
0.5V
1.0V
2.5V
5.0V
10.0V
Voltage (V)
Day 0
Day 1
Day 5
Day 7


Effect of voltage on SF188 metabolic activity
Fold change in metabolic activity
1.5
1.0
0.5
0.0
0V
0.5V
1.0V
2.5V
5.0V
10.0V
Voltage (V)
Day 0
Day 1
Day 5
Day 7

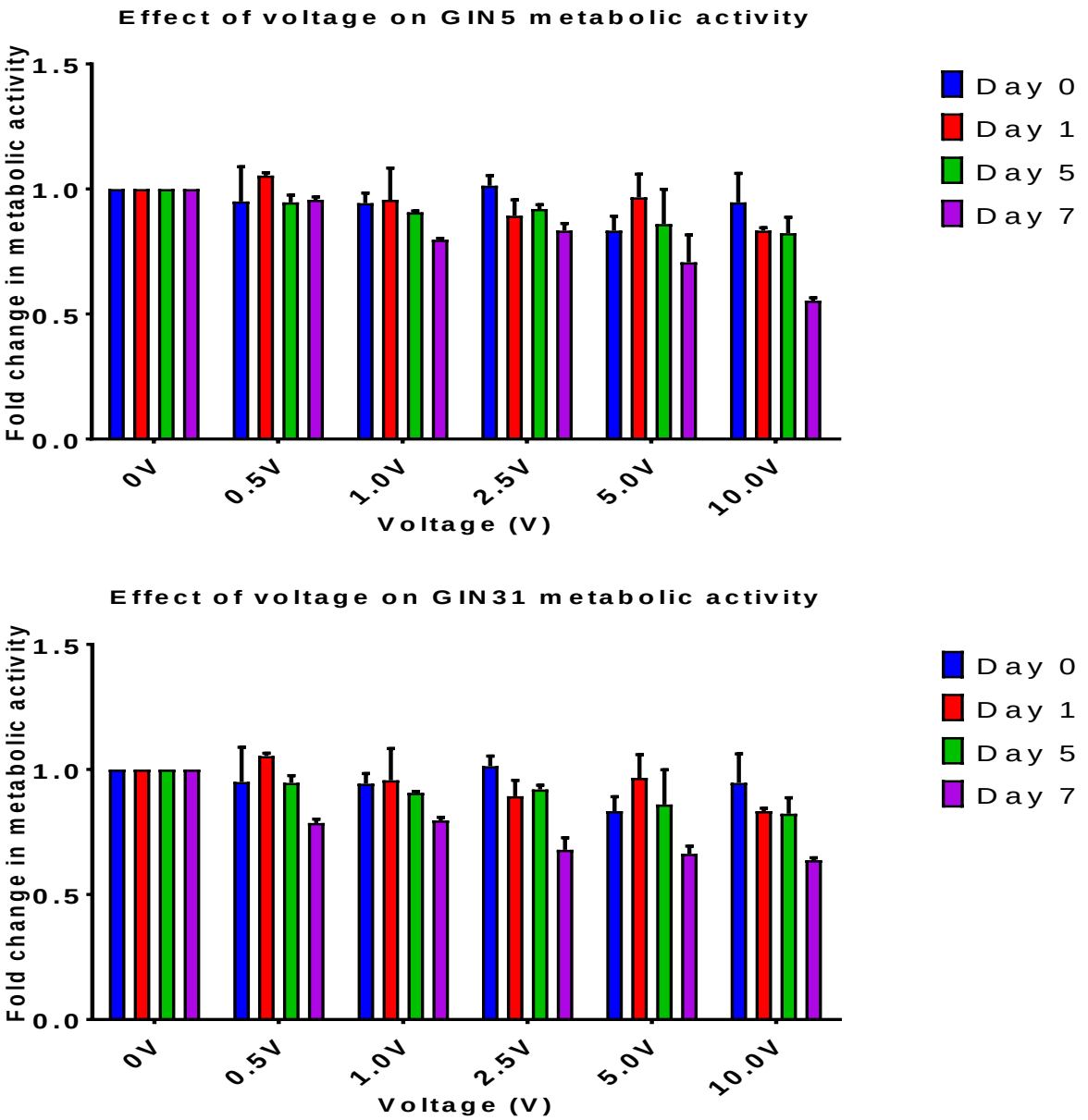


Figure 7. The effects of DBS delivered electric fields on U87, KNS42, SF188, GIN-5 and GIN-31 cell lines. Metabolic activity was assessed with Presto Blue assay and normalised to 0V sham control. Cells were treated with DBS electric fields over a panel of voltages at 130Hz and with a 450µs pulse width for 7 days, with assessment of metabolic activity taken on day 0, 1, 5 and the end-point of day 7 with the Presto Blue assay.

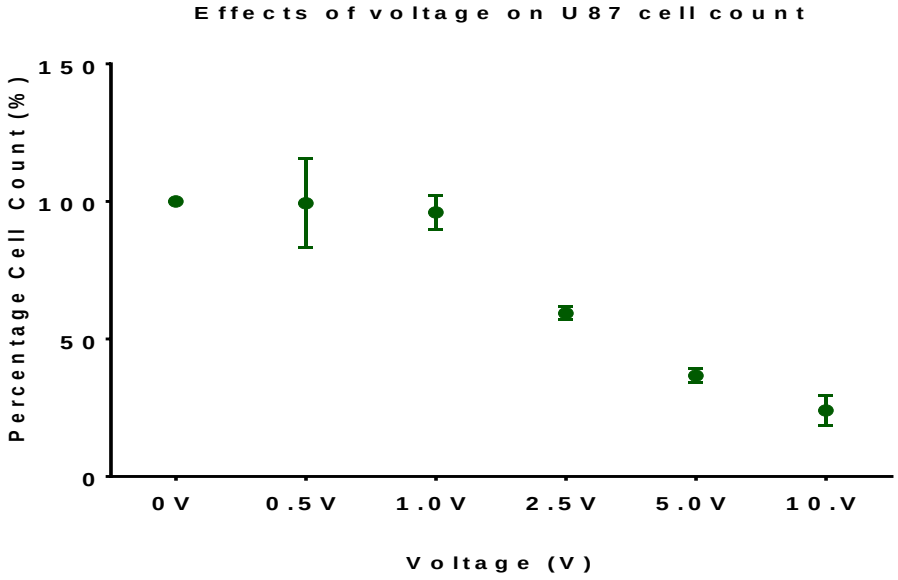
3.3. Electric fields delivered from DBS Leads reduce cell counts in GBM cell lines in a voltage dependent manner

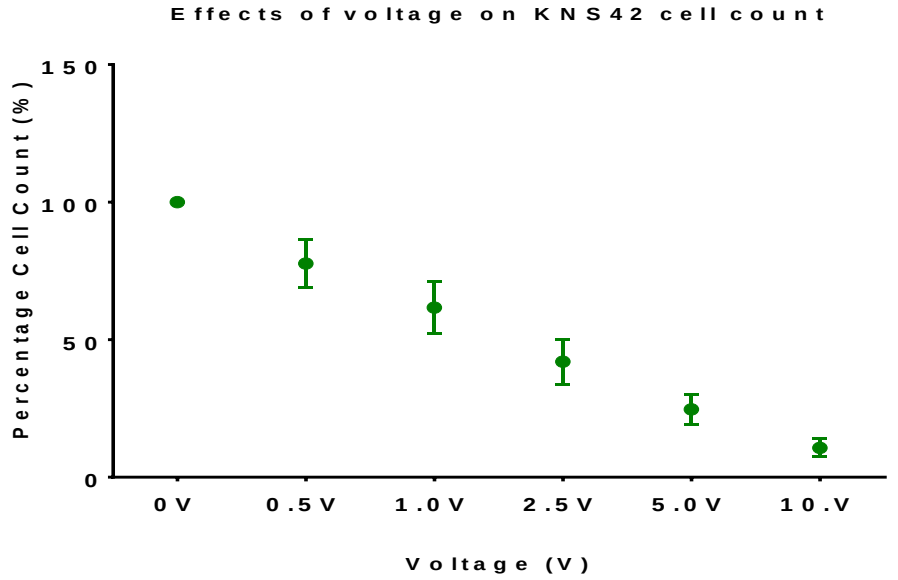
3.3.1. Results

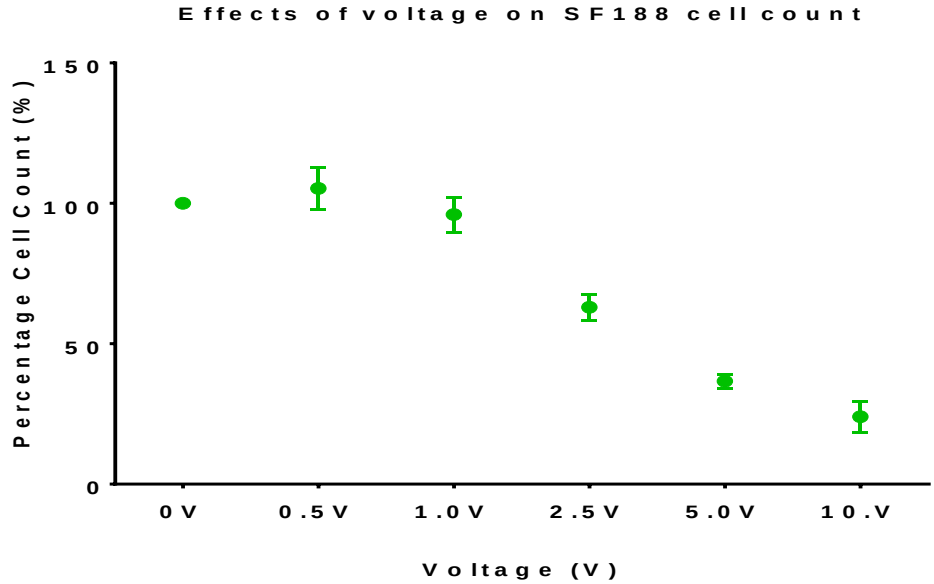
We next investigated how electromagnetic treatment would influence cell counts of GBM cell lines, as well as how this correlated with previous observations of reductions in metabolic activity, and cell counts were taken via haemocytometer. The reductions in cell counts were correlated with the reductions seen in metabolic activities across all cell lines, with a maximum reduction of cell count occurring following a 10.0V/130Hz/450μS treatment; a reduction of 85% ($p=<0.0001$; Unpaired t-test) in U87 cells, 89% ($p=<0.0001$; Unpaired t-test) reduction in KNS42 cells, ($p=<0.0001$; Unpaired t-test) in U87 cells, 76% ($p=<0.0001$; Unpaired t-test) reduction in SF188 cells, and 64% ($p=<0.0001$; Unpaired t-test) reduction in GIN-5 cells (Figure 8.).

3.3.2. Discussion

As with previous observations, there appeared to be no significant difference between 5.0V and 10.0V treatments at the 7 day time-point for our commercial lines, but a difference of 21% ($p=<0.0001$) was seen between 5.0V and 10.0V for the GIN-5 primary cell line. We also observed that the cell counts between the regions of the flask were variable, and there was a significant correlation between the distance of the region from the Lead and the greater amount of cells counted. Together, these observations confirm the correlation between cell viability and cell count in our cell lines, as well as that there may be a reduction in the intensity of the electric fields throughout the flask.


Effects of voltage on U87 cell count
Percentage Cell Count (%)
150
100
50
0
0V
0.5V
1.0V
2.5V
5.0V
10.V
Voltage (V)


Effects of voltage on KNS42 cell count
Percentage Cell Count (%)
150
100
50
0
0V
0.5V
1.0V
2.5V
5.0V
10.V
Voltage (V)


Effects of voltage on SF188 cell count
Percentage Cell Count (%)
150
100
50
0
0V
0.5V
1.0V
2.5V
5.0V
10.V
Voltage (V)

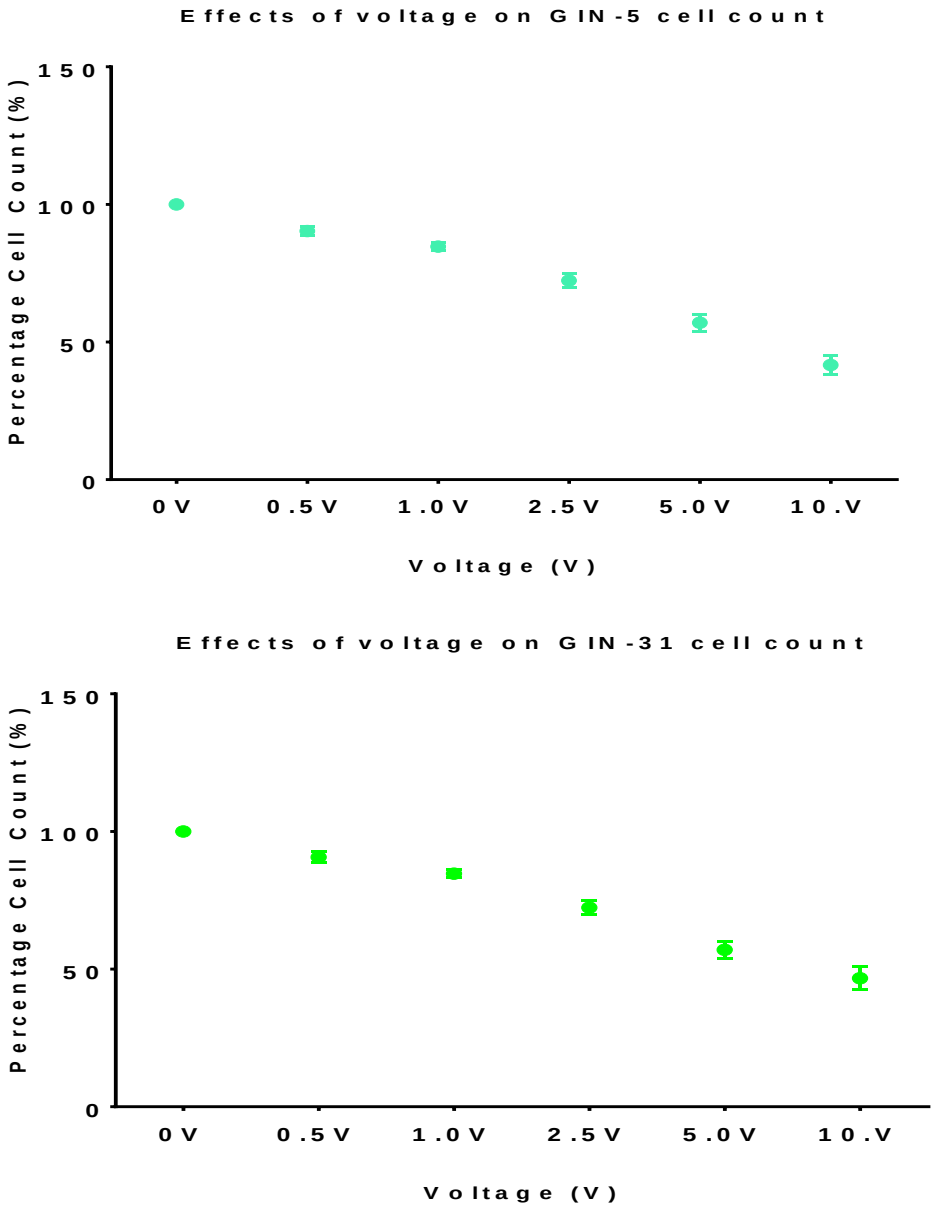


Figure 8. The effects of DBS delivered electric fields on U87, KNS42, SF188, GIN-5 and GIN-31 cell lines. Cell counts were performed with haemocytometer and normalised to 0V sham control. Cells were treated with DBS electric fields over a panel of voltages at 130Hz and with a 450μs pulse width for 7 days, with cell counts performed at the end-point.

3.4. The frequency of electric fields delivered from DBS leads has a profound effect on the metabolic activity of GBM cell lines

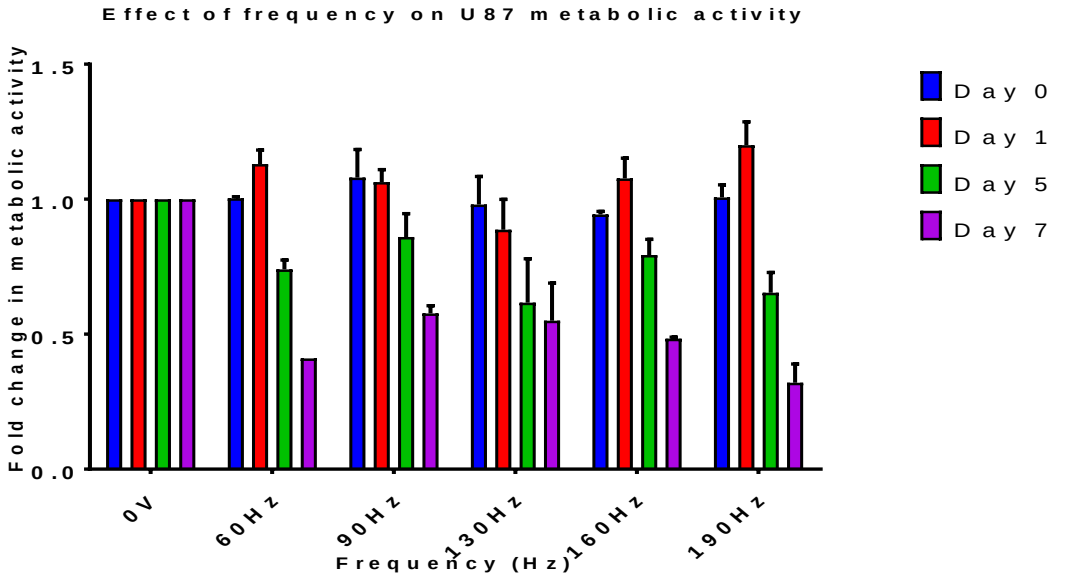
3.4.1. Results

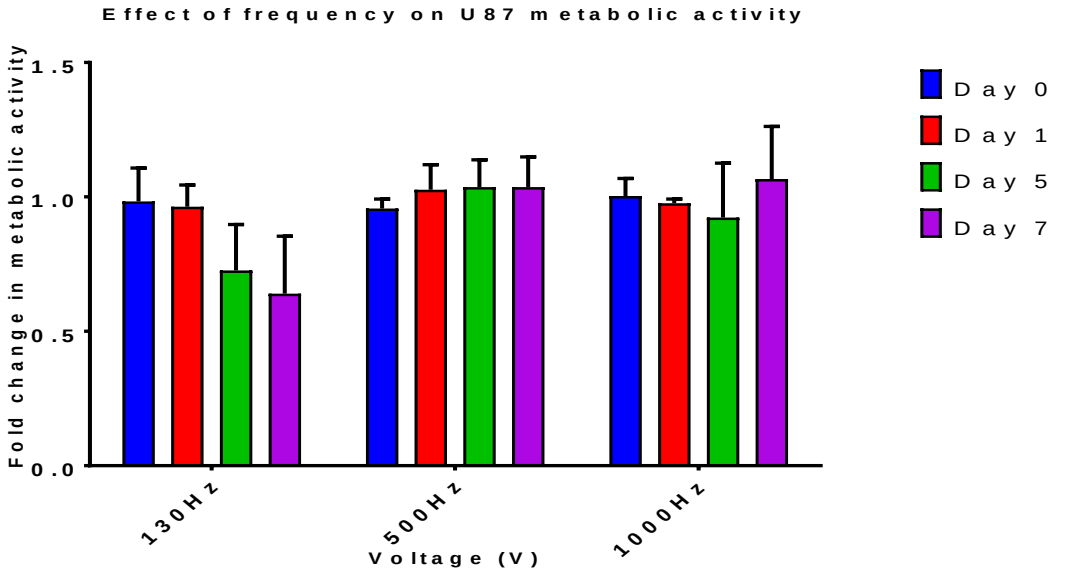
We next decided to investigate the influence of frequency on cell viability at an intensity shown to be effective. The panel of frequencies selected was; 60Hz, 90Hz, 130Hz, 160Hz, 190Hz, 500Hz and 1000Hz, in order to cover a spectrum of clinically relevant frequency parameters (60Hz, 90Hz, 130Hz, 160Hz, 190Hz) as well as frequencies outside what is therapeutically relevant (500Hz and 1000Hz). Cells again were treated for 7 days, with the 'clinical' frequencies run at 5.0V and the 'non-clinical' frequencies run at 1.0V, as these intensities were the highest possible programmed voltages from the pulse generators. Frequencies bordering on the limits of clinically relevant, 60Hz and 190Hz, were correlated with the greatest reduction in metabolic activity at end-point across the U87 (60%, p=<0.0001 and 65%, p=<0.0001, respectively) and SF188 (58%, p=<0.0001 and 71%, p=<0.0001, respectively) cell lines. Relative to treatment with 130Hz, these reductions translate to a further reduction in U87 (15% and 20%, respectively, however did not achieve significance) and SF188 (19%, p=0.0081 and 32%, p=<0.0001). These frequencies tested all followed the time-dependent manner of effect as previously shown with 130Hz. No reduction in metabolic activity was seen for the 500Hz and 1000Hz treated cells relative to untreated cells. The U87 and SF188 cell lines were used as they've shown efficacy at 7 days with both 1.0V and 5.0V DBS electric fields in previous experiments (Figure 9.).

3.4.2. Discussion

We tested frequencies outside the threshold of clinically relevant for DBS purposes (~130Hz) (Agnesi et al., 2013) to test whether the effects of DBS electric fields were frequency specific. Of particular interest were the experiments performed at 1000Hz as this frequency is above the threshold of stimulating neurons (Agnesi et al., 2013). However, these experiments demonstrated no significant efficacy, as did the 500Hz experiments either. These frequencies were only able to be delivered at an intensity of 1.0V

(an intensity shown to have very little efficacy in previous experiments), as the DBS pulse generators used were not designed to deliver such high frequencies and intensities. It would be interesting to observe the effects of these frequencies using devices capable of delivering these electrics with adequate intensity as frequencies as the frequencies diverging away from 130Hz appeared to have greater efficacy in our U87 and SF188 cell lines in a time-dependent manner, reinforcing the emphasis on a chronic treatment.


Effect of frequency on U87 metabolic activity
Fold change in metabolic activity
1.5
1.0
0.5
0.0
0V
60Hz
90Hz
130Hz
160Hz
190Hz
Frequency (Hz)
Day 0
Day 1
Day 5
Day 7


Effect of frequency on U87 metabolic activity
Fold change in metabolic activity
1.5
1.0
0.5
0.0
130Hz
500Hz
1000Hz
Voltage (V)
Day 0
Day 1
Day 5
Day 7

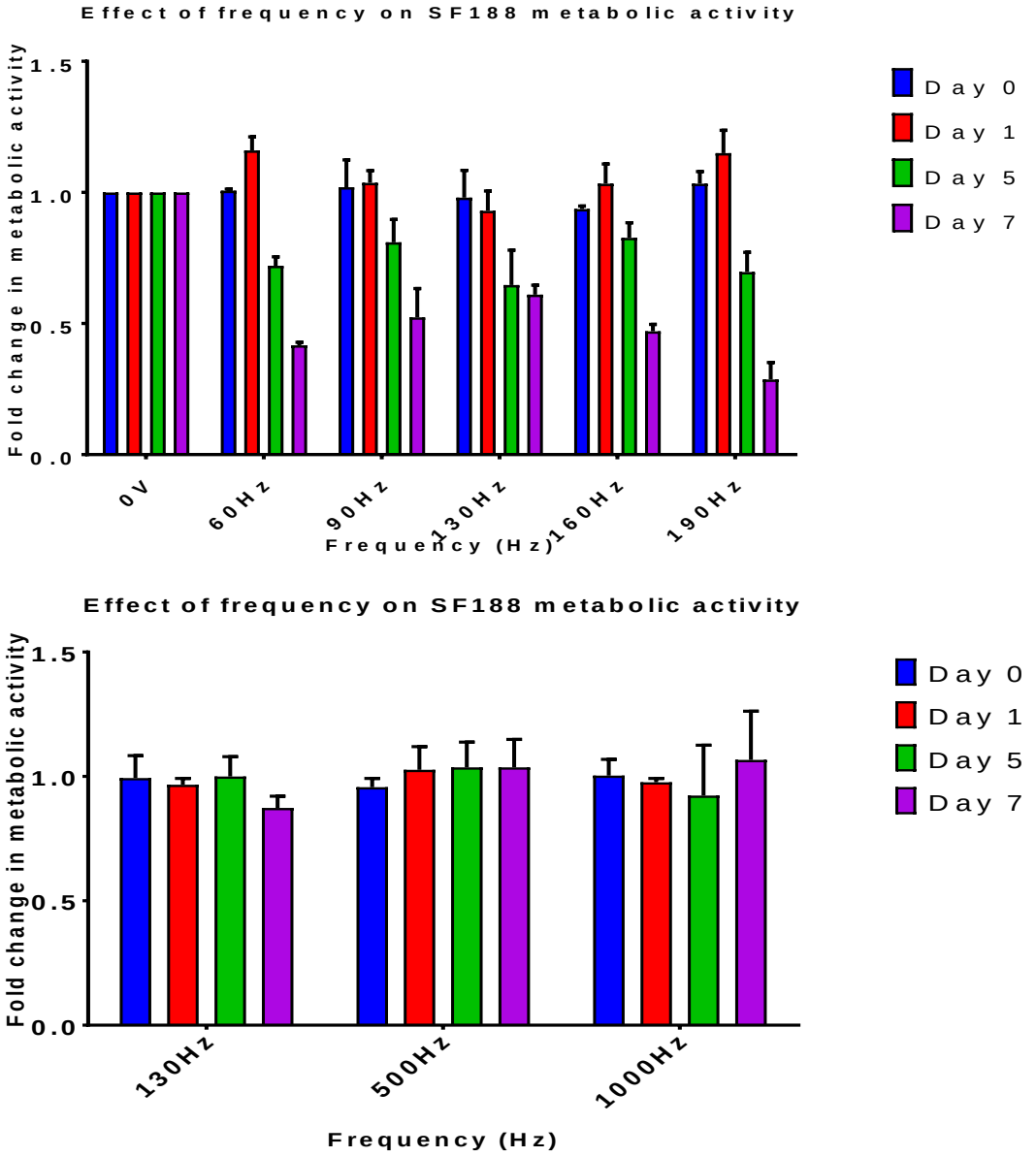


Figure 9. The effects of the higher and lower frequency DBS delivered electric fields on U87 and SF188 cell lines. Metabolic activity was assessed with Presto Blue assay and normalised to 0V sham control cells. Cells were treated with electric fields at 5V over a panel of frequencies; 60Hz, 90Hz, 130Hz, 160Hz, and 190Hz. DBS electric fields at 500Hz and 1000Hz were delivered at 1.0V and compared to 1.0V/130Hz/450µs treatment. An intensity of 5V and 1.0V was selected as it had been previously shown to be significantly effective on all cell lines (Higher intensities were not selected as the pulse generators could not be programmed across all frequencies at such a high intensity). Cells were treated with DBS electric fields for 7 days, with assessment of metabolic activity taken on day 0, 1, 5 and the end-point of day 7 with the Presto Blue assay.

3.5. Electric fields delivered from DBS Leads demonstrate efficacy against Ependymoma and Medulloblastoma cell lines

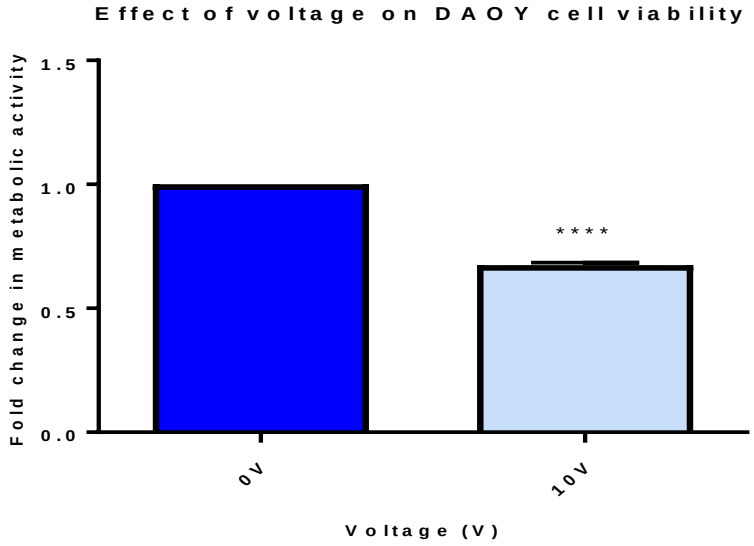
3.5.1. Results

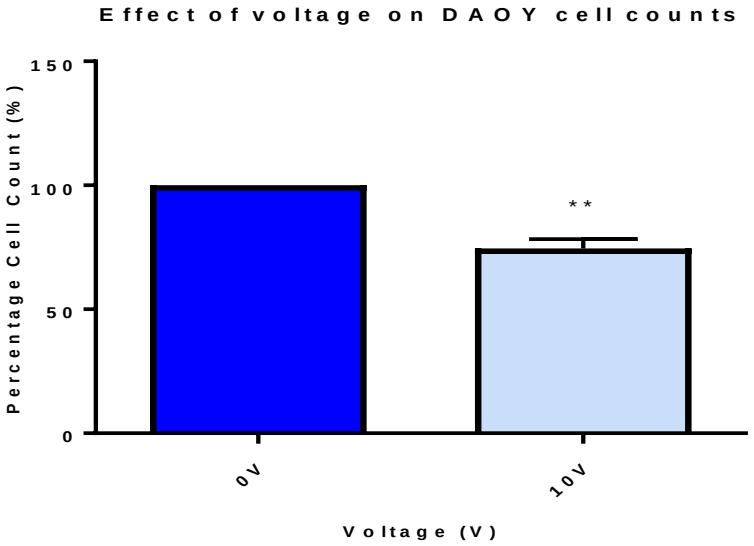
We next investigated whether the efficacy of DBS electric fields was restricted to GBM cell lines. We tested electric fields at 10.0V/130Hz/450μS pulse-width for a 7 day treatment on the Ependymoma and Medulloblastoma cell lines BXD-1425EPN and DAOY, respectively. Both cell lines were susceptible to the DBS electric fields, but at varying degrees. BXD-1425EPN cells were highly affected by the DBS treatment with a reduction in viability of 84% ($p=0.0001$, unpaired t-test) and a reduction in cell count counted via haemocytometer of 80% ($p=0.0006$, unpaired t-test). DAOY cells were less affected by the treatment, with a reduction in viability of 23% ($p=0.0009$, unpaired t-test) and a reduction in cell count counted via haemocytometer of 26% ($p=0.0218$, unpaired t-test). These two cell lines were chosen as the growth rates of both cell lines are comparable, as it has been shown that slower growing cell lines are typically less affected, but there is a clear difference in efficacy achieved (Figure 10.).

3.5.2. Discussion

Previous literature on various electric fields has demonstrated efficacy in multiple tumour types (Kirson et al., 2009d, Kirson et al., 2004, Voloshin et al., 2016, Xu et al., 2016, Sebastiano et al., 2018), and our data show that brain tumour cell lines other than GBM cell lines may be susceptible to DBS electric fields at 10.0V/130Hz/450μS. There was a strong correlation between the doubling time of our GBM cell lines and their responsiveness to DBS electrical treatment in previous experiments, however, observations with these cell lines is counter to previous data. Both the BXD-1425EPN and DAOY cell lines have doubling times comparable to the SF188 GBM cell lines (~18 hours), but their responsiveness was highly variable; EPN-1425EPN had a ~20% reduction in cell viability and DAOY had ~60% less of a reduction in cell viability, relative to SF188 cells. These data highlight how factors other than cell

cycling and doubling time may account for the responsiveness to DBS electric fields, such as genetics and ion channel expression. Literature has identified a plethora of dysregulated ion channels in gliomas (Pollak et al., 2017, Litan and Langhans, 2015, Molenaar, 2011), but such extensive characterisation has not been produced for Medulloblastoma. These differences in ion channel expression, and clear differences in tumour genetics (Brennan et al., 2013a, Kool et al., 2012, Godfraind et al., 2012), may produce varying membrane potential dependencies of this potential for cell cycle progression, and ultimately varying degrees of a viable target for DBS electric field therapy.


Effect of voltage on DAOY cell viability
Fold change in metabolic activity
1.5
1.0
0.5
0.0
****
0V
10V
Voltage (V)


Effect of voltage on DAOY cell counts
Percentage Cell Count (%)
150
100
50
0
**
0V
10V
Voltage (V)

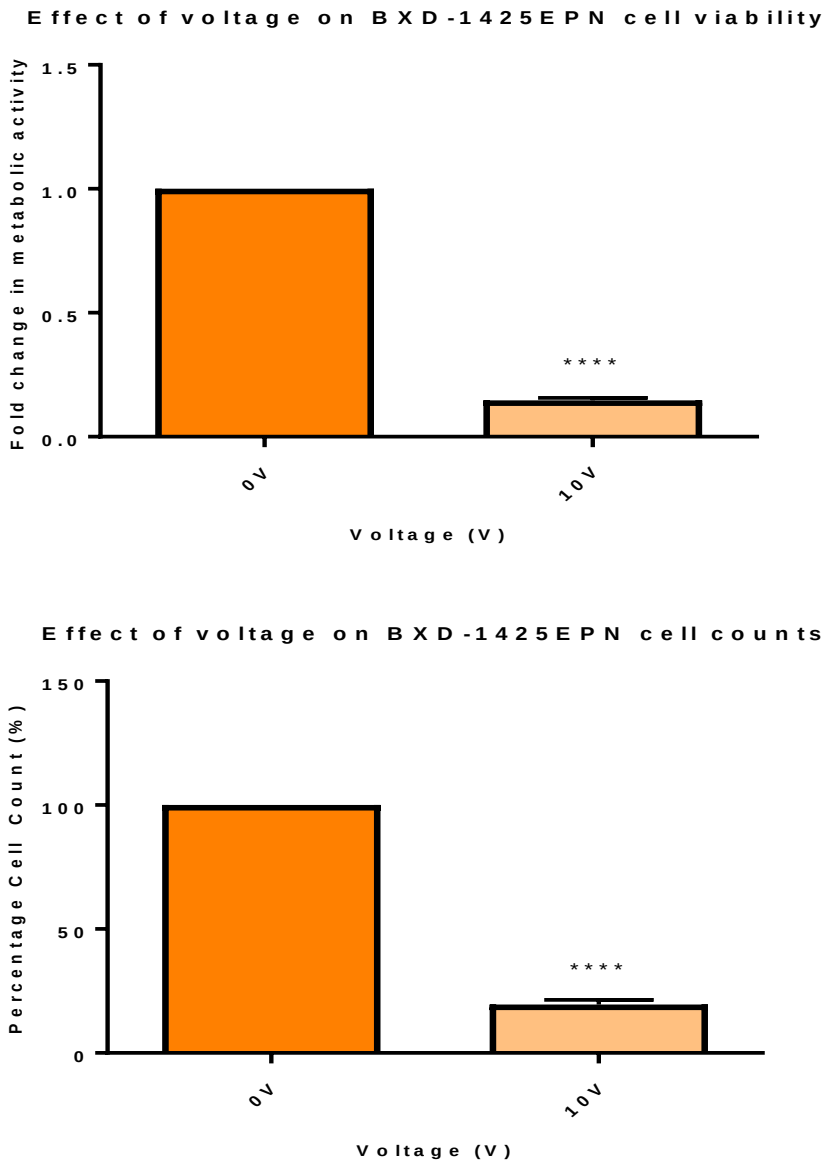


Figure 10. The effects of DBS delivered electric fields on BXD-1425 and DAOY cell lines. Metabolic activity was assessed with Presto Blue and cell counts performed with haemocytometer and normalised to 0V sham control. Cells were treated with 10V/130Hz/450µs for 7 days, with measurements taken at the end-point.

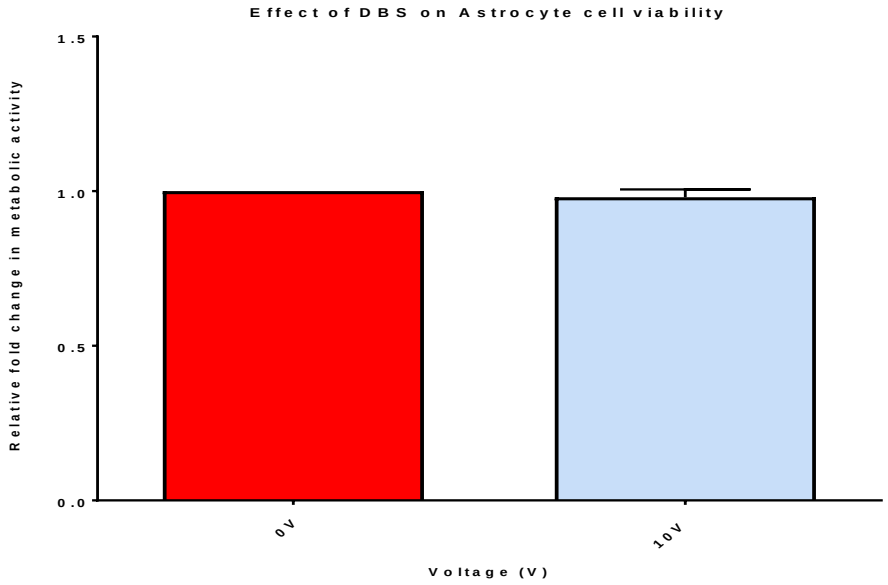
3.6. Electric fields delivered from DBS Leads has no effect on cell viability of non-dividing H1-hESC-derived Astrocytes

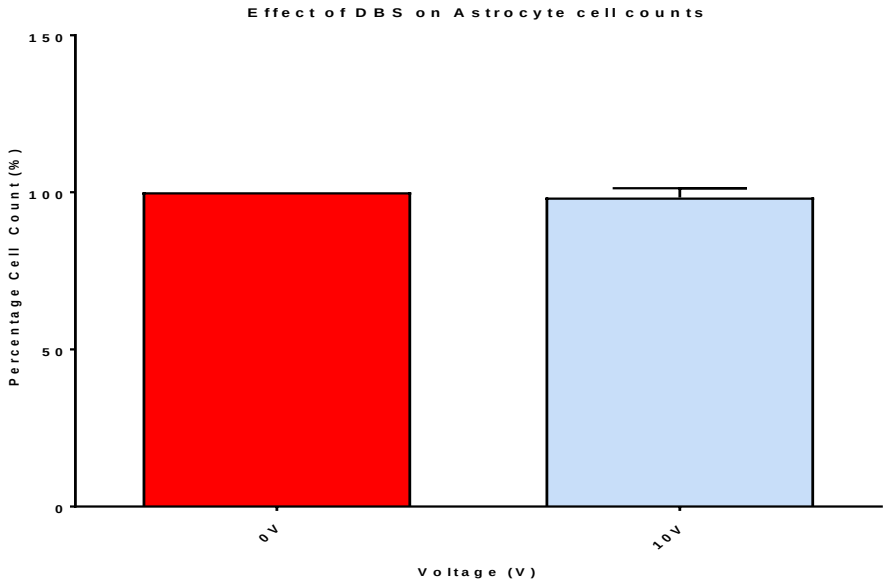
3.6.1. Results

Following showing efficacy of DBS electric fields on a panel of GBM, Ependymoma and Medulloblastoma cell lines, we assessed the effect of DBS electric fields on non-dividing astrocytes to determine whether an actively dividing cell was a necessity for effective DBS treatment. We derived non-dividing astrocytes from H1-hESC cells and subjected the cells to a 7 day DBS electric treatment at 10.0V/130Hz/450µS pulse-width, followed by a Presto Blue assay for assessment of cell viability and a cell count relative to the control cells. Both the cell viability assay and cell counts showed that DBS electric fields did not prove to be cytotoxic to the non-dividing astrocytes. We also performed the same experiment with dividing neural stem cells, which were also differentiated from H1-hESC cells. The cell viability measurements showed a reduction of 64% ($p=<0.0001$; Unpaired t-test) following the DBS treatment, and the cell count reduction reflected this with a reduction of 59% ($p=<0.0001$; Unpaired t-test) (Figure 11.).

3.6.2. Conclusion

Previous reports have hypothesised that an actively dividing cell is the target of electric field treatment (Kirson et al., 2004), and few reports have shown how these treatments have little to no efficacy on non-dividing cells (Xu et al., 2016, Sebastiano et al., 2018, Kirson et al., 2004, Jo et al., 2018). Our data demonstrates how DBS electric field treatment at 10.0V/130Hz/450µS had no effect on cell viability or cell count on our astrocyte cell line, where the treatment had significant effect on our neural stem cell line. Given that our astrocytes were derived from the neural stem cell line, these data further demonstrates how DBS electrical treatment targets actively dividing cells, not just cancer cells specifically.


Effect of DBS on Astrocyte cell viability
Relative fold change in metabolic activity
1.5
1.0
0.5
0.0
0 V
10 V
Voltage (V)


Effect of DBS on Astrocyte cell counts
Percentage Cell Count (%)
150
100
50
0
0 V
10 V
Voltage (V)

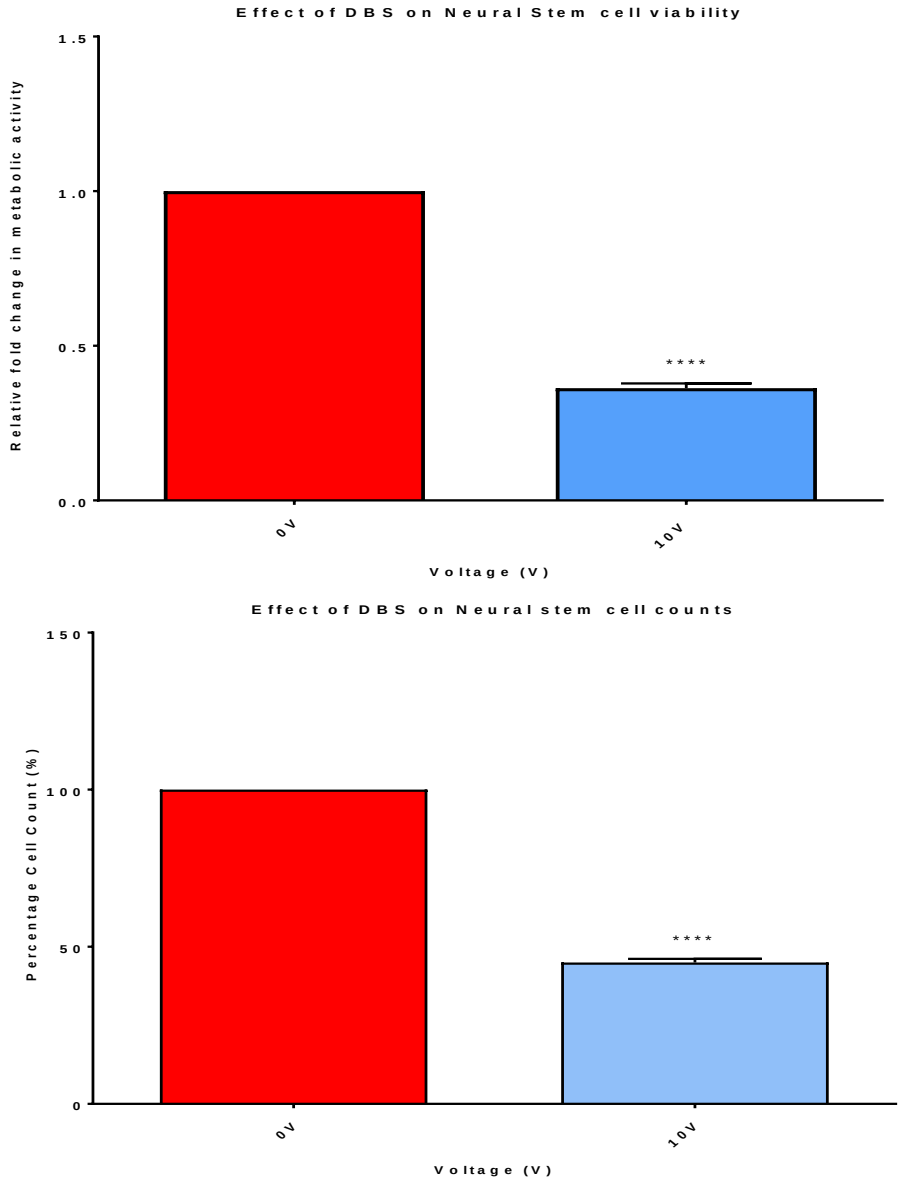


Figure 11. The effects of DBS electric fields on H1-hESC-derived astrocytes and human neural stem cell lines. Metabolic activity assessed with Presto Blue assay and cell counts measured with haemocytometer normalised to 0V control cells. Cells were treated with 10V/130Hz/450μs DBS electric fields for 7 days with measurements taken at the end-point.

3.7. Efficacy of DBS electric fields treatment may be increased with the addition of multiple DBS Leads

3.7.1. Results

Following observations of the variance of DBS electric fields intensity throughout a cell culture flask, and the appearance of greater efficacy within closer-proximity to the Lead, we sought to improve efficacy through using multiple Leads within a single flask. We inserted two Leads into a single T25 flask and introduced DBS electric treatment at 10.0V/130Hz/450µS pulse-width for 7 days, and compared to a SHAM-control flask as well as a flask treated with a single Lead at 10.0V/130Hz/450µS pulse-width. Indeed, efficacy was significantly increased relative to a single Lead by introducing a second Lead into the flask. Relative to a single Lead, the cell lines U87, SF188, and GIN-31 had a decrease in cell viability of 12% ($p=0.0062$, ordinary one-way ANOVA), 25% ($p=0.0021$, ordinary one-way ANOVA), and 11% ($p=<0.0001$, ordinary one-way ANOVA), respectively (Figure 12.).

3.7.2. Discussion

We tested the efficacy benefits of a multiple DBS Lead approach as this may be of greater clinical importance as multiple leads may be used in the clinic potentially without any compounding toxicities, as well as potentially producing a larger area of effect. As with previous observations, the efficacy of the DBS treatment with multiple Leads was correlated with the growth rate of the cell line used, with the fastest growing cell line – SF188, having a greater response to the multiple Lead treatment relative to the slowest growing cell line – GIN-31. Overall, multiple DBS Leads produced a more efficacious treatment relative to a single Lead approach. We also investigated different programming approaches with these experiments as detailed in Figure 13., however, no significant difference between the approaches was seen with regards to efficacy in vitro. These distinct programming approaches were used to confirm the hypothesis that DBS electric fields, unlike TTFields (Kirson et al., 2007, Giladi et al., 2015c), are not axis dependent to exhibit efficacy. This was to be expected as the

frequency used with DBS electric fields is too low to physically interact with polar molecules as TTFields does (Gera et al., 2015, Giladi et al., 2015c).

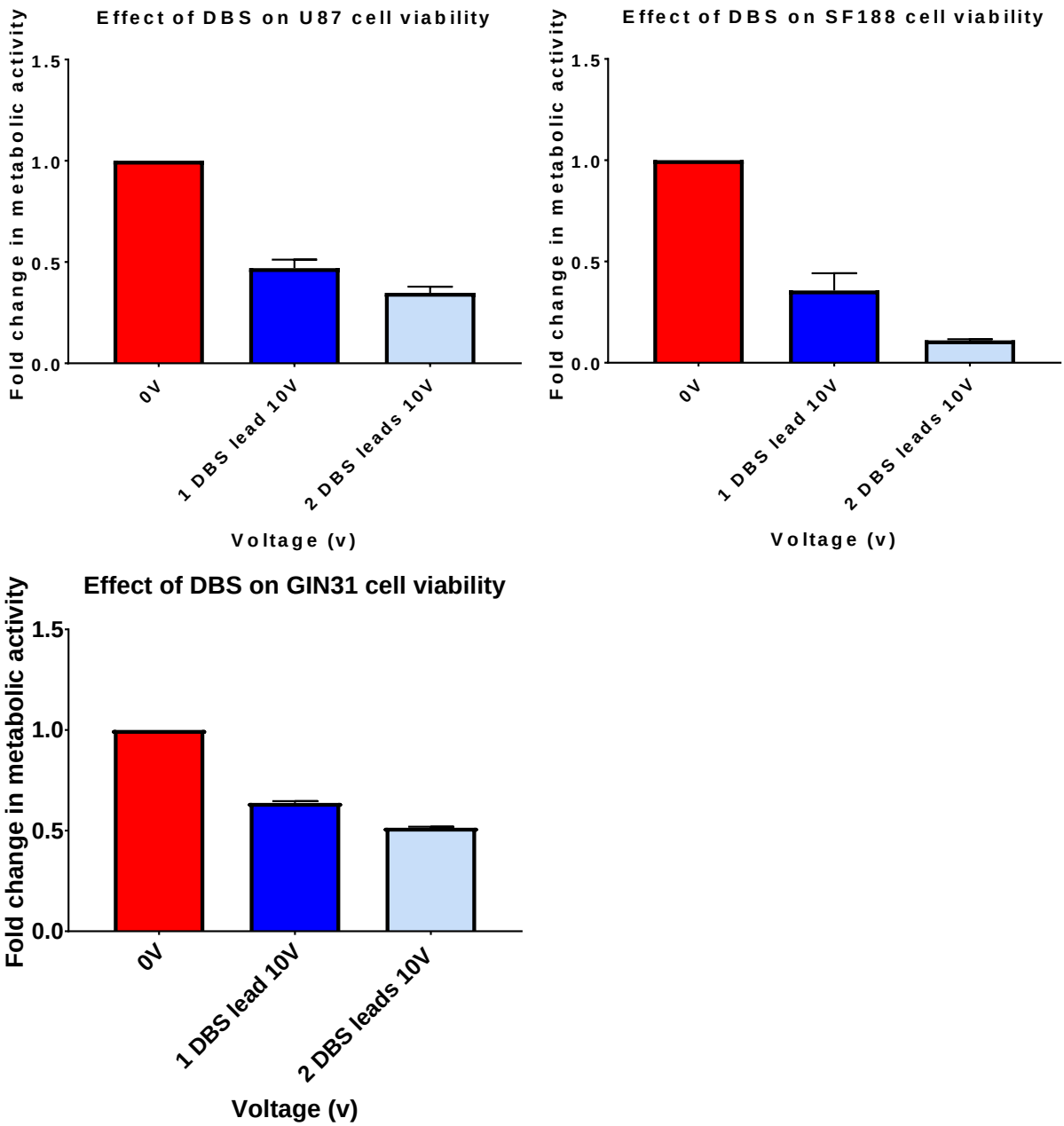


Figure 12. The effects of multiple DBS Leads delivering electric fields on U87, SF188 and GIN-31 cell lines. Metabolic activity assessed with Presto Blue assay and normalised to 0V control cells. Cells were treated with 10V/130Hz/450µs DBS electric fields for 7 days with measurements taken at the end-point.

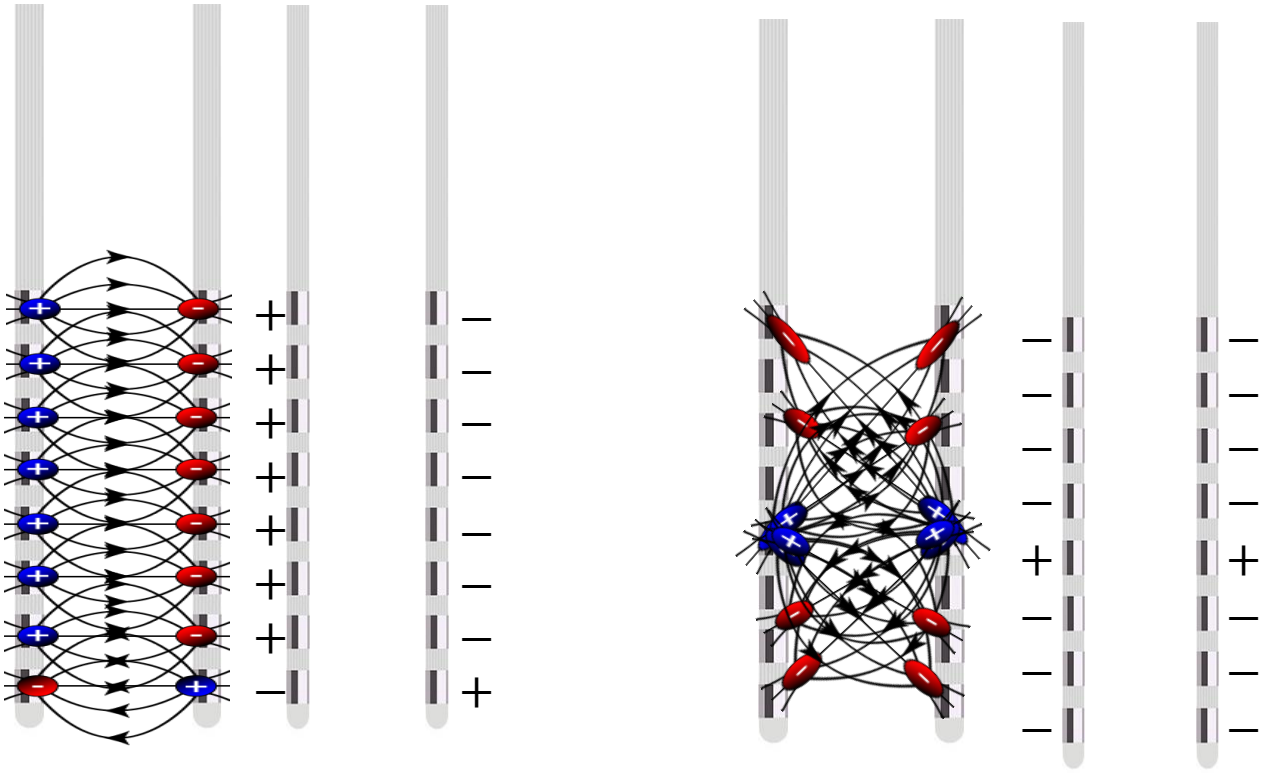
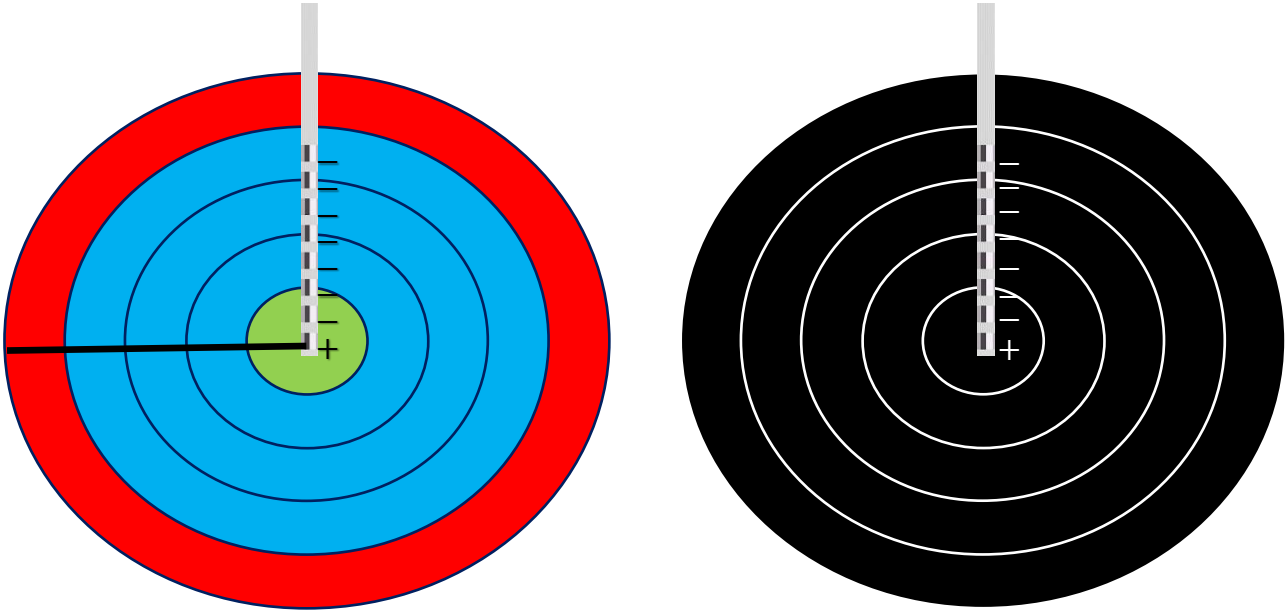


Figure 13. The different programming strategies and their proposed electric field mappings. Each strategy was programmed in a bipolar configuration with varying numbers of cathode and anode contacts to manipulate the field intensities along the contacts.

3.8. Electric fields delivered from DBS Leads reduce in intensity throughout the cell culture flasks

3.8.1. Results and Discussion

Given the previous observations in the reduction in efficacy of the DBS electric fields relative to the distance away from the Lead, we investigated as to whether the intensity of the electric fields did indeed reduce throughout the cell culture flasks. We used a 10cm petri dish, which has a greater surface area than the T25 flasks used, containing medium in order to fully submerge the Leads. The stimulator was run at; 10.0V/130Hz/450μS, 5.0V/60-190Hz/450μS, and 1.0V/500-1000Hz/450μS pulse-width and the relative intensity of the electric fields was measured with a multimeter in 1cm increments from the Lead to the edge of the petri dish (Figure 14.). The measurements confirmed that the relative intensity of the electric fields delivered at 10.0V/130Hz/450μS and 5.0V/60-190Hz/450μS pulse-width should fall no more than 20% within the T25 flasks, given that the distance of the 20% reduction is greater than what is possible within the T25 flasks used. However, the measurements also confirmed that the intensity of the electric fields delivered at 1.0V/500-1000Hz/450μS did not resonate within the petri dish, as only a reading could be taken when the Lead was physically in contact with the multimeter. These data do not rule out efficacy of 500-1000Hz frequency electric fields having efficacy, but does confirm that electric fields at these frequencies cannot be delivered at a high enough intensity to have efficacy from our Medtronic neurostimulators. It is also worth noting that the electrical resistance of the human brain is likely to be greater than that of the culture medium, thus limiting the spread of the electric field.



Intensity: 5.0V

Frequency: 60-190Hz

Pulse Width: 450µs

Intensity: 1.0V

Frequency: 500-1000Hz

Pulse Width: 450µs

KEY: 100% Intensity / 90% Intensity / 80% Intensity / 0% Intensity

Figure 14. The intensity of DBS electric fields within a petri dish relative to the distance from the cathode contact of the Lead. Due to technological constraints, DBS electric fields could only be delivered at 5.0V for 60-190Hz (Left) and 1.0V for 500-1000Hz (Right). The key denotes the colours associated with the measured relative intensity of the electric field. The Petri dishes used had a diameter of 5cm and the increments shown in the diagrams are of 1cm intervals.

3.9. Electric fields delivered from DBS Leads have lasting effects on growth rates of GBM cell lines

3.9.1. Results

We next tested the hypothesis that there was no long-term effect of treatment on cells associated with electrical fields treatment unlike traditional chemotherapies. Cells were treated with DBS electric fields at 10.0V/130Hz/450μS for 7 days, and then were re-seeded against control cells. The previously treated cells had further electric treatment withdrawn, and these cells were grown alongside the control cells for a further 7 days before cell viability analysis. Interestingly, the withdrawn cells expressed significantly reduced growth rates following extended DBS treatment, with reductions in viability of 43% in U87 ($p=0.0099$, paired t-test), 41% in KNS42 ($p=0.0011$, paired t-test), and 33% in GIN-31 ($p=0.0179$, paired t-test) cell lines (Figure 15.).

3.9.2. Discussion

It is well known that chemotherapies exhibit long-term effects on cells following withdrawal, but the notion of an electrical current having long-term effects is not well defined. However, data suggests a reduction in clonogenic potential of various TTFields treated cancer cell lines (Silginer et al., 2017, Giladi et al., 2017). Our data also shows that although there is no defined half-life associated with DBS electric fields per se, the mechanism of action may remain active for some time following the treatment. A clear mechanism of action that still remain active following DBS electric field treatment is still to be determined. Notably, DBS electric field treatment did not result in any noticeable morphological changes of the treated cells, unlike TTFields treated cells (Gera et al., 2015), therefore it may be possible that long-term consequences of DBS treatment may be genetic as opposed to physical.

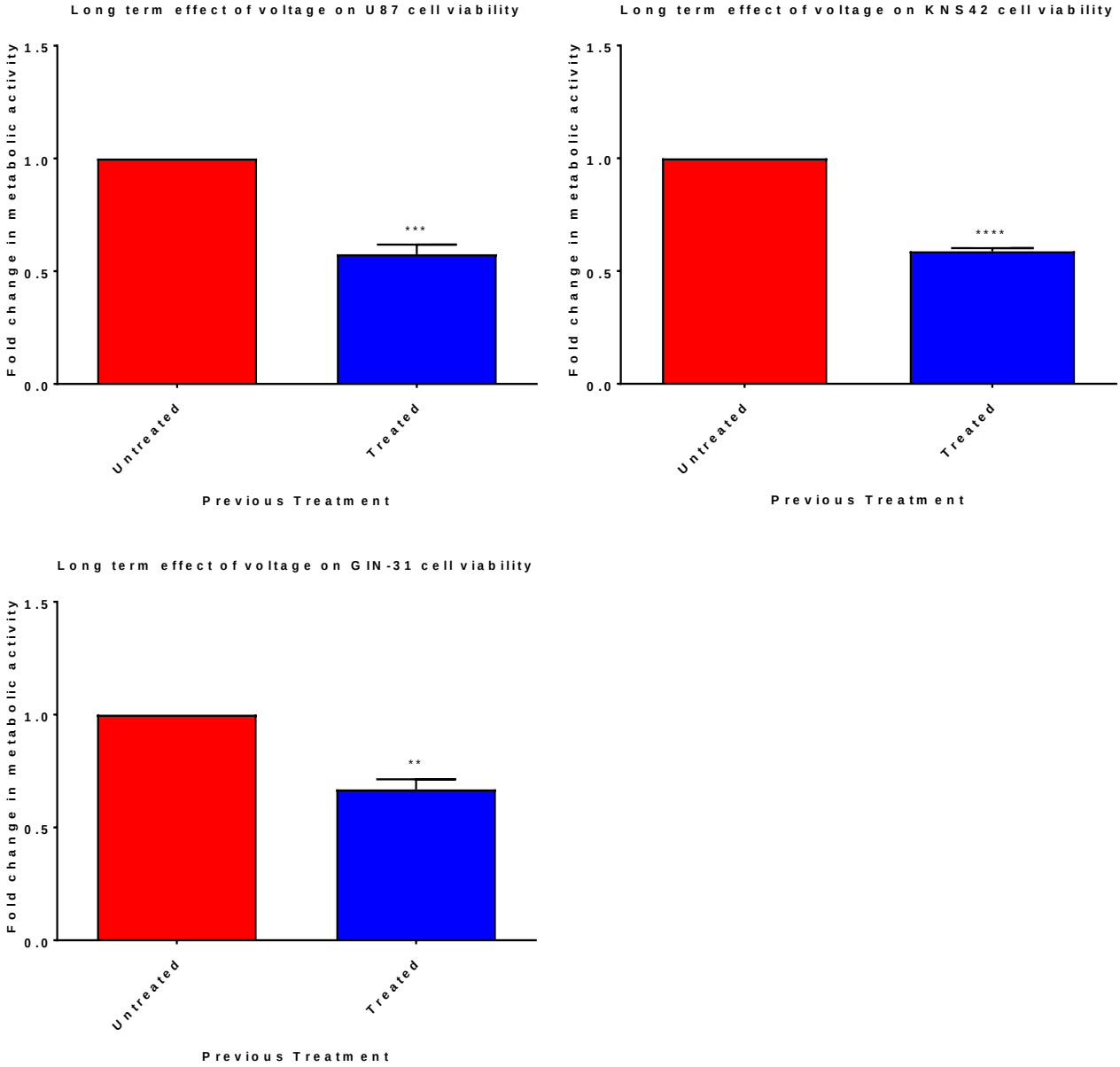


Figure 15. The long-term effects of DBS electric fields on U87, KNS42 and GIN31 cell lines. Metabolic activity assessed with Presto Blue assay and cell counts measured with haemocytometer normalised to previously non-treated 0V sham control cells. Treated cells were treated with 10V/130Hz/450µs DBS electric fields for 7 days, before being re-seeded against non-treated cells, and then grown without further treatment for 7 days with measurements taken at the end-point.

3.10. Electric fields delivered from DBS Leads do not cause temperature increases within cell culture flasks

3.10.1. Results and Discussion

We next looked into possible mechanisms for the previous observations on the effects of DBS electric fields on GBM cells. So we decided to first measure the temperature of all the flasks used to rule out heating as a mechanism of action. All flasks used were measured to average a temperature of 37^0C following no less than 24 hours of continuous treatment at 10.0V/130Hz/450µS, so reductions in cell viability can be concluded to not be a result of heating from the DBS electric fields (Figure 16.).

FLASK	No Wire	0V (SHAM)	0.5V	1.0V	2.5V	5.0V	10.0V
TEMPERATURE (^{0}C)	37.0	37.0	37.0	37.0	37.0	37.0	37.0

Figure 16. The effects of DBS electric fields on the temperature of growth medium. Temperature measurements were taken in triplicate with a temperature probe after no shorter than 24 hours of continuous treatment.

3.11. Electric fields delivered from DBS Leads have promote G0-phase accumulation of GBM cell lines

3.11.1. Results

Given that reductions in cell viability were achieved in all cell lines with DBS treatment, we sought to further characterise this phenomenon. Cells were treated with DBS electric fields at 10.0V/130Hz/450µS for 7 days and then their cell cycle profiles were analysed using Propidium iodide staining and flow cytometry. A few key observations arose following the cell cycle analysis. Firstly, DBS treatment appears to have minimal cytotoxicity activity as shown through the lack of cell accumulation in the subG0-phase, however, U87 cell accumulation did achieve significance ($p=0.0019$, Ordinary two-way ANOVA). Secondly, there was significant G0-phase accumulation following treatment for U87, KNS42, and SF188 cells, with an increase of 15% ($p=<0.0001$, Ordinary two-way ANOVA), 14% ($p=<0.0001$, Ordinary two-way ANOVA), and 17% ($p=<0.0001$, Ordinary two-way ANOVA) respectively. Thirdly, S-phase depletion following DBS treatment was apparent in our cell lines U87, KNS42, and SF188, with a decrease of 13% ($p=<0.0001$, Ordinary two-way ANOVA), 10% ($p=<0.0001$, Ordinary two-way ANOVA), and 18% ($p=<0.0001$, Ordinary two-way ANOVA), respectively. Lastly, there was no significant effect on the G2-phase of the cell cycle following DBS treatment for any of our cell lines (Figure 17.).

3.11.2. Discussion

One of the accepted mechanisms of actions of TTFields on cancer cells is accumulation of treated cells in the G2/M phase of the cell cycle (Kessler et al., 2018). Here we have demonstrated how significantly lower frequency electric fields cause accumulation of cells in the earlier stages of the cell cycle, G0 phase, as opposed to the latter stages, G2/M phase. The lack of accumulation in the G2/M phase would most likely be due to the DBS electric fields delivered being a frequency which is too low to physically interact with mitotic proteins like electric fields in the >50KHz ranges (Gera et al., 2015, Giladi et al., 2015c). Based off this observation,

coupled with the current literature, a mechanism of action through perturbing the depolarised V_m of the cancer cells to target their hyper proliferative phenotype. Cucullo and colleagues demonstrated how stimulation of cancer cells with low frequency electric fields may reduce proliferation through an increase in expression of inwards-rectifying potassium channels (Cucullo et al., 2005a). An increase in these channels may facilitate greater influx of potassium ions into the cancer cells, which typically have a significantly reduced intracellular concentration of potassium ions (Steve Haltiwanger). It's in part the lack of intracellular potassium ions which account for the depolarised, and the subsequent proliferative state (Yang and Brackenbury, 2013), of the cancer cells. It's noteworthy that potassium efflux is an essential process to allow progression through the G1/S phase and ultimately through the mitotic cycle (Yang and Brackenbury, 2013). Thereby, we propose that the low frequency DBS electric fields may be influencing potassium influx, destabilising the depolarised V_m of the cancer cell, and thus promoting G0 phase accumulation of the treated cells.

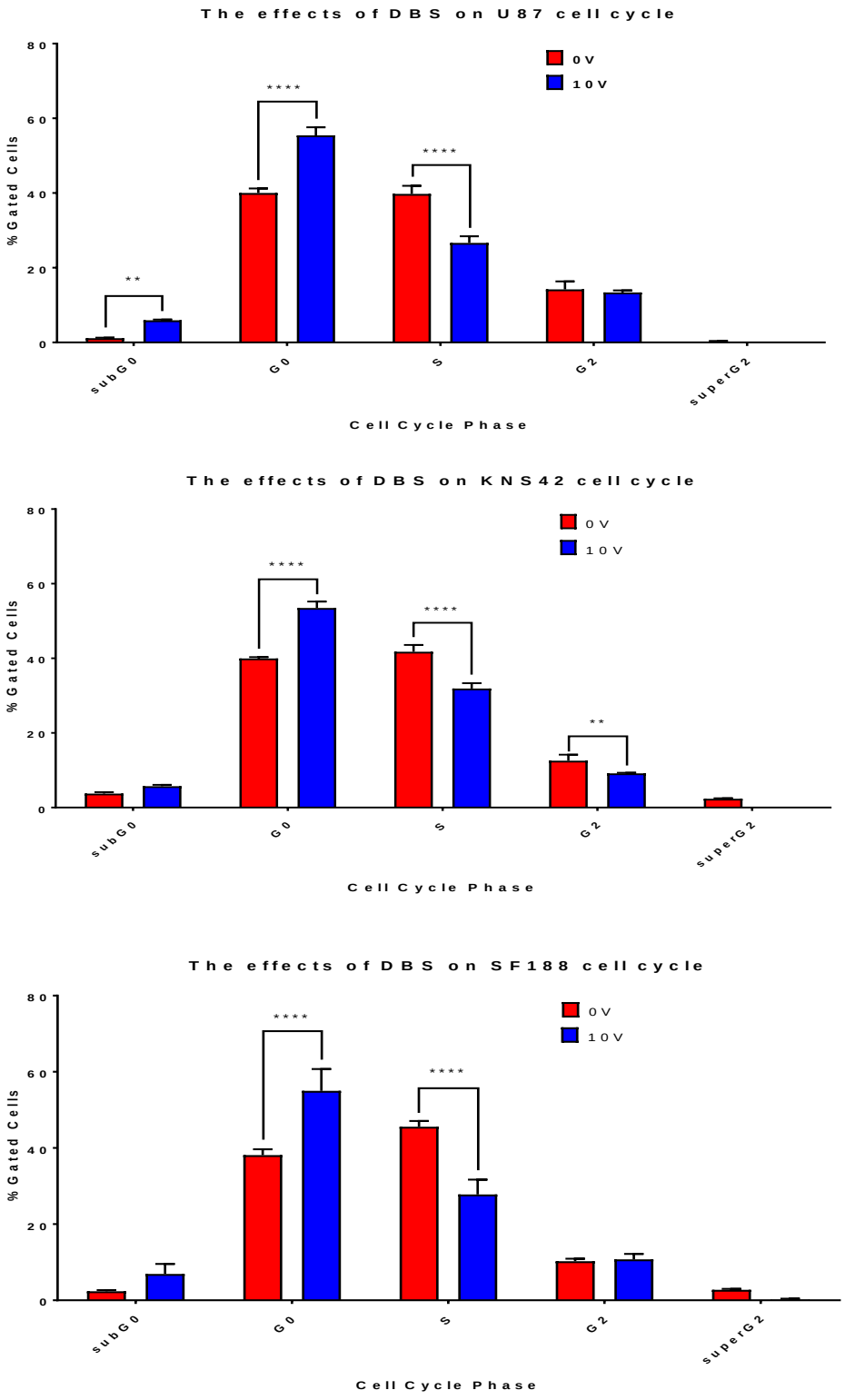


Figure 17. The effects of DBS electric fields on the cell cycling of U87, KNS42 and SF188 cell lines. Cell cycle analysis was performed via PI staining and flow cytometry with analysis with Weasel. Cells were treated for 7 days before being assessed with flow cytometry, with a minimum of 10,000 cells being analysed.

3.12. The efficacy of electric fields delivered from DBS Leads may be increased with the addition of mitotic inhibitors in GBM cell lines

3.12.1. Results and Discussion

After we established DBS treatment promoted G0-phase accumulation, we looked to further augment this with combinations of mitotic inhibitors. The mitotic inhibitors used were Paclitaxel and Mebendazole as they both targeted the latter stages of the cell cycle, the G2/M phase, this strategy allows targeting of multiple stages of the cell cycle for greater coverage. We first established the IC50 of Paclitaxel (0.36-4.6nM) and Mebendazole (0.03-1.2μM) on our cell lines and then took a lower and a higher dose and treated our cell lines as a monotherapy and in combination with DBS treatment for 5 days for comparison. We first confirmed that our cell lines were sensitive to the mitotic inhibitors used, with reductions of cell viability of 53% and 70% (p=<0.0001; ordinary one-way ANOVA) for U87 cells, 39% and 65% (p=0.0037 and p=<0.0001; ordinary one-way ANOVA) for SF188 cells, 61% and 69% (p=<0.0001; ordinary one-way ANOVA) for KNS42 cells, and 30% and 49% (p=0.0001 and p=<0.0001;ordinary one-way ANOVA) for GIN-31 cells for Paclitaxel and Mebendazole, respectively (Figure 18.).

Significant reductions in cell viability were also seen when comparing the higher and lower doses of Paclitaxel in combination with DBS treatment at 10.0V/130Hz/450μS to the Paclitaxel-alone treated flasks. The additive effect of the addition of DBS treatment netted an additional reduction in cell viability of 32% and 72% (p=0.0005 and p=<0.0001, two-way ANOVA) for U87 cells, 43% and 67% (p=0.0005 and p=0.0117, two-way ANOVA) for SF188 cells, 17% and 58% (p=0.0035 and p=<0.0001, two-way ANOVA) for KNS42 cells, and 16% and 19% (p=0.0254 and p=0.0054, two-way ANOVA). Cell viability analysis showed that DBS treatment in combination with Paclitaxel does significantly increase efficacy at higher doses, but not at the lower doses we used, with our panel of cell lines. Comparing the higher and lower doses of Paclitaxel in combination with DBS treatment at 10.0V/130Hz/450μS to untreated

controls, reductions in cell viability were recorded in U87 cells at 86% and 81% (p=<0.0001, two-way ANOVA), SF188 cells at 82% and 77% (p=<0.0001, two-way ANOVA), KNS42 cells at 78% and 71% (p=<0.0001, two-way ANOVA), and GIN-31 cells at 43% and 30% (p=<0.0001, two-way ANOVA), respectively (Figure 19.).

Using the same analysis strategy, we also looked to see how combinations with Mebendazole affected our cells. Reductions in cell viability were seen when comparing the higher and lower doses of Mebendazole in combination with DBS treatment at 10.0V/130Hz/450μS to the Mebendazole-alone treated flasks. The addition of DBS treatment to Mebendazole had an additional reduction in cell viability of 8% and 53% (p=0.0024 and p=<0.0001, two-way ANOVA) for U87 cells, 21% and 49% (p=<0.0001, two-way ANOVA) for SF188 cells, 9% and 42% (p=0.0137 and p=<0.0001, two-way ANOVA) for KNS42 cells, and 9% and 17% (p=0.0043 and p=<0.0001, two-way ANOVA) Cell viability analysis showed that DBS treatment in combination with Mebendazole does significantly increase efficacy at the higher doses used, but not at lower doses. Comparing the higher and lower doses of Mebendazole in combination with DBS treatment at 10.0V/130Hz/450μS to untreated controls, reductions in cell viability were recorded in U87 cells at 78% and 59% (p=<0.0001, two-way ANOVA), SF188 cells at 84% and 59% (p=<0.0001, two-way ANOVA), KNS42 cells at 78% and 53% (p=<0.0001, two-way ANOVA), and GIN-31 cells at 58% and 36% (p=<0.0001, two-way ANOVA), respectively. However, no significant improvements in efficacy were seen when comparing DBS treated cells at 10.0V/130Hz/450μS to DBS treated cells in combination with lower doses of Mebendazole, unlike this combination with Paclitaxel (Figure 19.).

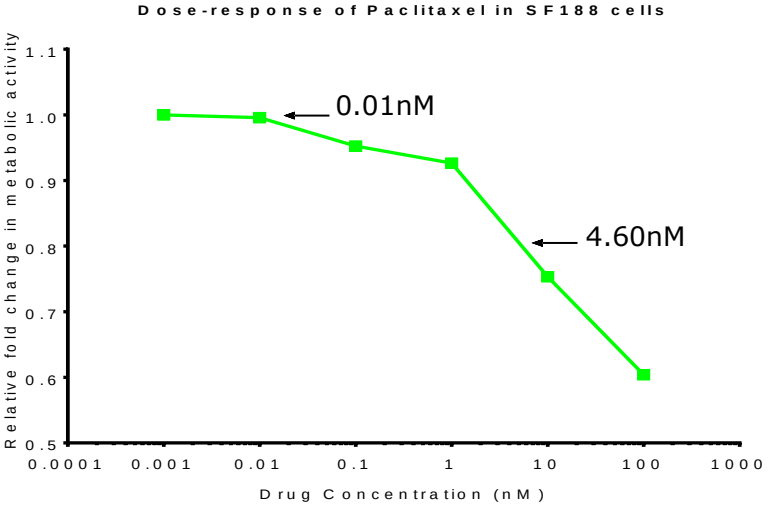
Interestingly, the combinations of DBS treatment with our lower doses of Paclitaxel produced a marginal, but significant, increase in efficacy, but this was not true for Mebendazole. The additive effect of DBS electric fields to both the lower and higher doses of Paclitaxel and Mebendazole is, however, very encouraging, as the minimal side effects associated with the therapy would reduce overlapping toxicities associated with combinational therapeutic strategies in the clinic. It is worth noting that

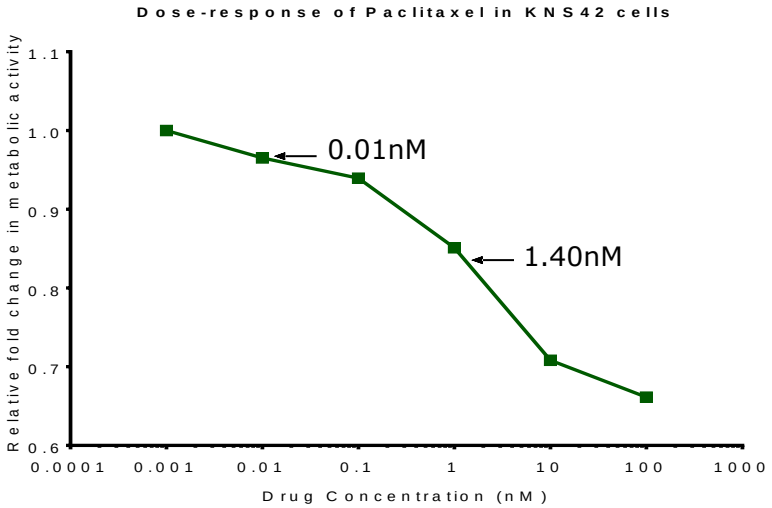
the largest increase in efficacy was DBS in combination with low dose chemotherapies compared to low dose chemotherapies alone, suggesting that low dose chemotherapies may be potentiated by DBS electric fields.

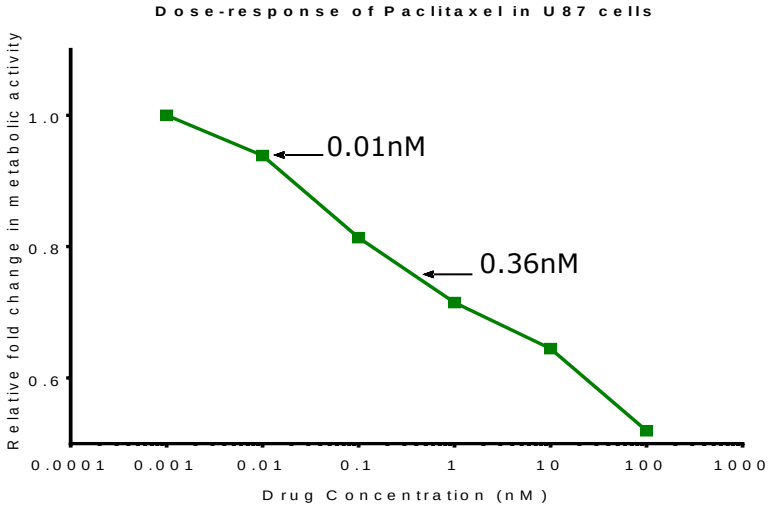
Following the treatments as monotherapies and as combinations, we analysed the cell cycling through flow cytometry of the cells to elucidate how mitotic inhibitors with and without DBS treatment affect cells with that regard. We analysed the cell cycle profile of a lower and higher dose of Paclitaxel with and without DBS treatment at 10.0V/130Hz/450μS, and a few key observations were made. Firstly, we confirmed that Paclitaxel promotes G2/M-phase accumulations when given in at a high enough dose of our GBM cell lines as expected as it functions through tubulin interaction; with U87 cells experiencing an increase of 9% ($p=0.025$; two-way ANOVA), SF188 cells having an increase of 8% ($p=0.024$; two-way ANOVA) and KNS42 cells showing an increase of 7% ($p=0.036$; two-way ANOVA). Interestingly, G0-phase accumulation as opposed to G2/M-phase accumulation was achieved with the lower dose Paclitaxel; with U87 cells experiencing an increase of 20% ($p=<0.0001$; two-way ANOVA), SF188 cells having an increase of 19% ($p=<0.0001$; two-way ANOVA), and KNS42 cells showing an increase of 19% ($p=<0.0001$; two-way ANOVA). This G0-phase accumulation appears to parallel what we've observed with DBS treatment as a monotherapy. Secondly, combining DBS with a higher dose of Paclitaxel appeared to create a significant increase in subG0-phase accumulation relative to either treatments alone, with an increase of 13% ($p=<0.0001$; two-way ANOVA) in U87 cells, 10% ($p=0.0009$; two-way ANOVA) in SF188 cells, and 9% ($p=0.0035$; to-way ANOVA) in KNS42 cells when compared to cell lines treated with high dose Paclitaxel alone. This combination did also cause a significant depletion of G0-phase accumulation, with no significant differences in accumulation in the G2/M-phase for our cells, when compared to DBS treated cells alone. Lastly, combining the lower dose of Paclitaxel with DBS treatment has no significant effect on the cell cycle, which is counter to what we see with the effects of combination with regards to efficacy (Figure 20.).

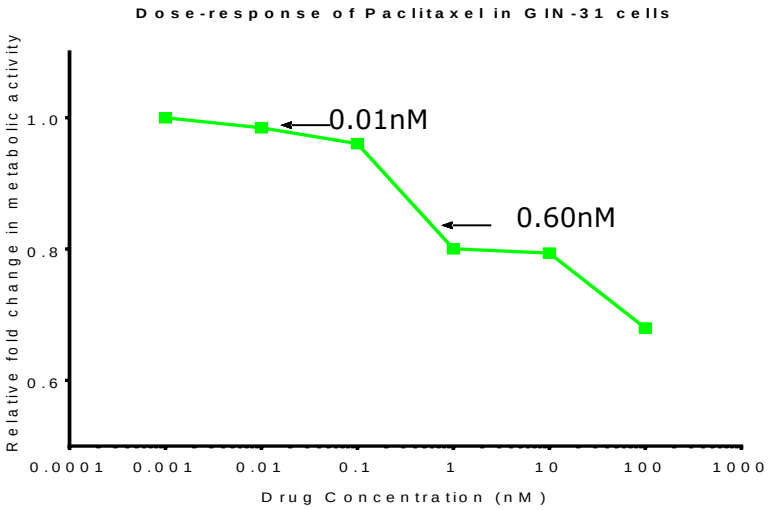
In summary, paclitaxel promotes G2-phase accumulation of our cells and combining paclitaxel to DBS promotes a significant increase in subG0-

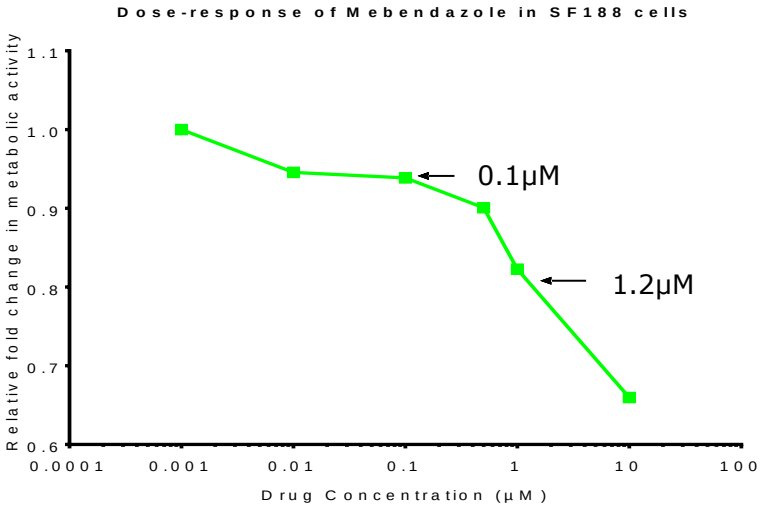
phase accumulation in addition to the G2-phase. Lastly, the lower dose of Paclitaxel used appears to cause G0-phase accumulation of cells but this did not seem to translate to a reduction in cell growth.

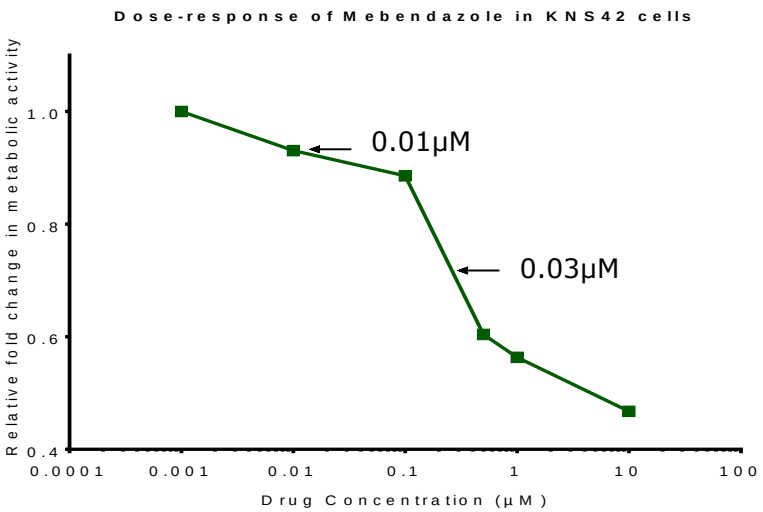

Dose-response of Paclitaxel in SF188 cells
Relative fold change in metabolic activity
1.1
1.0
0.9
0.8
0.7
0.6
0.5
0.01nM
4.60nM
0.0001
0.001
0.01
0.1
1
10
100
1000
Drug Concentration (nM)

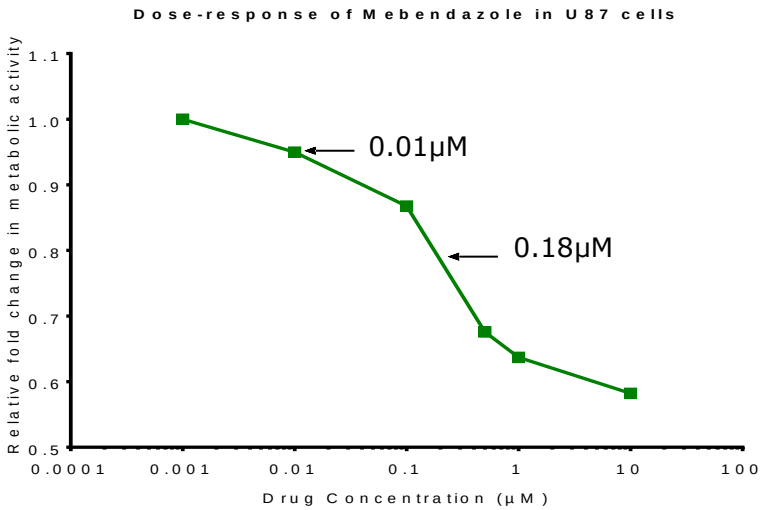

Dose-response of Paclitaxel in KNS42 cells
Relative fold change in metabolic activity
1.1
1.0
0.9
0.8
0.7
0.6
0.01nM
1.40nM
0.0001
0.001
0.01
0.1
1
10
100
1000
Drug Concentration (nM)


Dose-response of Paclitaxel in U87 cells
Relative fold change in metabolic activity
1.0
0.8
0.6
0.01nM
0.36nM
0.0001
0.001
0.01
0.1
1
10
100
1000
Drug Concentration (nM)


Dose-response of Paclitaxel in GIN-31 cells
Relative fold change in metabolic activity
1.0
0.8
0.6
0.01nM
0.60nM
0.0001
0.001
0.01
0.1
1
10
100
1000
Drug Concentration (nM)


Dose-response of Mebendazole in SF188 cells
Relative fold change in metabolic activity
1.1
1.0
0.9
0.8
0.7
0.6
0.1μM
1.2μM
0.0001
0.001
0.01
0.1
1
10
100
Drug Concentration (μM)


Dose-response of Mebendazole in KNS42 cells
Relative fold change in metabolic activity
1.0
0.8
0.6
0.4
0.01μM
0.03μM
0.0001
0.001
0.01
0.1
1
10
100
Drug Concentration (μM)



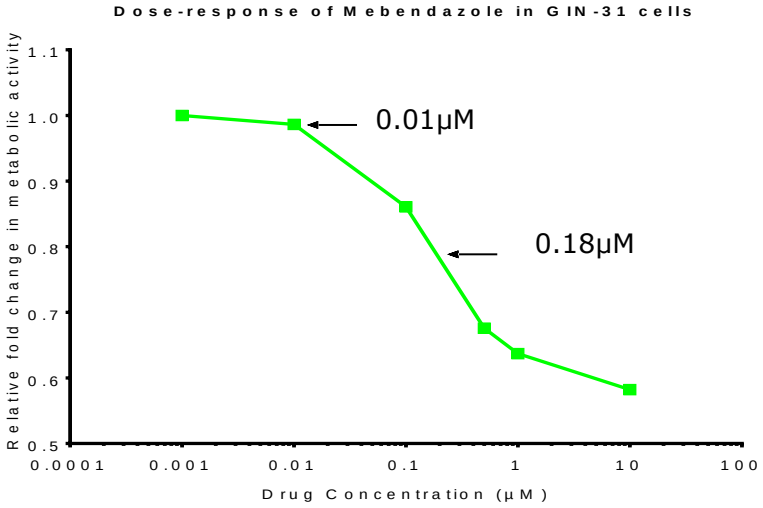
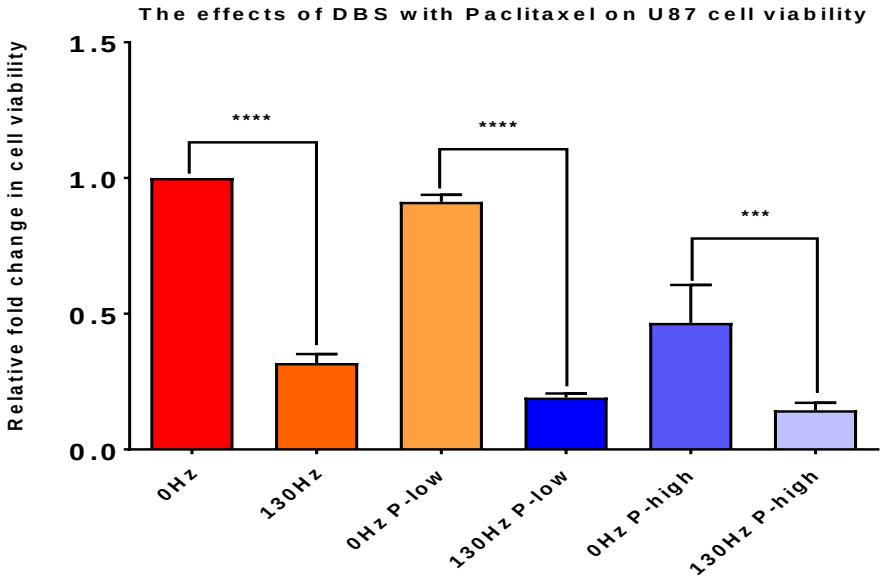
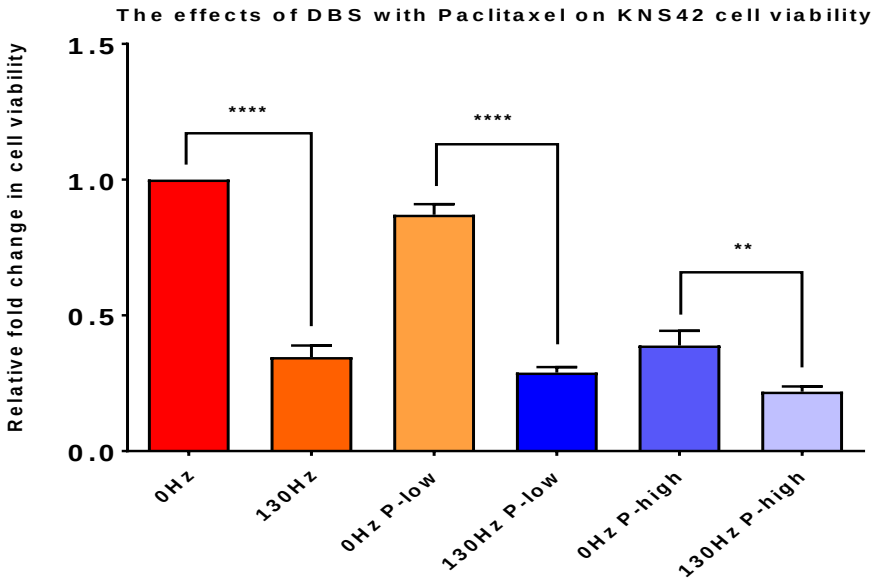
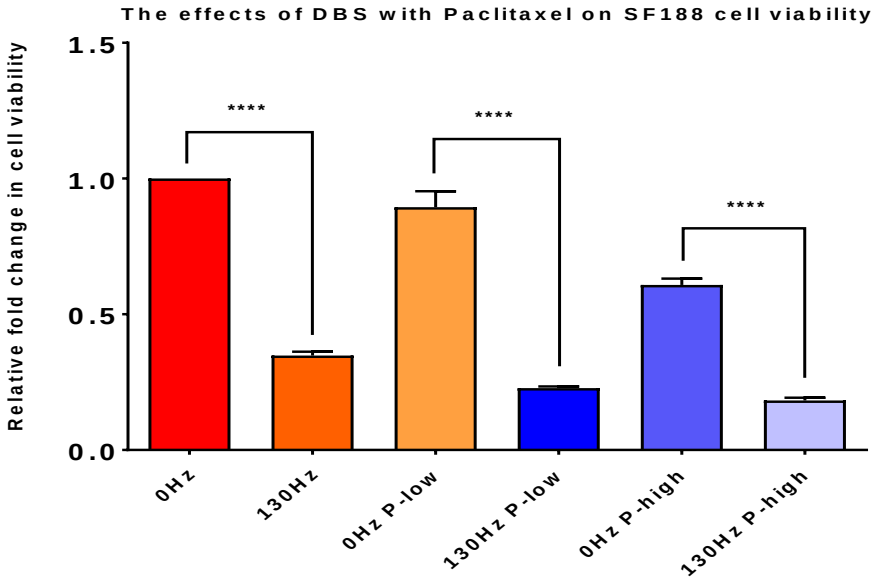
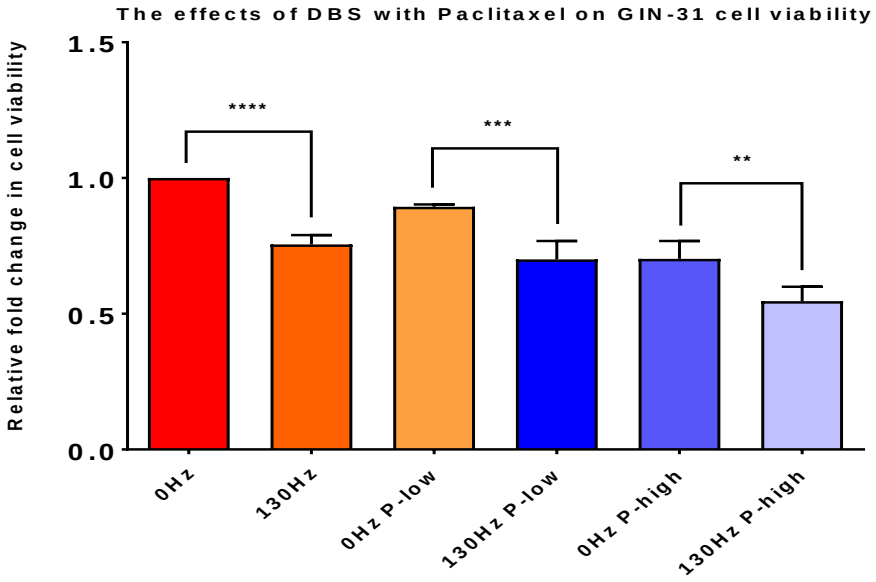


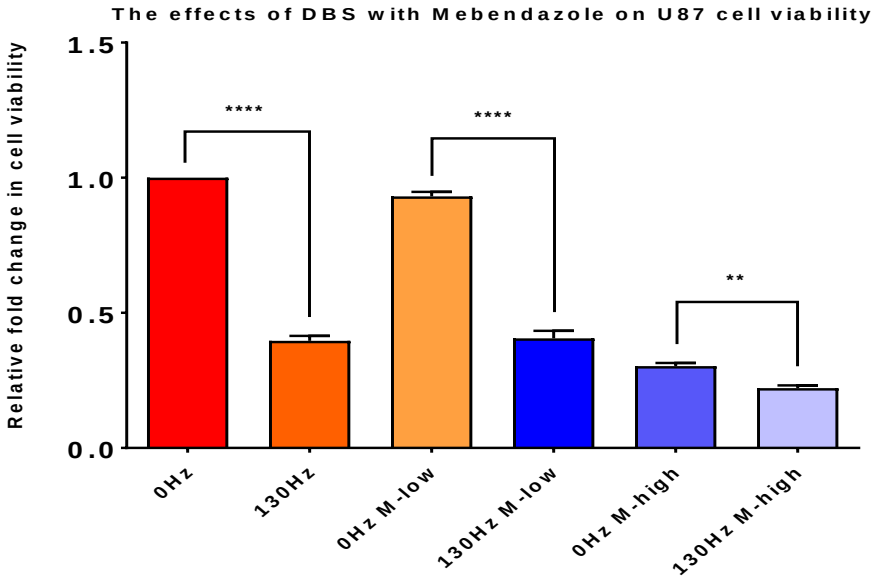
Figure 18. The dose-response curves of SF188, KNS42, U87, and GIN-31 cell lines treated with Paclitaxel and Mebendazole. The graphs show the 'high-dose' and 'low-dose' concentrations of the drugs used in our combination studies with TTFields.

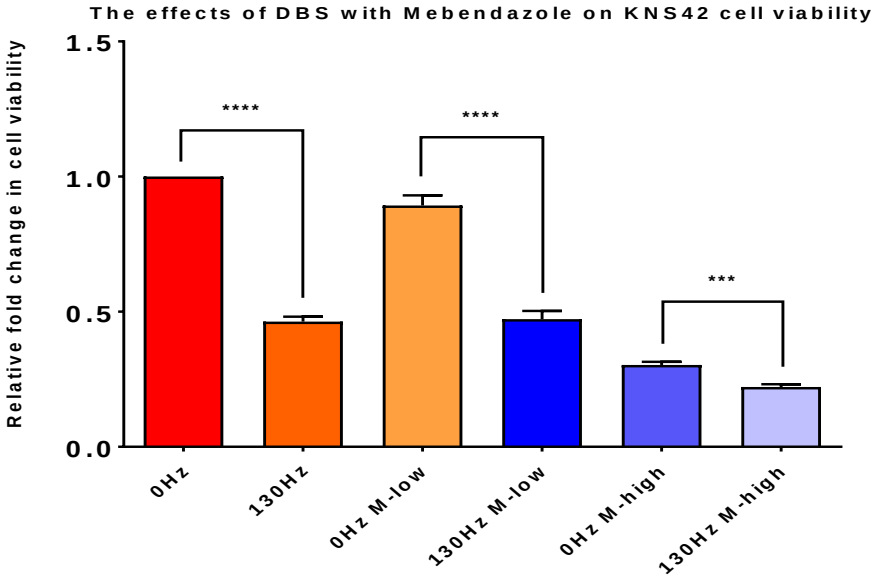

The effects of DBS with Paclitaxel on U87 cell viability
Relative fold change in cell viability
1.5
1.0
0.5
0.0
****
****
***
0Hz
130Hz
0Hz P-low
130Hz P-low
0Hz P-high
130Hz P-high


The effects of DBS with Paclitaxel on KNS42 cell viability
Relative fold change in cell viability
1.5
1.0
0.5
0.0
****
****
**
0Hz
130Hz
0Hz P-low
130Hz P-low
0Hz P-high
130Hz P-high


The effects of DBS with Paclitaxel on SF188 cell viability
Relative fold change in cell viability
1.5
1.0
0.5
0.0
****
****
****
0Hz
130Hz
0Hz P-low
130Hz P-low
0Hz P-high
130Hz P-high


The effects of DBS with Paclitaxel on GIN-31 cell viability
Relative fold change in cell viability
1.5
1.0
0.5
0.0
****
***
**
0Hz
130Hz
0Hz P-low
130Hz P-low
0Hz P-high
130Hz P-high


The effects of DBS with Mebendazole on U87 cell viability
Relative fold change in cell viability
1.5
1.0
0.5
0.0
****
****
**
0Hz
130Hz
0Hz M-low
130Hz M-low
0Hz M-high
130Hz M-high


The effects of DBS with Mebendazole on KNS42 cell viability
Relative fold change in cell viability
1.5
1.0
0.5
0.0
****
****
***
0Hz
130Hz
0Hz M-low
130Hz M-low
0Hz M-high
130Hz M-high

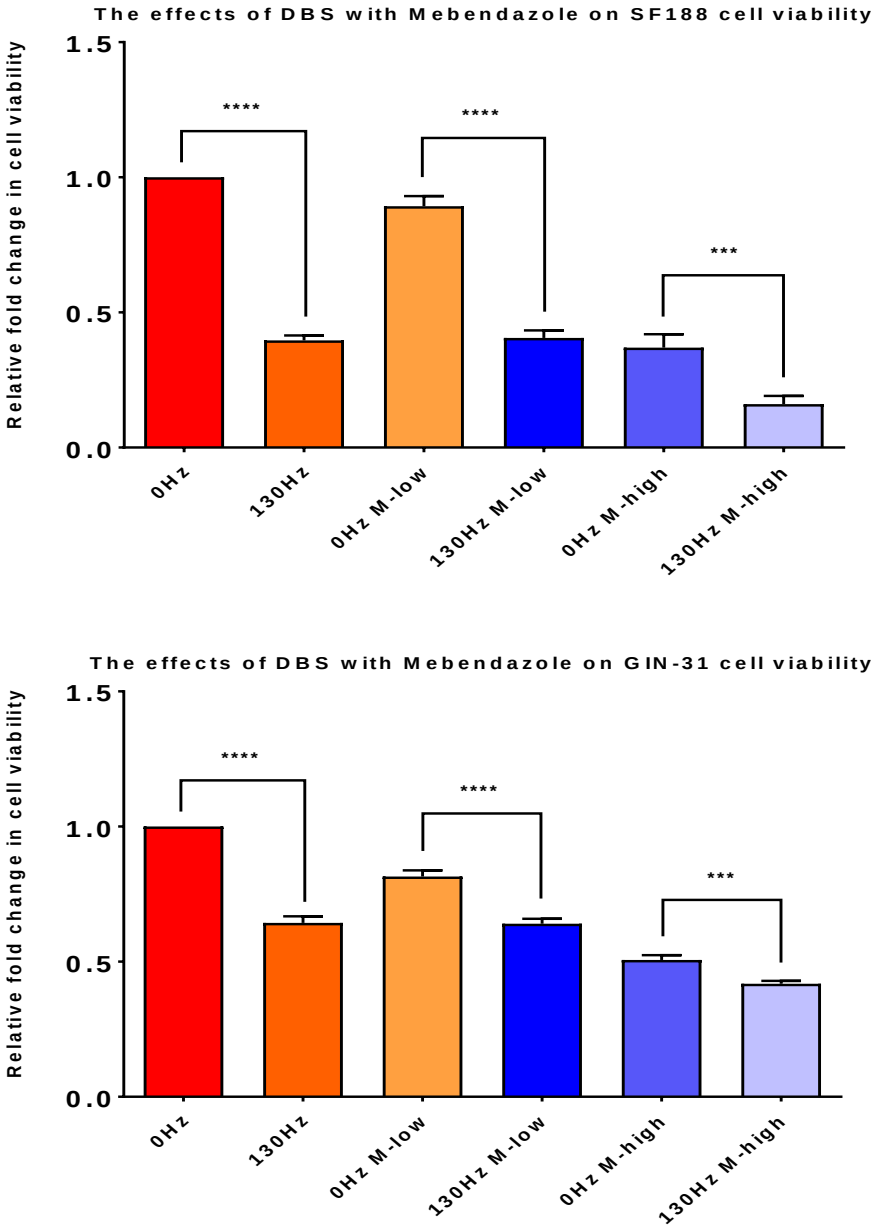
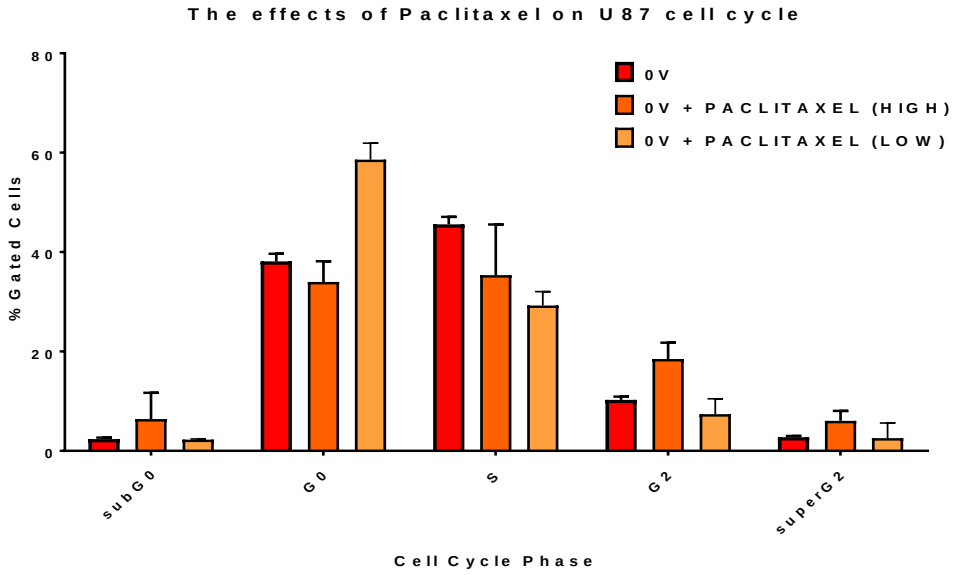
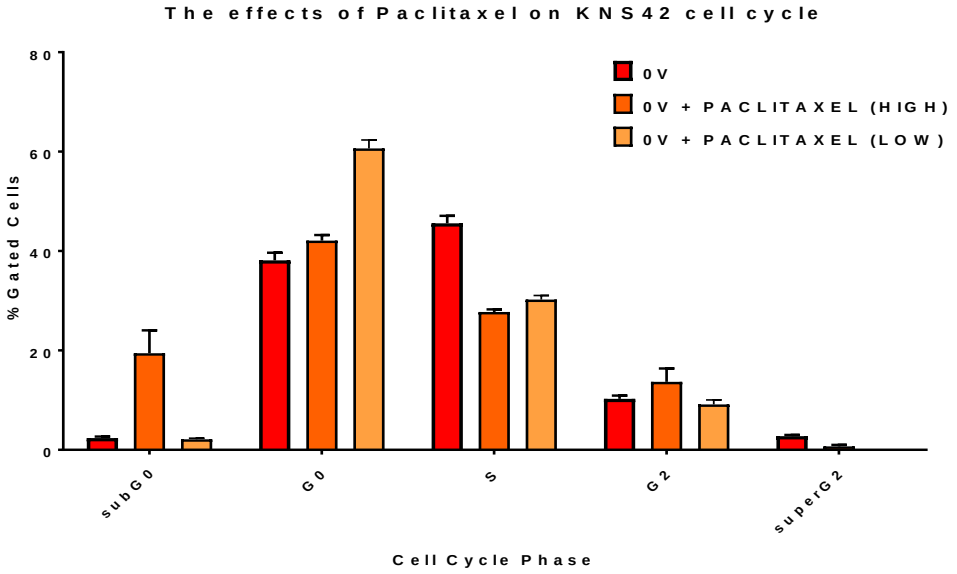
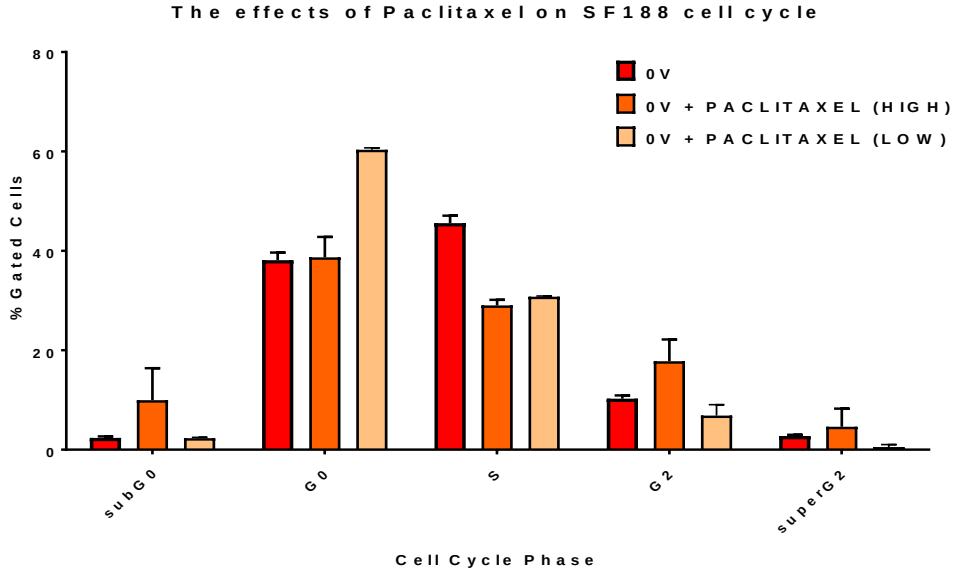
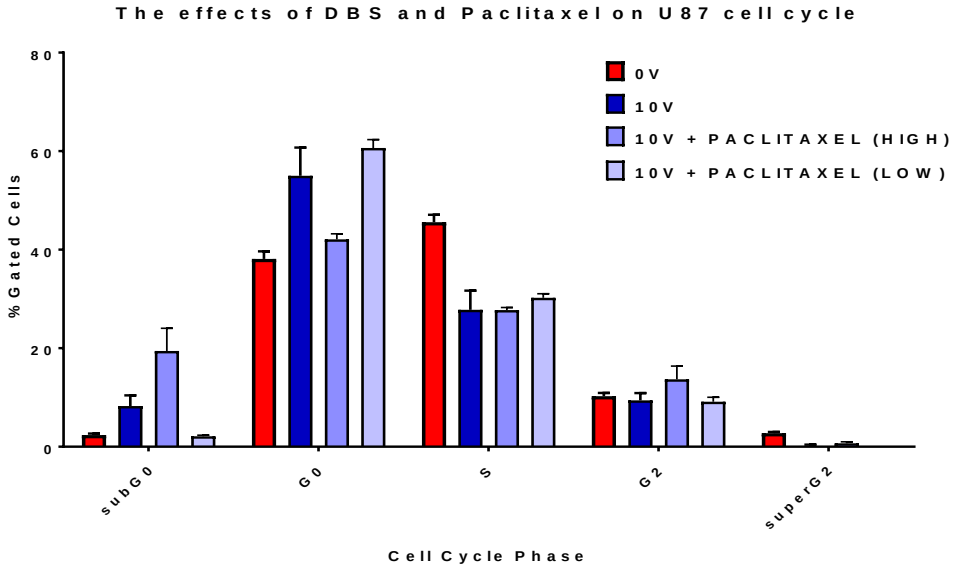


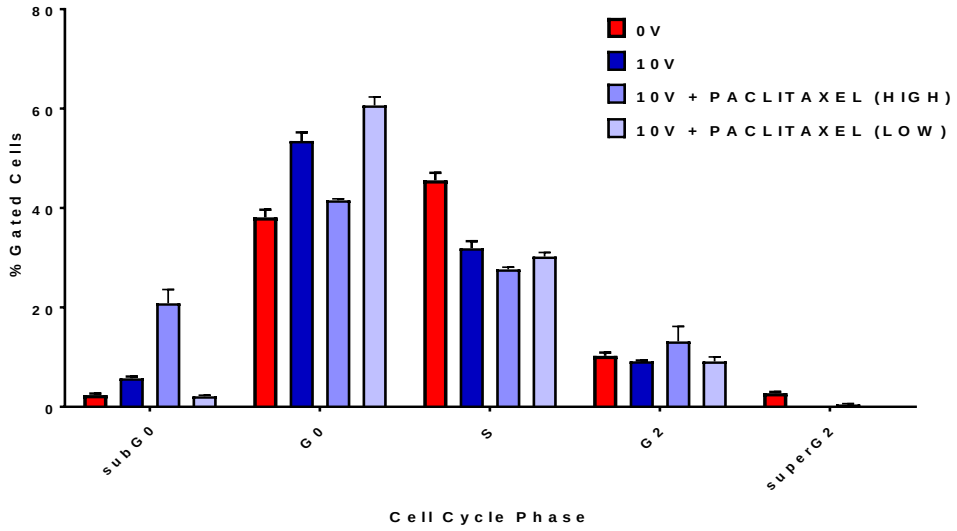
Figure 19. The effects of DBS electric fields in combination with Paclitaxel and Mebendazole on U87, KNS42, SF188 and GIN-31 cell lines. Metabolic activity was assessed with Presto Blue, and all conditions were normalised to 0V sham control cells. Cells were treated with and without 10V/130Hz/450µs DBS electric fields, with and without a high or low dose of Paclitaxel or Mebendazole for 5 days, with measurements taken at the end-point.


The effects of Paclitaxel on U87 cell cycle
0V
0V + PACLITAXEL (HIGH)
0V + PACLITAXEL (LOW)
% Gated Cells
0
20
40
60
80
subG0
G0
S
G2
superG2
Cell Cycle Phase


The effects of Paclitaxel on KNS42 cell cycle
0V
0V + PACLITAXEL (HIGH)
0V + PACLITAXEL (LOW)
% Gated Cells
0
20
40
60
80
subG0
G0
S
G2
superG2
Cell Cycle Phase


The effects of Paclitaxel on SF188 cell cycle
0V
0V + PACLITAXEL (HIGH)
0V + PACLITAXEL (LOW)
% Gated Cells
0
20
40
60
80
subG0
G0
S
G2
superG2
Cell Cycle Phase


The effects of DBS and Paclitaxel on U87 cell cycle
0V
10V
10V + PACLITAXEL (HIGH)
10V + PACLITAXEL (LOW)
% Gated Cells
0
20
40
60
80
subG0
G0
S
G2
superG2
Cell Cycle Phase


The effects of DBS and Paclitaxel on KNS42 cell cycle
0V
10V
10V + PACLITAXEL (HIGH)
10V + PACLITAXEL (LOW)
% Gated Cells
0
20
40
60
80
subG0
G0
S
G2
superG2
Cell Cycle Phase

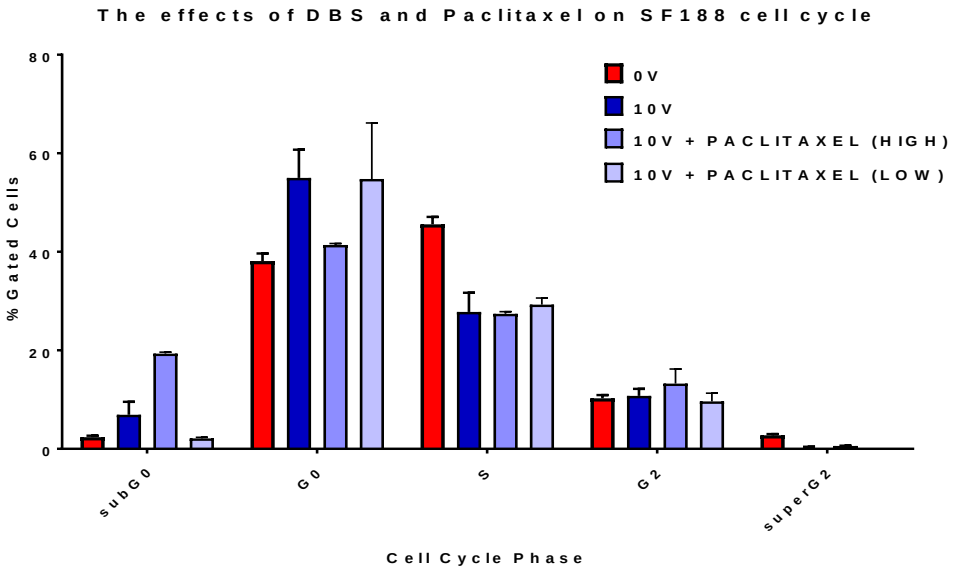

The effects of DBS and Paclitaxel on SF188 cell cycle
0V
10V
10V + PACLITAXEL (HIGH)
10V + PACLITAXEL (LOW)
% Gated Cells
0
20
40
60
80
subG0
G0
S
G2
superG2
Cell Cycle Phase

Figure 20. The effects of DBS electric fields in combination with Paclitaxel and Mebendazole on the cell cycling of U87, KNS42 and SF188 cell lines. Cell cycle analysis was performed via PI staining and flow cytometry with analysis with Weasel. Cells were treated with and without 10V/130Hz/450μs DBS electric fields, with and without a high or low dose of Paclitaxel or Mebendazole for 5 days, before being assessed with flow cytometry, with a minimum of 10,000 cells being analysed.

3.13. The efficacy of electric fields delivered from DBS Leads may be increased with the addition of Temozolomide in GBM cell lines

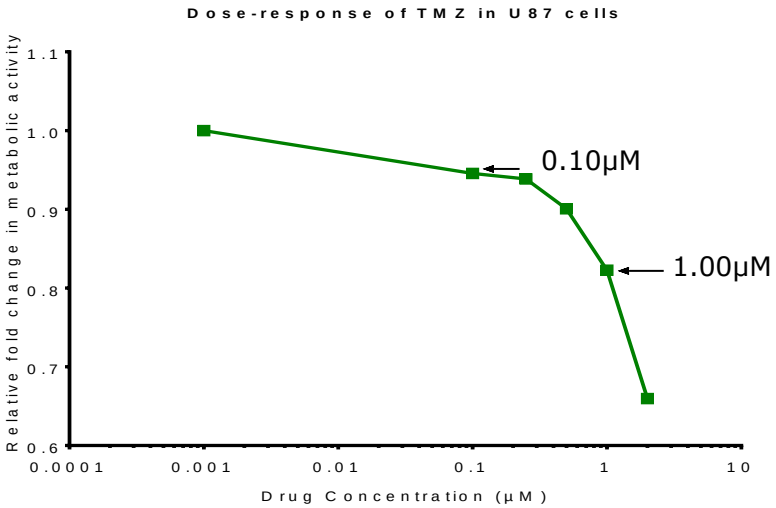
3.13.1. Results and Discussion

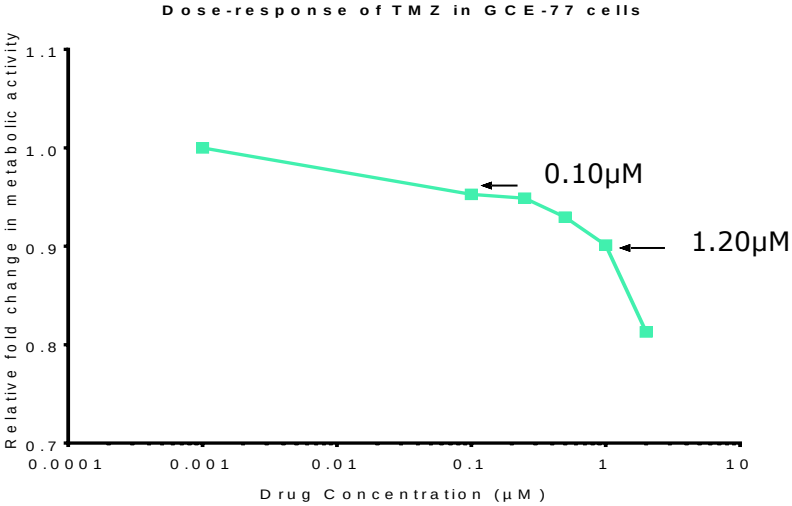
Next, we sought to combine DBS treatment with TMZ, as is this clinically relevant to GBM patients. Similarly to the previous used mitotic inhibitors, TMZ is also known to cause G2/M-phase, albeit through different mechanisms. But this would also fulfil the criteria of targeting multiple stages of the cell cycle through differing mechanisms. We used multiple cell lines, ensuring to include MGMT-methylated (U87 and GCE-77) and MGMT-wt (GIN-28 and GIN-31) cell lines to be more representative of the clinical challenges of GBM treatment. We first established an IC50 of TMZ (0.8-1.2μM) on our cell lines, and then took a lower and a higher dose and treated our cell lines as a monotherapy and in combination with DBS treatment for 5 days to form a comparison. All our cell lines tested were similarly responsive to TMZ alone, with an average reduction in viability across the cell lines of 28%, however the dose of drug used varied highly. This is as expected for our cell lines given their differing MGMT statuses, which is reflected by their IC50 values (Figure 21.).

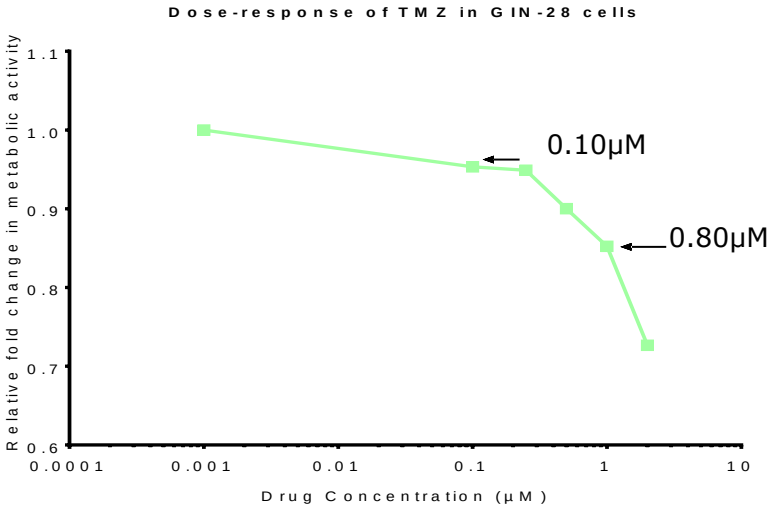
Significant reductions in cell viability were seen when comparing the higher and lower doses of TMZ in combination with DBS treatment at 10.0V/130Hz/450μS to the TMZ-alone treated flasks. The additive effect of the addition of DBS treatment netted an additional reduction in cell viability of 28% and 26% (p=<0.0001, two-way ANOVA) for U87 cells, 22% and 28% (p=0.0005 and =<0.0001, two-way ANOVA), 5% and 3% (p=0.0134 and 0.6271, two-way ANOVA) for GIN-28 cells, and 8% and 12% (p=0.0002 and p=<0.0001, two-way ANOVA) for GIN-31 cells. Cell viability analysis showed that DBS treatment in combination with TMZ does significantly increase efficacy with both the lower and higher doses. Comparing the higher and lower doses of TMZ in combination with DBS treatment at 10.0V/130Hz/450μS to untreated controls, reductions in cell viability were recorded in U87 cells at 56% and 45% (p=<0.0001, ordinary one-way ANOVA), GCE-77 cells at 30% and 43% (p=<0.0001, ordinary

one-way ANOVA), GIN-28 cells at 32% and 20% (p=<0.0001, ordinary one-way ANOVA), and GIN-31 cells at 34% and 23% (p=<0.0001, ordinary one-way ANOVA), respectively (Figure 22.).

Interestingly, our MGMT-wt cell lines (GIN-31 and GIN-28) both demonstrated a modest, but significant, reduction in cell viability following the combinational route. The apparent additive effect of DBS electric fields to both the lower and higher doses of TMZ is also encouraging, as the minimal side effects associated with DBS therapy would reduce overlapping toxicities associated with the already significant co-morbidities of the current GBM standard of care.


Dose-response of TMZ in U87 cells
Relative fold change in metabolic activity
1.1
1.0
0.9
0.8
0.7
0.6
0.10μM
1.00μM
0.0001
0.001
0.01
0.1
1
10
Drug Concentration (μM)


Dose-response of TMZ in GCE-77 cells
Relative fold change in metabolic activity
1.1
1.0
0.9
0.8
0.7
0.10μM
1.20μM
0.0001
0.001
0.01
0.1
1
10
Drug Concentration (μM)


Dose-response of TMZ in GIN-28 cells
Relative fold change in metabolic activity
1.1
1.0
0.9
0.8
0.7
0.6
0.10μM
0.80μM
0.0001
0.001
0.01
0.1
1
10
Drug Concentration (μM)

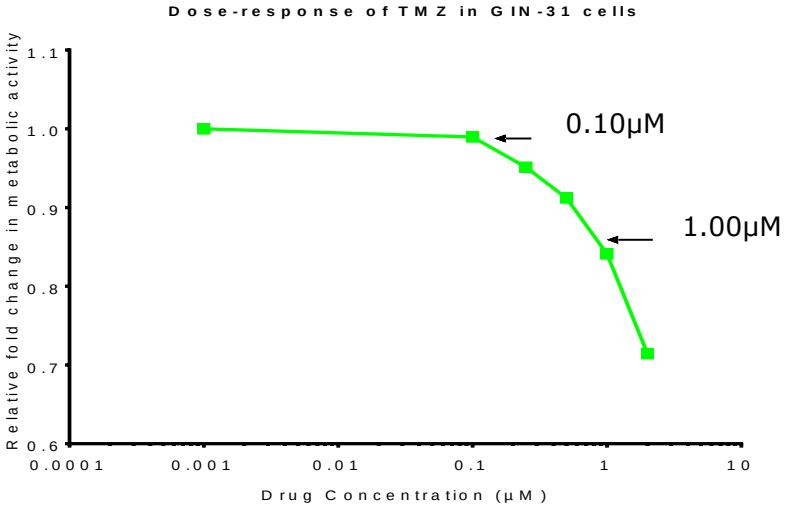
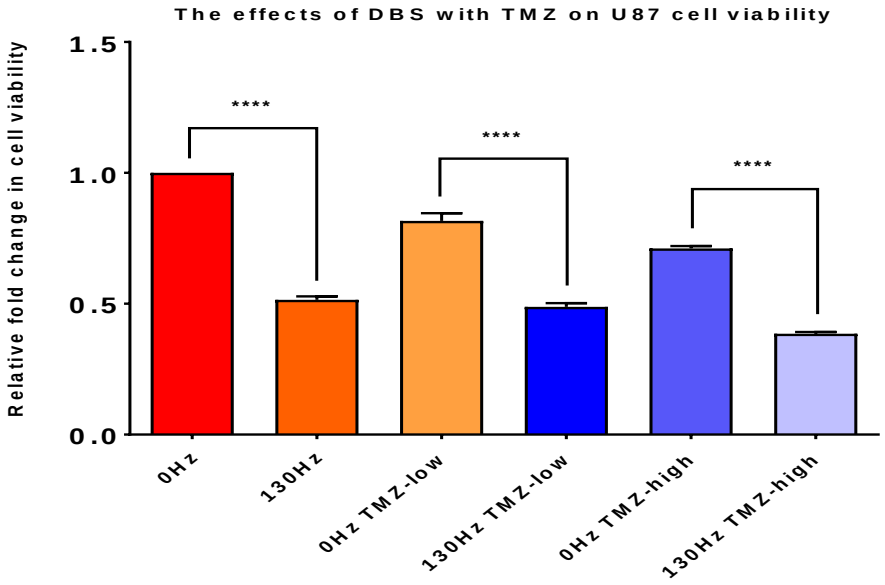
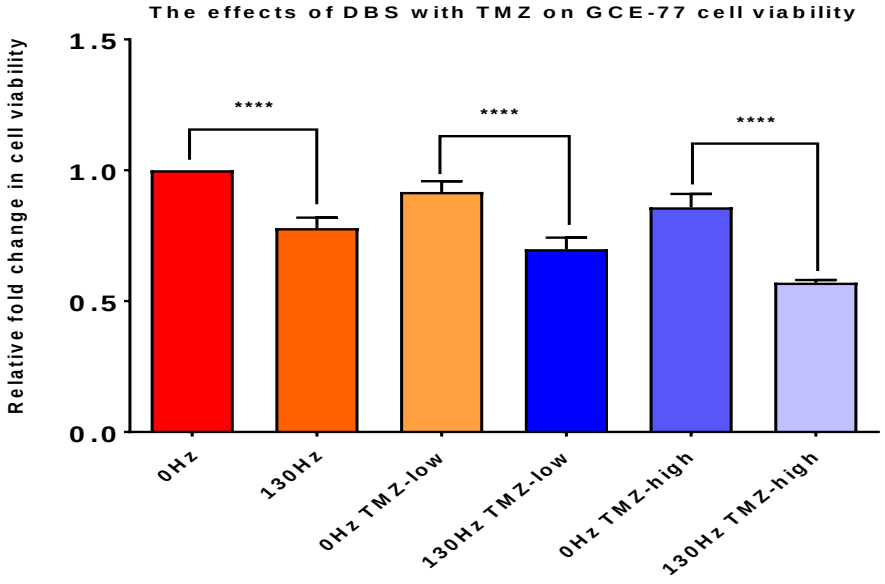
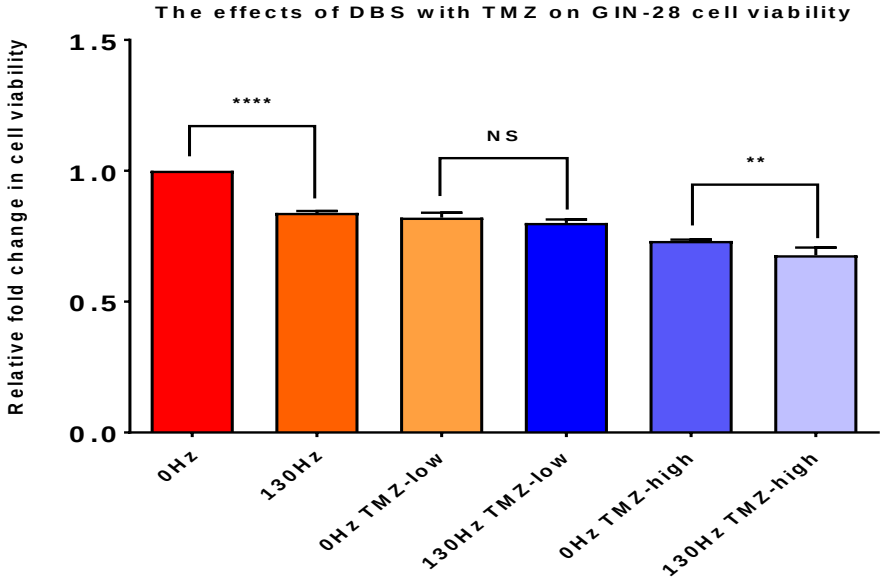


Figure 21. The dose-response curves of U87, GCE-77, GIN-28 and GIN-31 cell lines treated with TMZ. The graphs show the 'high-dose' and 'low-dose' concentrations of the drugs used in our combination studies with DBS electric fields.


The effects of DBS with TMZ on U87 cell viability
Relative fold change in cell viability
1.5
1.0
0.5
0.0
****
****
****
0Hz
130Hz
0Hz TMZ-low
130Hz TMZ-low
0Hz TMZ-high
130Hz TMZ-high


The effects of DBS with TMZ on GCE-77 cell viability
Relative fold change in cell viability
1.5
1.0
0.5
0.0
****
****
****
0Hz
130Hz
0Hz TMZ-low
130Hz TMZ-low
0Hz TMZ-high
130Hz TMZ-high


The effects of DBS with TMZ on GIN-28 cell viability
Relative fold change in cell viability
1.5
1.0
0.5
0.0
****
NS
**
0Hz
130Hz
0Hz TMZ-low
130Hz TMZ-low
0Hz TMZ-high
130Hz TMZ-high

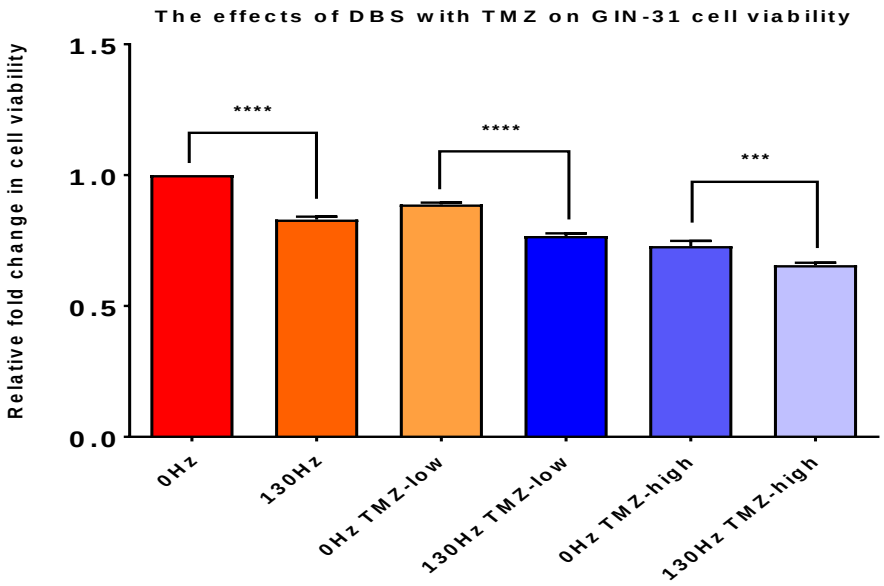


Figure 22. The effects of DBS electric fields in combination with TMZ on U87, GCE-77, GIN-28 and GIN-31 cell lines. Metabolic activity was assessed with Presto Blue, and all conditions were normalised to 0V sham control cells. Cells were treated with and without 10V/130Hz/450µs DBS electric fields, with and without a high or low dose of TMZ for 5 days, with measurements taken at the end-point.

4. Conclusions

The primary objectives of this chapter were to establish;

1. If electric fields delivered from Medtronic DNS devices had efficacy against our panel of high-grade brain tumour cell lines?
2. How the frequency and intensity of these DBS electric fields may influence their effects?
3. Through which mechanisms do DBS electric fields affect brain tumour cell lines?
4. Can the efficacy of chemotherapies be increased with the addition of DBS electric fields?

4.1. Main Findings

4.1.1. DBS Electric fields have anti-proliferative effects on high-grade brain tumour cell lines

In this chapter we have established through preliminary experiments involving manipulations of the DBS parameters that DBS electric fields have an anti-proliferative effect on our commercial and primary GBM, paediatric Medulloblastoma, and paediatric Ependymoma cell lines. Efficacy was shown to be positively correlated with greater field intensities, with a greater amount of DBS Leads, with frequencies within the range tested which diverge away from 130Hz, as well with a greater treatment time.

Other key observations include; DBS treatment efficacy was typically correlated with the doubling time of the cell lines tested, and DBS treatment had seemingly no effect on our non-dividing astrocyte cell line while having an anti-proliferative effect on our actively-dividing neural stem cell line.

4.1.2. DBS Electric Fields cause cell cycle arrest of GBM cell lines

Here we've established that GBM cell lines treated with DBS electric fields over an extended period arrest predominantly in the G0-phase of the cell cycle, causing depletion of cells within the S-phase, as well as causing minimal sub-G0-phase accumulation – implying a minimal cytotoxic effect of the treatment. The accumulation of cells in the G0-phase may be

attributed to manipulation of ion influx/efflux via electric fields, hypotheses discussed more thoroughly in Chapter 1, Sections 6.7.

4.1.3. DBS Electric Fields efficacy may be augmented with the addition of chemotherapies

We lastly established that the efficacy of TMZ, Paclitaxel, and Mebendazole may be increased with the addition of DBS electric fields. As with Paclitaxel we showed via flow cytometry how a synergistic effect of the combination treatment may produce a superior cytotoxic effect, with DBS electric fields not producing a significant cytotoxic effect when used as a monotherapy.

4.2. Future Work

This preliminary study into the effects of DBS electric fields on brain tumour cell lines has provided data demonstrating the feasibility of DBS electric fields *in vitro*, but has highlighted many avenues for future work;

1. Characterisation of the effects of DBS electric fields on a more extensive panel of normal brain cell lines.
2. Further combinational studies with approved chemotherapies and more targeted agents following a more characterised mechanism of action of DBS electric fields.
3. Further exploration of the influence of frequency on the efficacy of DBS electric fields.

4.2.1. Future Work Hypotheses

1. DBS electric fields will have very little to no effect on the viability of non-proliferative normal brain cell lines.
2. The efficacy of chemotherapies may be improved with the addition of DBS electric fields.
3. The efficacy of DBS electric fields may be improved with the optimisation of frequency and intensity.

4.2.2. DBS Electric Fields and the Brain

Here we have shown how DBS electric fields have an anti-proliferative effect on human neural stem cells, but do not on human astrocytes. Of

course, the brain consists of many cell types, with populations of dividing cells and non-dividing cells throughout neurogenesis (von Bartheld et al., 2016, Llaguno and Parada, 2016, Zong et al., 2012). We would like to test DBS electric fields on a more extensive panel of non-dividing and dividing brain cell lines, with the hypothesis that DBS electric fields do not have an anti-proliferative effect on non-dividing cells, regardless of cell type. It is worth noting that DBS therapy has been implemented safely in the clinic for decades for neurological disorders, so it is reasonable to believe that DBS electric fields therapy in patients do not pose a significant neurotoxic risk.

4.2.3. DBS Electric Fields and the Combination Approach

We have combined DBS electric fields with TMZ, Paclitaxel, and Mebendazole to satisfy the criteria of; combination with a clinically relevant agent (TMZ), and combination with an agents which targets the cell cycle (Paclitaxel and Mebendazole). We would like to test DBS electric fields in combination with other clinically relevant chemotherapies for brain tumours as well as agents which target stages of the cell cycle other than the G2/M phase. Furthermore, following greater elucidation of the mechanisms of action for DBS electric fields, we would also like to combine targeted therapies of these mechanisms to produce a synergistic treatment.

4.2.4. DBS Electric Fields and Frequency

We tested a range of frequencies against out brain tumour cell lines, each with varying efficacies, however, as we were repurposing Medtronic DBS devices we were limited by their capabilities. We took the frequencies tested up to 1000Hz, but the intensity was shown to be too low to have a significant anti-proliferative effect. This does not mean that 1000Hz electric fields have no efficacy, it would be very interesting to use devices capable of delivering such frequencies outside of the clinically relevant but at a higher intensity and how these effect brain tumour cell lines.

CHAPTER 4

ELECTROGENOMICS

Chapter 3: Tumour Treating Fields for the Treatment of Paediatric Brain Tumours

1. Introduction

Since the start of this project, Stupp and colleagues (Stupp et al., 2017a) published the final report of the EF-14 clinical trial, where the final patients to be randomised were included in the trial data. This report reported that TTFields in combination with TMZ was superior to TMZ as a monotherapy, while having no overlapping toxicities. Furthermore, significant increases in long-term survival were observed for some patients (Stupp et al., 2017a). Despite criticism and scepticism of TTFields (Wick, 2016), the therapy suggests a first advancement in survival for primary GBM patients since the addition of TMZ to radiotherapy (Stupp et al., 2005). This apparent improvement to a dismal prognosis patient population without apparent additive negative QoL effects provides an attractive treatment paradigm for paediatric patients with limited therapeutic options.

Here we present the first pre-clinical investigations into the effects of TTFields on paediatric GBM, Medulloblastoma, and Ependymoma cell lines, as well as a primary adult invasive margin derived cell line using the Inovitro system.

1.1. Hypotheses

TTFields delivered from the Inovitro system have an anti-proliferative effect, with emphasis targeting the G2/M phase of the cell cycle, on brain tumour cell lines and this effect may be augmented with the addition of chemotherapies.

1.2. Aims and Objectives

This chapter presents our investigations into the anti-cancer effects of TTFields on paediatric GBM, Medulloblastoma, and Ependymoma cell lines. The aims of this chapter were to;

1) Characterise the effect of manipulations in frequency of TTFields on paediatric brain tumour cell lines;

2) Investigate the effect of TTFields on human neural stem cells and astrocytes;
3) Investigate the efficacy of TTFields in combination with mitotic inhibitors,

The objectives for this study were;

1) Assess how TTFields influence the metabolic activity, cell count, and the cell cycle of treated paediatric brain tumour cell lines;
2) Assess how, and to what extent, TTFields influence the metabolic activity and cell count of the treated human normal brain cell lines;
3) Assess how the efficacy of TTFields may be improved with the addition of the mitotic inhibitors – Paclitaxel and Mebendazole, and how these may influence the cell viability of paediatric brain tumour cell lines.

2. Tumour Treating Fields Methods

2.1. Cell Culture and Cell Lines

All cell lines and basic cell subculture techniques used in this chapter as described in Chapter 2, Section 2.1.

2.2. Tumour Treating Fields Experiments

2.2.1. Base Plate and Dish Maintenance

Dishes and dish covers were rinsed under running tap water, and then rinsed with deionized water before being air-dried face down. Following the use of chemotherapeutic agents, dishes were soaked with light detergent for 30 minutes before being thoroughly rinsed with running tap water (to avoid any traces of the detergent in the dishes), dishes and dish covers were then rinsed with deionized water before being air-dried face down.

The now dry dishes with their covers were then sealed in autoclave bags. The bags were placed into an autoclave, making sure that the dishes were face down. The bags were then autoclaved for 60 minutes at no more than 120^0C. The bags were then removed from the autoclave and dried for 30 minutes before subsequent use.

2.2.2. Experimental Setup

Dishes and dish lids were sterilized as described in 'Base Plate and Dish Maintenance'. Sterilized 22mm glass coverslips were inserted into the dishes. A cell suspension was prepared in appropriate growth medium and at an appropriate cell concentration. These cell concentrations were selected as to allow control cells to achieve no more than ~90% confluency after 72 hours of growth. A volume of 200µL of cell suspension was pipetted as a drop onto the centre of each coverslip, and the dish covered with the dish lid. Coverslips were coated in Geltrex and washed thoroughly before seeding astrocytes and neural stem cell lines. The cells were then incubated overnight at 37^0C in an incubator to allow the cells to adhere to the coverslips. The dishes were attached to the baseplates after 24 hours by placing the dishes onto the baseplate contacts, gently pushed down and rotated clockwise until the dish locks into place. Any remaining medium was aspirated, and then replaced with 2ml of the appropriate growth medium (a sterile tip was used to gently tap around the edges of the

inserted coverslip to release any air bubbles caught under the coverslip). The dishes were then covered with their lids and then used for TTFields treatment.

CELL LINE	SEEDING DENSITY
SF188	25,000/ml
KNS42	50,000/ml
GIN-31	25,000/ml
U87	50,000/ml
DKFZ-EPN1	30,000/ml
BXD-EPN1	25,000/ml
DAOY	25,000/ml
UW228-3	20,000/ml
ASTROCYTES	40,000/ml
NEURAL STEM CELLS	8,000/ml

Table 1. Table outlining the seeding densities of cells used for 72 hours TTFields treated experiments.

2.2.3. TTFields Application

The baseplates with attached dishes were then transferred to a refrigerated incubator.

NOTE: Application of TTFields with Inovitro generates heat, so a refrigerated incubator was used to compensate and maintain 37^0C within the dishes. The temperature of the incubator was maintained between 18-22^0C, with 37^0C culture medium temperature being maintained and tracked with the Inovitro software.

The baseplate was connected to the TTFields generator with the flat cable and was switched on. The Inovitro application system software was opened and the experiment settings were defined (the name of the experiment and the frequency settings were defined depending upon the nature of the experiment). The TTFields experiment was then started using the software. Dishes had to be verified that they connected properly (properly connected dishes appear as light blue, while not properly connected dishes

appear as orange on the monitor). Dishes which were not verified were slowly, and repeatedly disconnected and then reconnected again until contact is restored, and the dishes become verified.

The TTFields application was then run for 24 hours. If the experiment has reached its endpoint, then the experiment is stopped by selecting 'END EXPERIMENT' on the software and then the experiment can be further processed – further analyses are described in the Section 2.3. If the experiment had not reached endpoint then the baseplates were disconnected from the TTFields generator, and then transferred to a laminar flow hood. Growth medium was aspirated from the dishes and then replaced. The baseplate was then returned to the refrigerated incubator, reconnected, and the experiment was continued by selecting 'CONTINUE' on the software. This process is repeated every 24 hours until the endpoint of the experiment has been reached.

2.2.4. TTFields Control Samples

Control cells (the same cell line used in the parallel TTFields experiment) were seeded onto coverslips. The cells were then incubated overnight at 37^0C in an incubator to allow the cells to adhere to the coverslips. Any remaining medium was aspirated, and then replaced with 2ml of the appropriate growth medium. The control dishes were then placed into a CO_2 incubator at 37^0C. The medium was replaced every 24 hours to control for the TTFields-treated cell's medium conditions.

2.2.5. TTFields Experiment End-point

Following selecting 'END EXPERIMENT', the experiment's records were saved (the records detail the dish temperature, current and a resistance data in real time). The TTFields generator was then switched off and the detached from the baseplates, which were then removed from the refrigerated incubator. The dishes were then detached from the baseplate and placed into a laminar flow hood. The coverslips were then aseptically removed from the dishes and transferred into sterile 6-well plates containing growth medium for further analyses described in 'Analyses of TTFields Treated Cells' section.

2.3. Analyses of Tumour Treating Fields Treated Cells

2.3.1 Cell Storage for Further Analysis

Coverslips contained in 6-well plates had their growth medium removed, cells were washed with HBSS, and 500µL of Trypsin was added to each coverslip. Trypsinised cells were incubated in a CO_2 incubator and incubated for 5-10 minutes at 37^0C to allow the cells to detach. The Trypsin was neutralised with 500µL of growth medium and the cells were transferred to a falcon tube. The cells were then centrifuged at 120g for 5 minutes to pellet the cells. The cell pellet was washed with PBS and then re-centrifuged at 120 x g for 5 minutes to re-pellet the cells. The cells were 'flash-frozen' in liquid nitrogen before being stored at -80^0C.

2.3.2. Cell Count Measurements

Cells treated with TTFields were counted manually with a haemocytometer. Given the low amount of cell yield per treatment – counts were performed from an average of 4 dishes (n=4). Coverslips contained in 6-well plates had their growth medium removed, cells were washed with HBSS, and 500µL of Trypsin was added to each coverslip. Trypsinised cells were incubated in a CO_2 incubator and incubated for 5-10 minutes at 37^0C to allow the cells to detach. The Trypsin was neutralised with 500µL of growth medium and the cells were transferred to a falcon tube. The cells were then centrifuged at 120 x g for 5 minutes to pellet the cells. The supernatant was removed, and the pellet was suspended in minimal fresh growth medium (up to 500µL), and then cells were transferred onto a haemocytometer to be counted under a microscope.

Cells from 4 quadrants of the haemocytometer were counted and an average taken. The total amount of cells was calculated using the following calculation;

$$\textbf{Cells/ml} = \frac{\textbf{Average number of cells counted X } 10^4}{\textbf{Initial volume of cells/ml}}$$

2.3.3. Cell Viability Measurements

Cells treated with TTFields had their cell viability assessed with Presto Blue. Coverslips contained in 6-well plates had their growth medium removed, cells were washed with HBSS, and then Presto Blue diluted 1:10 with growth medium was added to the wells. The 6-well plates were then transferred to a CO_2 incubator and incubated for 30 minutes at 37^0C. Following incubation, the 100µL Presto Blue was transferred to a black-bottom 96 well plate in preparation to be analysed via UV/Vis Spectroscopy with the FLUOstar Omega (BMG Labtech).

2.3.4. TTFields Frequency Titration

Cell lines were treated as described in 'Experimental Setup' and 'TTFields Application' but over a range of frequencies to determine the most efficacious frequency for each cell line. The frequencies programmed for the dishes in each experiment were 100kHz, 200kHz, 300kHz and 400kHz. Upon reaching the end-point of the experiment, cell viability was assessed with Presto Blue as described in 'Cell Viability'. The most efficacious frequency was determined by comparing the viabilities of the treated cells across all the frequencies to the non-treated control cells, with the lowest viability being associated with the most efficacious frequency.

2.3.5. Cell Cycle Analysis

Cell cycle analysis was performed using flow cytometry, and Weasel V.3.1. was used to analyse the data. Coverslips contained in 6-well plates had their growth medium removed, cells were washed with HBSS, and 500µL of Trypsin was added to each coverslip. Trypsinised cells were incubated in a CO_2 incubator and incubated for 5-10 minutes at 37^0C to allow the cells to detach. The Trypsin was neutralised with 500µL of growth medium and the cells were transferred to a falcon tube. The cells were then centrifuged at 120g for 5 minutes to pellet the cells. The supernatant was removed, and the pellet was suspended in cold PBS. The cells were then fixed with cold 70% ethanol and incubated overnight at 4^oC. The fixed cells were then pelleted via centrifugation at 300 x g for 5 minutes, and the ethanol supernatant was discarded. The pellet was again, resuspended in cold PBS and repelleted via centrifugation at 300 x g for 5 minutes. The

supernatant was thoroughly removed, and the cell pellet was then resuspended in Propidium Iodide (PI) solution (0.1% Triton X-100, 10µg/ml PI (Molecular Probes, Inc.) and 100µg/ml DNase-free RNase A in cold PBS. The cells were then incubated at room temperature in a dark room for 30 minutes before being transferred to flow cytometry. The PI stained cells were analysed with the FC500 Flow Cytometer (Beckman Coulter) and the data was then processed with Weasel V.3.1. software.

The flow cytometry data file was opened in Weasel. A histogram was produced with the 'Histogram' feature, and a 'Cell Cycle Fit' curve was applied to the data. The percentage of the cells under the curve are used to calculate the percentage of cells in their corresponding cell cycle phase; SubG0 (Apoptotic cells), G0 (Quiescence), S (Synthesis), G2/M (Mitosis), and SuperG2 (Artefactual - where DNA content is measured above n=2).

2.3.6. Withdrawal Analysis

Coverslips contained in 6-well plates had their growth medium removed, cells were washed with HBSS, and 500µL of Trypsin was added to each coverslip. Trypsinised cells were incubated in a CO_2 incubator and incubated for 5-10 minutes at 37^0C to allow the cells to detach. The Trypsin was neutralised with 500µL of growth medium and the cells were transferred to a falcon tube. The cells were counted as described in 'Cell Count' to quantify the cells and then the cells were then reseeded into T25 flasks in 5ml growth medium at the appropriate seeding density, as outlined in Table 2.. Untreated cells were also similarly seeded in T25 flasks in 5ml to be grown alongside treated cells. Both the treated and untreated cells were then grown for 7 days without any further electrical treatments. Following 7 days of growth the flasks had their viability measured, as described in 'Cell Viability', as well performing cell counts, as described in 'Cell Count'.

CELL LINE	SEEDING DENSITY
U87	7,000/ml
KNS42	6,000/ml
GIN31	8,000/ml

Table 2. Table outlining the seeding densities of cells used in Withdrawal of TTFields experiments.

2.3.7. TTFields in Combination with Mitotic Inhibitors

Before treatment, an IC50 was determined for Paclitaxel and Mebendazole for the cell lines; SF188, KNS42, GIN31, U87, UW228-3, AND BXD-EPN1. A cell suspension was prepared at an appropriate cell concentration as detailed in Table 3.

CELL LINE	SEEDING DENSITY
SF188	10,000/ml
KNS42	20,000/ml
GIN31	10,000/ml
U87	30,000/ml
UW228-3	10,000/ml
BXD-EPN1	20,000/ml

Table 3. Table showing the seeding densities used for 48 hours IC50 experiments using 96-well plates.

These cell concentrations were selected as to allow control cells to achieve no more than ~90% confluency after 48 hours of growth. A volume of 100µL of cell suspension was pipetted into each well, and then were incubated overnight at 37^0C in an incubator to allow the cells to adhere to the plate. Following 24 hours, the growth medium was removed and replaced with growth medium and the appropriate drug concentration as described in Table 4.

DRUG	CONDITION					
PACLITAXEL	MEDIUM + DMSO	MEDIUM + 100.0nM	MEDIUM + 10.0nM	MEDIUM + 1.0nM	MEDIUM + 0.1nM	MEDIUM + 0.01nM
MEBENDAZOLE	MEDIUM + DMSO	MEDIUM + 10.0μM	MEDIUM + 1.0μM	MEDIUM + 0.5μM	MEDIUM + 0.1μM	MEDIUM + 0.01μM

Table 4. Table showing the drug concentrations used to produce a dose-response curve used for 48 hours IC50 experiments using 96-well plates.

The cells were incubated for 48 hours at 37^0C in an incubator. Cell viability was measured via Presto Blue following 48 hours of treatment. Growth medium was removed from each of the wells and then Presto Blue diluted 1:10 with growth medium was added to the wells. The 6-well plates were then transferred to a CO_2 incubator and incubated for 30 minutes at 37^0C. Following incubation, the 100μL Presto Blue was transferred to a black-bottom 96 well plate in preparation to be analysed via UV/Vis Spectroscopy. The cell viability values obtained from the spectroscopy was used to produce a dose-response curve with Graphpad Prism V.7. in order to calculate an IC50.

TTFields experimental setup and application was run as described in the sections 'Experimental Setup' and 'TTFields Application' but with alterations to the growth medium used. All of the dishes were run at the most efficacious frequency determined via 'TTFields Frequency Titration' for the standard 72 hours treatment. The 6 conditions used were; TTFields treated without drug, TTFields treated with high dose drug, TTFields treated with low dose drug, no TTFields without drug, no TTFields with high dose drug, and no TTFields with low dose drug. All the dishes had their growth medium/growth medium with drug replaced every 24 hours until the end-point was reached. Cell viability was then assessed, as described in 'Cell Viability', and then the efficacy of the TTFields with/without the additional drug additions was compared to the non-TTFields treated cells with/without the additional drug additions.

3. Tumour Treating Fields Results and Discussion

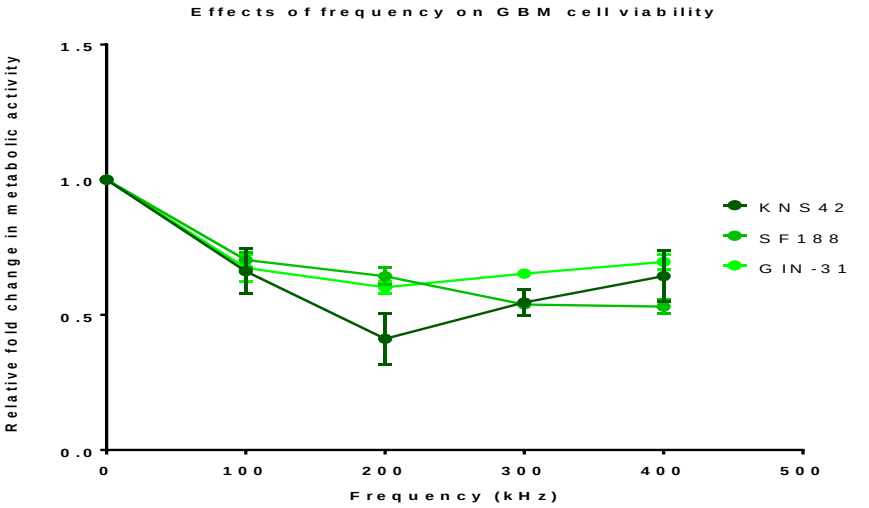
3.1. Tumour Treating Fields demonstrate variable efficacy in a frequency dependent manner

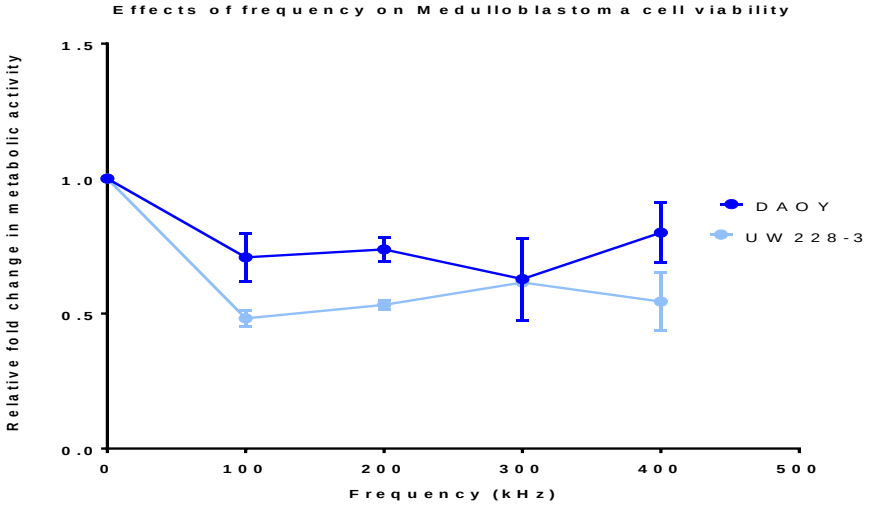
3.1.1. Results

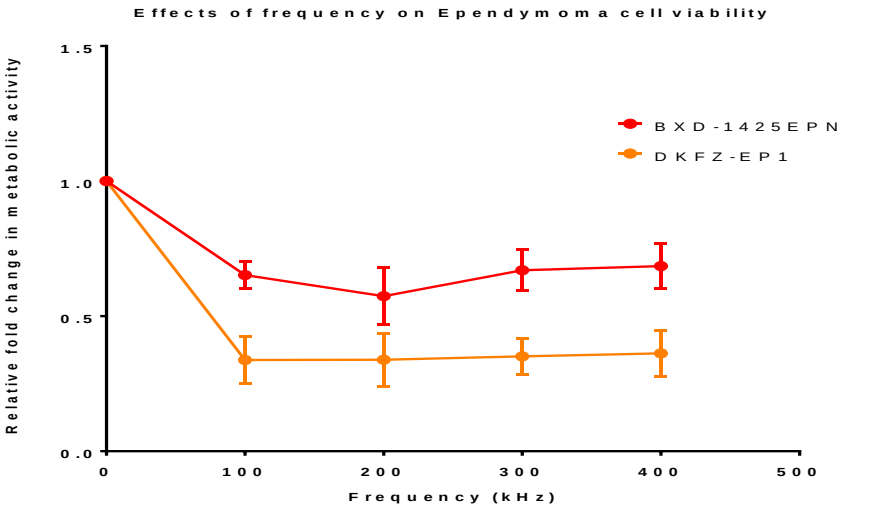
First, we had to determine the optimum frequency of TTFields for our cell lines. TTFields have been tested in various cancer cell lines within 100-500kHz range (Kirson et al., 2007), and thus far, TTFields have been trialled within adult GBM patients using a frequency of 200kHz (Stupp et al., 2017a). We ran our panel of paediatric GBM, Medulloblastoma and Ependymoma cell lines over a 100-400kHz range for a 72 hour treatment. We then measured cell viability via Presto Blue, and we validated the relation to Presto Blue to cell viability through cell counts. We confirmed that all our cell lines were sensitive to TTFields treatment across the frequencies tested. The GBM cell lines, KNS42, SF188, and GIN-31 had an optimal frequency of 200kHz, 400kHz, and 200kHz, respectively, while experiencing a reduction of 61%, 50%, and 40% cell count ($p=<0.0001$; unpaired t-test). The Medulloblastoma cell lines, DAOY and UW228-3, had an optimal frequency of 300kHz and 100kHz, with reduction of 30% and 47% in the cell counts ($p=<0.0001$; unpaired t-test). Lastly, the Ependymoma cell lines tested, DKFZ-EPN1 and BXD-1425EPN, had optimal frequencies of 100kHz and 200kHz, with reductions of cell counts of 60% and 40% ($p=<0.0001$; unpaired t-test). Cell counts were taken of the optimal frequency treated cells over $n=16$ dishes due to low yield of treated cells. We noticed that the cell lines had varying responses to TTFields as a treatment, as well as with response to different frequencies, it appeared that the Ependymoma cell lines had the most similar responses to the frequencies used. Interestingly, the paediatric GBM cell line SF188 was determined to have an optimal frequency of 400kHz as opposed to the accepted 200kHz for adult GBM in the clinic, however, KNS42 cells were most affected by TTFields at 200kHz (Figure 1.).

3.1.2. Discussion

We found that TTFields in the range of 100-400kHz over a 72 hour treatment period demonstrated efficacy across all of cell lines, in line with data suggesting efficacy against actively dividing cells regardless of cell type (Kirson et al., 2004, Kirson et al., 2009d, Porat et al., 2017). It has also been observed that the optimal frequency determined for cell lines is consistent for tumours of the same origin (Porat et al., 2017). However, we've shown how our cell lines each have a clear optimal frequency despite being of the same tumour type, apart from our Ependymoma cell lines which more interestingly appear to be equally influenced throughout the whole range of 100-400kHz TTFields. We also demonstrated a variable optimal frequency for our panel of GBM cell lines, our adult primary cell line (GIN-31) and paediatric cell line (KNS42) had an optimal frequency of 200kHz – which is in line with what is utilised in the clinic for adult GBM patients (Stupp et al., 2012b, Stupp et al., 2017a), while our other paediatric cell line (SF188) had an optimal frequency of 400kHz. These data highlight the need for further development of strategies for patient optimisation of TTFields treatment. Our Medulloblastoma cell lines had variable responses to the TTFields, with regards to efficacy and optimal frequency, despite being of the same genetic subgroup (SHH/Group 2), moreover, a key difference between the cell lines is that DAOY are tetraploid (Ivanov et al., 2016). Therefore, cell lines should have their own classification (i.e. responders and non-responders) which is independent of the cell lines classification relative to their cancer type. Lastly, observations of the optimal frequencies and their corresponding cell type's cell size aligns with the hypothesis that the optimal frequency is inversely proportional to the cell size (Wenger et al., 2018, Kirson et al., 2007). However, both Ependymoma cell lines appeared to be equally affected by all frequencies despite being highly varied in their cell morphology and cell size.


Effects of frequency on GBM cell viability
Relative fold change in metabolic activity
1.5
1.0
0.5
0.0
0
100
200
300
400
500
Frequency (kHz)
KNS42
SF188
GIN-31


Effects of frequency on Medulloblastoma cell viability
Relative fold change in metabolic activity
1.5
1.0
0.5
0.0
0
100
200
300
400
500
Frequency (kHz)
DAOY
UW228-3


Effects of frequency on Ependymoma cell viability
Relative fold change in metabolic activity
1.5
1.0
0.5
0.0
0
100
200
300
400
500
Frequency (kHz)
BXD-1425EPN
DKFZ-EP1

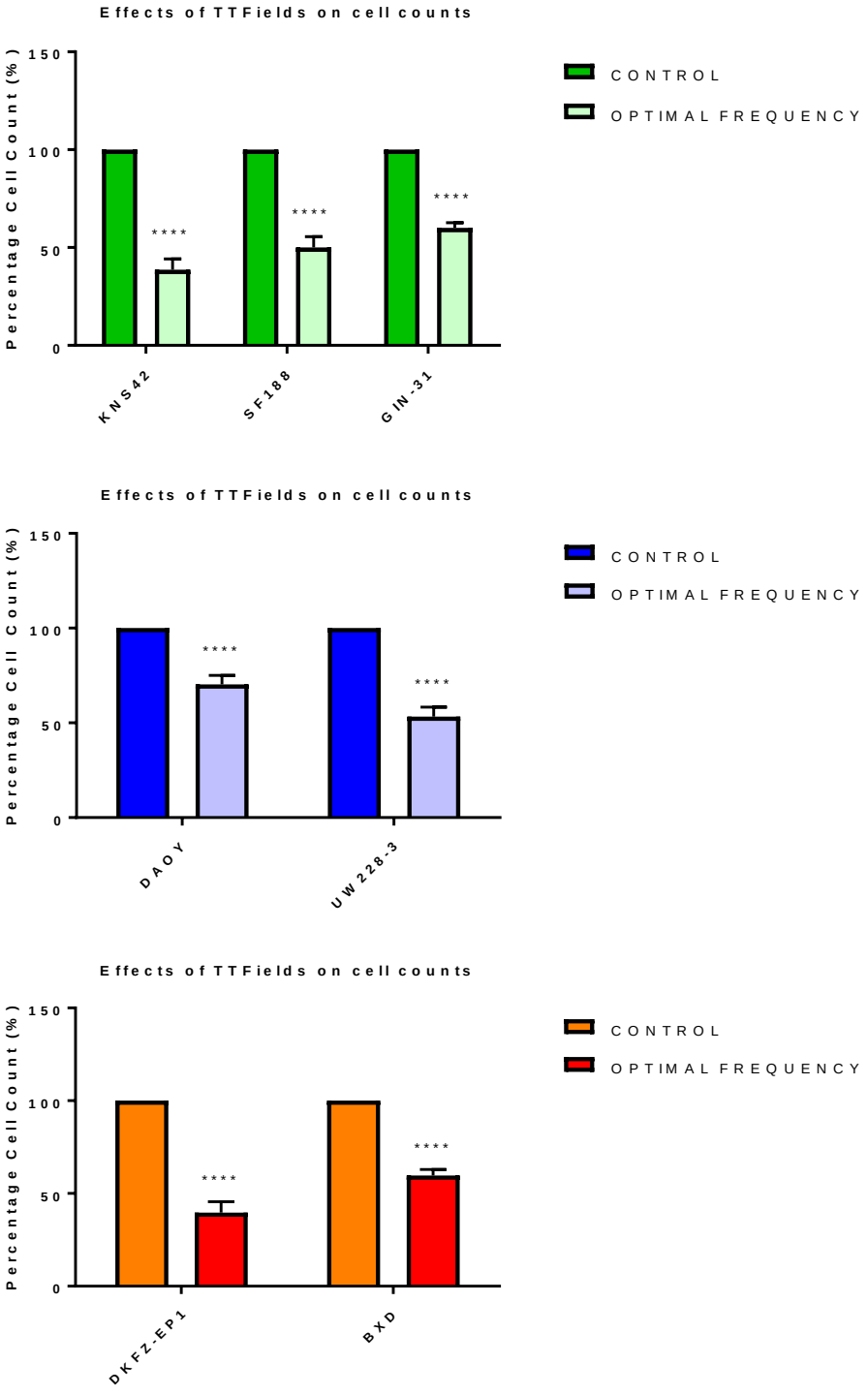


Figure 1. The effects of TTFields on KNS42, SF188, GIN-31, DAOY, UW228-3, DKFZ-EPN1 and BXD-1425 cell lines on metabolic activity, assessed with Presto Blue assay and cell counts measured with haemocytometer normalised to 0kHz control cells. Cells were treated with TTFields over a panel of frequencies for 72 hours with measurements taken at the end-point.

3.2. Tumour Treating Fields have no effect on the cell viability of non-dividing hiP-derived Astrocytes

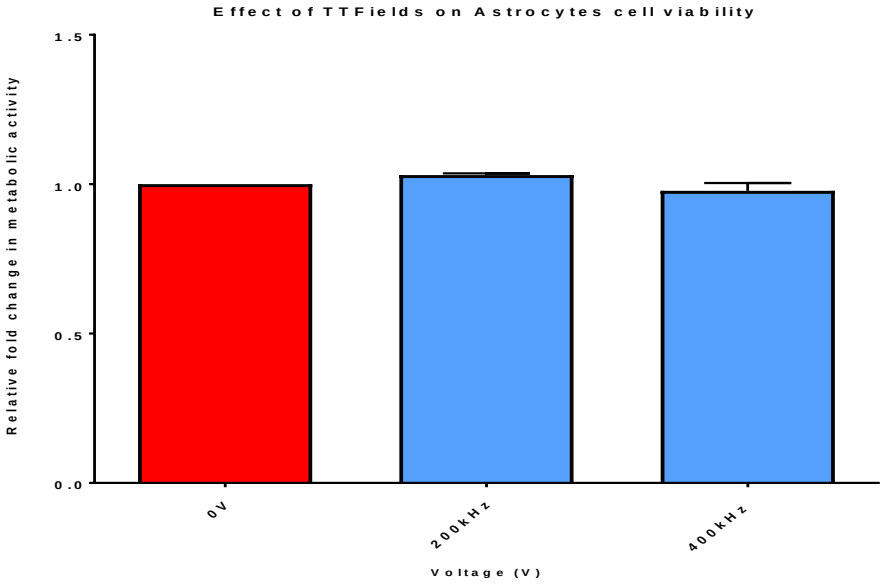
3.2.1. Results

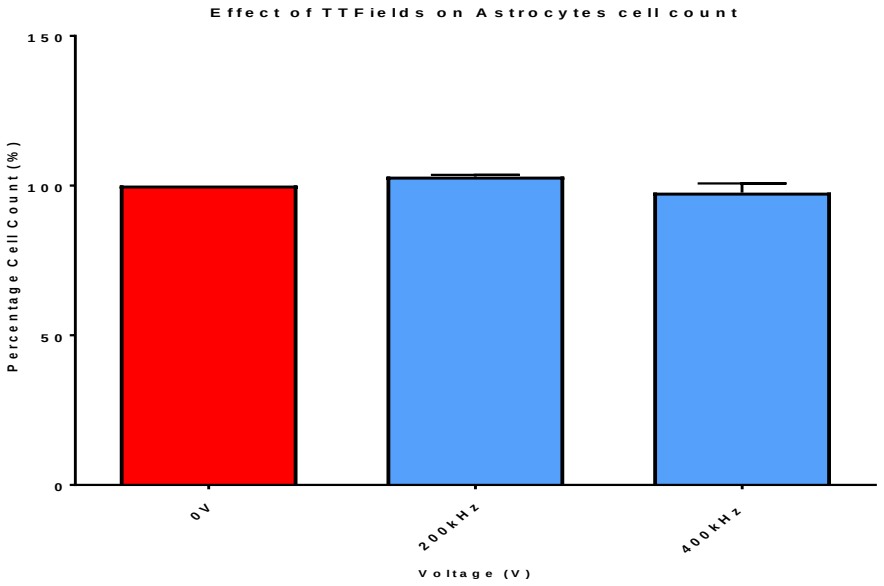
Following showing efficacy of TTFields on our panel of paediatric GBM, Ependymoma and Medulloblastoma cell lines, we assessed the effect of TTFields on dividing neural stem cells as well as non-dividing astrocytes, which were differentiated from the neural stem cells, to determine whether TTFields only affect actively dividing cells. We derived non-dividing astrocytes from neural stem cells and treated the cells for 72 hours at 200kHz and 400kHz, and then measured cell viability via a Presto Blue assay and performed a cell count. The cell viability measurements showed no significant differences between the untreated and TTFields treated cells, as well no difference between 200kHz and 400kHz treatments. We also performed cell counts from representative images of the treated and non-treated cells, and further confirmed no significant effects of TTFields treatment. We then subjected our dividing neural stem cells to TTFields treatment for 72 hours at either 200kHz or 400kHz. The cell viability measurements showed a reduction in cell viability of 33% and 32% ($p=0.0018$ and $p=0.0024$; ordinary one-way ANOVA) following treatment with 200kHz and 400kHz TTFields, respectively. There were no significant differences between the 200kHz and 400kHz treatments. These data confirm the hypothesis that TTFields only cause a decrease in viability in actively dividing cells (Figure 2.).

3.2.2. Discussion

Previous literature has stated that an actively dividing cell is the target of TTFields treatment (Kirson et al., 2004), a few reports have shown how TTFields and electric fields at similar frequencies have no significant efficacy on non-dividing cells (Xu et al., 2016, Sebastiano et al., 2018, Kirson et al., 2004, Jo et al., 2018), and in Chapter 2, Section 3.5 we have shown that DBS electric fields do not affect our non-dividing human astrocyte cell line. Our data confirms that TTFields treatment at 200KHz and 400KHz have no effect on the cell viability or cell count on our human astrocyte cell line, but the treatment did have a significant effect on our

neural stem cell line, as DBS electric fields did. Given that our astrocyte cell line was derived from the neural stem cell line, these data confirm that TTFields targets mitotic cells, and not just cancer cells specifically.


Effect of TTFields on Astrocytes cell viability
Relative fold change in metabolic activity
1.5
1.0
0.5
0.0
0V
200kHz
400kHz
Voltage (V)


Effect of TTFields on Astrocytes cell count
Percentage Cell Count (%)
150
100
50
0
0V
200kHz
400kHz
Voltage (V)

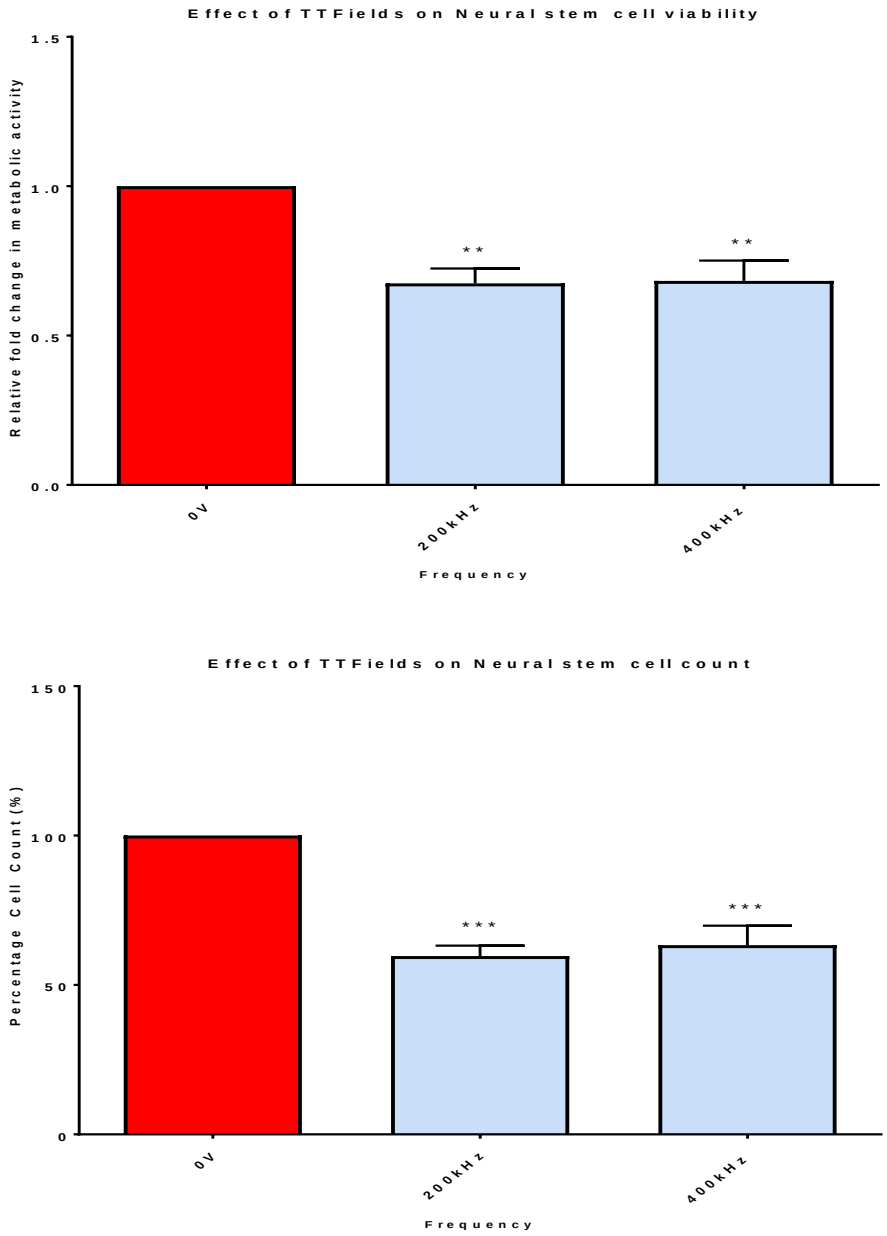


Figure 2. The effects of TTFields on human astrocyte and human neural stem cell lines on the metabolic activity, assessed with Presto Blue assay and cell counts measured with haemocytometer normalised to 0kHz control cells. Cells were treated with 200kHz and 400kHz TTFields for 72 hours with measurements taken at the end-point.

3.3. Tumour Treating Fields have lasting effects on growth rates of brain tumour cell lines following withdrawal from treatment

3.3.1. Results

Following post-hoc observations regarding compliance and outcome with TTFields therapy, we next tested the effects of treatment withdrawal as with our DBS experiments, to see if there were long lasting effects on cell growth and morphology. Cells were treated TTFields for 72 hours at their determined optimal frequency, and then were re-seeded against control cells. The previously treated cells had further TTFields treatment withdrawn, and these cells were grown alongside the control cells for 7 days before cell viability analysis. The withdrawal cells had a significantly compromised growth rate compared to the control cells, with reductions in viability of 71% in U87 ($p=<0.0001$, unpaired t-test), 84% in KNS42 ($p=<0.0001$, unpaired t-test), 78% in SF188 ($p=<0.0001$, unpaired t-test), and 66% in GIN-31 ($p=<0.0001$, unpaired t-test) cell lines (Figure 3.). This data reiterates that electrical treatment may have effects beyond the scope of acute responses as the affected cells clearly require recovery time to overcome the previous TTFields treatment.

3.3.2. Discussion

Reported data shows a reduced clonogenic potential of TTFields treated cancer cells (Silginer et al., 2017, Giladi et al., 2017), as well as our own observations in Chapter 2, Section 3.8 showing reduced cell growth rates following DBS electric fields treatment of brain tumour cell lines. Our data for TTFields treated cells shows how our commercial paediatric GBM cell lines (SF188 and KNS42), commercial adult GBM (U87), and our primary adult GBM cell line (GIN-31) all had significant reductions in viability long-term following TTFields treatment. Interestingly, although the TTFields treatment is shorter, and therefore less efficacious than our 7 day DBS electric fields treatment, the TTFields treated cells exhibited a much more significant reduced cell viability in the long-term. The reduced cell viability following treatment may be a combination of the resulting genetic and/or morphological modifications which are a consequence of TTFields treatment (Gera et al., 2015). As to whether long-term genetic

modifications are a consequence of TTFields treated cells is subject to future investigations.

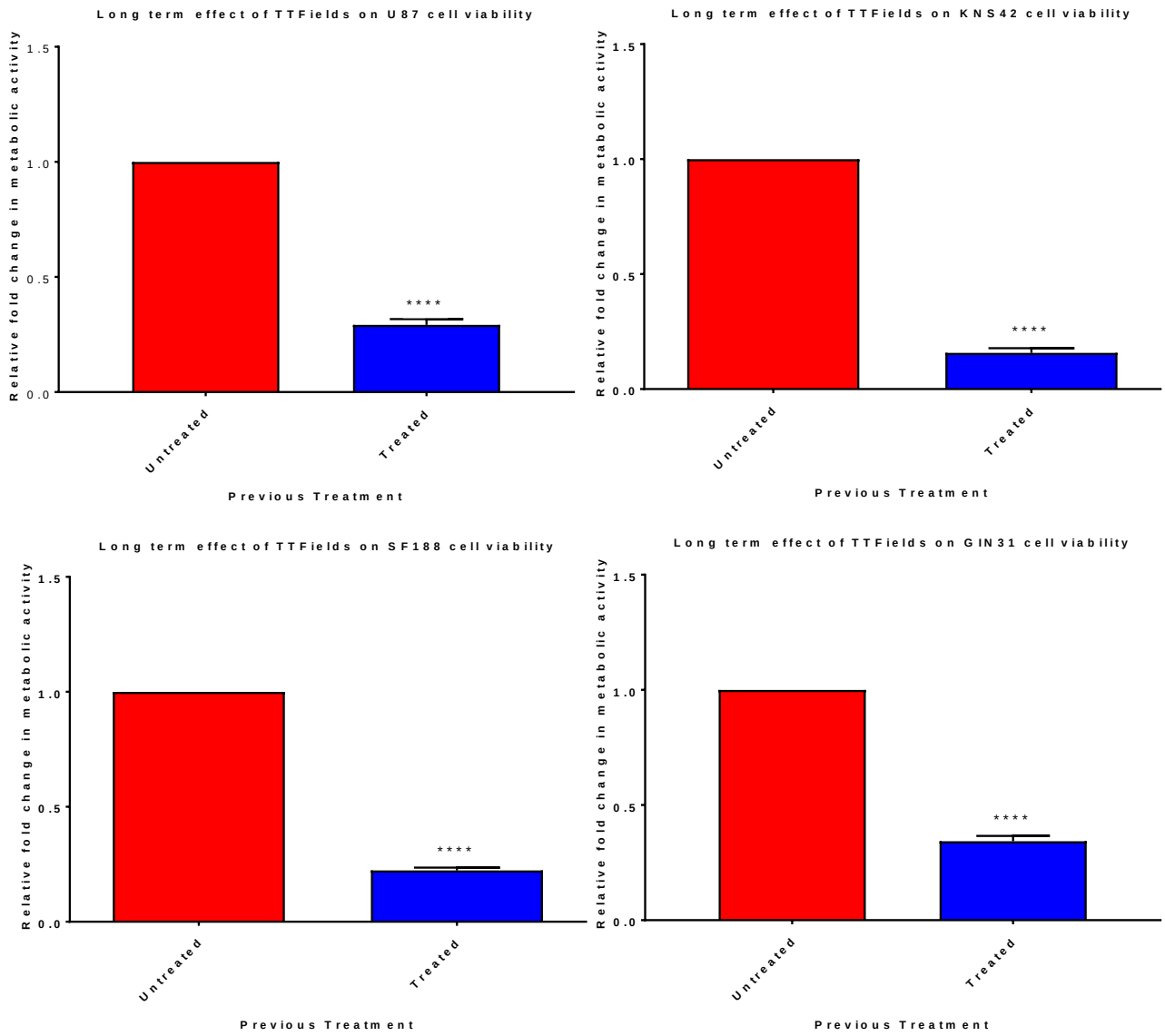


Figure 3. The long-term effects of TTFields on U87, KNS42, SF188 and GIN-31 cell lines on metabolic activity, assessed with Presto Blue assay and cell counts measured with haemocytometer normalised to 0kHz control cells. Cells were treated with TTFields at their determined optimal frequency for 72 hours, and then were re-seeded against non-treated cells, controlling for seeding densities. Previously treated cells and non-treated control cells were then regrown for 7 days with no further treatment before measurements taken at the end-point.

3.4. Tumour Treating Fields promote G2/M-phase accumulation in paediatric brain tumour cell lines

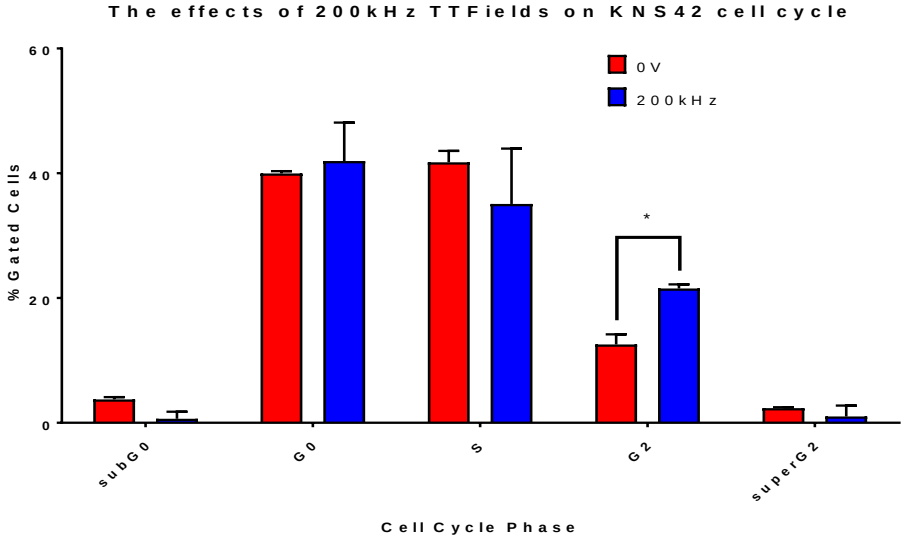
3.4.1. Results

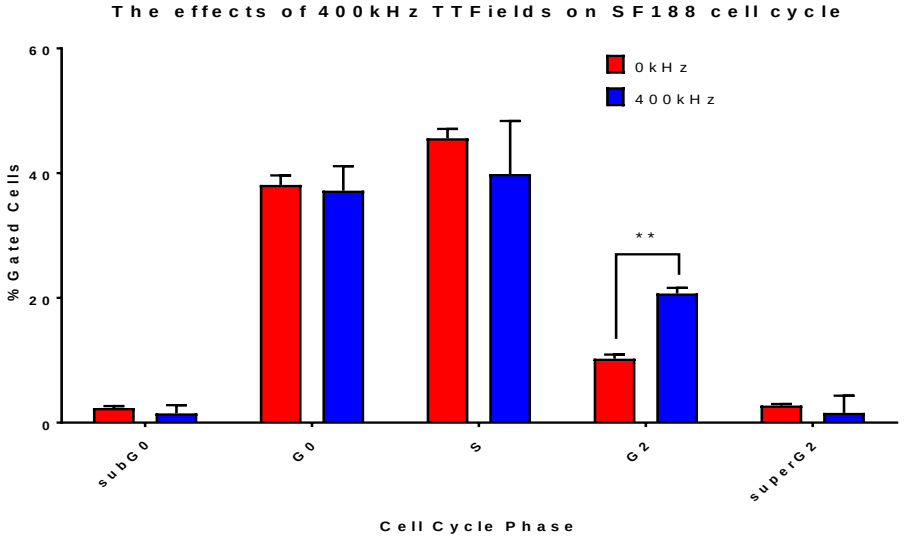
TTFields have previously been shown to promote G2/M-phase accumulation through interactions with tubulin dynamics (Kirson et al., 2004, Giladi et al., 2015c, Gera et al., 2015). Our panel of paediatric brain tumour cell lines were treated with TTFields for 72 hours at their optimal frequencies, and their cell cycling was analysed using PI staining and flow cytometry. Our observations are in-line with previous data (Silginer et al., 2017), TTFields treatment caused G2/M-phase accumulation for all cell lines; with an increase of 9% and 11% ($p=0.0297$ and $p=0.0037$; ordinary two-way ANOVA) for KNS42 and SF188 cell lines, 11% and 12% ($p=<0.0001$; ordinary two-way ANOVA) for DAOY and UW228-3 cell lines, and 13% and 8% ($p=0.0040$ and $p=0.0024$; ordinary two-way ANOVA) for BXD-1425EPN and DKFZ-EPN1 cell lines, respectively. The cell lines; DAOY, UW228-3, and DKFZ-EPN1 also had significant G0-phase depletion; 8%, 7%, and 7% ($p=0.0002$, $p=<0.0001$ and $p=0.0057$; ordinary two-way ANOVA), respectively. These cell lines also experienced a slight S-phase accumulation as well; 6%, 4%, and 10% ($p=0.0131$, $p=<0.0001$ and $p=<0.0001$; ordinary two-way ANOVA). None of the cell lines had significant levels of subG0-phase accumulation, suggesting that TTFields has a predominantly cytostatic over a cytotoxic effect in our tested paediatric brain tumour cell lines (Figure 4.).

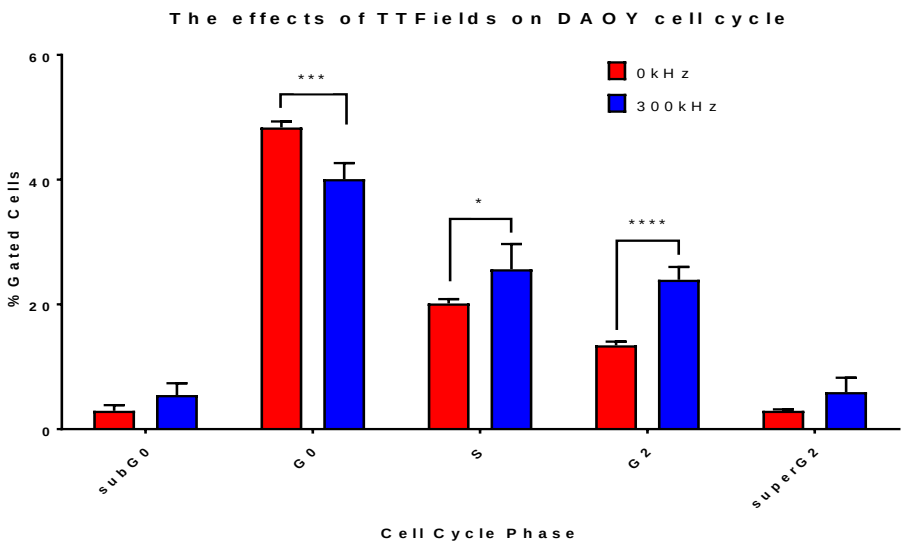
3.4.2. Discussion

An accepted consequence of TTFields treatment on cancer cells is the accumulation of treated cells in the G2/M phase of the cell cycle due to the microtubule interactions of the electric fields (Kessler et al., 2018). We have confirmed these observations in our cell lines, which is not unexpected, because although clear genetic differences are present between cell lines – actively dividing cells require microtubules along with other mitotic proteins which are targeted by TTFields (Mukhtar et al., 2014). Interestingly, none of our panel of brain tumour cell lines underwent significant levels of apoptosis, which is in line with other reports

of TTFields not inducing significant apoptosis in glioma models (Silginer et al., 2017, Kessler et al., 2018). The mechanisms by which each cell type evades apoptosis is subject to further investigation.


The effects of 200kHz TTFields on KNS42 cell cycle
0V
200kHz
% Gated Cells
60
40
20
0
*
subG0
G0
S
G2
superG2
Cell Cycle Phase


The effects of 400kHz TTFields on SF188 cell cycle
0kHz
400kHz
% Gated Cells
60
40
20
0
**
subG0
G0
S
G2
superG2
Cell Cycle Phase


The effects of TTFields on DAOY cell cycle
0kHz
300kHz
% Gated Cells
60
40
20
0
***
*
****
subG0
G0
S
G2
superG2
Cell Cycle Phase

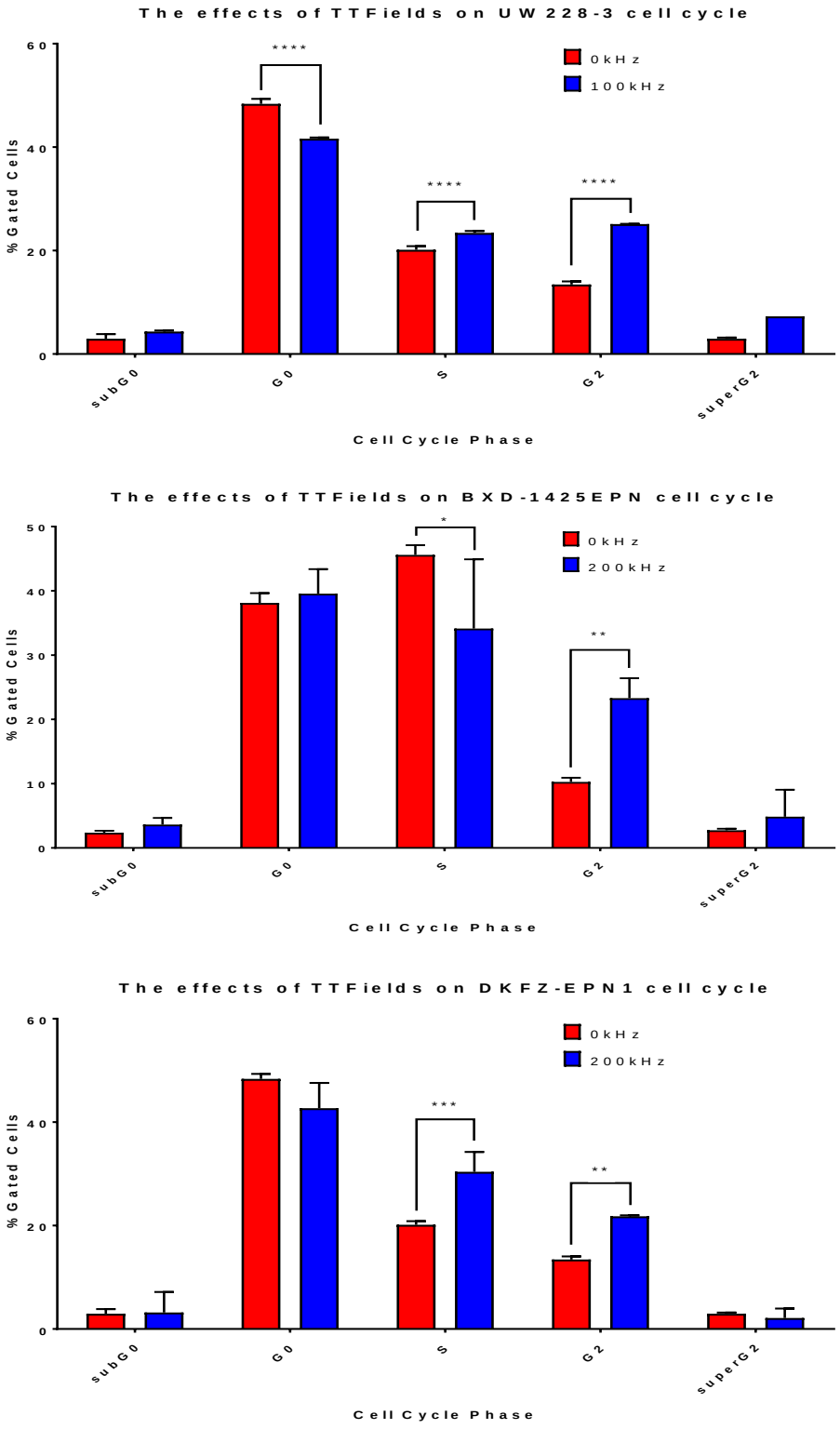


Figure 4. The effects of TTFields on cell cycling of KNS42, SF188, DAOY, UW228-3, BXD-1425 and DKFZ-EPN1 cell lines assessed via flow cytometry with PI staining. Cells were treated with TTFields at their determined optimal frequency for 72 hours before a minimum of 10,000 cells were stained with PI and analysed with flow cytometry. The cell cycle phases are; sub-G0 (Apoptotic readings), G0 (Quiescence), S (Synthesis), G2 (Division), super-G2 (Artefactual readings).

3.5. The efficacy of Tumour Treating Fields may be increased with the addition of mitotic inhibitors in brain tumour cell lines

3.5.1. Results and Discussion

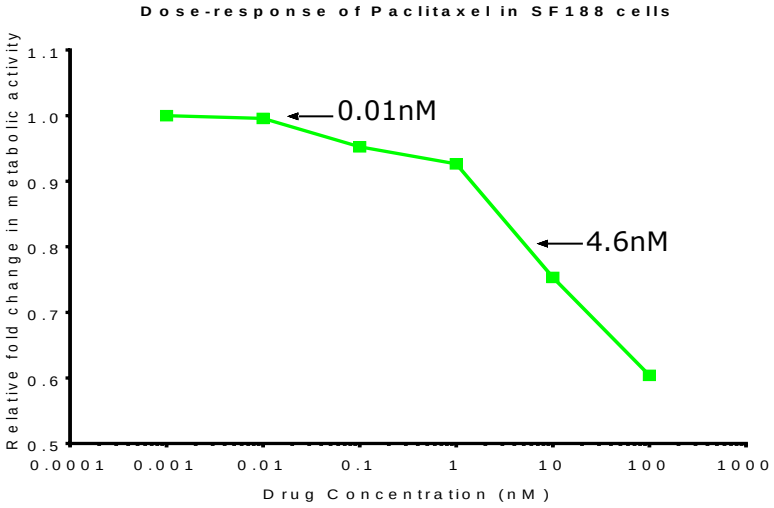
As our data suggests that TTFields target the G2/M-phase of the cell cycle, we decided to further target this phase with the tubulin-interacting mitotic inhibitors, Paclitaxel and Mebendazole. This strategy of targeting the same region of the cell cycle with different therapies seeks to overcome the axis-dependent nature of TTFields which most likely limits efficacy of the treatment. We established an IC50 of Paclitaxel (0.4-4.6nM) and Mebendazole (0.02-1.2μM) on our brain tumour cell lines, and then took a lower and a higher dose and treated our cell lines as a monotherapy and in combination with TTFields for a 72 hour treatment for comparison (Figure 5.). We first confirmed that our cell lines were sensitive to the mitotic inhibitors used, with reductions of cell viability of 30% and 39% ($p=0.0034$ and $p=<0.0001$; two-way ANOVA) for SF188 cells, 32% and 28% ($p=<0.0001$; two-way ANOVA) for UW228-3 cells, and 23% and 30% ($p=<0.0001$; two-way ANOVA) for BXD-1425EPN cells, for Paclitaxel and Mebendazole, respectively.

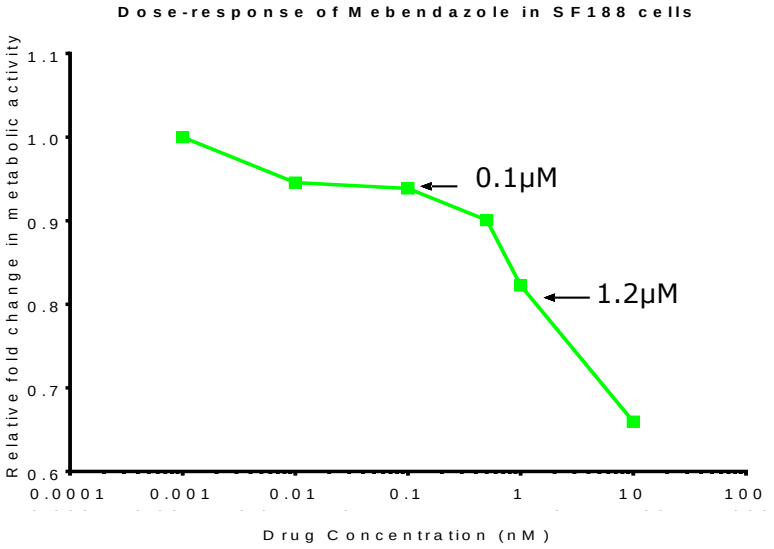
Significant effects were seen when comparing the combination treated cells to the higher and lower Paclitaxel-alone treated cells. An additive effect of TTFields was observed for all cell lines, with an additional reduction in cell viability of 33% and 38% ($p=0.0013$ and $p=0.0004$, two-way ANOVA) for SF188 cells, 22% and 34% ($p=0.0006$ and $p=<0.0001$, two-way ANOVA) for UW228-3 cells, and 34% and 27% ($p=<0.0001$, two-way ANOVA) for BXD-1425EPN cells, respectively. Cell viability analysis also showed that TTFields treatment in combination with a higher dose of Paclitaxel and Mebendazole produced a more efficacious treatment than either as a monotherapy. Cell viability analysis demonstrated that TTFields treatment in combination with Paclitaxel significantly increase efficacy at higher doses, but not at lower doses, with our panel of paediatric cell lines. Comparing the higher and lower doses of Paclitaxel in combination with TTFields treatment at their determined optimal frequency to untreated

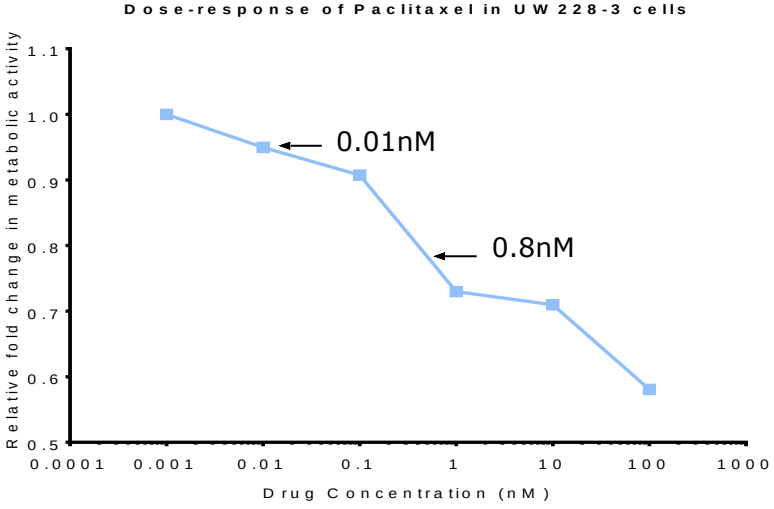
controls, reductions in cell viability were 63% and 46% (p=<0.0001, two-way ANOVA) in SF188 cells, 54% and 42% (p=<0.0001, two-way ANOVA) in UW228-3 cells, and 56% and 36% (p=<0.0001, two-way ANOVA) in BXD-1425EPN cells, respectively.

Following the trend seen with Paclitaxel combinations, reductions in cell viability were seen with the higher and lower doses of Mebendazole in combination with TTFields treatment compared to the Mebendazole-alone treated flasks. The addition of TTFields treatment to Mebendazole had an additive reduction in cell viability of 22% and 41% (p=0.0037 and p=<0.0001, two-way ANOVA) for SF188 cells, 29% and 24% (p=<0.0001, two-way ANOVA) for UW228-3 cells, and 16% and 19% (p=<0.0001, two-way ANOVA) for BXD-1425EPN cells, respectively Cell viability analysis showed that TTFields treatment in combination with Mebendazole also significantly increase efficacy at the higher doses, but also does not have significant effects at lower doses. Comparing the higher and lower doses of Mebendazole in combination with TTFields treatment to untreated controls, reductions in cell viability were 61% and 55% (p=<0.0001, two-way ANOVA) in SF188 cells, 57% and 36% (p=<0.0001, two-way ANOVA) in UW228-3 cells, and 46% and 33% (p=<0.0001, two-way ANOVA) in BXD-1425EPN cells, respectively (Figure 6.).

Unlike the combination of mitotic inhibitors with DBS, the combination of TTFields with a lower dose of Paclitaxel and Mebendazole did not produce any significant benefit compared to the electric fields treatment as a monotherapy. This may be due to the reduced treatment time of 3 days with TTFields as opposed to 5 days with DBS. Though overall, the increase in efficacy achieved with higher doses and TTFields is encouraging as this may translate to the clinic as it has already been well established through multiple trials that TTFields therapy yields very minimal overlapping toxicities when combined with further chemotherapies.


Dose-response of Paclitaxel in SF188 cells
Relative fold change in metabolic activity
1.1
1.0
0.9
0.8
0.7
0.6
0.5
0.01nM
4.6nM
0.0001
0.001
0.01
0.1
1
10
100
1000
Drug Concentration (nM)


Dose-response of Mebendazole in SF188 cells
Relative fold change in metabolic activity
1.1
1.0
0.9
0.8
0.7
0.6
0.1μM
1.2μM
0.0001
0.001
0.01
0.1
1
10
100
Drug Concentration (nM)


Dose-response of Paclitaxel in UW228-3 cells
Relative fold change in metabolic activity
1.1
1.0
0.9
0.8
0.7
0.6
0.5
0.01nM
0.8nM
0.0001
0.001
0.01
0.1
1
10
100
1000
Drug Concentration (nM)

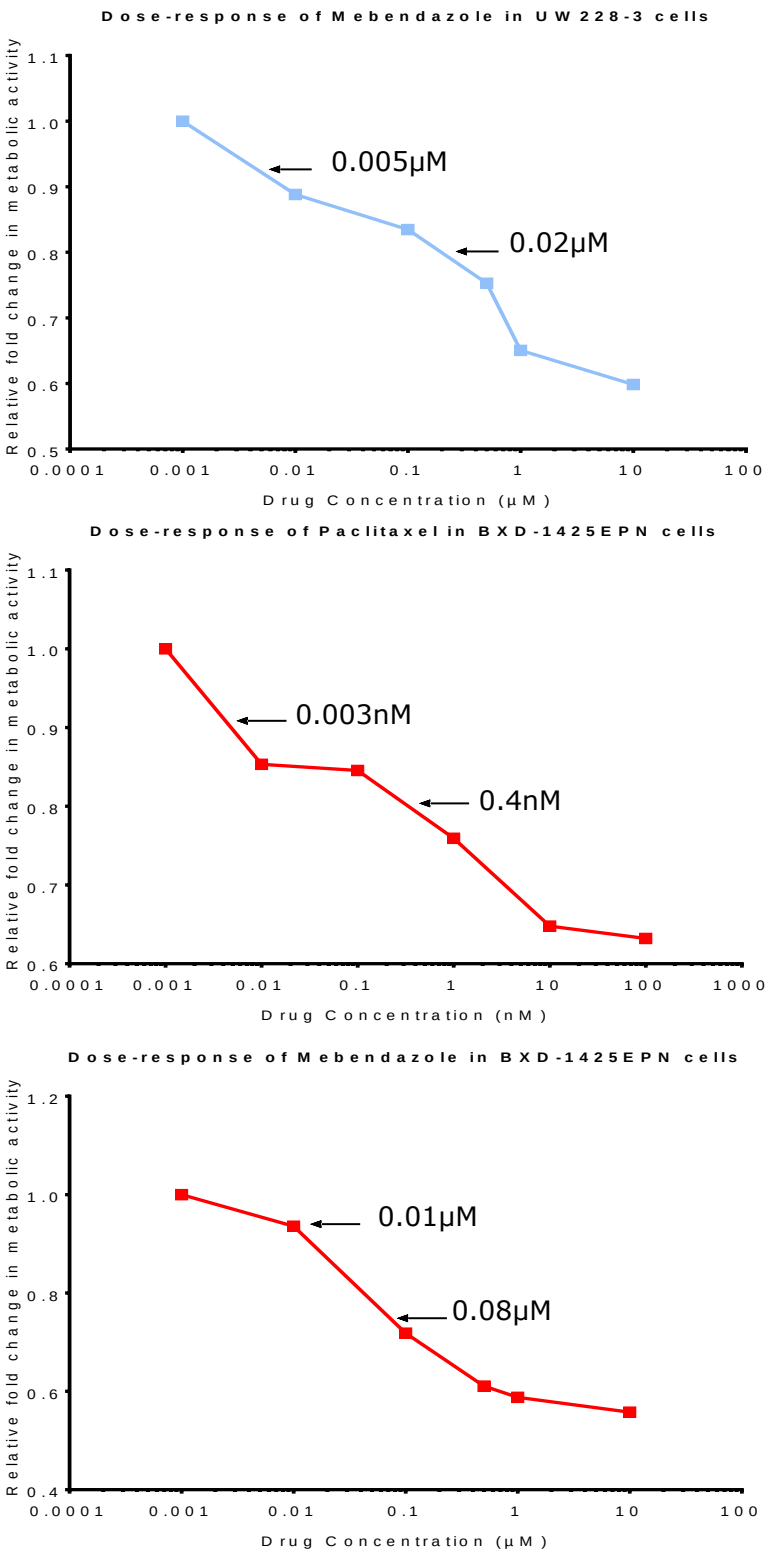
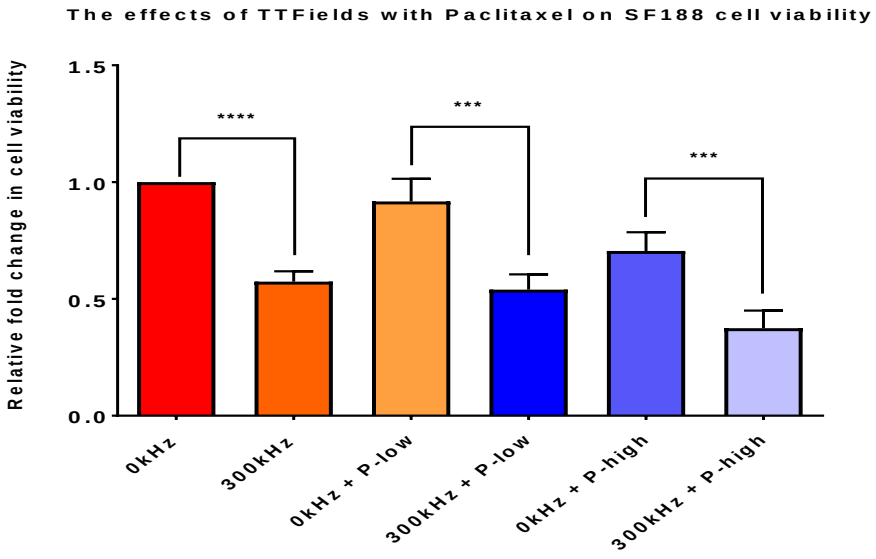
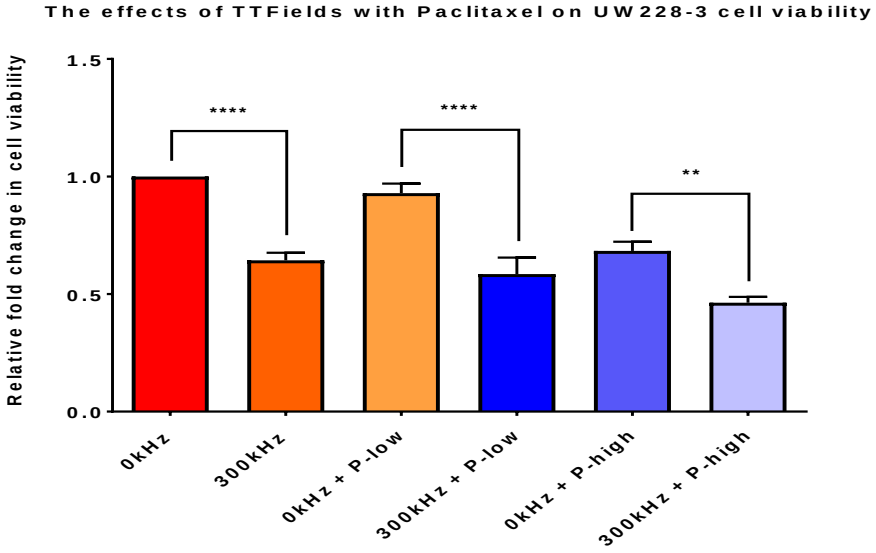
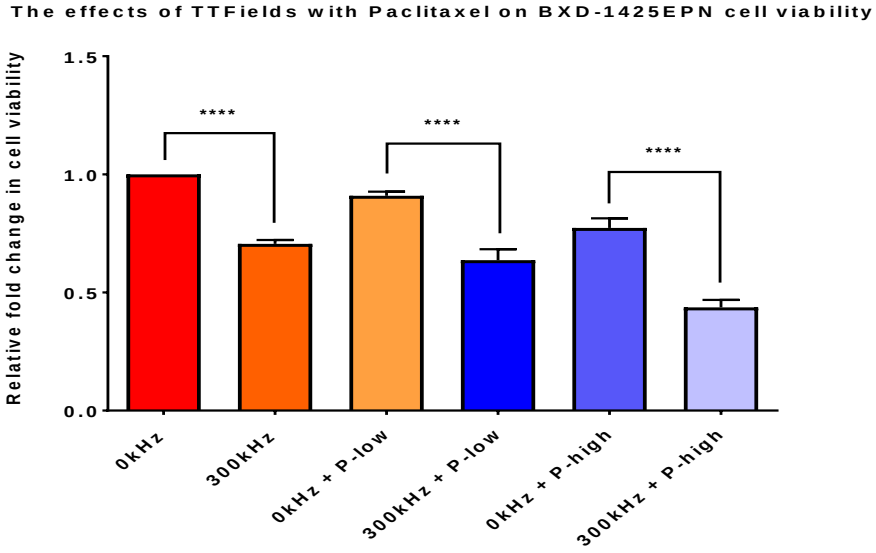


Figure 5. The dose-response curves of SF188, UW228-3 and BXD-1425EPN cell lines treated with Paclitaxel and Mebendazole. The graphs show the 'high-dose' and 'low-dose' concentrations of the drugs used in our combination studies with TTFields.


The effects of TTFields with Paclitaxel on SF188 cell viability
Relative fold change in cell viability
1.5
1.0
0.5
0.0
****
***
***
0kHz
300kHz
0kHz + P-low
300kHz + P-low
0kHz + P-high
300kHz + P-high


The effects of TTFields with Paclitaxel on UW228-3 cell viability
Relative fold change in cell viability
1.5
1.0
0.5
0.0
****
****
**
0kHz
300kHz
0kHz + P-low
300kHz + P-low
0kHz + P-high
300kHz + P-high


The effects of TTFields with Paclitaxel on BXD-1425EPN cell viability
Relative fold change in cell viability
1.5
1.0
0.5
0.0
****
****
****
0kHz
300kHz
0kHz + P-low
300kHz + P-low
0kHz + P-high
300kHz + P-high

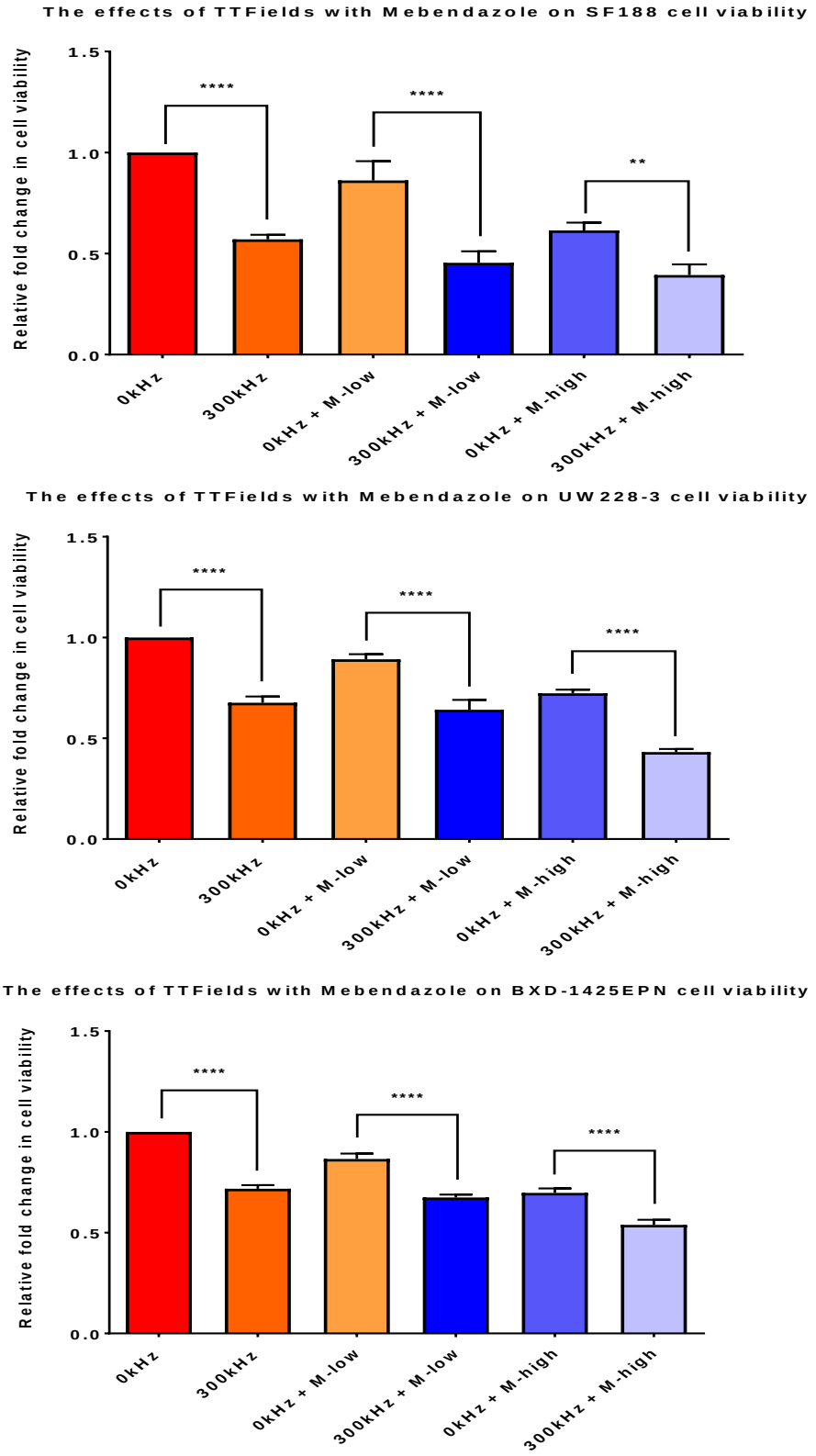


Figure 6. The effects of TTFields in combination with Paclitaxel and Mebendazole on SF188, UW228-3 and BXD-1425EPN cell lines on the metabolic activity assessed with Presto Blue assay. The 'high dose' being the IC50 of the drug and the low dose being described in Figure 6. Cells were treated with their determined optimal frequency TTFields for 72 hours

in combination with high dose and low dose chemotherapy and compared to non-TTFields treated cells in combination with high dose and low dose chemotherapy.

4. Conclusions

The primary objectives of this chapter were to establish;

1. If TTFields had efficacy against our panel of high-grade brain tumour cell lines at clinically deliverable frequencies?
2. How the frequency may be optimised to each tumour, and its cell types?
3. Confirm whether TTFields cause arrest G2/M arrest in paediatric brain tumour cell lines?
4. Can the efficacy of mitotic inhibitors be augmented with the addition of TTFields?

4.1. Main Findings

4.1.1. TTFields have anti-proliferative effects on high-grade paediatric brain tumour cell lines

In this chapter we have shown that TTFields have an anti-proliferative effect on our paediatric GBM, paediatric Medulloblastoma, paediatric Ependymoma, and our primary adult invasive margin cell lines. Efficacy was achieved with TTFields of a clinically deliverable frequency and intensity. Efficacy was correlated with frequency, with clear optimal frequencies being established for our cell lines, with exception of the Ependymoma cell lines. The optimal frequency was largely correlated with cell size, and overall efficacy was correlated with the doubling time of the cell. Lastly, TTFields was shown to have no effect on our non-dividing astrocyte cell line while having an anti-proliferative effect on our actively-dividing neural stem cell line, similar to our observations with DBS electric fields in Chapter 2, Section 3.5.

4.1.2. TTFields cause mitotic arrest at the G2/M checkpoint in paediatric brain tumour cell lines

Here we report that our brain tumour cell lines arrest at the G2/M checkpoint following 72 hours of TTFields treatment, while having as well as causing minimal sub-G0-phase accumulation – implying a minimal cytotoxic effect of the treatment. The accumulation of cells in the G2/M phase followed extended TTFields treatment is in line with all other *in vitro* TTFields literature.

4.1.3. TTFields efficacy may be augmented with the addition of mitotic inhibitors

Lastly, we demonstrated that the efficacy of TTFields can be improved with the addition of the G2/M targeting agents, Paclitaxel and Mebendazole, across our paediatric brain tumour cell lines.

4.2. Future Work

This study into the effects of TTFields on paediatric brain tumour cell lines has provided data demonstrating efficacy *in vitro*, and has identified many directions for future work;

1. Characterisation of the effects of TTFields on a more extensive panel of normal brain cell lines.
2. Further combinational studies with chemotherapies used for each tumour type in the clinic, with potential for a targeted approach following a more thorough elucidation of genetic and pathways targets of TTFields treatment.
3. Further exploration of the influence of frequency on a larger panel of paediatric brain tumour cell lines.

4.2.1. Future Work Hypotheses

1. TTFields will have very little to no effect on the viability of non-proliferative normal brain cell lines.
2. The efficacy of chemotherapies may be improved with the addition of TTFields.
3. The efficacy of TTFields may be improved with the optimisation of frequency for each cell line, independent upon tumour type.

4.2.2. TTFields and the Brain

Here we have shown that TTFields have an anti-proliferative effect on our human neural stem cell line, but do not on our human astrocyte cell line. The brain consists of many different cell types, with populations of non-dividing and actively dividing cells, especially throughout neurogenesis in children (von Bartheld et al., 2016, Llaguno and Parada, 2016, Zong et al., 2012, Sorrells et al., 2018). We would like to test TTFields on a more extensive panel of non-dividing and dividing brain cell lines, extending beyond astrocytes and neural stem cells. This is because the developing

brain of a paediatric patient may be more mitotically active than an adult patient, and we've shown how TTFields have an anti-proliferative effect on neural stem cells. TTFields exhibits minimal side-effects beyond skin-related toxicities, and the notion that TTFields may have anti-proliferative effects within the developing brain may also limit this therapy to certain patient populations due to risk of long-term neurocognitive deficits as with other therapies (Freund et al., 2015, Sanders et al., 2007). Although, all current therapies carry significant risks of toxicity to the developing brain.

4.2.3. TTFields and the Combination Approach

We have combined TTFields with Paclitaxel and Mebendazole to augment the microtubule perturbing effects of TTFields with microtubule targeting agents to enhance the efficacy. We would like to test TTFields in combination with other clinically relevant chemotherapies and radiotherapy for paediatric brain tumours. We would also like to combine TTFields with agents which target stages of the cell cycle other than the G2/M phase to assess how this combinational approach affects the efficacy of the treatment. Furthermore, following greater characterisation of the mechanisms of action of TTFields other than G2/M specific mechanisms, we would like to combine TTFields with these targeted therapies and characterise these interactions.

4.2.4. TTFields and Paediatric Brain Tumours

Previous reports have shown how cell lines from the same origin have the same optimal frequency (Kirson et al., 2004, Kirson et al., 2009d). We tested a panel of paediatric brain tumours against a range of TTFields frequencies, demonstrating variable optimal frequencies between tumour types and their cell lines. We would like to expand our panel of cell lines in number, as well as to other high-grade paediatric tumour types, and assess how the optimal frequency differs between the cell lines and elucidate as for what reason the frequencies differ.

CHAPTER 4

ELECTROGENOMICS

Chapter 4: Electrogenomics

1. Introduction

Many reports have demonstrated mechanisms of action, notably G2/M accumulation through perturbation of mitotic proteins, which may or may not account solely for the efficacy observed with TTFields treatment (Gera et al., 2015, Giladi et al., 2015c, Shteingauz et al., 2018). Karanam and colleagues postulated that TTFields may function through novel mechanisms not yet described, and took a genome-wide RNA-seq approach assessing differential changes in gene expression and pathway signalling between 'more-responsive' and 'less-responsive' NSCLC cell lines (Karanam et al., 2017). The gene expression analyses confirmed previous reports (Gera et al., 2015, Kirson et al., 2004) through demonstrating dysregulation of mitotic genes and pathways. The novel finding was the apparent downregulation of BRCA1 signalling following TTFields treatment, with a more pronounced downregulation in the more-responsive cell lines, suggesting an inverse correlation between sensitivity to TTFields and BRCA1 pathway signalling (Karanam et al., 2017). These observations give further credence to data regarding increases in TTFields efficacy before or following IR treatment (Giladi et al., 2017, Ho Kim et al., 2016), given how BRCA1 signalling is involved with DNA double strand break-repair (Karanam et al., 2017). Another conclusion of this study was suggesting a combination of TTFields with poly ADP ribose polymerase (PARP) inhibitors to target both single strand break- and double strand break-repair mechanisms of cancer cells to increase efficacy (Karanam et al., 2017), however, this has yet to be explored.

We hypothesise that a similar genome-wide approach may provide both novel mechanisms of DBS electric fields and TTFields treatment, and novel candidates for combinational therapeutics. This chapter presents our exploratory study of our two distinct electric treatment modalities on the genome of our commercial adult (U87), commercial paediatric (KNS42), and primary adult (GIN-31) GBM cell lines.

1.1. Hypotheses

DBS electric fields and TTFields will have significant effects upon the genetic profiles of the GBM cell lines, with particular emphasis on cell cycle and DNA-repair genes and pathways.

1.2. Aims and Objectives

This chapter presents the genetic aberrations of both DBS electric fields and TTFields treatment on our U87, KNS42 and GIN-31 GBM cell lines. The aims of this chapter were to;

1) Characterise genome-wide gene expression effects of DBS electric fields and TTFields on GBM cell lines;
2) Identify common and differential mechanisms of DBS electric fields and TTFields.

The objectives for this study were;

1) Assess how DBS electric fields and TTFields influence gene expression levels via RNA-seq;
2) Assess which molecular pathways are implicated through gene expression changes in GBM cell lines treated with DBS electric fields and TTFields;
3) Validate RNA-seq results with Western blot;
4) Propose novel mechanisms and suggest novel therapeutic targets for future combinational studies.

2. Methods

2.1. Cell Culture and Cell Lines

All cell lines and basic cell subculture techniques used in this chapter as described in Chapter 2, Section 2.1.

2.2. Gene Expression Analysis

2.2.1. Electric Fields Treated Cell Sample Collection

Cells were treated as described in dedicated DBS (Chapter 2, Section 2.2) and TTFields (Chapter 3, Section 2.2) methods sections. Cells had their growth medium removed, cells were washed with HBSS, and Trypsin was added. Trypsinised cells were incubated in a CO_2 incubator and incubated for 5-10 minutes at 37^0C to allow the cells to detach. The Trypsin was neutralised with an equal volume of growth medium. The cells were then centrifuged at 120 x g for 5 minutes to pellet the cells. The supernatant was removed, the pellet was washed with PBS, then centrifuged at 120 x g for 5 minutes to repellet the cells. The cells were then 'flash frozen' in liquid nitrogen before being stored long-term at -80^0C ready for further analysis.

2.2.2. RNA Extraction

RNA extraction was performed using the mirVana™ miRNA Isolation Kit (ThermoFisher™). Cells pellets stored at -80^0C were thawed on ice before adding 300µL of miRNA Homogenate Additive to the cells. The cells and additive were mixed via vortexing and then were incubated on ice for 10 minutes. Following incubation, 300µL of Acid-Phenol: Chloroform was added to the sample mix, and then vortexed for 30 seconds to mix before centrifuging for 5 minutes at 10,000 x g. Centrifuging separated the mix into 3 phases, the upper aqueous phase was transferred to a fresh tube and 400µL of room temperature 100% ethanol was added. A collection tube with a filter cartridge was prepared for each sample used. The cell/ethanol mix was pipetted onto the filter cartridge and centrifuged for 15 seconds at 10,000 x g. The flow-through was discarded, and then 700µL of miRNA Wash Solution 1 was added to the filter cartridge and then centrifuged at 10,000 x g for 10 seconds, with the flow-through discarded.

This process was repeated 2 more times with 500µL of Wash Solution 2, and the flow through was discarded one last time, and the filter cartridge was transferred to a fresh collection tube. Up to 50µL of nuclease-free water pre-heated to 95^0C was pipetted into the centre of the filter. The collection tubes were centrifuged at 10,000 x g for 30 seconds to collect the final RNA product.

2.2.3. RNA Amplification

Samples which did not meet the minimum RNA requirements for microarray analysis (50ng/µl in 20µl) were amplified with the Repli-g™ WTA Single Cell kit (QIAGEN) (Table 2.). Following RNA extraction, 8µl of RNA was transferred into a microcentrifuge tube. 3µl of Denaturation Buffer was added to the RNA and mixed by gently vortexing and briefly centrifuging. The mix was then incubated for 3 minutes at 95°C and then cooled to 4°C. 2µl of the gDNA Wipeout Buffer was added to the mix before being vortexed and centrifuged briefly. The mix was then incubated for 10 minutes at 42°C and then cooled to 4°C. The Quantiscript RT mix was freshly prepared as detailed in Table 1**.**, and then 6µl of Quantiscript RT mix was added to the mix before being vortexed and centrifuged briefly. The mix was then incubated for 60 minutes at 42°C, then for 3 minutes at 95°C, before being cooled to 4°C. The Ligation mix was freshly prepared as detailed in Table 1**.**, and then 10µl of the Ligation mix was added to the mix before being vortexed and centrifuged briefly. The mix was then incubated for 30 minutes at 24°C, then for 5 minutes at 95°C, before being cooled to 4°C. The REPLI-g SensiPhi Amplification mix was the freshly prepared as detailed in Table 1**.**, and then 3µl of REPLI-g SensiPhi Amplification mix was added to the mix before being vortexed and centrifuged briefly. The mix was then incubated for 120 minutes at 30°C, then for 5 minutes at 65°C, before being cooled to 4°C. The amplified cDNA product was then stored at -20°C until further use.

Reagent	Components	Quantity
Quantiscript RT Mix	RT/Polymerase Buffer Oligo dT Primer Quantiscript RT Enzyme Mix	4µl 1µl 1µl
Ligation Mix	Ligase Buffer Ligase Mix	8µl 2µl
REPLI-g SensiPhi Amplification Mix	REPLI-g sc Reaction Buffer REPLI-g SensiPhi DNA Polymerase	29µl 1µl

Table 1. Table showing reagents used in the RNA amplification and their components.

STEP	CONDITION	TIME
Denaturation	95^0C 4^0C	3 minutes ∞
gDNA Removal	42^0C 4^0C	10 minutes ∞
Reverse Transcription	42^0C 95^0C 4^0C	60 minutes 3 minutes ∞
Ligation	24^0C 95^0C 4^0C	30 minutes 5 minutes ∞
Whole Transcriptome Amplification	30^0C 65^0C 4^0C	120 minutes 5 minutes ∞

Table 2. Table showing the steps and conditions of the RNA amplification.

2.2.4. Microarray Analysis

We used the Human Clariom™ S Array (ThermoFisher™) for an unbiased, whole transcriptome gene expression analysis of DBS and TTFields treated cells. Microarray processing was performed by Dr. Marcos Castellenos and Dr. Iqbal Khan of Nottingham Arabidopsis Stock Centre (NASC), University of Nottingham.

2.2.4.1.1. RNA Quality and Quantification

The Agilent 2100 Bioanalyzer was used with either a 'Eukaryote Total RNA Nano Assay' (Agilent Technologies™) for RNA samples or the 'High Sensitivity DNA Assay' (Agilent Technologies™) for the amplified RNA samples. The quality control measurements included RNA concentration (ng/µl), RNA Integrity Number (RIN) score, as well as the rRNA ratio (28S/18S). The accepted values we used were; RNA concentration >50ng/µl, a RIN score of >9.0, and an rRNA ratio of >2.0.

2.2.4.1.2. First-Strand cDNA Synthesis

First, a master mix containing 4µl of First-Strand Buffer and 1µl First-Strand Enzyme per RNA reaction plus 5% for pipetting error was prepared on ice, vortexed and then centrifuged briefly. On ice, 5µl of total RNA was added to a 5µl aliquot of the First-Strand Master Mix, vortexed and then centrifuged briefly. The RNA mix was then incubated in a thermal cycler for 1 hour at 25^0C, 1 hour at 42^0C, 2 minutes at 4^0C, and then stored on ice before moving immediately to Second-Strand cDNA Synthesis.

2.2.4.1.3. Second-Strand cDNA Synthesis

A master mix containing 18µl of First-Strand Buffer and 2µl Second-Strand Enzyme per First-Strand cDNA reaction plus 5% for pipetting error was prepared on ice, vortexed and then centrifuged briefly. On ice, 20µl of Second-Strand Master Mix was added to a 10µl aliquot of the First-Strand cDNA, vortexed and then centrifuged briefly. The cDNA mix was then incubated in a thermal cycler for 1 hour at 16^0C, 10 minutes at 65^0C, 2 minutes at 4^0C, and then stored on ice before moving immediately to Synthesize cRNA by *in vitro* transcription.

2.2.4.1.4. Synthesize cRNA by in vitro Transcription

A master mix containing 24µl of IVT Buffer and 6µl IVT Enzyme per Second-Strand cDNA reaction plus 5% for pipetting error was prepared at

room temperature, vortexed and then centrifuged briefly. At room temperature, 30µl of IVT Master Mix was added to a 30µl aliquot of the Second-Strand cDNA, vortexed and then centrifuged briefly. The cDNA mix was then incubated for 16 hour at 40^0C, 2 minutes at 4^0C, and then stored on ice before moving immediately to Purify cRNA.

2.2.4.1.5. Purify cRNA

Purification beads are added to each cRNA, mixed by pipetting up and down, and then the mix is transferred to a U-bottom plate. The cRNA-purification bead mix is then incubated for 10 minutes at room temperature to allow cRNA to bind to the purification beads. The U-bottom plate is transferred to a magnetic stand to pellet/capture the purification beads, and the supernatant is aspirated and discarded. The purification beads were then washed with 200µl of 80% ethanol for 30 seconds. The 80% ethanol was then aspirated and discarded. A further two washes with 80% ethanol was performed, and then the remaining purification bead pellet was air-dried.

The cRNA was eluted by adding 27µl of 65^0C nuclease-free water and incubated for 1 minute at room temperature. The solution was mixed by pipetting up and down. The solution was then transferred to a magnetic stand to capture the purification beads. The nuclease-free water, which now contains the cRNA, was aspirated and transferred to a fresh tube and then stored on ice before assessing cRNA yield via a NanoDrop Spectrophotometer and Second-Cycle Single-Strand cDNA Synthesis.

2.2.4.1.6. Second-Cycle Single-Strand cDNA Synthesis

A cRNA sample with a concentration of 625ng/µL was made up with nuclease-free water to a volume of 24µL, producing a solution of 15µg of cRNA. The cRNA was mixed with 4µL of 2^{nd}-Cycle Primers on ice, vortexed, and then centrifuged briefly. The mix was then incubated in a thermal cycler for 5 minutes at 70^0C, 5 minutes at 25^0C, 2 minutes at 4^0C, and then stored on ice.

A master mix containing 8µl of 2^{nd}-Cycle ss-cDNA Buffer and 4µl 2^{nd}-Cycle ss-cDNA Enzyme per 2^{nd}-Cycle ss-cDNA reaction plus 5% for pipetting error was prepared on ice, vortexed and then centrifuged briefly. On ice,

12µl of 2nd-Cycle ss-cDNA Master Mix was added to a 28µl aliquot of the cRNA-2nd-Cycle Primer mix, vortexed and then centrifuged briefly. The cRNA mix was then incubated in a thermal cycler for 10 minutes at 25^{0}C, 1.5 hours at 42^{0}C, 10 minutes at 70^{0}C, 2 minutes at 4^{0}C, and then stored on ice before moving immediately to Hydrolyze RNA Using RNase H.

2.2.4.1.7. Hydrolyze RNA Using RNase H

On ice, 4µl of RNase H is added to each 40µl 2nd-Cycle ss-cDNA sample, and then vortexed and centrifuged briefly. The 2nd-Cycle ss-cDNA mix was then incubated in a thermal cycler for 45 minutes at 37^{0}C, 5 minutes at 95^{0}C, 2 minutes at 4^{0}C, and then stored on ice. On ice, 11µl of nuclease-free water was added to each 44µl hydrolysed 2nd-Cycle ss-cDNA sample, vortexed, centrifuged briefly and then stored on ice before moving immediately to Purify Second-Cycle Single-Strand cDNA.

2.2.4.1.8. Purify Second-Cycle Single-Strand cDNA

Purification beads are added to each cRNA, mixed by pipetting up and down, and then the mix is transferred to a U-bottom plate. The cRNA-purification bead mix is then incubated for 10 minutes at room temperature to allow cRNA to bind to the purification beads. The U-bottom plate is transferred to a magnetic stand to pellet/capture the purification beads, and the supernatant is aspirated and discarded. The purification beads were then washed with 150µl of 100% ethanol for 20 minutes. The 100% ethanol was then aspirated and discarded. The purification beads were then washed with 200µl of 80% ethanol for 30 seconds. The 80% ethanol was then aspirated and discarded. A further two washes with 80% ethanol was performed, and then the remaining purification bead pellet was air-dried.

The ss-cDNA was eluted by adding 30µl of 65^{0}C nuclease-free water and incubated for 1 minute at room temperature. The solution was mixed by pipetting up and down. The solution was then transferred to a magnetic stand to capture the purification beads. The nuclease-free water, which now contains the ss-cDNA, was aspirated and transferred to a fresh tube and then stored on ice before assessing cDNA yield via a NanoDrop Spectrophotometer and Fragment and Label Single-Stranded cDNA.

2.2.4.1.9. Fragment and Label Single-Stranded cDNA

An ss-cDNA sample with a concentration of 1765ng/µL was made up with nuclease-free water to a volume of 31.2µL, producing a solution of 5.5µg of ss-cDNA. On ice, a master mix containing 10µl of nuclease-free water, 4.8µL of 10X cDNA Fragmentation Buffer, 1.0µL UDG 10U/µL, and 1.0µL APE 1 1,000U/µL per ss-cDNA reaction plus 5% for pipetting error was prepared at room temperature, vortexed and then centrifuged briefly. The 31.2µL ss-cDNA was mixed with 16.8µL of Fragmentation Master Mix on ice, vortexed, and then centrifuged briefly. The mix was then incubated in a thermal cycler for 1 hour at 37^0C, 2 minutes at 93^0C, 2 minutes at 4^0C, and then stored on ice.

On ice, a master mix containing 12µl of 5X TdT Bugger, 1.0µL of DNA Labelling Reagent 5mM, 2.0µL of TdT 30U/µL per fragmented ss-cDNA reaction plus 5% for pipetting error was prepared at room temperature, vortexed and then centrifuged briefly. The 45µL fragmented ss-cDNA was mixed with 15µL of Labelling Master Mix on ice, vortexed, and then centrifuged briefly. The mix was then incubated in a thermal cycler for 1 hour at 37^0C, 10 minutes at 70^0C, 2 minutes at 4^0C, and then stored on ice before moving immediately to Cartridge Array Hybridization.

2.2.4.10. Cartridge Array Hybridization

The GeneChip™ experiments were performed using a GeneChip™ Fluidics Station 450 (ThermoFisher™).

A master mix containing 2.3µg of fragmented and labelled ss-DNA, 1.7µl of Control Oligo B2 3nM, 5µl of 20X Hybridization Controls, 50µl of 2X Hybridization Mix, 7µl of DMSO, 9.3µl of Nuclease-free water for a total volume of 73µl per fragmented and labelled ss-DNA reaction plus 5% for pipetting error was prepared at room temperature, vortexed and then centrifuged briefly.

At room temperature, 73µl of the Hybridization Master Mix was added to a 27µl aliquot of 2.3µg fragmented and labelled ss-cDNA, vortexed and then centrifuged briefly. The ss-cDNA mix was then incubated in a thermal cycler for 5 minutes at 95^0C, then 5 minutes at 45^0C before immediately moving onto the next step.

The GeneChip™ Cartridge Array was prepared before use by inserting a pipette tip into the right upper septum (Illustrated in Figure 1.) to allow venting. 80µl of Hybridization master mix was pipetted into a septum, and then the arrays were then inserted into the hybridization oven and incubated for 16 hours at 45^{0}C and 60rpm before moving onto GeneChip™ Array Wash and Stain.

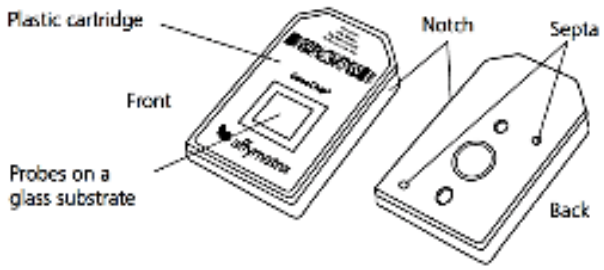


Image 1. GeneChip™ Cartridge Array

2.2.4.11. GeneChip™ Array Wash and Stain

The arrays were removed from the hybridization oven and the hybridization master mix was aspirated and stored on ice for future use. At room temperature, Wash Buffer A was added to the array. Vials were placed into the GeneChip™ Fluidics Station 450; 600µl Stain Cocktail 1 was added in sample holder 1, 600µl Stain Cocktail 2 in sample holder 2, and 800µl Array Holding Buffer in sample holder 3 – the fluidics protocol used for this process was 'FS450_0007'.

2.2.4.12. Array Strip Hybridization on the GeneAtlas™ Instrument

The previously aspirated hybridization master mix was reused, 120µl of this master was added to the middle of appropriate wells in the hybridization tray (Illustrated in Figure 2.). The hybridization tray was then placed into the Hybridization Station for 15 minutes at 45^{0}C. The results were collected and then analysed.

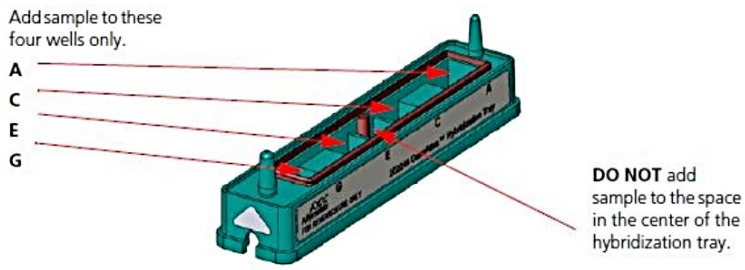


Image 2. GeneChip™ Hybridization Tray

2.2. Gene Target Analysis

Bioinformatic analyses were performed using the Partek® Genomics Suite® package, Partek® Pathway™, Gene Ontology Enrichment Analysis and Visualization tool (GOrilla), and Enrichr (Ma'ayan Laboratories). Analyses using Partek® were performed by Dr. Marcos Castellenos of Nottingham Arabidopsis Stock Centre (NASC), University of Nottingham.

2.2.4. Hierarchical Clustering Analysis

Hierarchical clustering analyses were performed using Partek®. The criteria of significant genes were; false discovery rate (Bonferroni Correction) and p-value of <0.05, and a fold-change of <-2.0 and >2.0. An unsupervised clustering method was used and analyses were displayed as heatmaps on a genome-wide scale, as well as heatmaps of the top 20 commonly differentially expressed genes within each electrical treatment. Samples G0 and K0 were untreated, samples G10 and K10 were treated with DBS electric fields, and samples G200 and K200 were treated with TTFields.

2.2.5. Volcano Plot Analysis

Volcano plots were produced using Partek®. The criteria of significant genes were; false discovery rate and p-value of <0.05, and a fold-change of <-2.0 and >2.0. The plots displays the fold-change (x-axis) and p-value (y-value) simultaneously for the differentially expressed genes of each cell line for each electrical treatment. Samples G0 and K0 were untreated, samples G10 and K10 were treated with DBS electric fields, and samples G200 and K200 were treated with TTFields.

2.2.6. Venn Diagram Analysis

Venn diagrams were produced using Partek®. The criteria of significant genes were; false discovery rate (Bonferroni Correction) and p-value of <0.05, and a fold-change of <-2.0 and >2.0. The number of commonly differentially expressed genes were generated for each treatment by comparing treated cell lines to their control samples, and then comparing to the other cell lines within the treatment condition. Comparisons between the electrical treatments were also performed. Samples G0 and K0 were untreated, samples G10 and K10 were treated with DBS electric fields, and samples G200 and K200 were treated with TTFields.

2.2.7. Gene Target Identification

Gene lists were produced using Partek®. The criteria of significant genes were; false discovery rate and p-value of <0.05, and a fold-change of <-2.0 and >2.0. The gene targets selected for western blot validation were ND5, BTNL9, and CTSD. Each of these genes were significantly differentially expressed following electrical treatments and were common between the electrical treatments. ND5 was on average the most downregulated gene following electrical treatments, BTNL9 was the only gene in the top 50 significant genes which was upregulated, and CTSD gene has been implicated in neurodegeneration mechanisms which have been identified as significant through our KEGG pathway analyses. Samples G0 and K0 were untreated, samples G10 and K10 were treated with DBS electric fields, and samples G200 and K200 were treated with TTFields.

2.2.8. Gene Ontology Analysis

Gene Ontology analyses were performed independently using Enrichr (Chen et al., 2013, Kuleshov et al., 2016). Enrichr was used at http://amp.pharm.mssm.edu/Enrichr/ and gene lists produced from each of the electrical treatments were entered into the 'gene list box' and submitted into the database to produce gene ontology lists. Samples G0 and K0 were untreated, samples G10 and K10 were treated with DBS electric fields, and samples G200 and K200 were treated with TTFields.

2.2.9. KEGG Pathway Analysis

KEGG Pathway analyses were performed independently using Enrichr (Chen et al., 2013, Kuleshov et al., 2016). Enrichr was used at http://amp.pharm.mssm.edu/Enrichr/ and gene lists produced from each of the electrical treatments were entered into the 'gene list box' and submitted into the database to produce KEGG Pathway lists. Diagrams of the KEGG pathways were produced using https://www.genome.jp/kegg/pathway/ . Samples G0 and K0 were untreated, samples G10 and K10 were treated with DBS electric fields, and samples G200 and K200 were treated with TTFields.

2.2.10. Western Blot for Validation

2.2.10.1. Bradford Assay for Protein Quantification

Cell pellets were removed from -80^{0}C storage and placed on ice. Up to 50µl of protease cocktail buffer was added, with the volume added being dependent upon cell pellet size. Samples were then incubated on ice for 20 minutes. Samples were then centrifuged for 30 minutes at 13,000 x g for 30 minutes. The cell lysate was then retrieved and transferred to a fresh Eppendorf tube.

The concentration of protein was calculated by comparing values to known concentrations of BSA (Bovine Serum Albumin). Reference samples were produced as described in Table 3., and then briefly vortexed. Protein samples were produced by adding 2µl lysate to 1ml Protein Assay dye (Bio-Rad Laboratories) to be compared to BSA control samples.

Solution	Concentration of BSA (µg/ml)							
BSA (µl)	0	1	5	10	15	20	30	40
Protein Assay Dye (µl)	1,000	999	995	990	985	980	970	960
Total Volume (ml)	1	1	1	1	1	1	1	1

Table 3. Table showing the reagents used for the reference samples in the Bradford Assay.

200µl of the BSA standards and the protein lysate were added to a 96 well plate in triplicate, and then the absorbance was read using FLUOstar Omega (BMG Labtech). The absorbance of the triplicates were averaged and plot as an XY scatter graph. The concentration of the protein lysate was determined by comparing to the linear concentrations of BSA using y=mx+c.

2.2.10.2. Western Blot

Gel cassettes were assembled in a casting frame before adding the gel buffers. A 10% acrylamide gel was prepared consisting of a 1.5µm lower gel and a 1.5µm upper gel (Table 4.). The lower gel was poured into the gel cassette and was incubated for one hour at room temperature to allow it to set. The upper gel was then poured on top of the now set lower gel and a comb was inserted into the upper gel before it was set to form wells for protein loading. The upper gel was incubated for one hour at room temperature.

Lower Gel	
Reagent	Volume
Lower Gel Buffer	2.0ml
Acrylamide	2.66ml
Distilled H_2O	3.34ml
10% Ammonium Persulphate Solution (APS)	50.0µl
Tetramethylethylenediamine (TEMED)	6.6µl
Upper Gel	
Reagent	Volume
Upper Gel Buffer	1.25ml

Acrylamide	0.62ml
Distilled H_2O	3.0ml
10% Ammonium Persulphate Solution (APS)	25.0µl
Tetramethylethylenediamine (TEMED)	5.0µl

Table 4. Table showing the reagents used for the lower and upper gels in the Western Blot.

After the upper gel had set, the comb was removed. The gel cassette was then inserted into the Electrode assembly and then placed inside a minitank. 1X Electrode buffer was produced (Table 5.) and then was used to fill the minitank, making sure to cover the gel assembly, and the comb was removed from the upper gel.

Electrode Buffer 1X	
Reagent	Quantity/Volume
Tris Base	30.0g
Glycine	144.0g
Sodium Dodecyl Sulfate (SDS)	10.0g
Distilled H_2O	1L
Transfer Buffer 1X	
Reagent	Quantity/Volume
Tris Base	3.03g
Glycine	14.4g
Methanol	200ml
Distilled H_2O	800ml
Tris Buffered Saline (TBS) 10X	
Reagent	Quantity/Volume
Tris Base	24.2g
NaCl	80.0g

Distilled H_2O	1000ml
TBS-T (Tween) 1X	
Reagent	Quantity/Volume
TBS	1000ml
Tween	1.0ml
Distilled H_2O	1000ml
Marvel-TBS-T	
Reagent	Quantity/Volume
TBS-T	500ml
1% Marvel Milk Powder	25.0g

Table 5. Table showing the reagents used for 10X Electrode Buffer.

A total of 20µg of protein was combined with 20% of the volume used of 1:20 β-mercaptoethanol and then boiled at 99^0C for 3 minutes. The samples were then centrifuged at 13,000rpm for 1 minute before being loaded into the gel. A ladder was used to control for protein size of the samples. The gel was run for 60 minutes at 140.0V to allow adequate separation of our samples.

The gel cassette was removed from the Electrode apparatus and transferred into Transfer buffer (Table 5.) for 10 minutes. A nitrocellulose membrane was used for the transfer step, and was first soaked in transfer buffer for 10 minutes. The gel was removed from the gel cassette and placed onto the nitrocellulose membrane before being secured into the Transfer apparatus, submerged in Transfer buffer, and then run overnight at 25V at 4^oC. The nitrocellulose membrane was then removed from the Transfer apparatus and transferred into blocking solution, the solution we used was Marvel-TBS-T (Table 5.), for 60 minutes at room temperature. The membrane was then washed in TBS-T (Table 5.) twice for 5 minutes at room temperature. The membrane was then incubated for 60 minutes at room temperature in a specific primary antibody (Table 6.) on a rocker. The membrane was then washed twice in Marvel-TBS-T for 5 minutes, and then washed in TBS-T for 5 minutes at room temperature. The membrane was then incubated in the appropriate secondary antibody (Table 6.) for

60 minutes at room temperature on a rocker. The secondary antibody was removed and the membrane was then washed three times in Marvel-TBST for 5 minutes, washed in TBS-T for 5 minutes, and then washed in TBS for 5 minutes at room temperature.

Western Blot Antibodies		
Target	Dilution	Secondary Antibody
ND5 (Abcam) – 67kDa	1:100	Rabbit
BTNL-9 (Abcam) – 50kDa	1:1000	Rabbit
CTSD (Abcam) – 46kDa	1:2000	Rabbit
GAPDH (Abcam) – 36kDa	1:10,000	Mouse

Table 6. Table showing the primary and secondary antibodies used for Western blot.

The membrane was then incubated in ECL (Enhanced Chemiluminescence) plus western blotting detection solutions for 5 minutes at room temperature. Excess solution was removed and the membrane was transferred to a photography cassette, and placed on top of photographic film for an appropriate exposure time (Table 16.) in the dark room. After exposure, the photographic film was then washed in the film developer solution until the protein bands become visible, then washed in the fixing solution, and then washed in water briefly before drying.

3. Gene Expression Results and Discussion

3.1. DBS electric fields and TTFields treatment causes gene expression changes in GBM cell lines

3.1.1. Results and Discussion

Firstly, we ran our DBS electric fields treated at 10.0V/130Hz/450µS for 5 days and TTFields treated at 200kHz for 3 days GBM cell lines on Clariom™ S Human Assays to produce genome-wide expression data for further analysis. We chose 5 days treatment for the DBS treated cells as we have previously shown this time-point to have significant efficacy while improving cell yield for the experiment. We also chose 3 days treatment for the TTFields treated cells as we have characterised the effects of TTFields on our cell lines at this time point, as TTFields treatment of a shorter time has been demonstrated to produce different effects with regards to cell cycle accumulation (Silginer et al., 2017).

From our heat maps with hierarchical clustering analyses (Figure 1.) and our volcano plots (Figure 2.), we have demonstrated that electrical treatment, whether DBS electric fields or TTFields, significantly biases towards the downregulation of genes of treated GBM cell lines. Consistent clustering of our samples was typically apparent, however, our U87 cells treated with DBS electric fields (U10) clustered with all of our untreated samples (Figure 1A). Peculiar results for our U10 samples were also shown in our volcano plots (Figure 2C), with these samples showing a bias towards upregulation of genes, dissimilar from all other treatments which appear to be relatively uniform. We believe that it's more likely that there was a problem with the U10 samples hybridising to the CHIPs, rather than U87 cells responding uniquely to DBS electric fields. This is because of a few reasons; our U10 samples were collected in the exact same fashion as the other samples following their respective treatment, our U10 samples passed the QC process like the other samples ruling out the possibility of low quality samples, lastly, all of our previous experiments have shown clear similarities between our cell lines following DBS electric field treatment. However, the possibility of U87 cells having a distinct genetic signature following DBS electric fields treatment is also to be considered.

Based off the assumption that the U10 sample data is unreliable due to technical errors, we chose to exclude the data in further analyses, including; production of gene lists, pathway analyses, and gene ontologies.

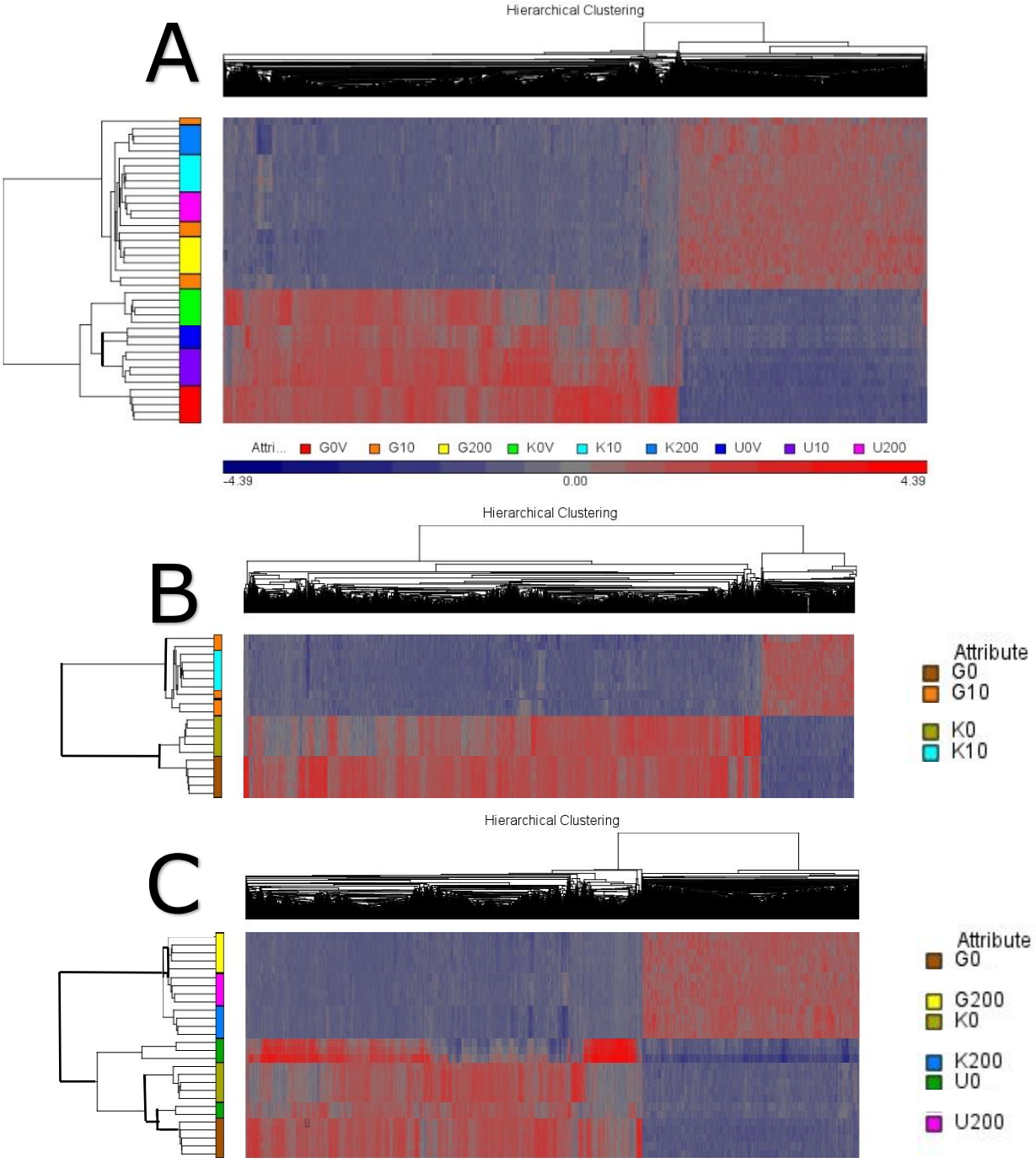


Figure 1. Hierarchical clustering analysis of the gene expression patterns of up-regulation and down-regulation of GBM cell lines following electrical treatment. A) Heat map showing all cell lines treated with 130Hz/10V/450µs electric fields or 200kHz TTFields and untreated cells. B) Heat map showing KNS42 and GIN-31 cells treated with 130Hz/10V/450µs (K10 and G10) electric fields and untreated cells (K0 and G0). This heat map excludes U87 cells. C) Heat map showing U87, KNS42 and GIN-31 cells treated with 200kHz TTFields (U200, K200 and G200) and untreated cells (U0, K0 and G0). **Key**; Blue = downregulation, Red = Upregulation.

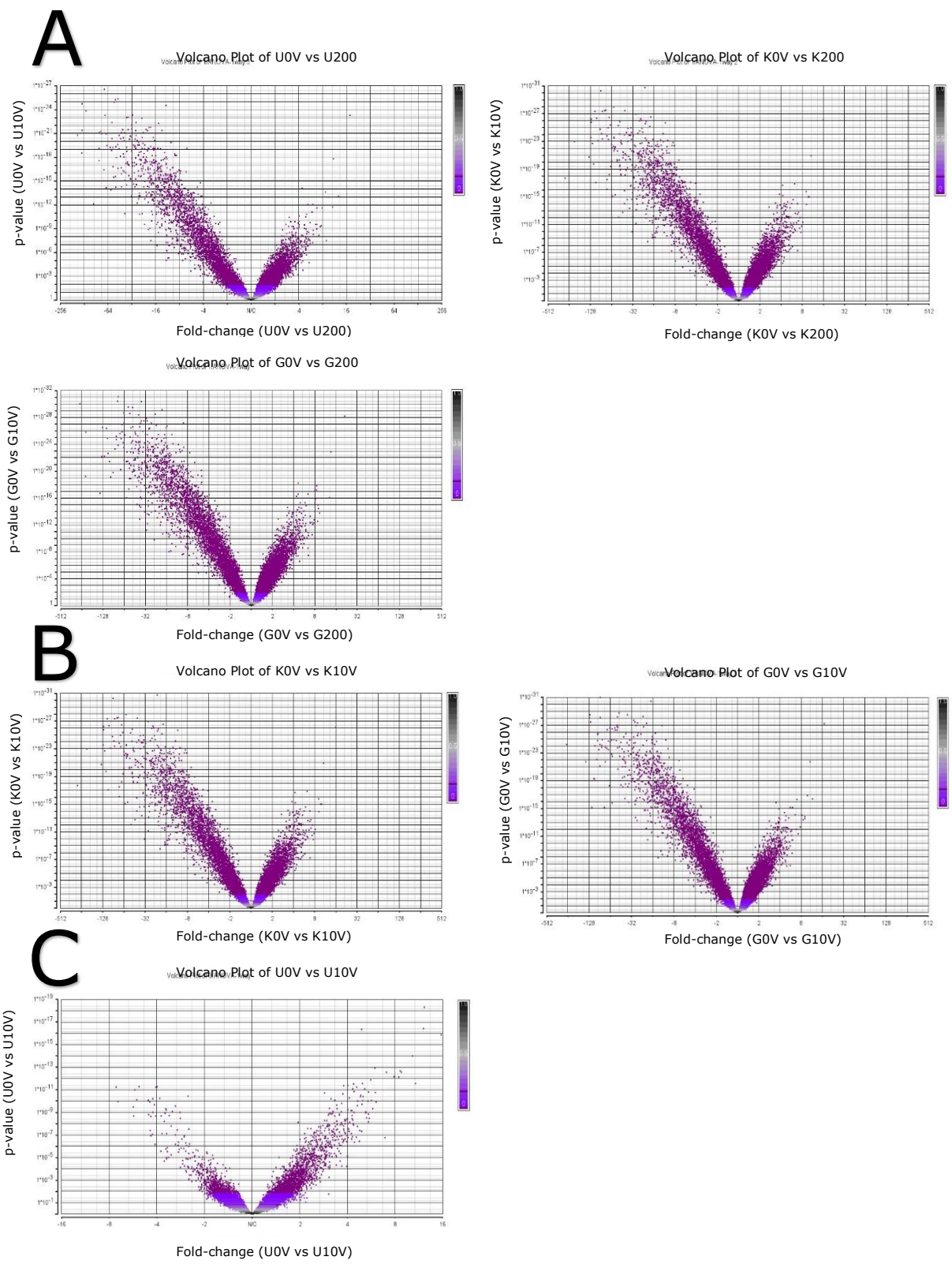


Figure 2. Volcano plots demonstrating the gene expression patterns of up-regulation and down-regulation of GBM cell lines following electrical treatment. A) Volcano plots of U87, KNS42 and GIN-31 cells treated with 200kHz TTFields for 72 hours relative to untreated cells. B) Volcano plots of KNS42 and GIN-31 cells treated with 130Hz/10V/450µs electric fields for 5 days relative to untreated cells. C) Volcano plot of U87 cells treated with 130Hz/10V/450µs electric fields for 5 days relative to untreated cells.

3.2. DBS electric fields and TTFields treatment causes similar genetic aberrations

3.2.1. Results and Discussion

We next interrogated the DBS electric fields and TTFields treated data sets to see whether there were any common differentially expressed genes following electrical treatment, and to also describe differences in their mechanisms on the genetic level. We produced gene lists to show how genes are differentially expressed following DBS electric fields and TTFields treatment, as well as how these differ between cell lines (Appendix 1.). We took these gene lists and compared the number of differentially expressed genes for each treatment, between the treatments, and between the cell lines (Figure 3.). We also showed via Venn diagrams (Figure 3A. and 3E.) how including U10 samples very significantly reduces the number of commonly differentially expressed genes, further re-affirming why we excluded these samples from our analyses. We observed significant overlap between the electrical treatments, the number of commonly expressed genes between the cell lines of a given treatment were 3345 genes for DBS electric fields (Figure 3C.) and 2690 genes for TTFields (Figure 3B.) treated cells, whereas the number of commonly expressed genes between these two treatments is 2376 (Figure 3D).

We produced a list of the top 20 differentially expressed genes (Figure 4.), with significance determined by p-value, for DBS electric fields and TTFields treatments, and we observed 16 of these 20 genes to be common to both treatments. Of these 16 genes, it also appears that these genes are involved in mitochondrial and ER functioning; including, electron transport, metabolism, ion signalling and protein folding. It is worth noting that all of these associated genes are significantly downregulated, implying that these processes are also downregulated. The downregulation of mitochondrial and ER functioning may potentially be a result of the prolonged mitotic arrest from the electrical treatment, these observations have already been made in TTFields studies where it has been shown that prolonged TTFields exposure may promote ER stress (Shteingauz et al., 2018). Furthermore, the pathway proposed by Shteingauz and colleagues

described ATP (Adenosine triphosphate) depletion also being a product of TTFields exposure (Shteingauz et al., 2018). ATP production through metabolic pathways, such as glycolysis and the citric acid cycle, is reliant upon reduction of NAD^+ to NADH (Nicotinamide Adenine Dinucleotide) (Jang et al., 2013). This redox process of donating and accepting electrons is reliant upon the electron transport chain, and therefore, it may also be potentially a novel mechanism of electric fields treatments on GBM cell lines. Lastly, only one of our top 20 genes was significantly upregulated following electrical treatment, BTNL9 (Figure 4.). BTNL9 is a butyrophilin-like protein involved with the T-cell immune response (Guo and Wang, 2015). A proposed mechanism of TTFields is through immunogenic cell death (Giladi et al., 2016), with an immune response being observed in response to TTFields *in vitro* and *in vivo* (Kirson et al., 2009b, Kirson et al., 2009c). So our results suggest that both TTFields and DBS electric fields treatment may promote an immune response in our GBM cell lines.

Lastly, we chose 3 gene targets to validate our gene expression data via western blotting – and we chose the genes ND5, CTSD, and BTNL9. Our western blot confirmed the expression patterns observed with the gene expression data translated to the changes observed at the protein level (Figure 6.).

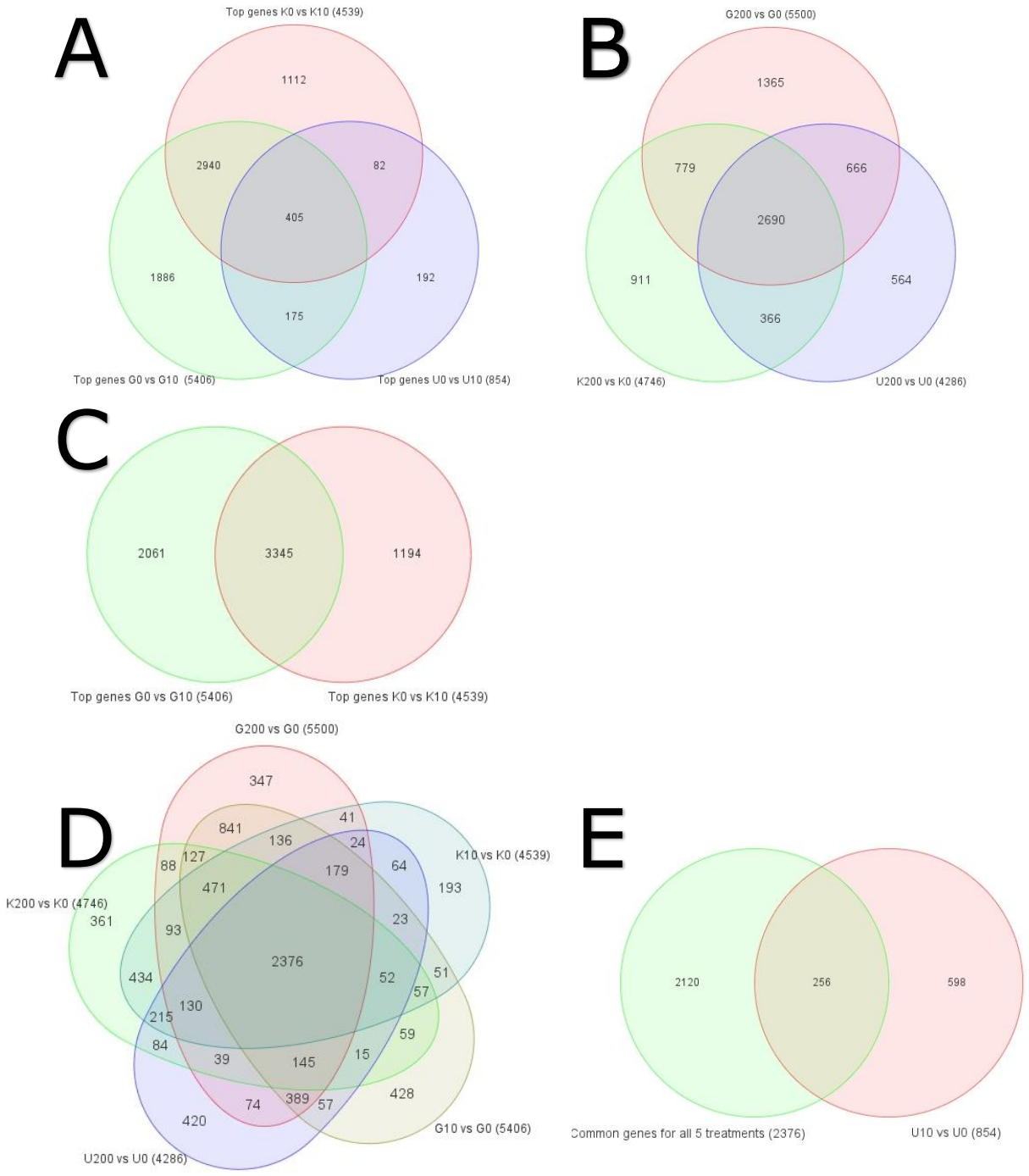


Figure 3: Venn diagrams demonstrating the common gene expression patterns of DBS electric fields and TTFields treated GBM cell lines. A) Venn diagram of U87, KNS42 and GIN-31 cells treated with 130Hz/10V/450µs electric fields showing numbers of common and differentially expressed genes. B) Venn diagram of U87, KNS42 and GIN-31 cells treated with 200kHz TTFields showing numbers of common and differentially expressed

genes. C) Venn diagram of KNS42 and GIN-31 cells treated with 130Hz/10V/450µs electric fields showing numbers of common and differentially expressed genes. D) Venn diagram of KNS42 and GIN-31 cells treated with130Hz/10V/450µs electric fields compared with U87, KNS42 and GIN-31 cells treated with 200kHz TTFields showing numbers of common and differentially expressed genes. E) Venn diagram showing U87 cells treated with 130Hz/10V/450µs electric fields compared to all other treatments and cell lines showing numbers of common and differentially expressed genes.

DBS Electric Fields Treatment		TTFields Treatment	
Gene Symbol	**Gene Function**	**Gene Symbol**	**Gene Function**
SLC20A2	Encodes a protein that is a type 3 sodium-dependent phosphate transport to regulate cellular phosphate homeostasis.	**MAX**	Encodes a protein which forms homodimers and heterodimers with other family members; Mad, Mxi1 and Myc.
PLK1	Encodes a protein which regulates the maturation of the centrosome and formation of the spindle.	**ND6**	Encodes one of the subunits of the mitochondrial membrane respiratory chain NADH Dehydrogenase (Complex I).
MAX	Encodes a protein which forms homodimers and heterodimers with other family members; Mad, Mxi1 and Myc.	**UBE2A**	Encodes a protein which is a member of the E2 ubiquitin-conjugating enzyme family.
ND6	Encodes one of the subunits of the mitochondrial membrane respiratory chain NADH Dehydrogenase (Complex I).	**TRAM1**	Encodes a multi-pass membrane protein that is part of the mammalian endoplasmic reticulum
LDHB	Encodes a subunit of lactate dehydrogenase enzyme, which catalyses the conversion of pyruvate and lactate.	**CALR**	Encodes a protein that acts as a Ca^{2+} binding protein in ER.
ND5	Encodes one of the subunits of the mitochondrial membrane respiratory chain NADH Dehydrogenase (Complex I).	**SEP15**	Encodes a protein which regulates the quality control of protein folding within the ER.
TRAM1	Encodes a multi-pass membrane protein that is part of the ER.	**PDP1**	Encodes one of the subunits of the Pyruvate Dehydrogenase Complex, and located within the mitochondria.

PDP1	Encodes one of the subunits of the Pyruvate Dehydrogenase Complex, and located within the mitochondria.	**RPL5**	Encodes a protein of the L18P ribosomal protein family, which are components of the 60S subunit.
CALR	Encodes a protein that acts as a Ca^{2+} binding protein in ER.	**ND5**	Encodes one of the subunits of the mitochondrial membrane respiratory chain NADH Dehydrogenase (Complex I).
SEP15	Encodes a protein which regulates the quality control of protein folding within the ER.	**SELT**	Encodes a Selenoprotein, containing a Selenocysteine (Sec) residue.
DDX5	Encodes a protein Involved in the regulation of pre-mRNA splicing	**RHOA**	Encodes Rho small GTPases, which regulate signal transduction cascades.
HNRNPH1	Encodes a protein associated with pre-mRNAs in the nucleus and regulates pre-mRNA processing.	**DDX5**	Encodes a protein Involved in the regulation of pre-mRNA splicing
KCMF1	Encodes potassium channel modulatory factor proteins.	**HNRNPH1**	Encodes a protein associated with pre-mRNAs in the nucleus and regulates pre-mRNA processing.
TMEM138	Encodes multi-pass transmembrane proteins.	**KCMF1**	Encodes potassium channel modulatory factor proteins.
THEM179B	Encodes multi-pass transmembrane proteins.	**TMEM138**	Encodes multi-pass transmembrane proteins.
SELT	Encodes a Selenoprotein, containing a Selenocysteine (Sec) residue.	**THEM179B**	Encodes multi-pass transmembrane proteins.
PTPRA	Encodes a protein that is a member of the protein tyrosine phosphatase (PTP) family.	**ND3**	Encodes one of the subunits of the mitochondrial membrane respiratory chain NADH Dehydrogenase (Complex I).
RHOA	Encodes Rho small GTPases, which regulate signal transduction cascades.	**UBE2D2**	Encodes a protein which is a member of the E2 ubiquitin-conjugating enzyme family.

HIST1H4J	Encodes a replication-dependent histone that is a member of the H4 family of histones.	**HIST1H4J**	Encodes a replication-dependent histone that is a member of the H4 family of histones.
BTNL9	Encodes proteins involved in the immune response through regulation of T-cells.	**BTNL9**	Encodes proteins involved in the immune response through regulation of T-cells.

Figure 4. Table listing the top 20 significantly differentially expressed genes following DBS electric fields and TTFields treatment and their gene functions as described by https://www.genecards.org/. The top 20 genes on this list were determined by greatest significance via p-value.

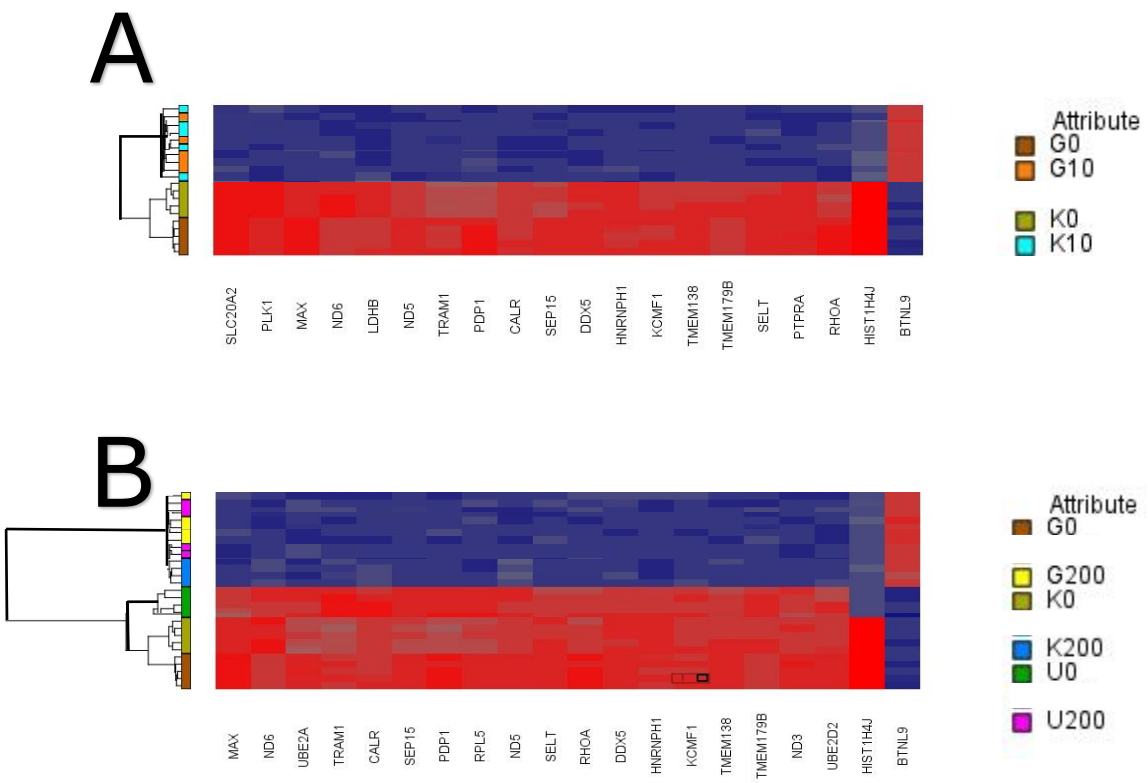


Figure 5. Heat maps of the gene expression patterns of the up-regulation and down-regulation of the previously determined top 20 significant genes of our GBM cell lines following electrical treatment. A) Heat map showing KNS42 and GIN-31 cells treated with 130Hz/10V/450µs electric fields and the top 20 differentially expressed genes. B) Heat map showing all our cell lines treated with 130Hz/10V/450µs electric fields and the top 20 differentially expressed genes. Key; Blue = downregulation, Red = Upregulation.

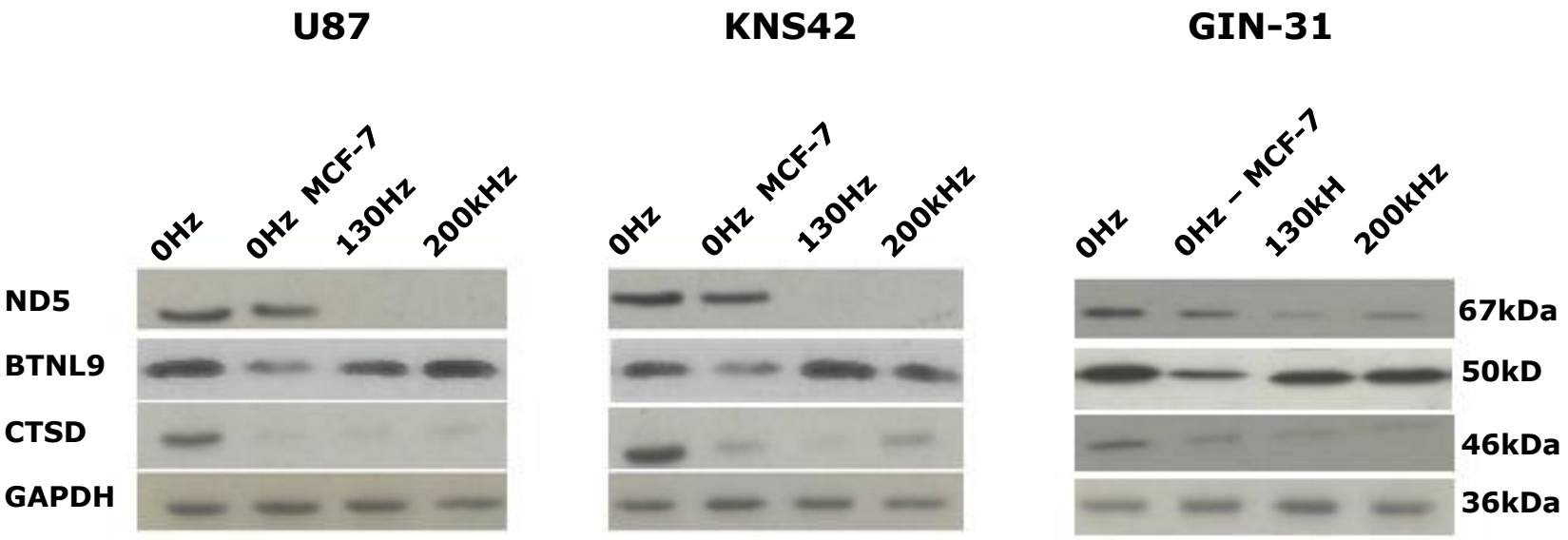


Figure 6. Western blots of the protein expression patterns of GBM cell lines treated with DBS electric fields and TTFields. The targets chosen were ND5, BTNL9 and CTSD and were assessed in the U87, KNS42 and GIN-31 cell lines to cover adult, paediatric and primary GBM cell lines. The positive control were breast carcinoma MCF-7 cells and the housekeeping gene chosen was GAPDH. Protein was extracted from samples following 5 days of electrical treatment and 5 days of continuous growth for the untreated samples. The results confirm the gene expression patterns of the targets as observed in the gene expression data; ND5 and CTSD become downregulated following electrical treatment, BTNL9 becomes upregulated following electrical treatment, and GIN-31 cells are less affected by electrical treatment relative to U87 and KNS42 cells as observed on the gene and protein level.

3.3. Gene Ontology and KEGG Pathway Analyses

3.3.1. Results and Discussion

We next performed gene ontology analyses of our data sets to give further context to our gene list data and to give further insight into the underlying mechanisms of electrical treatments. We used the 'Enrichr' tool from http://amp.pharm.mssm.edu/Enrichr/ to produce the top 50 gene function ontologies (Figure 7. And Figure 8.), as well as the top 25 cellular component ontologies (Figure 9.) for our DBS electric fields and TTFields treated GBM cell lines. The U10 samples were excluded from the DBS electric fields ontologies. Firstly, the top 2 gene function ontologies; Protein targeting to ER (GO:0045047) and SRP-dependent co-translocation protein targeting to membrane (GO:0006614), are both functions which coincide with our previous observations regarding a large proportion of the most significantly differentially expressed genes being related to ER functioning. Secondly, three out of five of the top 25 cellular component ontologies are mitochondrial related, which also is in line with previous genetic observations. Collectively, these ontology analyses validate our gene list data, with our top gene ontologies being heavily associated with our top gene picks, as well as striking resemblances between the ontologies of both are electrical treatments.

We also performed a KEGG Pathway analysis (KEGG: Kyoto Encyclopedia of Genes and Genomes) using the Enrichr tool in order to examine the biological pathways involved with electrical treatment. Very interestingly, the top 3 KEGG pathways are common between the electrical treatments, and they are all associated with neurodegenerative diseases; Parkinson, Alzheimer, and Huntington disease (Figure 10-12.). Although these diseases have their own pathologies, they share similarities with regards to their causative factors (Lin and Beal, 2006). All three of the aforementioned diseases have been shown to have significant downregulation of NADH Dehydrogenase, among other oxidative phosphorylation complexes, and we have previously shown significant downregulation of ND3, ND5 and ND6 (subunits of the NADH Dehydrogenase (Bai et al., 2000)) in our electrical treated cell lines. Of note, inhibitors of this complex are used in Parkinson disease models to

recapitulate the disease (Marella et al., 2009). Furthermore, Ca^{2+} signalling has been implicated in neurodegeneration diseases (Marambaud et al., 2009), and we have also shown downregulation of CALR, which acts as a Ca^{2+} binding protein within the ER (Biwer et al., 2018). Recently, TTFields treatment of GBM cell lines was shown to reduce intracellular Ca^{2+} concentrations, suggesting a Ca^{2+} signalling-mediated stress response to the treatment (Neuhaus et al., 2019). The significance of Ca^{2+} signalling in GBM cells has been noted and associated with tumour survival mechanisms (Leclerc et al., 2016), GBM tumourigenesis, and neurogenesis (Toth et al., 2016).

Index	Name	P-value	Adjusted p-value	Z-score	Combined score
1	protein targeting to ER (GO:0045047)	1.816e-36	1.262e-33	-2.08	171.25
2	SRP-dependent cotranslational protein targeting to membrane (GO:0006614)	9.716e-40	4.727e-36	-1.84	165.42
3	peptide biosynthetic process (GO:0043043)	6.353e-37	5.294e-34	-1.92	160.06
4	nuclear-transcribed mRNA catabolic process, nonsense-mediated decay (GO:0000184)	2.481e-33	1.097e-30	-1.99	149.46
5	viral transcription (GO:0019083)	7.424e-34	3.612e-31	-1.78	135.90
6	viral process (GO:0016032)	2.022e-35	1.229e-32	-1.69	134.77
7	viral gene expression (GO:0019080)	2.140e-34	1.157e-31	-1.58	122.20
8	cotranslational protein targeting to membrane (GO:0006613)	2.582e-39	6.280e-36	-1.37	121.64
9	gene expression (GO:0010467)	6.457e-38	1.047e-34	-1.26	107.61
10	cellular macromolecule biosynthetic process (GO:0034645)	5.550e-27	2.077e-24	-1.75	105.58
11	translation (GO:0006412)	6.529e-37	5.294e-34	-1.22	101.95
12	cellular protein metabolic process (GO:0044267)	1.003e-37	1.219e-34	-1.18	100.28
13	ncRNA processing (GO:0034470)	6.049e-23	1.839e-20	-1.91	97.64
14	rRNA metabolic process (GO:0016072)	1.840e-22	5.267e-20	-1.92	96.23
15	rRNA processing (GO:0006364)	8.658e-26	3.009e-23	-1.61	92.74
16	mRNA splicing, via spliceosome (GO:0000398)	1.394e-21	3.392e-19	-1.73	82.94
17	nuclear-transcribed mRNA catabolic process (GO:0000956)	1.291e-29	5.235e-27	-1.23	81.57
18	mitochondrial ATP synthesis coupled electron transport (GO:0042775)	7.324e-19	1.620e-16	-1.88	78.45
19	positive regulation of ubiquitin protein ligase activity (GO:1904668)	1.868e-17	3.366e-15	-2.00	77.17
20	mitochondrial electron transport, NADH to ubiquinone (GO:0006120)	1.713e-12	1.894e-10	-2.66	71.98
21	mRNA processing (GO:0006397)	1.144e-21	3.091e-19	-1.46	70.43
22	cytoplasmic translation (GO:0002181)	1.118e-18	2.365e-16	-1.66	68.76
23	neutrophil degranulation (GO:0043312)	1.086e-15	1.651e-13	-1.97	67.75
24	regulation of hematopoietic progenitor cell differentiation (GO:1901532)	1.280e-13	1.639e-11	-2.27	67.24
25	mitochondrial ATP synthesis coupled proton transport (GO:0042776)	0.000001365	0.00005444	-4.87	65.80
26	neutrophil degranulation (GO:0043312)	2.158e-12	3.140e-10	-1.97	52.95
27	ATP biosynthetic process (GO:0006754)	9.812e-10	7.963e-8	-2.46	51.03
28	mRNA processing (GO:0006397)	6.607e-16	1.162e-13	-1.45	50.83
29	neutrophil mediated immunity (GO:0002446)	6.266e-12	8.012e-10	-1.90	48.92
30	regulation of translation (GO:0006417)	2.517e-14	4.086e-12	-1.56	48.78
31	ATP metabolic process (GO:0046034)	2.530e-10	2.372e-8	-2.19	48.46
32	regulation of mRNA stability (GO:0043488)	4.422e-13	6.911e-11	-1.69	48.04
33	proteasome-mediated ubiquitin-dependent protein catabolic process (GO:0043161)	1.047e-16	2.008e-14	-1.29	47.50
34	RNA splicing, via transesterification reactions with bulged adenosine as nucleophile (GO:0000377)	6.503e-17	1.307e-14	-1.25	46.66
35	purine ribonucleoside monophosphate biosynthetic process (GO:0009168)	8.868e-10	7.338e-8	-2.23	46.56
36	positive regulation of ubiquitin protein ligase activity (GO:1904668)	2.634e-10	2.416e-8	-1.98	43.61
37	mitochondrial transport (GO:0006839)	9.548e-15	1.612e-12	-1.32	42.76
38	ER to Golgi vesicle-mediated transport (GO:0006888)	2.909e-12	4.092e-10	-1.61	42.64
39	proteasomal protein catabolic process (GO:0010498)	1.633e-12	2.461e-10	-1.55	42.10
40	regulation of hematopoietic progenitor cell differentiation (GO:1901532)	5.407e-9	3.356e-7	-2.21	42.09
41	cristae formation (GO:0042407)	3.088e-7	0.00001277	-2.78	41.63
42	mitochondrial respiratory chain complex assembly (GO:0033108)	8.107e-11	9.246e-9	-1.74	40.37
43	Wnt signaling pathway, planar cell polarity pathway (GO:0060071)	1.954e-9	1.397e-7	-2.01	40.26
44	ribosome assembly (GO:0042255)	2.530e-10	2.372e-8	-1.78	39.26
45	RNA metabolic process (GO:0016070)	3.475e-9	2.328e-7	-1.91	37.16
46	regulation of mitotic cell cycle phase transition (GO:1901990)	2.700e-9	1.838e-7	-1.83	36.15
47	inner mitochondrial membrane organization (GO:0007007)	1.307e-9	9.847e-8	-1.74	35.61
48	nucleic acid metabolic process (GO:0090304)	1.279e-10	1.349e-8	-1.52	34.67
49	regulation of protein localization to Cajal body (GO:1904869)	0.000005512	0.0001736	-2.86	34.61
50	establishment of protein localization to mitochondrion (GO:0072655)	1.759e-8	9.394e-7	-1.93	34.38

Figure 7. Table showing the top 50 gene function ontologies of DBS electric fields treated GBM cell lines, with significance determined via the combined score. The gene ontologies were generated from KNS42 and GIN-31 data, with U87 data being excluded.

Index	Name	P-value	Adjusted p-value	Z-score	Combined score
1	protein targeting to ER (GO:0045047)	6.570e-42	1.061e-38	-2.09	197.89
2	SRP-dependent cotranslational protein targeting to membrane (GO:0006614)	3.017e-44	1.462e-40	-1.84	184.54
3	peptide biosynthetic process (GO:0043043)	6.603e-40	6.397e-37	-1.92	173.26
4	nuclear-transcribed mRNA catabolic process, nonsense-mediated decay (GO:0000184)	4.212e-37	3.401e-34	-2.00	167.28
5	viral process (GO:0016032)	6.059e-37	4.193e-34	-1.69	140.78
6	cotranslational protein targeting to membrane (GO:0006613)	1.048e-43	2.538e-40	-1.37	135.49
7	viral transcription (GO:0019083)	2.322e-33	1.022e-30	-1.78	133.79
8	viral gene expression (GO:0019080)	7.757e-34	3.757e-31	-1.58	120.11
9	translation (GO:0006412)	7.158e-41	8.669e-38	-1.22	113.23
10	cellular macromolecule biosynthetic process (GO:0034645)	6.702e-27	2.497e-24	-1.75	105.25
11	gene expression (GO:0010467)	6.283e-36	3.804e-33	-1.25	101.48
12	cellular protein metabolic process (GO:0044267)	7.769e-36	4.181e-33	-1.17	94.83
13	rRNA metabolic process (GO:0016072)	1.143e-21	3.462e-19	-1.92	92.79
14	nuclear-transcribed mRNA catabolic process (GO:0000956)	2.903e-32	1.172e-29	-1.23	89.05
15	ncRNA processing (GO:0034470)	3.994e-20	1.075e-17	-1.91	85.11
16	rRNA processing (GO:0006364)	4.636e-23	1.604e-20	-1.61	82.64
17	cytoplasmic translation (GO:0002181)	7.339e-22	2.370e-19	-1.67	81.25
18	mitochondrial ATP synthesis coupled electron transport (GO:0042775)	5.193e-19	1.258e-16	-1.88	79.19
19	mRNA splicing, via spliceosome (GO:0000398)	3.181e-19	8.110e-17	-1.73	73.62
20	neutrophil degranulation (GO:0043312)	9.706e-17	1.741e-14	-1.97	72.80
21	mitochondrial electron transport, NADH to ubiquinone (GO:0006120)	3.671e-12	4.135e-10	-2.66	70.01
22	positive regulation of ubiquitin protein ligase activity (GO:1904668)	6.159e-16	9.323e-14	-2.00	69.93
23	mitochondrial ATP synthesis coupled proton transport (GO:0042776)	7.081e-7	0.00003363	-4.90	69.33
24	neutrophil mediated immunity (GO:0002446)	3.019e-16	4.874e-14	-1.90	67.93
25	positive regulation of protein ubiquitination involved in ubiquitin-dependent protein catabolic process (GO:2000060)	2.184e-14	3.112e-12	-1.86	58.55
26	mRNA processing (GO:0006397)	4.445e-18	9.363e-16	-1.46	58.15
27	ribosome biogenesis (GO:0042254)	1.916e-21	5.460e-19	-1.20	57.31
28	negative regulation of ubiquitin protein ligase activity (GO:1904667)	1.348e-18	2.969e-16	-1.36	56.16
29	negative regulation of ubiquitin-protein ligase activity involved in mitotic cell cycle (GO:0051436)	1.591e-16	2.752e-14	-1.51	54.80
30	anaphase-promoting complex-dependent catabolic process (GO:0031145)	5.676e-17	1.057e-14	-1.46	54.49
31	regulation of cellular amino acid metabolic process (GO:0006521)	3.854e-11	3.522e-9	-2.22	53.34
32	RNA splicing, via transesterification reactions with bulged adenosine as nucleophile (GO:0000377)	5.565e-19	1.284e-16	-1.25	52.62
33	respiratory electron transport chain (GO:0022904)	1.622e-17	3.274e-15	-1.35	52.06
34	regulation of hematopoietic progenitor cell differentiation (GO:1901532)	7.538e-11	6.295e-9	-2.23	51.96
35	regulation of ubiquitin-protein ligase activity involved in mitotic cell cycle (GO:0051439)	5.146e-17	9.970e-15	-1.34	50.16
36	regulation of mitotic cell cycle phase transition (GO:1901990)	2.933e-12	3.383e-10	-1.86	49.42
37	positive regulation of ubiquitin-protein ligase activity involved in regulation of mitotic cell cycle transition (GO:0051437)	1.490e-15	2.187e-13	-1.44	49.18
38	negative regulation of G2/M transition of mitotic cell cycle (GO:0010972)	1.759e-11	1.763e-9	-1.91	47.40
39	proteasomal protein catabolic process (GO:0010498)	5.979e-14	8.045e-12	-1.54	46.94
40	regulation of mRNA stability (GO:0043488)	7.536e-13	9.607e-11	-1.68	46.78
41	regulation of translation (GO:0006417)	7.095e-14	9.288e-12	-1.54	46.74
42	mitochondrial respiratory chain complex assembly (GO:0033108)	1.952e-12	2.306e-10	-1.73	46.71
43	proteasome-mediated ubiquitin-dependent protein catabolic process (GO:0043161)	5.508e-16	8.607e-14	-1.28	45.05
44	neutrophil activation involved in immune response (GO:0002283)	2.584e-16	4.316e-14	-1.23	44.06
45	Wnt signaling pathway, planar cell polarity pathway (GO:0060071)	3.648e-10	2.718e-8	-2.00	43.43
46	regulation of G2/M transition of mitotic cell cycle (GO:0010389)	1.269e-11	1.356e-9	-1.71	42.98
47	regulation of transcription from RNA polymerase II promoter in response to hypoxia (GO:0061418)	4.085e-14	5.654e-12	-1.31	40.24
48	ER to Golgi vesicle-mediated transport (GO:0006888)	1.783e-11	1.763e-9	-1.58	39.10
49	mitochondrial translational termination (GO:0070126)	1.512e-10	1.220e-8	-1.72	38.87
50	regulation of stem cell differentiation (GO:2000736)	1.414e-9	9.255e-8	-1.85	37.62

Figure 8. Table showing the top 50 gene function ontologies of TTFields treated GBM cell lines, with significance determined via the combined score. The gene ontologies were generated from U87, KNS42 and GIN-31 data.

Index	Name	P-value	Adjusted p-value	Z-score	Combined score
1	mitochondrial proton-transporting ATP synthase complex (GO:0005753)	2.002e-8	4.309e-7	-8.20	145.39
2	mitochondrial inner membrane (GO:0005743)	9.288e-37	3.799e-34	-1.70	141.25
3	cytosolic part (GO:0044445)	1.803e-27	2.066e-25	-1.61	99.38
4	mitochondrion (GO:0005739)	7.369e-25	6.028e-23	-1.79	99.37
5	cytosolic large ribosomal subunit (GO:0022625)	3.006e-19	1.756e-17	-2.13	90.68
6	focal adhesion (GO:0005925)	1.865e-33	3.815e-31	-1.12	84.77
7	cytosolic ribosome (GO:0022626)	2.020e-27	2.066e-25	-1.32	81.15
8	large ribosomal subunit (GO:0015934)	4.394e-20	2.995e-18	-1.49	66.56
9	ficolin-1-rich granule lumen (GO:1904813)	3.227e-12	1.320e-10	-2.12	55.98
10	spliceosomal snRNP complex (GO:0097525)	1.372e-12	6.234e-11	-2.01	54.90
11	mitochondrial respiratory chain complex I (GO:0005747)	2.631e-13	1.345e-11	-1.89	54.87
12	ribosome (GO:0005840)	3.786e-12	1.408e-10	-2.07	54.50
13	spliceosomal tri-snRNP complex (GO:0097526)	5.551e-9	1.261e-7	-2.13	40.48
14	small ribosomal subunit (GO:0015935)	5.639e-11	1.647e-9	-1.43	33.80
15	cytosolic small ribosomal subunit (GO:0022627)	1.913e-10	5.216e-9	-1.44	32.12
16	cytoplasmic vesicle lumen (GO:0060205)	3.526e-10	9.014e-9	-1.39	30.30
17	spliceosomal complex (GO:0005681)	2.408e-11	8.206e-10	-1.23	30.01
18	polysomal ribosome (GO:0042788)	3.823e-8	7.818e-7	-1.73	29.54
19	U2 snRNP (GO:0005686)	8.401e-7	0.00001273	-2.10	29.32
20	secretory granule lumen (GO:0034774)	4.014e-11	1.263e-9	-1.21	29.03
21	U4/U6 x U5 tri-snRNP complex (GO:0046540)	2.637e-7	0.000004686	-1.86	28.14
22	U6 snRNP (GO:0005688)	0.000003967	0.00005409	-2.25	27.99
23	ficolin-1-rich granule (GO:0101002)	1.067e-9	2.568e-8	-1.16	24.05
24	mitochondrial inner membrane presequence translocase complex (GO:0005744)	0.00007642	0.0007624	-2.41	22.80
25	precatalytic spliceosome (GO:0071011)	0.000005879	0.00007514	-1.84	22.15

Index	Name	P-value	Adjusted p-value	Z-score	Combined score
1	mitochondrial proton-transporting ATP synthase complex (GO:0005753)	1.266e-12	3.021e-11	-8.28	226.90
2	cytosolic part (GO:0044445)	3.459e-51	6.191e-49	-1.62	188.79
3	mitochondrial inner membrane (GO:0005743)	1.313e-49	1.567e-47	-1.67	188.31
4	mitochondrion (GO:0005739)	6.080e-40	4.353e-38	-1.79	161.48
5	cytosolic large ribosomal subunit (GO:0022625)	1.559e-33	7.975e-32	-2.13	160.62
6	cytosolic ribosome (GO:0022626)	1.586e-52	5.680e-50	-1.34	159.89
7	ribosome (GO:0005840)	3.829e-27	1.713e-25	-2.12	129.24
8	large ribosomal subunit (GO:0015934)	1.435e-33	7.975e-32	-1.49	112.93
9	focal adhesion (GO:0005925)	5.746e-41	5.143e-39	-1.11	102.88
10	mitochondrial respiratory chain complex I (GO:0005747)	5.977e-18	1.945e-16	-1.85	73.49
11	small ribosomal subunit (GO:0015935)	5.481e-22	2.180e-20	-1.47	71.77
12	cytosolic small ribosomal subunit (GO:0022627)	5.261e-21	1.883e-19	-1.47	68.56
13	polysomal ribosome (GO:0042788)	9.354e-17	2.576e-15	-1.77	65.39
14	ficolin-1-rich granule lumen (GO:1904813)	4.154e-13	1.062e-11	-2.04	58.17
15	polysome (GO:0005844)	9.228e-17	2.576e-15	-1.50	55.40
16	spliceosomal snRNP complex (GO:0097525)	4.489e-11	8.928e-10	-1.89	45.09
17	U2 snRNP (GO:0005686)	4.834e-8	6.180e-7	-2.09	35.14
18	mitochondrial envelope (GO:0005740)	1.029e-8	1.417e-7	-1.83	33.74
19	spliceosomal complex (GO:0005681)	3.847e-12	8.608e-11	-1.20	31.53
20	nuclear chromatin (GO:0000790)	3.715e-9	5.782e-8	-1.62	31.41
21	spliceosomal tri-snRNP complex (GO:0097526)	1.327e-7	0.000001584	-1.97	31.24
22	nucleolus (GO:0005730)	1.361e-10	2.564e-9	-1.31	29.85
23	U6 snRNP (GO:0005688)	0.000001107	0.00001133	-2.17	29.72
24	mitochondrial intermembrane space (GO:0005758)	2.055e-7	0.000002373	-1.89	29.14
25	cytoplasmic vesicle lumen (GO:0060205)	7.920e-10	1.418e-8	-1.36	28.40

Figure 9. Tables showing the top 25 cellular component ontologies of DBS electric fields and TTFields treated GBM cell lines, with significance determined via the combined score. The gene ontologies were generated from KNS42 and GIN-31 data for the DBS electric fields treated cells and U87, KNS42 and GIN-31 data for the TTFields treatment.

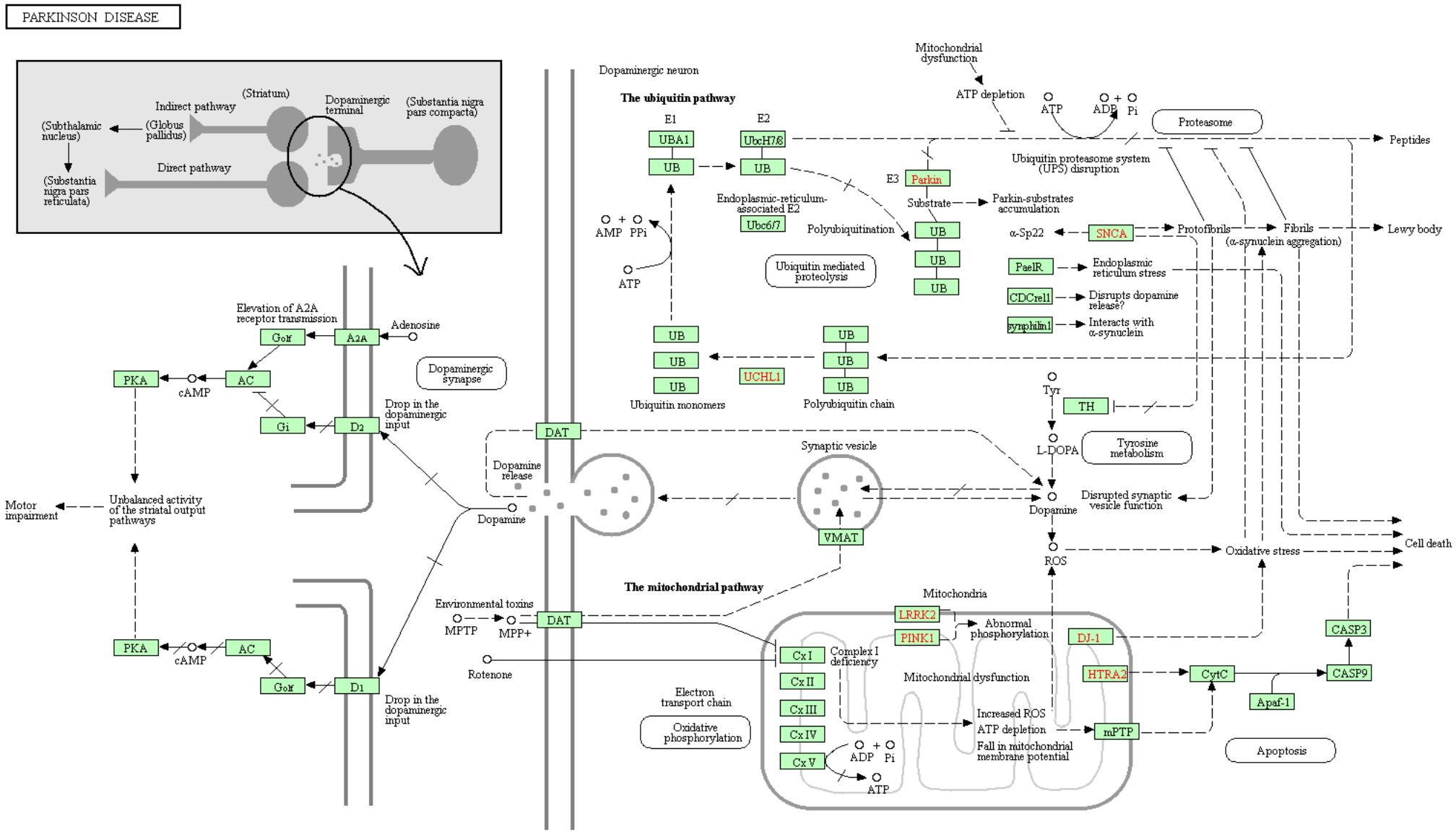


Figure 10. KEGG Pathway analysis of the effects of DBS electric fields and TTFields treatment on GBM cell lines. The KEGG Pathway describes the Parkinson Disease pathway. The KEGG Pathways were generated from KNS42 and GIN-31 data for the DBS electric fields treated cells and U87, KNS42 and GIN-31 data for the TTFields treatment. Image from https://www.genome.jp/kegg-bin/show_pathway?hsa05012 .

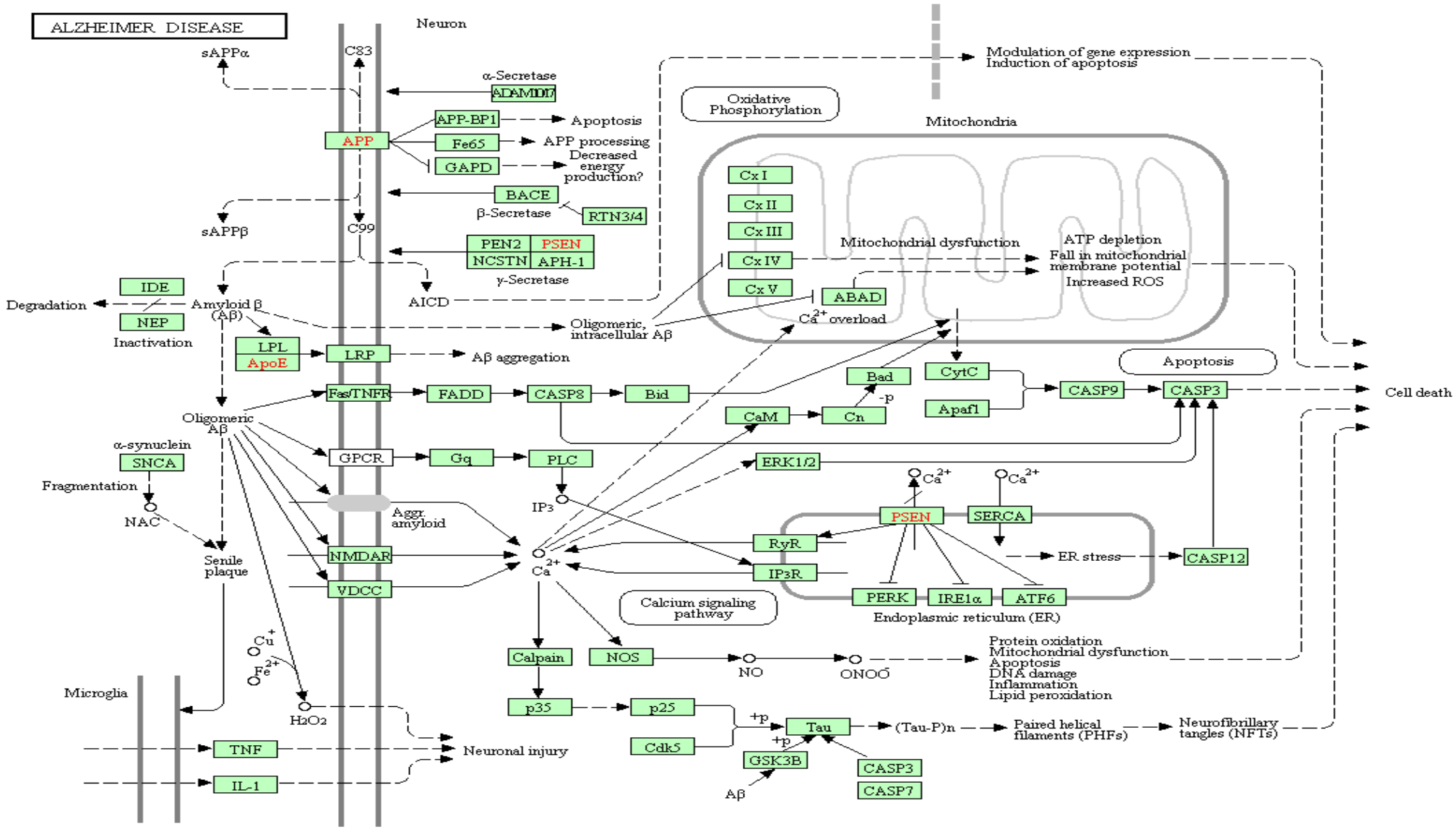


Figure 11. KEGG Pathway analysis of the effects of DBS electric fields and TTFields treatment on GBM cell lines. The KEGG Pathway describes the Alzheimer Disease pathway. The KEGG Pathways were generated from KNS42 and GIN-31 data for the DBS electric fields treated cells and U87, KNS42 and GIN-31 data for the TTFields treatment. Image from https://www.genome.jp/kegg/pathway/hsa/hsa05010.html .

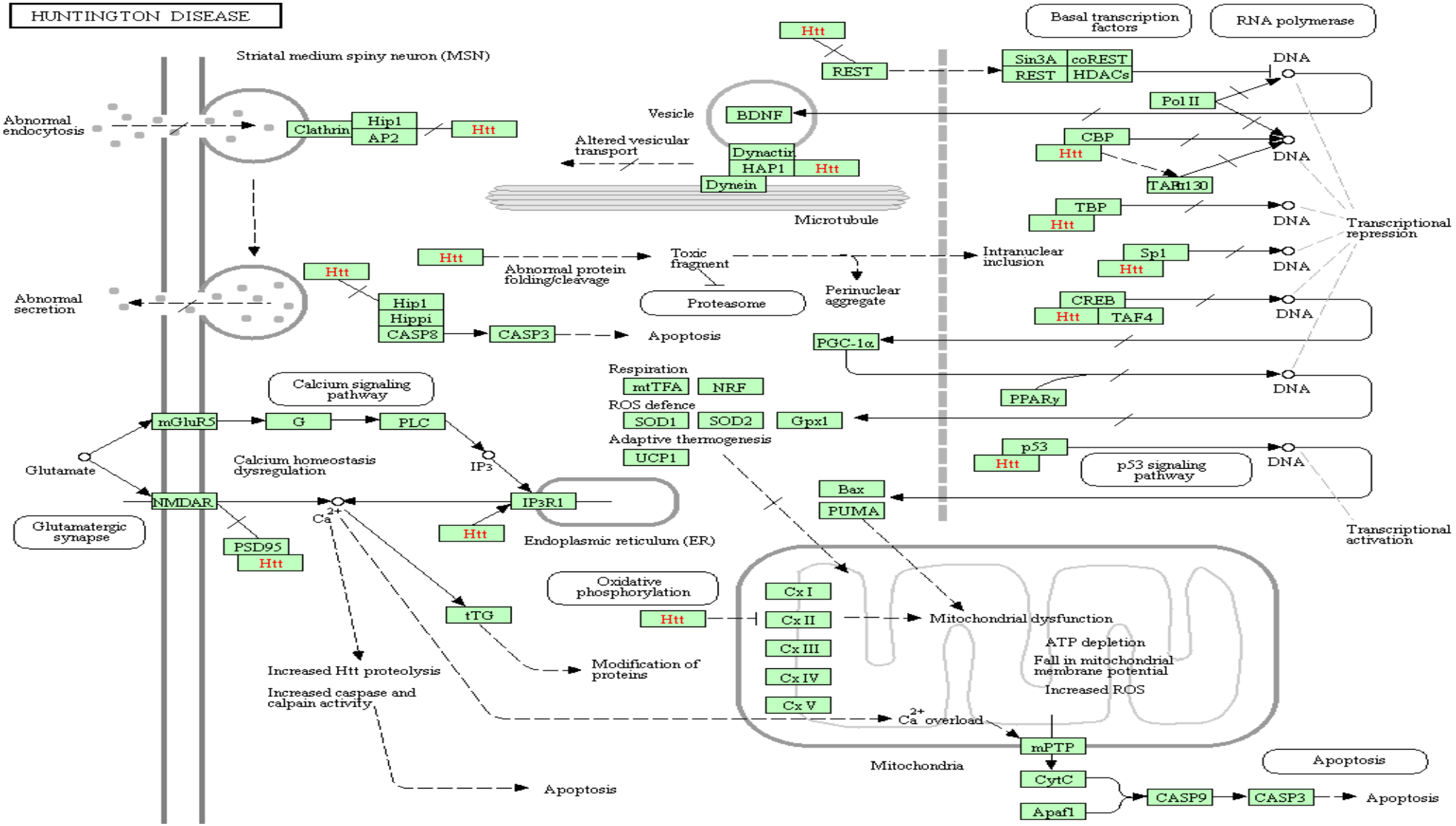


Figure 12. KEGG Pathway analysis of the effects of DBS electric fields and TTFields treatment on GBM cell lines. The KEGG Pathway describes the H Disease pathway. The KEGG Pathways were generated from KNS42 and GIN-31 data for the DBS electric fields treated cells and U87, KNS42 and GIN-31 data for the TTFields treatment. Image from https://www.genome.jp/kegg-bin/show_pathway?hsa05016 .

4. Conclusions

The primary objectives of this chapter were to establish;

5. If DBS electric fields and TTFields treatment cause significant genetic dysregulation within our panel of GBM cell lines?
6. Whether the differences in the electrical treatments would be demonstrated on the genetic level?
7. Can the gene expression profiles of electrically treated cells elucidate novel mechanisms of action, while providing novel opportunities for therapeutic targeted therapies?

4.1. Main Findings

4.1.1. DBS electric fields and TTFields treatments cause similar genetic changes in GBM cell lines

In this chapter we have shown that electrical treatment affects our GBM cell lines on the genetic level, which was analysed via RNA-seq. Interestingly, clear similarities were observed despite the differences in mechanisms described in previous chapters. Firstly, we've shown striking similarities within the expression patters of electrically treated cells with our hierarchical clustering analyses and volcano plots, with a significant bias towards downregulation of gene expression following treatment. Secondly, our Venn diagram analysis of differentially expressed genes showed significant overlap between the cell lines following a given electrical treatment, owing to the hypothesis that electrical treatment is largely non-specific with regards to its anti-proliferative effects. A significant overlap of differentially expressed genes was further observed when DBS electric fields and TTFields treated cells were compared. Lastly, the heat maps of the top 20 significantly expressed genes of the electrical treatments also have significant overlap, with 16 out of the 20 genes being common between the electrical treatments. Interestingly, a large proportion of these genes encode proteins relating to the endoplasmic reticulum, mitochondria, and the electron transport chain.

4.1.2. Electrical treatment promotes dysregulation of mitochondrial and endoplasmic reticulum processes in GBM cell lines

Here we have shown through our gene ontology analyses that a large proportion of the top ontologies are located within the ER and mitochondrion (Figure 9.), and associated with mitochondrial and ER functioning (Figure 7. and 8.). Given how the genes associated with these functions are significantly downregulated in our electrically treated cells, it's reasonable to believe that these functions are also perturbed. These observations are not to be wholly unexpected as ER stress as a result of TTFields has been reported upon previously (Shteingauz et al., 2018). However, whether the ER stress response is a direct target or merely a consequence of prolonged electrical treatment is to be determined. Our KEGG pathway analyses demonstrated common neurodegenerative pathways, all of which are associated with mitochondrial and metabolic dysfunction.

4.1.3. Electrical treatment may potentially target metabolic pathways through interactions with electron transport chain in GBM cell lines

We lastly observed that also, a large proportion of the top differentially expressed genes of the electrically treated cells were involved with mitochondrial functioning and the electron transport chain. Of particular importance to the electron transport chain are the subunits ND3, ND5 and ND6, which were all shown to be significantly downregulated in our GBM cells following electrical treatment. We speculate that the dysregulation of the electron transport chain following electrical treatment may be due to either a downregulation of metabolism as a response to prolonged mitotic arrest or more interestingly, the electric fields influencing ion transfer within these systems to inhibit these ion driven metabolic pathways.

4.2. Future Work

This genome-wide analysis of the effects of DBS electric fields and TTFields treatment on GBM cell lines has provided novel insights into the mechanisms of both our electrical treatments, and has highlighted many unanswered questions which may be addressed in further work, but the most pertinent may be how this therapy may be translated into the clinic;

1. Can electric fields be combined with targeted, novel therapeutic agents to enhance their efficacy?

4.2.1. Future Work Hypotheses

1. The genetic data and gene ontologies may guide future drug combinations to improve efficacy of electric fields treatment.

4.2.2. Electric Fields in a Combinational Approach

Here we have shown that both DBS electric fields and TTFields treatment affect gene expression, and their associated pathways, in a similar fashion – with observations into the effects of electric fields on metabolism through dysregulation of ER and mitochondrial functioning. There may be a several potential different therapeutic approaches with electric fields treatment, which may be built upon with further investigations into the underlying mechanisms of electric fields. Firstly, it has yet to be determined through with mechanism electric fields are promoting ER stress, and if these mechanisms differ between the electrical treatments despite having similar end-points. For example, TTFields has been shown to physically manipulate sufficiently polar proteins (Gera et al., 2015, Kirson et al., 2004, Giladi et al., 2015c), while DBS electric fields function at a frequency too low to achieve such perturbations. So whether downregulations of key proteins, such as ND5, is achieved through physical perturbation of regulatory proteins is yet to be determined, as well as whether interactions with proteins via TTFields cause downregulation at the gene level at all. Secondly, these processes may be dysregulated through manipulations of action potentials via electric fields. We know that biological processes are electrically regulated (Yang and Brackenbury, 2013), and that electric fields of similar frequencies to the ones tested may dysregulate ion flux (Cucullo et al., 2005b, Neuhaus et al., 2019). But most likely, a combination of these mechanisms, rather than a single underlining mechanism, may be promoting ER stress and thus providing therapeutic opportunities.

Taken together, novel approaches with electric fields therapy may involve combination with; ion channel inhibitors, whether K^+, Na^+ or Cl^- ion channels in order to potentiate the effects or inhibiting stress responses to

electric fields treatment e.g. Ca^{2+} channel inhibitors (Meister et al., 2010). Combination with novel agents targeting the ER stress response, whether being to potentiate ER stress with traditional chemotherapies (Yadav et al., 2014) or to inhibit resistance mechanisms e.g. targeting autophagy as a resistance mechanism to ER stress with the addition of chloroquine (Kimura et al., 2013).

CHAPTER 4

ELECTROGENOMICS

Chapter 5: Conclusions

1. Introduction

This thesis has documented our investigations in the effects of DBS electric fields on GBM and TTFields treatment on paediatric brain tumour cell lines. We have shown with our preliminary and our more exploratory experiments that these electrical treatments have clear differences, but also a significant amount of similarities. In this chapter we will highlight the key similarities and differences between the electrical treatments, as well as discussing future investigations surrounding electrical based therapies.

2. Discussion

2.1. Optimisation of Electric Fields

We have shown that both of our electrical treatments exhibit efficacy against our brain tumour cell lines, and this efficacy may be increased with a degree of optimisation. DBS electric fields efficacy was increased through increasing the intensity of the field (Chapter 2, Section 3.1) and through manipulation of frequency between 60Hz and 190Hz (Chapter 2, Section 3.3). TTFields treatment efficacy was increased through manipulation of the frequency between 100kHz and 400kHz (Chapter 3, Section 3.1), we did not explore the effects of manipulating the intensity of TTFields as this has already been established *in vitro* (Porat et al., 2017). The range of frequencies showing significant differences in frequencies is interesting, with DBS electric fields appearing to have a more 'precise' optimisation process relative to TTFields, however, the difference in the mechanisms of actions may potentially reflect this.

2.2. Mitotic Arrest

We have demonstrated how both of our electrical treatments cause significant shifts in cell cycle phase accumulations, with DBS electric fields promoting G0-phase accumulation (Chapter 2, Section 3.10) and TTFields treatments promoting G2/M-phase accumulation (Chapter 3, Section 3.4) in brain tumour cell lines. The accumulation of TTFields treated cells in the

G2/M phase has been observed in many different cell lines and tumour types, and has been attributed to perturbation of key mitotic proteins e.g. tubulin and Septin proteins (Giladi et al., 2015c, Gera et al., 2015). A number of mitotic proteins have been investigated, however, many proteins may be influenced by an alternating electric field if there is sufficient current and the protein has a sufficiently high dipole moment (Gera et al., 2015). The accumulation of DBS electric fields treated cells in the G0-phase is speculated to occur through manipulation of ion flux and its effects on the electrical activity of the cancer cells. This hypothesis arose from previous literature reporting how electric fields at a very similar frequency to our DBS electric fields treatment, having anti-proliferative effects on tumour cell lines through interactions with inwards-rectifying K^+ channels (Cucullo et al., 2005a). These anti-proliferative effects may be explained through perturbation of ion flux and how this may dysregulate the electrical processes of the cell cycle. However, recent TTFields investigations into ion flux has described how Ca^{2+} signalling may be activated as a response to TTFields (Neuhaus et al., 2019). Given the similarities between our electrical treatments, it would be interesting to characterise the effects of both treatments on a larger array of ions and their respective channels.

2.3. Combination with Chemotherapy

We have tested a variety of chemotherapies in combination with DBS electric fields – TMZ, Paclitaxel and Mebendazole on GBM cell lines (Chapter 2, Section 3.11-12), and in combination with TTFields treatment – Paclitaxel and Mebendazole on paediatric GBM, Medulloblastoma and Ependymoma cell lines (Chapter 3, Section 3.5). We showed that the efficacy of all these chemotherapies may be increased with the addition of electric fields treatment. Of particular note, we tested a variety of MGMT-wt and MGMT-methylated GBM cell lines and still observed an increase in the efficacy in the MGMT-wt cell lines when combining electric fields treatment. This may be of future clinical relevance given how MGMT-wt tumours are typically more chemoresistant to chemotherapies, particularly alkylating agents (Hegi et al., 2005). TTFields combined with TMZ has shown to increase efficacy irrespective of MGMT status *in vitro* (Clark et

al., 2016) and *in vivo* (Stupp et al., 2017a). The combination of electric fields to chemotherapies, especially with those with limited efficacy against certain patient subgroups, offers a clinical strategy whereby an additional potentially efficacious therapy may be administered without overlapping or significant toxicities (Stupp et al., 2012b, Stupp et al., 2017a). We also chose to combine both of our electrical treatments with mitotic inhibitors which target the G2/M-phase of the cell cycle through targeting tubulin (Jordan and Wilson, 2004, Voloshin et al., 2016) in an attempt to augment the mitotic arrest effects observed with our electric fields treatments. We demonstrated an increase in efficacy when combined with our electrical treatments, as well as influencing the cell cycling of cells treated with DBS electric fields and promoting a significant increase in apoptosis (Chapter 2, Figure…..). The increase in apoptosis from the combinational route with DBS electric fields is in-line with reports on similar phenomenon with TTFields in combination with mitotic inhibitors (Voloshin et al., 2016).

2.4. Gene Expression

We lastly examined how electric fields affect treated GBM cells on the genetic level to help guide future research and identify novel mechanisms of action. Firstly, we clearly observed striking similarities between the gene expression profiles of DBS electric fields and TTFields treated cells (Chapter 4, Section 3.2), as with the gene ontologies (Chapter 4, Section 3.3). A significant number of the affected genes and pathways were associated with mitochondrial and endoplasmic reticulum functioning synonymous with the unfolded protein and the ER stress response. Autophagy as a response to ER stress and aneuploidy in TTFields cell lines has been shown before (Shteingauz et al., 2018). However, given the proposed differential mechanisms of action between our electric fields treatments, it most likely that DBS electric fields have a yet to be elucidated underlying function which may be addressed with future research. Overall, the gene expression analyses provided novel target genes and pathways which may provide a platform for targeted drug combination studies in the future.

3. Future Directions

We conclude this thesis and investigations into DBS electric fields and TTFields treatment on brain tumour cell lines with some future directions, which may elucidate further the underlying mechanisms of electrical treatment upon brain tumour cell lines *in vitro*.

3.1. Measuring Ion Flux

We have described previously literature pertaining to the concept of cellular process, in particular the cell cycle, being electrically driven and regulated by membrane potentials (Yang and Brackenbury, 2013). A plethora of ion channels have been implicated in glioblastoma pathogenesis (Pollak et al., 2017, Molenaar, 2011) (Figure 1.), of which may potentially be targeted with electric fields.

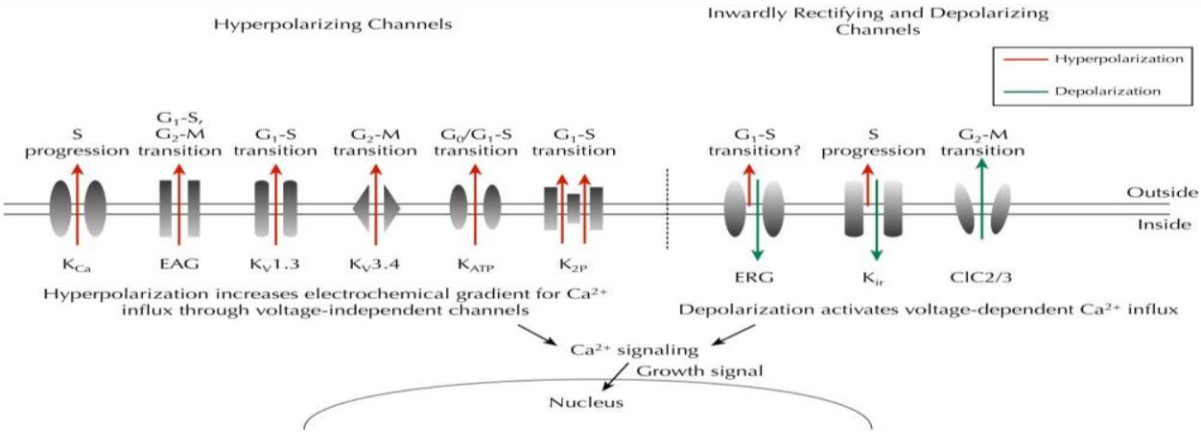


Figure 1. Diagram detailing key hyperpolarizing, depolarizing, and inwards-rectifying ion channels that regulate membrane potentials and their respective cell cycle phase, and how they regulate Ca^{2+} signalling and subsequent growth signalling in cancer. Abbreviations: Hyperpolarizing channels; KCa - Ca2+-activated K+ channel, EAG - Ether à go-go channel, Kv - Voltage-gated K+ channel, KATP - ATP-sensitive K+ channel, K2P - Two-pore domain K+ channel, and Depolarizing and Inwards-rectifying channels; ERG - EAG-related gene K+ channel, Kir - Classic inward-rectifier K+ channel, ClC2/3 - Chloride 2/3 channel. Image from (Yang and Brackenbury, 2013).

Neuhaus and colleagues have described using patch clamp experiments to measure Ca^{2+} flux as a response to TTFields treatment (Neuhaus et al., 2019), the focus on Ca^{2+} ions was attributed to Ca^{2+} signalling being implicated in gliomagenesis and proliferation (Leclerc et al., 2016, Zhang et al., 2017). Given how TTFields has been shown to promote Ca^{2+} signalling, it is reasonable to expect that other ions and their channels may be perturbed by TTFields. The same can be said for DBS electric fields as Cucullo and colleagues demonstrated how low frequency electric fields dysregulated inwards rectifying K^{+} channels (Cucullo et al., 2005a). Therefore, we propose experiments designed to implicate ion channels and measure ion flux following DBS electric fields and TTFields treatment of GBM cell lines. We would seek to characterise the ion flux patterns of electrically treated cells and how these drive the cell cycle and are perturbed to cause mitotic arrest. Of particular interest would be if Ca^{2+} signalling is activated following DBS electric fields due to its survival promoting characteristics (Leclerc et al., 2016). The resulting experiments may be able to elucidate novel mechanisms of action for both electrical treatments, identify resistance mechanisms, as well as providing targeted ion channel therapeutic opportunities for a combinational approach to electrotherapies. We would also seek to measure the membrane potentials of the untreated cell lines and see how electric fields may alter this value, it would also be interesting to measure previously treated and recovered cells as these cells exhibited a reduced proliferative capacity relative to untreated cell lines.

3.1.1. Hypothesis

1. Electric fields treatment may perturb ion flux and is measurable to an extent that the ion flux may be aligned with the previous observations of the cell cycling aberrations as a result of electrical treatment.

3.2. Characterising Endoplasmic Reticulum Stress

Our gene ontology analyses have highlighted pathways indicative of ER stress being highly enriched in both DBS electric fields and TTFields treated GBM cell lines in Chapter 4, Section 3.3, as well the a large proportion of

the most significantly differentially expressed genes of these treatments being related to ER functioning in Chapter 4, Section 3.3. Cancer cells exhibiting ER stress and subsequently promoting the unfolded-protein response as a response to therapies is a known phenomenon (Avril et al., 2017) with ER stress being a result of many different stimuli (Lin et al., 2008). ER stress may be induced by, but not limited to; reduced metabolic activity, hypoxia, oxidative stress, as well as mutations in ER related proteins (Clarke et al., 2014). Underlying mechanisms of action of DBS electric fields and TTFields treatment may be described through identification of which, if any, of these processes which promote ER stress become biased through electrical treatment. Of particular interest would be the oxidative stress and metabolic stress aspects. Dysregulation of the electron transport chain as a result of electrical fields, as determined by gene ontology and gene target analyses in Chapter 4, Section 3.3, may reduce cell viability from oxidative stress via free radicals produced from metabolic pathways (Matsuzaki et al., 2009, Cadenas and Davies, 2000). We've shown very significant downregulation of ND3, ND5, and ND6 – key components of Complex I of the electron transport chain, and this may potentially increase free radicals and oxidative stress (Cadenas and Davies, 2000, Matsuzaki et al., 2009). Interestingly, this mechanism of cell death has been implicated in many neurodegenerative diseases (Kim et al., 2015), and our KEGG pathway analyses implicated the Parkinson, Alzheimer, and Huntington disease in the mechanisms of electrical treatment in Chapter 4, Section 3.3. These particular KEGG pathways also include the processes of ER stress, mitochondrial dysfunction and ATP depletion. So we propose a series of experiments to measure to what extent ATP levels are reduced, as well as to what extent free radical levels are increased as a response to electric fields treatment. Uniquely to TTFields treatment, we would also determine the dipole moments of the significant endoplasmic reticulum, mitochondrial, and electron transport chain associated proteins and observe how the alternating electric field may perturb the localisation and conformational changes of these proteins. TTFields have been shown to disrupt localisation of Septin proteins to the cytokinetic furrow and thereby disrupt their proper functioning during

mitosis (Gera et al., 2015), so it may be reasonable to believe that similar perturbations of sufficiently charged proteins may disrupt cellular functions and reduce cell viability in TTFields treated cell lines.

3.2.1. Hypothesis

1. The endoplasmic reticulum stress which is a result of electrical treatment has a key driver which may be identified and further exploited to increase efficacy of electric fields.

Appendix

1. Appendix 1 – Gene Expression Data

Gene lists produced from Partek analysis are attached via USB and saved as an excel file – 'JB Thesis Electro Gene List'.

References

AGAOGLU, F. Y., AYAN, I., DIZDAR, Y., KEBUDI, R., GORGUN, O. & DARENDELILER, E. 2005. Ependymal tumors in childhood. *Pediatric blood & cancer,* 45**,** 298-303.

AGNESI, F., JOHNSON, M. D. & VITEK, J. L. 2013. Deep brain stimulation: how does it work? *Handb Clin Neurol,* 116**,** 39-54.

ALDAPE, K., ZADEH, G., MANSOURI, S., REIFENBERGER, G. & VON DEIMLING, A. 2015. Glioblastoma: pathology, molecular mechanisms and markers. *Acta neuropathologica,* 129**,** 829-848.

AMON, A. & ALESCH, F. 2017. Systems for deep brain stimulation: review of technical features. *Journal of Neural Transmission,* 124**,** 1083-1091.

ANDERSON, V. C., BURCHIEL, K. J., HOGARTH, P., FAVRE, J. & HAMMERSTAD, J. P. 2005. Pallidal vs subthalamic nucleus deep brain stimulation in Parkinson disease. *Archives of neurology,* 62**,** 554-560.

ANGER, M., KUES, W. A., KLIMA, J., MIELENZ, M., KUBELKA, M., MOTLIK, J., ESNER, M., DVORAK, P., CARNWATH, J. W. & NIEMANN, H. 2003. Cell cycle dependent expression of Plk1 in synchronized porcine fetal fibroblasts. *Mol Reprod Dev,* 65**,** 245-53.

ARMSTRONG, T. S., WEFEL, J. S., WANG, M., GILBERT, M. R., WON, M., BOTTOMLEY, A., MENDOZA, T. R., COENS, C., WERNER-WASIK, M. & BRACHMAN, D. G. 2013. Net clinical benefit analysis of radiation therapy oncology group 0525: a phase III trial comparing conventional adjuvant temozolomide with dose-intensive temozolomide in patients with newly diagnosed glioblastoma. *Journal of Clinical Oncology,* 31**,** 4076.

ASHBY, L., HASSELLE, M., CHOWDHARY, S., FATHALLAH-SHAYKH, H. & ZHU, J.-J. 2015. ATCT-04RETROSPECTIVE ANALYSIS OF TUMOR TREATING FIELDS (TTFIELDS) IN ADULTS WITH GLIOBLASTOMA: SAFETY PROFILE OF THE OPTUNE™ MEDICAL DEVICE IN PATIENTS WITH IMPLANTED NON-PROGRAMMABLE SHUNTS, PROGRAMMABLE SHUNTS, AND PACEMAKERS/DEFIBRILLATORS. *Neuro-Oncology,* 17**,** v1-v1.

AVRIL, T., VAULÉON, E. & CHEVET, E. 2017. Endoplasmic reticulum stress signaling and chemotherapy resistance in solid cancers. *Oncogenesis,* 6**,** e373.

BAI, Y., SHAKELEY, R. M. & ATTARDI, G. 2000. Tight control of respiration by NADH dehydrogenase ND5 subunit gene expression in mouse mitochondria. *Molecular and cellular biology,* 20**,** 805-815.

BARBAULT, A., COSTA, F. P., BOTTGER, B., MUNDEN, R. F., BOMHOLT, F., KUSTER, N. & PASCHE, B. 2009. Amplitude-modulated electromagnetic fields for the treatment of cancer: discovery of tumor-specific frequencies and assessment of a novel therapeutic approach. *Journal of Experimental & Clinical Cancer Research,* 28**,** 51.

BARGAGNA-MOHAN, P., HAMZA, A., KIM, Y.-E., HO, Y. K. A., MOR-VAKNIN, N., WENDSCHLAG, N., LIU, J., EVANS, R. M., MARKOVITZ, D. M. & ZHAN, C.-G. 2007. The tumor inhibitor and antiangiogenic agent withaferin A targets the intermediate filament protein vimentin. *Chemistry & biology,* 14**,** 623-634.

BARKHOUDARIAN, G. 2017. A feasibility study of the Nativis Voyager system in patients with recurrent glioblastoma multiforme (GBM): Interim results of first-in-human study. American Society of Clinical Oncology.

BASELGA, J., SCHOFFSKI, P., ROJO, F., DUMEZ, H., RAMOS, F., MACARULLA, T., CAJAL, R., KISKER, O., VAN OOSTEROM, A. & TABERNERO, J. 2006. A phase I pharmacokinetic (PK) and molecular pharmacodynamic (PD) study of the combination of two anti-EGFR therapies, the monoclonal antibody (MAb) cetuximab (C) and the tyrosine kinase inhibitor (TKI) gefitinib (G), in patients (pts) with advanced colorectal (CRC),

head and neck (HNC) and non-small cell lung cancer (NSCLC). *Journal of Clinical Oncology,* 24**,** 3006-3006.

BASKAR, R., LEE, K. A., YEO, R. & YEOH, K. W. 2012. Cancer and radiation therapy: current advances and future directions. *Int J Med Sci,* 9**,** 193-9.

BEGG, A. C., STEWART, F. A. & VENS, C. 2011. Strategies to improve radiotherapy with targeted drugs. *Nat Rev Cancer,* 11**,** 239-53.

BENABID, A., POLLAK, P., GROSS, C., HOFFMANN, D., BENAZZOUZ, A., GAO, D., LAURENT, A., GENTIL, M. & PERRET, J. 1994. Acute and long-term effects of subthalamic nucleus stimulation in Parkinson's disease. *Stereotactic and functional neurosurgery,* 62**,** 76-84.

BERGMAN, H., WICHMANN, T. & DELONG, M. R. 1990. Reversal of experimental parkinsonism by lesions of the subthalamic nucleus. *Science,* 249**,** 1436-1438.

BERNARD-ARNOUX, F., LAMURE, M., DUCRAY, F., AULAGNER, G., HONNORAT, J. & ARMOIRY, X. 2016. The cost-effectiveness of tumor-treating fields therapy in patients with newly diagnosed glioblastoma. *Neuro-oncology,* 18**,** 1129-1136.

BERNEY, A., VINGERHOETS, F., PERRIN, A., GUEX, P., VILLEMURE, J.-G., BURKHARD, P., BENKELFAT, C. & GHIKA, J. 2002. Effect on mood of subthalamic DBS for Parkinson's disease A consecutive series of 24 patients. *Neurology,* 59**,** 1427-1429.

BEURRIER, C., BIOULAC, B., AUDIN, J. & HAMMOND, C. 2001. High-frequency stimulation produces a transient blockade of voltage-gated currents in subthalamic neurons. *Journal of neurophysiology,* 85**,** 1351-1356.

BIGNER, S. H., MARK, J., BURGER, P. C., MAHALEY, M. S., BULLARD, D. E., MUHLBAIER, L. H. & BIGNER, D. D. 1988. Specific chromosomal abnormalities in malignant human gliomas. *Cancer research,* 48**,** 405-411.

BINDRA, R. S., SCHAFFER, P. J., MENG, A., WOO, J., MÅSEIDE, K., ROTH, M. E., LIZARDI, P., HEDLEY, D. W., BRISTOW, R. G. & GLAZER, P. M. 2004. Down-regulation of Rad51 and decreased homologous recombination in hypoxic cancer cells. *Mol Cell Biol,* 24**,** 8504-18.

BINGGELI, R. & WEINSTEIN, R. C. 1986. Membrane potentials and sodium channels: hypotheses for growth regulation and cancer formation based on changes in sodium channels and gap junctions. *Journal of theoretical biology,* 123**,** 377-401.

BIRBILIS, T. A., MATIS, G. K., ELEFTHERIADIS, S. G., THEODOROPOULOU, E. N. & SIVRIDIS, E. 2010. Spinal metastasis of glioblastoma multiforme: an uncommon suspect? *Spine,* 35**,** E264-E269.

BIWER, L. A., GOOD, M. E., HONG, K., PATEL, R. K., AGRAWAL, N., LOOFT-WILSON, R., SONKUSARE, S. K. & ISAKSON, B. E. 2018. Non–Endoplasmic Reticulum–Based Calr (Calreticulin) Can Coordinate Heterocellular Calcium Signaling and Vascular Function. *Arteriosclerosis, thrombosis, and vascular biology,* 38**,** 120-130.

BLACKISTON, D. J., MCLAUGHLIN, K. A. & LEVIN, M. 2009. Bioelectric controls of cell proliferation: ion channels, membrane voltage and the cell cycle. *Cell cycle,* 8**,** 3527-3536.

BONDY, M. L., SCHEURER, M. E., MALMER, B., BARNHOLTZ-SLOAN, J. S., DAVIS, F. G., IL'YASOVA, D., KRUCHKO, C., MCCARTHY, B. J., RAJARAMAN, P. & SCHWARTZBAUM, J. A. 2008. Brain tumor epidemiology: consensus from the Brain Tumor Epidemiology Consortium. *Cancer,* 113**,** 1953-1968.

BOUFFET, E., PERILONGO, G., CANETE, A. & MASSIMINO, M. 1998. Intracranial ependymomas in children: a critical review of prognostic factors and a plea for cooperation. *Medical and Pediatric Oncology: The Official Journal of SIOP—International Society of Pediatric Oncology (Societé Internationale d'Oncologie Pédiatrique,* 30**,** 319-329.

BRADA, M., HOANG-XUAN, K., RAMPLING, R., DIETRICH, P., DIRIX, L., MACDONALD, D., HEIMANS, J., ZONNENBERG, B., BRAVO-MARQUES, J. & HENRIKSSON, R. 2001. Multicenter phase II trial of temozolomide in patients with glioblastoma multiforme at first relapse. *Annals of Oncology,* 12**,** 259-266.

BRAY, F., FERLAY, J., SOERJOMATARAM, I., SIEGEL, R. L., TORRE, L. A. & JEMAL, A. 2018. Global cancer statistics 2018: GLOBOCAN estimates of incidence and mortality worldwide for 36 cancers in 185 countries. *CA: a cancer journal for clinicians*.

BREM, H., PIANTADOSI, S., BURGER, P., WALKER, M., SELKER, R., VICK, N., BLACK, K., SISTI, M., BREM, S. & MOHR, G. 1995. Placebo-controlled trial of safety and efficacy of intraoperative controlled delivery by biodegradable polymers of chemotherapy for recurrent gliomas. *The Lancet,* 345**,** 1008-1012.

BRENNAN, C. W., VERHAAK, R. G., MCKENNA, A., CAMPOS, B., NOUSHMEHR, H., SALAMA, S. R., ZHENG, S., CHAKRAVARTY, D., SANBORN, J. Z. & BERMAN, S. H. 2013a. The somatic genomic landscape of glioblastoma. *Cell,* 155**,** 462-477.

BRENNAN, C. W., VERHAAK, R. G., MCKENNA, A., CAMPOS, B., NOUSHMEHR, H., SALAMA, S. R., ZHENG, S., CHAKRAVARTY, D., SANBORN, J. Z., BERMAN, S. H., BEROUKHIM, R., BERNARD, B., WU, C. J., GENOVESE, G., SHMULEVICH, I., BARNHOLTZ-SLOAN, J., ZOU, L., VEGESNA, R., SHUKLA, S. A., CIRIELLO, G., YUNG, W. K., ZHANG, W., SOUGNEZ, C., MIKKELSEN, T., ALDAPE, K., BIGNER, D. D., VAN MEIR, E. G., PRADOS, M., SLOAN, A., BLACK, K. L., ESCHBACHER, J., FINOCCHIARO, G., FRIEDMAN, W., ANDREWS, D. W., GUHA, A., IACOCCA, M., O'NEILL, B. P., FOLTZ, G., MYERS, J., WEISENBERGER, D. J., PENNY, R., KUCHERLAPATI, R., PEROU, C. M., HAYES, D. N., GIBBS, R., MARRA, M., MILLS, G. B., LANDER, E., SPELLMAN, P., WILSON, R., SANDER, C., WEINSTEIN, J., MEYERSON, M., GABRIEL, S., LAIRD, P. W., HAUSSLER, D., GETZ, G., CHIN, L. & NETWORK, T. R. 2013b. The somatic genomic landscape of glioblastoma. *Cell,* 155**,** 462-77.

BRONISCER, A. & GAJJAR, A. 2004. Supratentorial high-grade astrocytoma and diffuse brainstem glioma: two challenges for the pediatric oncologist. *The oncologist,* 9**,** 197-206.

BRONSTEIN, J. M., TAGLIATI, M., MCINTYRE, C., CHEN, R., CHEUNG, T., HARGREAVES, E. L., ISRAEL, Z., MOFFITT, M., MONTGOMERY, E. B. & STYPULKOWSKI, P. 2015. The rationale driving the evolution of deep brain stimulation to constant-current devices. *Neuromodulation: Technology at the Neural Interface,* 18**,** 85-89.

BUCKNER, C. A., BUCKNER, A. L., KOREN, S. A., PERSINGER, M. A. & LAFRENIE, R. M. 2015. Inhibition of cancer cell growth by exposure to a specific time-varying electromagnetic field involves T-type calcium channels. *PLoS One,* 10**,** e0124136.

BUCKNER, J. C., BROWN, P. D., O'NEILL, B. P., MEYER, F. B., WETMORE, C. J. & UHM, J. H. Central nervous system tumors. Mayo Clinic Proceedings, 2007. Elsevier, 1271-1286.

BUTTERS, J. T., FIGUEROA, X. A. & BUTTERS, B. M. 2014. Non-thermal radio frequency stimulation of tubulin polymerization in vitro: a potential therapy for cancer treatment. *Open Journal of Biophysics,* 4**,** 147.

CADENAS, E. & DAVIES, K. J. 2000. Mitochondrial free radical generation, oxidative stress, and aging. *Free Radical Biology and Medicine,* 29**,** 222-230.

CANADY, K. S., ALI-OSMAN, F. & RUBEL, E. W. 1990. Extracellular potassium influences DNA and protein syntheses and glial fibrillary acidic protein expression in cultured glial cells. *Glia,* 3**,** 368-374.

CARÉN, H., POLLARD, S. M. & BECK, S. 2013. The good, the bad and the ugly: epigenetic mechanisms in glioblastoma. *Molecular Aspects of Medicine,* 34**,** 849-862.

CARICO, C., NUÑO, M., MUKHERJEE, D., ELRAMSISY, A., DANTIS, J., HU, J., RUDNICK, J., JOHN, S. Y., BLACK, K. L. & BANNYKH, S. I. 2012. Loss of PTEN is not associated with poor

survival in newly diagnosed glioblastoma patients of the temozolomide era. *PLoS One,* 7**,** e33684.

CAVALLI, F. M., REMKE, M., RAMPASEK, L., PEACOCK, J., SHIH, D. J., LUU, B., GARZIA, L., TORCHIA, J., NOR, C. & MORRISSY, A. S. 2017. Intertumoral heterogeneity within medulloblastoma subgroups. *Cancer cell,* 31**,** 737-754. e6.

CHAI, Y.-H., JUNG, S., LEE, J.-K., KIM, I.-Y., JANG, W.-Y., MOON, K.-S., KIM, J.-H., LEE, K.-H., KIM, S.-K. & JUNG, T.-Y. 2017. Ependymomas: prognostic factors and outcome analysis in a retrospective series of 33 patients. *Brain tumor research and treatment,* 5**,** 70-76.

CHAICHANA, K. L., CABRERA-ALDANA, E. E., JUSUE-TORRES, I., WIJESEKERA, O., OLIVI, A., RAHMAN, M. & QUINONES-HINOJOSA, A. 2014. When gross total resection of a glioblastoma is possible, how much resection should be achieved? *World neurosurgery,* 82**,** e257-e265.

CHAMBERLAIN, M. C. 2011. Bevacizumab for the treatment of recurrent glioblastoma. *Clin Med Insights Oncol,* 5**,** 117-29.

CHAN, K. S., KOH, C. G. & LI, H. Y. 2012. Mitosis-targeted anti-cancer therapies: where they stand. *Cell Death Dis,* 3**,** e411.

CHANG, E., POHLING, C., BEYGUI, N., PATEL, C. B., ROSENBERG, J., HA, D. H. & GAMBHIR, S. S. 2017. Synergistic inhibition of glioma cell proliferation by Withaferin A and tumor treating fields. *Journal of Neuro-Oncology***,** 1-10.

CHANG, E., POHLING, C., NATARAJAN, A., WITNEY, T. H., KAUR, J., XU, L., GOWRISHANKAR, G., D'SOUZA, A. L., MURTY, S. & SCHICK, S. 2016. AshwaMAX and Withaferin A inhibits gliomas in cellular and murine orthotopic models. *Journal of neuro-oncology,* 126**,** 253-264.

CHANG, S. M., THEODOSOPOULOS, P., LAMBORN, K., MALEC, M., RABBITT, J., PAGE, M. & PRADOS, M. D. 2004. Temozolomide in the treatment of recurrent malignant glioma. *Cancer,* 100**,** 605-611.

CHAUDHRY, A., BENSON, L., VARSHAVER, M., FARBER, O., WEINBERG, U., KIRSON, E. & PALTI, Y. 2015. NovoTTF™-100A System (Tumor Treating Fields) transducer array layout planning for glioblastoma: a NovoTAL™ system user study. *World J Surg Oncol,* 13**,** 316.

CHEN, E. Y., TAN, C. M., KOU, Y., DUAN, Q., WANG, Z., MEIRELLES, G. V., CLARK, N. R. & MA'AYAN, A. 2013. Enrichr: interactive and collaborative HTML5 gene list enrichment analysis tool. *BMC bioinformatics,* 14**,** 128.

CHENG, A.-L., KANG, Y.-K., CHEN, Z., TSAO, C.-J., QIN, S., KIM, J. S., LUO, R., FENG, J., YE, S. & YANG, T.-S. 2009. Efficacy and safety of sorafenib in patients in the Asia-Pacific region with advanced hepatocellular carcinoma: a phase III randomised, double-blind, placebo-controlled trial. *The lancet oncology,* 10**,** 25-34.

CHIBA, K., LORBEER, F. K., SHAIN, A. H., MCSWIGGEN, D. T., SCHRUF, E., OH, A., RYU, J., DARZACQ, X., BASTIAN, B. C. & HOCKEMEYER, D. 2017. Mutations in the promoter of the telomerase gene TERT contribute to tumorigenesis by a two-step mechanism. *Science,* 357**,** 1416-1420.

CHIKEN, S. & NAMBU, A. 2013. High-frequency pallidal stimulation disrupts information flow through the pallidum by GABAergic inhibition. *Journal of Neuroscience,* 33**,** 2268-2280.

CHIKEN, S. & NAMBU, A. 2016. Mechanism of Deep Brain Stimulation: Inhibition, Excitation, or Disruption? *Neuroscientist,* 22**,** 313-22.

CHINOT, O., ROUGE, T. D. L. M., MOORE, N., ZEAITER, A., DAS, A., PHILLIPS, H., MODRUSAN, Z. & CLOUGHESY, T. 2011. AVAglio: Phase 3 trial of bevacizumab plus temozolomide and radiotherapy in newly diagnosed glioblastoma multiforme. *Advances in therapy,* 28**,** 334-340.

CHINOT, O. L., WICK, W., MASON, W., HENRIKSSON, R., SARAN, F., NISHIKAWA, R., CARPENTIER, A. F., HOANG-XUAN, K., KAVAN, P., CERNEA, D., BRANDES, A. A., HILTON, M., ABREY, L. & CLOUGHESY, T. 2014. Bevacizumab plus radiotherapy-temozolomide for newly diagnosed glioblastoma. *N Engl J Med,* 370**,** 709-22.

CLARK, P. A., GAAL, J. T., STREBE, J. K., PASCH, C. A., DEMING, D. A., KUO, J. S. & ROBINS, H. I. 2016. The effects of tumor treating fields and temozolomide in MGMT expressing and non-expressing patient-derived glioblastoma cells. *J Clin Neurosci*.

CLARKE, H. J., CHAMBERS, J. E., LINIKER, E. & MARCINIAK, S. J. 2014. Endoplasmic reticulum stress in malignancy. *Cancer cell,* 25**,** 563-573.

CLEELAND, C. S., ZHAO, F., CHANG, V. T., SLOAN, J. A., O'MARA, A. M., GILMAN, P. B., WEISS, M., MENDOZA, T. R., LEE, J. W. & FISCH, M. J. 2013. The symptom burden of cancer: evidence for a core set of cancer-related and treatment-related symptoms from the Eastern Cooperative Oncology Group Symptom Outcomes and Practice Patterns study. *Cancer,* 119**,** 4333-4340.

COHEN, A. L., HOLMEN, S. L. & COLMAN, H. 2013. IDH1 and IDH2 mutations in gliomas. *Current neurology and neuroscience reports,* 13**,** 345.

COHEN, K. J., POLLACK, I. F., ZHOU, T., BUXTON, A., HOLMES, E. J., BURGER, P. C., BRAT, D. J., ROSENBLUM, M. K., HAMILTON, R. L. & LAVEY, R. S. 2011. Temozolomide in the treatment of high-grade gliomas in children: a report from the Children's Oncology Group. *Neuro-oncology,* 13**,** 317-323.

CONE, C. D. 1969. SECTION OF BIOLOGICAL AND MEDICAL SCIENCES: ELECTROOSMOTIC INTERACTIONS ACCOMPANYING MITOSIS INITIATION IN SARCOMA CELLS IN VITRO. *Transactions of the New York Academy of Sciences,* 31**,** 404-427.

CONE JR, C. D. 1970. Variation of the transmembrane potential level as a basic mechanism of mitosis control. *Oncology,* 24**,** 438-470.

CONE JR, C. D. 1971. Unified theory on the basic mechanism of normal mitotic control and oncogenesis. *Journal of Theoretical Biology,* 30**,** 151-181.

COSTA, F., DE OLIVEIRA, A., MEIRELLES, R., MACHADO, M., ZANESCO, T., SURJAN, R., CHAMMAS, M., DE SOUZA ROCHA, M., MORGAN, D. & CANTOR, A. 2011. Treatment of advanced hepatocellular carcinoma with very low levels of amplitude-modulated electromagnetic fields. *British journal of cancer,* 105**,** 640.

COSTELLO, J. F., FUTSCHER, B. W., TANO, K., GRAUNKE, D. M. & PIEPER, R. O. 1994. Graded methylation in the promoter and body of the O6-methylguanine DNA methyltransferase (MGMT) gene correlates with MGMT expression in human glioma cells. *Journal of Biological Chemistry,* 269**,** 17228-17237.

COUBES, P., CIF, L., EL FERTIT, H., HEMM, S., VAYSSIERE, N., SERRAT, S., PICOT, M. C., TUFFERY, S., CLAUSTRES, M. & ECHENNE, B. 2004. Electrical stimulation of the globus pallidus internus in patients with primary generalized dystonia: long-term results. *Journal of neurosurgery,* 101**,** 189-194.

CUCULLO, L., DINI, G., HALLENE, K. L., FAZIO, V., ILKANICH, E. V., IGBOECHI, C., KIGHT, K. M., AGARWAL, M. K., GARRITY-MOSES, M. & JANIGRO, D. 2005a. Very low intensity alternating current decreases cell proliferation. *Glia,* 51**,** 65-72.

CUCULLO, L., DINI, G., HALLENE, K. L., FAZIO, V., ILKANICH, E. V., IGBOECHI, C., KIGHT, K. M., AGARWAL, M. K., GARRITY-MOSES, M. & JANIGRO, D. 2005b. Very low intensity alternating current decreases cell proliferation. *Glia,* 51**,** 65-72.

DANG, L., WHITE, D. W., GROSS, S., BENNETT, B. D., BITTINGER, M. A., DRIGGERS, E. M., FANTIN, V. R., JANG, H. G., JIN, S., KEENAN, M. C., MARKS, K. M., PRINS, R. M., WARD, P. S., YEN, K. E., LIAU, L. M., RABINOWITZ, J. D., CANTLEY, L. C., THOMPSON, C. B., VANDER HEIDEN, M. G. & SU, S. M. 2010. Cancer-associated IDH1 mutations produce 2-hydroxyglutarate. *Nature,* 465**,** 966.

DAVIES, A. M., WEINBERG, U. & PALTI, Y. 2013. Tumor treating fields: a new frontier in cancer therapy. *Ann N Y Acad Sci,* 1291**,** 86-95.

DIAMOND, A. & JANKOVIC, J. 2005. The effect of deep brain stimulation on quality of life in movement disorders. *Journal of Neurology, Neurosurgery & Psychiatry,* 76**,** 1188-1193.

DIETRICH, J., RAO, K., PASTORINO, S. & KESARI, S. 2011. Corticosteroids in brain cancer patients: benefits and pitfalls. *Expert Rev Clin Pharmacol,* 4**,** 233-42.

DOMINGUEZ-BRAUER, C., THU, K. L., MASON, J. M., BLASER, H., BRAY, M. R. & MAK, T. W. 2015. Targeting Mitosis in Cancer: Emerging Strategies. *Mol Cell,* 60**,** 524-36.

DUBBINK, H. J., ATMODIMEDJO, P. N., KROS, J. M., FRENCH, P. J., SANSON, M., IDBAIH, A., WESSELING, P., ENTING, R., SPLIET, W. & TIJSSEN, C. 2015. Molecular classification of anaplastic oligodendroglioma using next-generation sequencing: a report of the prospective randomized EORTC Brain Tumor Group 26951 phase III trial. *Neuro-oncology,* 18**,** 388-400.

DUMONTET, C. & JORDAN, M. A. 2010. Microtubule-binding agents: a dynamic field of cancer therapeutics. *Nat Rev Drug Discov,* 9**,** 790-803.

DYE, R. B. & WILLIAMS, R. C. 1996. Assembly of microtubules from tubulin bearing the nonhydrolyzable guanosine triphosphate analogue GMPPCP [guanylyl 5'-(beta, gamma-methylenediphosphonate)]: variability of growth rates and the hydrolysis of GTP. *Biochemistry,* 35**,** 14331-9.

ELLER, J. L., LONGO, S. L., KYLE, M. M., BASSANO, D., HICKLIN, D. J. & CANUTE, G. W. 2005. Anti-epidermal growth factor receptor monoclonal antibody cetuximab augments radiation effects in glioblastoma multiforme in vitro and in vivo. *Neurosurgery,* 56**,** 155-162.

ELTAHAWY, H. A., SAINT-CYR, J., GILADI, N., LANG, A. E. & LOZANO, A. M. 2004. Primary dystonia is more responsive than secondary dystonia to pallidal interventions: outcome after pallidotomy or pallidal deep brain stimulation. *Neurosurgery,* 54**,** 613-621.

ELZINGA, G., CHUNG, A. T. & WONG, E. Safety analysis of bevacizumab plus NovoTTF-100A in patients with recurrent malignant gliomas. ASCO Annual Meeting Proceedings, 2013. 2082.

ESTELLER, M., HAMILTON, S. R., BURGER, P. C., BAYLIN, S. B. & HERMAN, J. G. 1999. Inactivation of the DNA repair gene O6-methylguanine-DNA methyltransferase by promoter hypermethylation is a common event in primary human neoplasia. *Cancer research,* 59**,** 793-797.

FAKHAR, K., HASTINGS, E., BUTSON, C. R., FOOTE, K. D., ZEILMAN, P. & OKUN, M. S. 2013. Management of deep brain stimulator battery failure: battery estimators, charge density, and importance of clinical symptoms. *PLoS One,* 8**,** e58665.

FANGUSARO, J. 2012. Pediatric high grade glioma: a review and update on tumor clinical characteristics and biology. *Front Oncol,* 2**,** 105.

FAURY, D., NANTEL, A., DUNN, S. E., GUIOT, M. C., HAQUE, T., HAUSER, P., GARAMI, M., BOGNÁR, L., HANZÉLY, Z., LIBERSKI, P. P., LOPEZ-AGUILAR, E., VALERA, E. T., TONE, L. G., CARRET, A. S., DEL MAESTRO, R. F., GLEAVE, M., MONTES, J. L., PIETSCH, T., ALBRECHT, S. & JABADO, N. 2007. Molecular profiling identifies prognostic subgroups of pediatric glioblastoma and shows increased YB-1 expression in tumors. *J Clin Oncol,* 25**,** 1196-208.

FENG, L., WANG, X. & JIN, H. 2011. Rabbit monoclonal antibody: potential application in cancer therapy. *Am J Transl Res,* 3**,** 269-74.

FERNET, M., MÉGNIN-CHANET, F., HALL, J. & FAVAUDON, V. 2010. Control of the G2/M checkpoints after exposure to low doses of ionising radiation: implications for hyper-radiosensitivity. *DNA Repair (Amst),* 9**,** 48-57.

FIELD, C. M., COUGHLIN, M., DOBERSTEIN, S., MARTY, T. & SULLIVAN, W. 2005. Characterization of anillin mutants reveals essential roles in septin localization and plasma membrane integrity. *Development,* 132**,** 2849-60.

FILALI, M., HUTCHISON, W. D., PALTER, V. N., LOZANO, A. M. & DOSTROVSKY, J. O. 2004. Stimulation-induced inhibition of neuronal firing in human subthalamic nucleus. *Experimental brain research,* 156**,** 274-281.

FINLAY, J. L., BOYETT, J. M., YATES, A. J., WISOFF, J. H., MILSTEIN, J. M., GEYER, J. R., BERTOLONE, S. J., MCGUIRE, P., CHERLOW, J. M. & TEFFT, M. 1995. Randomized phase III trial in childhood high-grade astrocytoma comparing vincristine, lomustine, and prednisone with the eight-drugs-in-1-day regimen. Childrens Cancer Group. *Journal of clinical oncology,* 13**,** 112-123.

FINLAY, J. L. & ZACHAROULIS, S. 2005. The treatment of high grade gliomas and diffuse intrinsic pontine tumors of childhood and adolescence: a historical–and futuristic–perspective. *Journal of neuro-oncology,* 75**,** 253-266.

FLEMING, A. B. & SALTZMAN, W. M. 2002. Pharmacokinetics of the carmustine implant. *Clinical pharmacokinetics,* 41**,** 403-419.

FOROUZANFAR, M., AFSHIN, A., ALEXANDER, L., ANDERSON, H., BHUTTA, Z. & BIRYUKOV, S. GBD 2015 Risk Factors Collaborators (2016) Global, regional, and national comparative risk assessment of 79 behavioural, environmental and occupational, and metabolic risks or clusters of risks, 1990-2015: A systematic analysis for the Global Burden of Disease Study 2015. *Lancet,* 388**,** 1659-1724.

FRANZINI, A., FERROLI, P., LEONE, M. & BROGGI, G. 2003. Stimulation of the posterior hypothalamus for treatment of chronic intractable cluster headaches: first reported series. *Neurosurgery,* 52**,** 1095-1101.

FRASER, S. P., DISS, J. K., CHIONI, A.-M., MYCIELSKA, M. E., PAN, H., YAMACI, R. F., PANI, F., SIWY, Z., KRASOWSKA, M. & GRZYWNA, Z. 2005. Voltage-gated sodium channel expression and potentiation of human breast cancer metastasis. *Clinical Cancer Research,* 11**,** 5381-5389.

FRENETTE, P., HAINES, E., LOLOYAN, M., KINAL, M., PAKARIAN, P. & PIEKNY, A. 2012. An anillin-Ect2 complex stabilizes central spindle microtubules at the cortex during cytokinesis. *PLoS One,* 7**,** e34888.

FREUND, D., ZHANG, R., SANDERS, M. & NEWHAUSER, W. 2015. Predictive risk of radiation induced cerebral necrosis in pediatric brain cancer patients after VMAT versus proton therapy. *Cancers,* 7**,** 617-630.

FRIEDMAN, H. S., PRADOS, M. D., WEN, P. Y., MIKKELSEN, T., SCHIFF, D., ABREY, L. E., YUNG, W., PALEOLOGOS, N., NICHOLAS, M. K. & JENSEN, R. 2009a. Bevacizumab alone and in combination with irinotecan in recurrent glioblastoma. *J clin oncol,* 27**,** 4733-4740.

FRIEDMAN, H. S., PRADOS, M. D., WEN, P. Y., MIKKELSEN, T., SCHIFF, D., ABREY, L. E., YUNG, W. K., PALEOLOGOS, N., NICHOLAS, M. K., JENSEN, R., VREDENBURGH, J., HUANG, J., ZHENG, M. & CLOUGHESY, T. 2009b. Bevacizumab alone and in combination with irinotecan in recurrent glioblastoma. *J Clin Oncol,* 27**,** 4733-40.

GAJJAR, A., CHINTAGUMPALA, M., ASHLEY, D., KELLIE, S., KUN, L. E., MERCHANT, T. E., WOO, S., WHEELER, G., AHERN, V. & KRASIN, M. J. 2006. Risk-adapted craniospinal radiotherapy followed by high-dose chemotherapy and stem-cell rescue in children with newly diagnosed medulloblastoma (St Jude Medulloblastoma-96): long-term results from a prospective, multicentre trial. *The lancet oncology,* 7**,** 813-820.

GAMBOA, N. T., KARSY, M., GAMBOA, J. T., YOON, N. K., DRISCOLL, M. J., SONNEN, J. A., SALZMAN, K. L. & JENSEN, R. L. 2018. Preoperative and intraoperative perfusion magnetic resonance imaging in a RELA fusion-positive anaplastic ependymoma: A case report. *Surgical neurology international,* 9.

GARCIA, P. A., ROSSMEISL, J. H., NEAL, R. E., ELLIS, T. L., OLSON, J. D., HENAO-GUERRERO, N., ROBERTSON, J. & DAVALOS, R. V. 2010. Intracranial nonthermal irreversible electroporation: in vivo analysis. *J Membr Biol,* 236**,** 127-36.

GASCOIGNE, K. E. & TAYLOR, S. S. 2008. Cancer cells display profound intra- and interline variation following prolonged exposure to antimitotic drugs. *Cancer Cell,* 14**,** 111-22.

GASPAR, N., MARSHALL, L., PERRYMAN, L., BAX, D. A., LITTLE, S. E., VIANA-PEREIRA, M., SHARP, S. Y., VASSAL, G., PEARSON, A. & REIS, R. M. 2010. MGMT-independent temozolomide resistance in paediatric glioblastoma cells associated with a PI3-kinase-mediated HOX/stem cell gene signature. *Cancer research***,** canres. 1250.2010.

GAUTSCHI, O., HEIGHWAY, J., MACK, P. C., PURNELL, P. R., LARA, P. N. & GANDARA, D. R. 2008. Aurora kinases as anticancer drug targets. *Clin Cancer Res,* 14**,** 1639-48.

GERA, N., YANG, A., HOLTZMAN, T. S., LEE, S. X., WONG, E. T. & SWANSON, K. D. 2015. Tumor treating fields perturb the localization of septins and cause aberrant mitotic exit. *PLoS One,* 10**,** e0125269.

GILADI, M., MUNSTER, M., SCHNEIDERMAN, R., VOLOSHIN, T., PORAT, Y., BLAT, R., SHERBO, S., BOMZON, Z., KIRSON, E. & WEINBERG, U. 2015a. Tumor Treating Fields (TTFields) Sensitize Glioma Tumor Cells to Radiation Therapy by Delaying DNA Damage Repair Through Homologous Recombination. *International Journal of Radiation Oncology• Biology• Physics,* 93**,** E524-E525.

GILADI, M., MUNSTER, M., SCHNEIDERMAN, R. S., VOLOSHIN, T., PORAT, Y., BLAT, R., ZIELINSKA-CHOMEJ, K., HÅÅG, P., BOMZON, Z. E. & KIRSON, E. D. 2017. Tumor treating fields (TTFields) delay DNA damage repair following radiation treatment of glioma cells. *Radiation Oncology,* 12**,** 206.

GILADI, M., SCHNEIDERMAN, R. S., VOLOSHIN, T., PORAT, Y., MUNSTER, M., BLAT, R., SHERBO, S., BOMZON, Z., URMAN, N. & ITZHAKI, A. 2015b. Mitotic spindle disruption by alternating electric fields leads to improper chromosome segregation and mitotic catastrophe in cancer cells. *Scientific reports,* 5**,** 18046.

GILADI, M., SCHNEIDERMAN, R. S., VOLOSHIN, T., PORAT, Y., MUNSTER, M., BLAT, R., SHERBO, S., BOMZON, Z., URMAN, N., ITZHAKI, A., CAHAL, S., SHTEINGAUZ, A., CHAUDHRY, A., KIRSON, E. D., WEINBERG, U. & PALTI, Y. 2015c. Mitotic Spindle Disruption by Alternating Electric Fields Leads to Improper Chromosome Segregation and Mitotic Catastrophe in Cancer Cells. *Sci Rep,* 5**,** 18046.

GILADI, M., VOLOSHIN, T., SHTEINGAUZ, A., MUNSTER, M., BLAT, R., PORAT, Y., SCHNEIDERMAN, R. S., CAHAL, S., ITZHAKI, A. & KIRSON, E. 2016. Alternating electric fields (TTFields) induce immunogenic cell death resulting in enhanced antitumor efficacy when combined with anti-PD-1 therapy. Am Assoc Immnol.

GILADI, M., ZIELINSKA-CHOMEJ, K., TICHON, A., TU, J., SCHNEIDERMAN, R. S., VIKTORSSON, K., KIRSON, E. D., PALTI, Y. & LEWENSOHN, R. M. The effect of alternating electric fields (TTFields) on inhibition of repair of DNA damage induced by ionizing radiation and sensitization of glioma and non-small cell lung cancer cells to radiation. ASCO Annual Meeting Proceedings, 2014. e22239.

GILBERT, M. R., DIGNAM, J., WON, M., BLUMENTHAL, D. T., VOGELBAUM, M. A., ALDAPE, K. D., COLMAN, H., CHAKRAVARTI, A., JERAJ, R. & ARMSTRONG, T. S. 2013. RTOG 0825: Phase III double-blind placebo-controlled trial evaluating bevacizumab (Bev) in patients (Pts) with newly diagnosed glioblastoma (GBM). American Society of Clinical Oncology.

GILBERT, M. R., DIGNAM, J. J., ARMSTRONG, T. S., WEFEL, J. S., BLUMENTHAL, D. T., VOGELBAUM, M. A., COLMAN, H., CHAKRAVARTI, A., PUGH, S., WON, M., JERAJ, R., BROWN, P. D., JAECKLE, K. A., SCHIFF, D., STIEBER, V. W., BRACHMAN, D. G., WERNER-WASIK, M., TREMONT-LUKATS, I. W., SULMAN, E. P., ALDAPE, K. D.,

CURRAN, W. J. & MEHTA, M. P. 2014. A randomized trial of bevacizumab for newly diagnosed glioblastoma. *N Engl J Med,* 370**,** 699-708.

GILDEN, J. K., PECK, S., CHEN, Y. C. & KRUMMEL, M. F. 2012. The septin cytoskeleton facilitates membrane retraction during motility and blebbing. *J Cell Biol,* 196**,** 103-14.

GM, C. 2000. The Cell: A Molecular Approach. 2nd Edition ed. Sunderland (MA): Sinauer Associates.

GODFRAIND, C., KACZMARSKA, J. M., KOCAK, M., DALTON, J., WRIGHT, K. D., SANFORD, R. A., BOOP, F. A., GAJJAR, A., MERCHANT, T. E. & ELLISON, D. W. 2012. Distinct disease-risk groups in pediatric supratentorial and posterior fossa ependymomas. *Acta neuropathologica,* 124**,** 247-257.

GOLDMAN, D. E. 1943. Potential, impedance, and rectification in membranes. *The Journal of general physiology,* 27**,** 37-60.

GONZALEZ-GOMEZ, P., BELLO, M. J., ARJONA, D., LOMAS, J., ALONSO, M. E., DE CAMPOS, J. M., VAQUERO, J., ISLA, A., GUTIERREZ, M. & REY, J. A. 2003. Promoter hypermethylation of multiple genes in astrocytic gliomas. *International journal of oncology,* 22**,** 601-608.

GRABOWSKI, M. M., RECINOS, P. F., NOWACKI, A. S., SCHROEDER, J. L., ANGELOV, L., BARNETT, G. H. & VOGELBAUM, M. A. 2014. Residual tumor volume versus extent of resection: predictors of survival after surgery for glioblastoma. *Journal of neurosurgery,* 121**,** 1115-1123.

GRILL, J., LE DELEY, M.-C., GAMBARELLI, D., RAQUIN, M.-A., COUANET, D., PIERRE-KAHN, A., HABRAND, J.-L., DOZ, F., FRAPPAZ, D. & GENTET, J.-C. 2001. Postoperative chemotherapy without irradiation for ependymoma in children under 5 years of age: a multicenter trial of the French Society of Pediatric Oncology. *Journal of Clinical Oncology,* 19**,** 1288-1296.

GRUNDY, R. G., WILNE, S. A., WESTON, C. L., ROBINSON, K., LASHFORD, L. S., IRONSIDE, J., COX, T., CHONG, W. K., CAMPBELL, R. H. & BAILEY, C. C. 2007. Primary postoperative chemotherapy without radiotherapy for intracranial ependymoma in children: the UKCCSG/SIOP prospective study. *The lancet oncology,* 8**,** 696-705.

GUAN, X., VENGOECHEA, J., ZHENG, S., SLOAN, A. E., CHEN, Y., BRAT, D. J., O'NEILL, B. P., DE GROOT, J., YUST-KATZ, S. & YUNG, W.-K. A. 2014. Molecular subtypes of glioblastoma are relevant to lower grade glioma. *PLoS One,* 9**,** e91216.

GUO, Y. & WANG, A. Y. 2015. Novel immune check-point regulators in tolerance maintenance. *Frontiers in immunology,* 6**,** 421.

GUTIN, P. H. & WONG, E. T. 2012. Noninvasive application of alternating electric fields in glioblastoma: a fourth cancer treatment modality. *Am Soc Clin Oncol Educ Book***,** 126-31.

HAMILTON, S. R., LIU, B., PARSONS, R. E., PAPADOPOULOS, N., JEN, J., POWELL, S. M., KRUSH, A. J., BERK, T., COHEN, Z. & TETU, B. 1995. The molecular basis of Turcot's syndrome. *New England Journal of Medicine,* 332**,** 839-847.

HANAJIMA, R., DOSTROVSKY, J. O., LOZANO, A. M., HUTCHISON, W. D., DAVIS, K. D., CHEN, R. & ASHBY, P. 2004. Somatosensory evoked potentials (SEPs) recorded from deep brain stimulation (DBS) electrodes in the thalamus and subthalamic nucleus (STN). *Clinical neurophysiology,* 115**,** 424-434.

HANIF, F., MUZAFFAR, K., PERVEEN, K., MALHI, S. M. & SIMJEE, S. U. 2017. Glioblastoma multiforme: A review of its epidemiology and pathogenesis through clinical presentation and treatment. *Asian Pacific journal of cancer prevention: APJCP,* 18**,** 3.

HARRISON, M. R., HOLEN, K. D. & LIU, G. 2009. Beyond taxanes: a review of novel agents that target mitotic tubulin and microtubules, kinases, and kinesins. *Clin Adv Hematol Oncol,* 7**,** 54-64.

HART, M. G., GARSIDE, R., ROGERS, G., SOMERVILLE, M., STEIN, K. & GRANT, R. 2011. Chemotherapy wafers for high grade glioma. *Cochrane Database of Systematic Reviews*.

HARTMANN, C., WOJTECKI, L., VESPER, J., VOLKMANN, J., GROISS, S., SCHNITZLER, A. & SÜDMEYER, M. 2015. Long-term evaluation of impedance levels and clinical development in subthalamic deep brain stimulation for Parkinson's disease. *Parkinsonism & related disorders,* 21**,** 1247-1250.

HASSELBALCH, B., LASSEN, U., HANSEN, S., HOLMBERG, M., SØRENSEN, M., KOSTELJANETZ, M., BROHOLM, H., STOCKHAUSEN, M.-T. & POULSEN, H. S. 2010. Cetuximab, bevacizumab, and irinotecan for patients with primary glioblastoma and progression after radiation therapy and temozolomide: a phase II trial. *Neuro-oncology,* 12**,** 508-516.

HATANPAA, K. J., BURMA, S., ZHAO, D. & HABIB, A. A. 2010. Epidermal growth factor receptor in glioma: signal transduction, neuropathology, imaging, and radioresistance. *Neoplasia,* 12**,** 675-84.

HAYASHI, M. T. & KARLSEDER, J. 2013. DNA damage associated with mitosis and cytokinesis failure. *Oncogene,* 32**,** 4593-601.

HEGI, M. E., DISERENS, A. C., GORLIA, T., HAMOU, M. F., DE TRIBOLET, N., WELLER, M., KROS, J. M., HAINFELLNER, J. A., MASON, W., MARIANI, L., BROMBERG, J. E., HAU, P., MIRIMANOFF, R. O., CAIRNCROSS, J. G., JANZER, R. C. & STUPP, R. 2005. MGMT gene silencing and benefit from temozolomide in glioblastoma. *N Engl J Med,* 352**,** 997-1003.

HENSON, P. M. & HUME, D. A. 2006. Apoptotic cell removal in development and tissue homeostasis. *Trends Immunol,* 27**,** 244-50.

HERMAN, J. G., JEN, J., MERLO, A. & BAYLIN, S. B. 1996. Hypermethylation-associated inactivation indicates a tumor suppressor role for p15INK4B. *Cancer research,* 56**,** 722-727.

HERSHEY, T., REVILLA, F., WERNLE, A., GIBSON, P. S., DOWLING, J. & PERLMUTTER, J. 2004. Stimulation of STN impairs aspects of cognitive control in PD. *Neurology,* 62**,** 1110-1114.

HERZOG, J., FIETZEK, U., HAMEL, W., MORSNOWSKI, A., STEIGERWALD, F., SCHRADER, B., WEINERT, D., PFISTER, G., MÜLLER, D. & MEHDORN, H. M. 2004. Most effective stimulation site in subthalamic deep brain stimulation for Parkinson's disease. *Movement disorders,* 19**,** 1050-1054.

HERZOG, J., REIFF, J., KRACK, P., WITT, K., SCHRADER, B., MÜLLER, D. & DEUSCHL, G. 2003. Manic episode with psychotic symptoms induced by subthalamic nucleus stimulation in a patient with Parkinson's disease. *Movement disorders: official journal of the Movement Disorder Society,* 18**,** 1382-1384.

HEYNINCK, K., LAHTELA-KAKKONEN, M., VAN DER VEKEN, P., HAEGEMAN, G. & BERGHE, W. V. 2014. Withaferin A inhibits NF-kappaB activation by targeting cysteine 179 in IKKβ. *Biochemical pharmacology,* 91**,** 501-509.

HO KIM, E., JIN KIM, Y., SOOK SONG, H., KYOUNG JEONG, Y., YOUNG LEE, J., SUNG, J., HOON YOO, S. & YOON, M. 2016. *Biological effect of an alternating electric field on cell proliferation and synergistic antimitotic effect in combination with ionizing radiation*.

HODGKIN, A. L. & KATZ, B. 1949. The effect of sodium ions on the electrical activity of the giant axon of the squid. *The Journal of physiology,* 108**,** 37-77.

HOFFMAN, L. M., DONSON, A. M., NAKACHI, I., GRIESINGER, A. M., BIRKS, D. K., AMANI, V., HEMENWAY, M. S., LIU, A. K., WANG, M. & HANKINSON, T. C. 2014. Molecular sub-group-specific immunophenotypic changes are associated with outcome in recurrent posterior fossa ependymoma. *Acta neuropathologica,* 127**,** 731-745.

HOFLAND, K. F., HANSEN, S., SORENSEN, M., ENGELHOLM, S., SCHULTZ, H. P., MUHIC, A., GRUNNET, K., ASK, A., COSTA, J. C. & KRISTIANSEN, C. 2014. Neoadjuvant bevacizumab and irinotecan versus bevacizumab and temozolomide followed by concomitant chemoradiotherapy in newly diagnosed glioblastoma multiforme: A randomized phase II study. *Acta Oncologica,* 53**,** 939-944.

HOLSHEIMER, J., DEMEULEMEESTER, H., NUTTIN, B. & DE SUTTER, P. 2000. Identification of the target neuronal elements in electrical deep brain stimulation. *European journal of neuroscience,* 12**,** 4573-4577.

HONASOGE, A. & SONTHEIMER, H. 2013. Involvement of tumor acidification in brain cancer pathophysiology. *Frontiers in physiology,* 4**,** 316.

HORIGUCHI, K., TOMIZAWA, Y., TOSAKA, M., ISHIUCHI, S., KURIHARA, H., MORI, M. & SAITO, N. 2003. Epigenetic inactivation of RASSF1A candidate tumor suppressor gene at 3p21. 3 in brain tumors. *Oncogene,* 22**,** 7862.

HOTTINGER, A. F., STUPP, R. & HOMICSKO, K. 2014. Standards of care and novel approaches in the management of glioblastoma multiforme. *Chin J Cancer,* 33**,** 32-9.

HOWLADER, N., NOONE, A., KRAPCHO, M., GARSHELL, J., MILLER, D., ALTEKRUSE, S., KOSARY, C., YU, M., RUHL, J. & TATALOVICH, Z. 2015. SEER cancer statistics review, 1975–2011. Bethesda: National Cancer Institute; 2014.

HUANG, H. C., SHI, J., ORTH, J. D. & MITCHISON, T. J. 2009. Evidence that mitotic exit is a better cancer therapeutic target than spindle assembly. *Cancer Cell,* 16**,** 347-58.

HUR, H., JUNG, S., JUNG, T.-Y. & KIM, I.-Y. 2008. Cerebellar glioblastoma multiforme in an adult. *Journal of Korean Neurosurgical Society,* 43**,** 194.

HWANG, Y., CHUMBALKAR, V., LATHA, K. & BOGLER, O. 2011. Forced dimerization increases the activity of ΔEGFR/EGFRvIII and enhances its oncogenicity. *Molecular Cancer Research***,** molcanres. 0229.2011.

IVANOV, D. P., COYLE, B., WALKER, D. A. & GRABOWSKA, A. M. 2016. In vitro models of medulloblastoma: choosing the right tool for the job. *Journal of biotechnology,* 236**,** 10-25.

JACKSON, J. R., PATRICK, D. R., DAR, M. M. & HUANG, P. S. 2007. Targeted anti-mitotic therapies: can we improve on tubulin agents? *Nat Rev Cancer,* 7**,** 107-17.

JAING, T.-H., WANG, H.-S., TSAY, P.-K., TSENG, C.-K., JUNG, S.-M., LIN, K.-L. & LUI, T.-N. 2004. Multivariate analysis of clinical prognostic factors in children with intracranial ependymomas. *Journal of neuro-oncology,* 68**,** 255-261.

JAMAL, M., RATH, B. H., WILLIAMS, E. S., CAMPHAUSEN, K. & TOFILON, P. J. 2010. Microenvironmental regulation of glioblastoma radioresponse. *Clin Cancer Res,* 16**,** 6049-59.

JANG, M., KIM, S. S. & LEE, J. 2013. Cancer cell metabolism: implications for therapeutic targets. *Experimental & molecular medicine,* 45**,** e45.

JENUWEIN, T. & ALLIS, C. D. 2001. Translating the histone code. *Science,* 293**,** 1074-1080.

JO, Y., HWANG, S.-G., JIN, Y. B., SUNG, J., JEONG, Y. K., BAEK, J. H., CHO, J.-M., KIM, E. H. & YOON, M. 2018. Selective toxicity of tumor treating fields to melanoma: an in vitro and in vivo study. *Cell death discovery,* 5**,** 46.

JOHNSON, K. J., CULLEN, J., BARNHOLTZ-SLOAN, J. S., OSTROM, Q. T., LANGER, C. E., TURNER, M. C., MCKEAN-COWDIN, R., FISHER, J. L., LUPO, P. J. & PARTAP, S. 2014. Childhood brain tumor epidemiology: a brain tumor epidemiology consortium review. *Cancer Epidemiology and Prevention Biomarkers,* 23**,** 2716-2736.

JORDAN, M. A. & WILSON, L. 2004. Microtubules as a target for anticancer drugs. *Nat Rev Cancer,* 4**,** 253-65.

KAATSCH, P. 2010. Epidemiology of childhood cancer. *Cancer treatment reviews,* 36**,** 277-285.

KANNER, A. A., WONG, E. T., VILLANO, J. L., RAM, Z. & INVESTIGATORS, E.-. 2014. Post Hoc analyses of intention-to-treat population in phase III comparison of NovoTTF-100A™ system versus best physician's choice chemotherapy. *Semin Oncol,* 41 Suppl 6**,** S25-34.

KARANAM, N. K., SRINIVASAN, K., DING, L., SISHC, B., SAHA, D. & STORY, M. D. 2017. Tumor-treating fields elicit a conditional vulnerability to ionizing radiation via the downregulation of BRCA1 signaling and reduced DNA double-strand break repair capacity in non-small cell lung cancer cell lines. *Cell death & disease,* 8**,** e2711.

KATAYAMA, Y., YAMAMOTO, T., KOBAYASHI, K., KASAI, M., OSHIMA, H. & FUKAYA, C. 2001. Motor cortex stimulation for post-stroke pain: comparison of spinal cord and thalamic stimulation. *Stereotactic and functional neurosurgery,* 77**,** 183-186.

KEPP, O., GALLUZZI, L., MARTINS, I., SCHLEMMER, F., ADJEMIAN, S., MICHAUD, M., SUKKURWALA, A. Q., MENGER, L., ZITVOGEL, L. & KROEMER, G. 2011. Molecular determinants of immunogenic cell death elicited by anticancer chemotherapy. *Cancer Metastasis Rev,* 30**,** 61-9.

KESSLER, A. F., FRÖMBLING, G. E., GROSS, F., HAHN, M., DZOKOU, W., ERNESTUS, R.-I., LÖHR, M. & HAGEMANN, C. 2018. Effects of tumor treating fields (TTFields) on glioblastoma cells are augmented by mitotic checkpoint inhibition. *Cell death discovery,* 5**,** 12.

KILLELA, P. J., REITMAN, Z. J., JIAO, Y., BETTEGOWDA, C., AGRAWAL, N., DIAZ, L. A., FRIEDMAN, A. H., FRIEDMAN, H., GALLIA, G. L. & GIOVANELLA, B. C. 2013. TERT promoter mutations occur frequently in gliomas and a subset of tumors derived from cells with low rates of self-renewal. *Proceedings of the National Academy of Sciences,* 110**,** 6021-6026.

KIM, G. H., KIM, J. E., RHIE, S. J. & YOON, S. 2015. The role of oxidative stress in neurodegenerative diseases. *Experimental neurobiology,* 24**,** 325-340.

KIMURA, T., TAKABATAKE, Y., TAKAHASHI, A. & ISAKA, Y. 2013. Chloroquine in cancer therapy: a double-edged sword of autophagy. *Cancer research,* 73**,** 3-7.

KIRSON, E. D., DBALÝ, V., TOVARYS, F., VYMAZAL, J., SOUSTIEL, J. F., ITZHAKI, A., MORDECHOVICH, D., STEINBERG-SHAPIRA, S., GURVICH, Z., SCHNEIDERMAN, R., WASSERMAN, Y., SALZBERG, M., RYFFEL, B., GOLDSHER, D., DEKEL, E. & PALTI, Y. 2007. Alternating electric fields arrest cell proliferation in animal tumor models and human brain tumors. *Proc Natl Acad Sci U S A,* 104**,** 10152-7.

KIRSON, E. D., GILADI, M., GURVICH, Z., ITZHAKI, A., MORDECHOVICH, D., SCHNEIDERMAN, R. S., WASSERMAN, Y., RYFFEL, B., GOLDSHER, D. & PALTI, Y. 2009a. Alternating electric fields (TTFields) inhibit metastatic spread of solid tumors to the lungs. *Clin Exp Metastasis,* 26**,** 633-40.

KIRSON, E. D., GILADI, M., GURVICH, Z., ITZHAKI, A., MORDECHOVICH, D., SCHNEIDERMAN, R. S., WASSERMAN, Y., RYFFEL, B., GOLDSHER, D. & PALTI, Y. 2009b. Alternating electric fields (TTFields) inhibit metastatic spread of solid tumors to the lungs. *Clinical & experimental metastasis,* 26**,** 633-640.

KIRSON, E. D., GURVICH, Z., SCHNEIDERMAN, R., DEKEL, E., ITZHAKI, A., WASSERMAN, Y., SCHATZBERGER, R. & PALTI, Y. 2004. Disruption of cancer cell replication by alternating electric fields. *Cancer Res,* 64**,** 3288-95.

KIRSON, E. D., SCHNEIDERMAN, R. S., DBALÝ, V., TOVARYŠ, F., VYMAZAL, J., ITZHAKI, A., MORDECHOVICH, D., GURVICH, Z., SHMUELI, E. & GOLDSHER, D. 2009c. Chemotherapeutic treatment efficacy and sensitivity are increased by adjuvant alternating electric fields (TTFields). *BMC medical physics,* 9**,** 1.

KIRSON, E. D., SCHNEIDERMAN, R. S., DBALÝ, V., TOVARYS, F., VYMAZAL, J., ITZHAKI, A., MORDECHOVICH, D., GURVICH, Z., SHMUELI, E., GOLDSHER, D., WASSERMAN, Y. & PALTI, Y. 2009d. Chemotherapeutic treatment efficacy and sensitivity are increased by adjuvant alternating electric fields (TTFields). *BMC Med Phys,* 9**,** 1.

KOLLER, W. C., LYONS, K. E., WILKINSON, S. B. & PAHWA, R. 1999. Efficacy of unilateral deep brain stimulation of the VIM nucleus of the thalamus for essential head tremor. *Movement disorders: official journal of the Movement Disorder Society,* 14**,** 847-850.

KOMLODI-PASZTOR, E., SACKETT, D. L. & FOJO, A. T. 2012. Inhibitors targeting mitosis: tales of how great drugs against a promising target were brought down by a flawed rationale. *Clin Cancer Res,* 18**,** 51-63.

KONDO, N., TAKAHASHI, A., ONO, K. & OHNISHI, T. 2010. DNA damage induced by alkylating agents and repair pathways. *J Nucleic Acids,* 2010**,** 543531.

KOOL, M., KORSHUNOV, A., REMKE, M., JONES, D. T., SCHLANSTEIN, M., NORTHCOTT, P. A., CHO, Y.-J., KOSTER, J., SCHOUTEN-VAN MEETEREN, A. & VAN VUURDEN, D. 2012. Molecular subgroups of medulloblastoma: an international meta-analysis of transcriptome, genetic aberrations, and clinical data of WNT, SHH, Group 3, and Group 4 medulloblastomas. *Acta neuropathologica,* 123**,** 473-484.

KOPS, G. J. & SHAH, J. V. 2012. Connecting up and clearing out: how kinetochore attachment silences the spindle assembly checkpoint. *Chromosoma,* 121**,** 509-25.

KOUZARIDES, T. 2007. SnapShot: Histone-modifying enzymes. *Cell,* 128**,** 802. e1-802. e2.

KREISL, T. N., KIM, L., MOORE, K., DUIC, P., ROYCE, C., STROUD, I., GARREN, N., MACKEY, M., BUTMAN, J. A. & CAMPHAUSEN, K. 2009a. Phase II trial of single-agent bevacizumab followed by bevacizumab plus irinotecan at tumor progression in recurrent glioblastoma. *Journal of clinical oncology,* 27**,** 740.

KREISL, T. N., KIM, L., MOORE, K., DUIC, P., ROYCE, C., STROUD, I., GARREN, N., MACKEY, M., BUTMAN, J. A., CAMPHAUSEN, K., PARK, J., ALBERT, P. S. & FINE, H. A. 2009b. Phase II trial of single-agent bevacizumab followed by bevacizumab plus irinotecan at tumor progression in recurrent glioblastoma. *J Clin Oncol,* 27**,** 740-5.

KREX, D., KLINK, B., HARTMANN, C., VON DEIMLING, A., PIETSCH, T., SIMON, M., SABEL, M., STEINBACH, J. P., HEESE, O. & REIFENBERGER, G. 2007. Long-term survival with glioblastoma multiforme. *Brain,* 130**,** 2596-2606.

KULESHOV, M. V., JONES, M. R., ROUILLARD, A. D., FERNANDEZ, N. F., DUAN, Q., WANG, Z., KOPLEV, S., JENKINS, S. L., JAGODNIK, K. M. & LACHMANN, A. 2016. Enrichr: a comprehensive gene set enrichment analysis web server 2016 update. *Nucleic acids research,* 44**,** W90-W97.

KUMAR, R., DAGHER, A., HUTCHISON, W., LANG, A. & LOZANO, A. 1999. Globus pallidus deep brain stimulation for generalized dystonia: clinical and PET investigation. *Neurology,* 53**,** 871-871.

KUNCEL, A. M., COOPER, S. E., WOLGAMUTH, B. R., CLYDE, M. A., SNYDER, S. A., MONTGOMERY JR, E. B., REZAI, A. R. & GRILL, W. M. 2006. Clinical response to varying the stimulus parameters in deep brain stimulation for essential tremor. *Movement disorders: official journal of the Movement Disorder Society,* 21**,** 1920-1928.

LACOUTURE, M. E., DAVIS, M. E., ELZINGA, G., BUTOWSKI, N., TRAN, D., VILLANO, J. L., DIMEGLIO, L., DAVIES, A. M. & WONG, E. T. 2014. Characterization and management of dermatologic adverse events with the NovoTTF-100A System, a novel anti-mitotic electric field device for the treatment of recurrent glioblastoma. *Semin Oncol,* 41 Suppl 4**,** S1-14.

LAI, A., TRAN, A., NGHIEMPHU, P. L., POPE, W. B., SOLIS, O. E., SELCH, M., FILKA, E., YONG, W. H., MISCHEL, P. S. & LIAU, L. M. 2011. Phase II study of bevacizumab plus temozolomide during and after radiation therapy for patients with newly diagnosed glioblastoma multiforme. *Journal of clinical oncology,* 29**,** 142.

LAKHAN, S. E. & HARLE, L. 2009. Difficult diagnosis of brainstem glioblastoma multiforme in a woman: a case report and review of the literature. *Journal of medical case reports,* 3**,** 87.

LAQUINTANA, V., TRAPANI, A., DENORA, N., WANG, F., GALLO, J. M. & TRAPANI, G. 2009. New strategies to deliver anticancer drugs to brain tumors. *Expert opinion on drug delivery,* 6**,** 1017-1032.

LAVIE, D., GLOTTER, E. & SHVO, Y. 1965. Constituents of Withania somnifera Dun. III. The side chain of withaferin A*, 1. *The Journal of Organic Chemistry,* 30**,** 1774-1778.

LECLERC, C., HAEICH, J., AULESTIA, F. J., KILHOFFER, M.-C., MILLER, A. L., NEANT, I., WEBB, S. E., SCHAEFFER, E., JUNIER, M.-P. & CHNEIWEISS, H. 2016. Calcium signaling orchestrates glioblastoma development: facts and conjunctures. *Biochimica et Biophysica Acta (BBA)-Molecular Cell Research,* 1863**,** 1447-1459.

LEE, D. X., WONG, E. & SWANSON, K. D. 2013. Disruption of cell division within anaphase by tumor treating electric fields (TTFields) leads to immunogenic cell death. Neuro Oncol.

LEE, S. M., KOH, H.-J., PARK, D.-C., SONG, B. J., HUH, T.-L. & PARK, J.-W. 2002. Cytosolic NADP+-dependent isocitrate dehydrogenase status modulates oxidative damage to cells. *Free Radical Biology and Medicine,* 32**,** 1185-1196.

LEE, S. M., SHIN, H., JANG, S.-W., SHIM, J.-J., SONG, I.-S., SON, K.-N., HWANG, J., SHIN, Y.-H., KIM, H.-H. & LEE, C.-K. 2004. PLP2/A4 interacts with CCR1 and stimulates migration of CCR1-expressing HOS cells. *Biochemical and biophysical research communications,* 324**,** 768-772.

LEE, Y., KOH, J., KIM, S.-I., WON, J. K., PARK, C.-K., CHOI, S. H. & PARK, S.-H. 2017. The frequency and prognostic effect of TERT promoter mutation in diffuse gliomas. *Acta neuropathologica communications,* 5**,** 62.

LEVIN, M. 2007. Gap junctional communication in morphogenesis. *Progress in biophysics and molecular biology,* 94**,** 186-206.

LEVINE, S. A., MCKEEVER, P. E. & GREENBERG, H. S. 1987. Primary cerebellar glioblastoma multiforme. *Journal of neuro-oncology,* 5**,** 231-236.

LI, F. P. & FRAUMENI, J. F. 1969. Soft-tissue sarcomas, breast cancer, and other neoplasms: a familial syndrome? *Annals of internal medicine,* 71**,** 747-752.

LI, F. P. & FRAUMENI JR, J. F. 1969. Rhabdomyosarcoma in children: epidemiologic study and identification of a familial caneer syndrome. *Journal of the National Cancer Institute,* 43**,** 1365-1373.

LI, Y. M., SUKI, D., HESS, K. & SAWAYA, R. 2016. The influence of maximum safe resection of glioblastoma on survival in 1229 patients: can we do better than gross-total resection? *Journal of neurosurgery,* 124**,** 977-988.

LIN, J. H., WALTER, P. & YEN, T. B. 2008. Endoplasmic reticulum stress in disease pathogenesis. *Annu. Rev. pathmechdis. Mech. Dis.,* 3**,** 399-425.

LIN, M. T. & BEAL, M. F. 2006. Mitochondrial dysfunction and oxidative stress in neurodegenerative diseases. *Nature,* 443**,** 787.

LITAN, A. & LANGHANS, S. A. 2015. Cancer as a channelopathy: ion channels and pumps in tumor development and progression. *Frontiers in cellular neuroscience,* 9**,** 86.

LIU, J., FAIRN, G. D., CECCARELLI, D. F., SICHERI, F. & WILDE, A. 2012. Cleavage furrow organization requires PIP(2)-mediated recruitment of anillin. *Curr Biol,* 22**,** 64-9.

LLAGUNO, S. R. A. & PARADA, L. F. 2016. Cell of origin of glioma: biological and clinical implications. *British journal of cancer,* 115**,** 1445.

LLOVET, J. M., RICCI, S., MAZZAFERRO, V., HILGARD, P., GANE, E., BLANC, J.-F., DE OLIVEIRA, A. C., SANTORO, A., RAOUL, J.-L. & FORNER, A. 2008. Sorafenib in advanced hepatocellular carcinoma. *New England journal of medicine,* 359**,** 378-390.

LOUIS, D. N., OHGAKI, H., WIESTLER, O. D., CAVENEE, W. K., BURGER, P. C., JOUVET, A., SCHEITHAUER, B. W. & KLEIHUES, P. 2007. The 2007 WHO classification of tumours of the central nervous system. *Acta neuropathologica,* 114**,** 97-109.

LOUIS, D. N., PERRY, A., REIFENBERGER, G., VON DEIMLING, A., FIGARELLA-BRANGER, D., CAVENEE, W. K., OHGAKI, H., WIESTLER, O. D., KLEIHUES, P. & ELLISON, D. W. 2016. The 2016 World Health Organization classification of tumors of the central nervous system: a summary. *Acta neuropathologica,* 131**,** 803-820.

LUKAS, R. V., RATERMANN, K. L., WONG, E. T. & VILLANO, J. L. 2017. Skin toxicities associated with tumor treating fields: case based review. *Journal of Neuro-Oncology,* 135**,** 593-599.

LUN, M., LOK, E., GAUTAM, S., WU, E. & WONG, E. T. 2011. The natural history of extracranial metastasis from glioblastoma multiforme. *Journal of neuro-oncology,* 105**,** 261-273.

LUO, J., KAPLITT, M. G., FITZSIMONS, H. L., ZUZGA, D. S., LIU, Y., OSHINSKY, M. L. & DURING, M. J. 2002. Subthalamic GAD gene therapy in a Parkinson's disease rat model. *Science,* 298**,** 425-429.

LYONS, K. E. & PAHWA, R. 2005. Long-term benefits in quality of life provided by bilateral subthalamic stimulation in patients with Parkinson disease. *Journal of neurosurgery,* 103**,** 252-255.

MAHER, E. A., BRENNAN, C., WEN, P. Y., DURSO, L., LIGON, K. L., RICHARDSON, A., KHATRY, D., FENG, B., SINHA, R., LOUIS, D. N., QUACKENBUSH, J., BLACK, P. M., CHIN, L. & DEPINHO, R. A. 2006. Marked genomic differences characterize primary and secondary glioblastoma subtypes and identify two distinct molecular and clinical secondary glioblastoma entities. *Cancer Res,* 66**,** 11502-13.

MAHVASH, M., HUGO, H.-H., MASLEHATY, H., MEHDORN, H. M. & STARK, A. M. 2011. Glioblastoma multiforme in children: report of 13 cases and review of the literature. *Pediatric neurology,* 45**,** 178-180.

MALMSTRÖM, A., GRØNBERG, B. H., MAROSI, C., STUPP, R., FRAPPAZ, D., SCHULTZ, H., ABACIOGLU, U., TAVELIN, B., LHERMITTE, B., HEGI, M. E., ROSELL, J., HENRIKSSON, R. & (NCBTSG), N. C. B. T. S. G. 2012. Temozolomide versus standard 6-week radiotherapy versus hypofractionated radiotherapy in patients older than 60 years with glioblastoma: the Nordic randomised, phase 3 trial. *Lancet Oncol,* 13**,** 916-26.

MARAMBAUD, P., DRESES-WERRINGLOER, U. & VINGTDEUX, V. 2009. Calcium signaling in neurodegeneration. *Molecular neurodegeneration,* 4**,** 20.

MARELLA, M., SEO, B. B., YAGI, T. & MATSUNO-YAGI, A. 2009. Parkinson's disease and mitochondrial complex I: a perspective on the Ndi1 therapy. *Journal of bioenergetics and biomembranes,* 41**,** 493-497.

MARGISON, G. P. & SANTIBÁÑEZ-KOREF, M. F. 2002. O6-alkylguanine-DNA alkyltransferase: role in carcinogenesis and chemotherapy. *Bioessays,* 24**,** 255-66.

MASSIMINO, M., GANDOLA, L., GIANGASPERO, F., SANDRI, A., VALAGUSSA, P., PERILONGO, G., GARRÈ, M. L., RICARDI, U., FORNI, M. & GENITORI, L. 2004. Hyperfractionated radiotherapy and chemotherapy for childhood ependymoma: final results of the first prospective AIEOP (Associazione Italiana di Ematologia-Oncologia Pediatrica) study. *International Journal of Radiation Oncology* Biology* Physics,* 58**,** 1336-1345.

MASSIMINO, M., MICELI, R., GIANGASPERO, F., BOSCHETTI, L., MODENA, P., ANTONELLI, M., FERROLI, P., BERTIN, D., PECORI, E. & VALENTINI, L. 2016. Final results of the second prospective AIEOP protocol for pediatric intracranial ependymoma. *Neuro-oncology,* 18**,** 1451-1460.

MATSUZAKI, S., SZWEDA, P. A., SZWEDA, L. I. & HUMPHRIES, K. M. 2009. Regulated production of free radicals by the mitochondrial electron transport chain: Cardiac ischemic preconditioning. *Advanced drug delivery reviews,* 61**,** 1324-1331.

MCINTYRE, C. C., SAVASTA, M., KERKERIAN-LE GOFF, L. & VITEK, J. L. 2004a. Uncovering the mechanism (s) of action of deep brain stimulation: activation, inhibition, or both. *Clinical neurophysiology,* 115**,** 1239-1248.

MCINTYRE, C. C., SAVASTA, M., WALTER, B. L. & VITEK, J. L. 2004b. How does deep brain stimulation work? Present understanding and future questions. *Journal of clinical neurophysiology,* 21**,** 40-50.

MEISTER, S., FREY, B., LANG, V. R., GAIPL, U. S., SCHETT, G., SCHLÖTZER-SCHREHARDT, U. & VOLL, R. E. 2010. Calcium Channel Blocker Verapamil Enhances Reticulum Stress and Death Induced by Proteasome Inhibition in Myeloma Cells. *Neoplasia,* 12**,** 550-IN3.

MESSAHEL, B., ASHLEY, S., SARAN, F., ELLISON, D., IRONSIDE, J., PHIPPS, K., COX, T., CHONG, W., ROBINSON, K. & PICTON, S. 2009. Relapsed intracranial ependymoma in children in the UK: patterns of relapse, survival and therapeutic outcome. *European journal of cancer,* 45**,** 1815-1823.

MILELLA, M., FALCONE, I., CONCIATORI, F., CESTA INCANI, U., DEL CURATOLO, A., INZERILLI, N., NUZZO, C., VACCARO, V., VARI, S. & COGNETTI, F. 2015. PTEN: multiple functions in human malignant tumors. *Frontiers in oncology,* 5**,** 24.

MOLENAAR, R. J. 2011. Ion channels in glioblastoma. *ISRN neurology,* 2011.

MONTGOMERY JR, E. B. 2006. Effects of GPi stimulation on human thalamic neuronal activity. *Clinical Neurophysiology,* 117**,** 2691-2702.

MORITZ, A. R. & HENRIQUES JR, F. 1947. Studies of thermal injury: II. The relative importance of time and surface temperature in the causation of cutaneous burns. *The American journal of pathology,* 23**,** 695.

MUKHTAR, E., ADHAMI, V. M. & MUKHTAR, H. 2014. Targeting microtubules by natural agents for cancer therapy. *Molecular cancer therapeutics,* 13**,** 275-284.

MUNSTER, M., ROBERTS, C. P., SCHMELZ, E. M., GILADI, M., BLAT, R., SCHNEIDERMAN, R. S., PORAT, Y., BOMZON, Z., URMAN, N., ITZHAKI, A., VOLOSHIN SELA, T., CAHAL, S., KIRSON, E. D., WEINBERG, U. & PALTI, Y. 2015. Abstract 5365: Alternating electric fields (TTFields) in combination with paclitaxel are therapeutically effective against ovarian cancer cells in vitro and in vivo. *Cancer Research,* 75**,** 5365-5365.

MUSTAFA, D. A., SWAGEMAKERS, S. M., BUISE, L., VAN DER SPEK, P. J. & KROS, J. M. 2014. Metabolic alterations due to IDH1 mutation in glioma: opening for therapeutic opportunities? *Acta Neuropathol Commun,* 2**,** 6.

MYCIELSKA, M. E., PALMER, C. P., BRACKENBURY, W. J. & DJAMGOZ, M. B. 2005. Expression of Na+-dependent citrate transport in a strongly metastatic human prostate cancer PC-3M cell line: regulation by voltage-gated Na+ channel activity. *The Journal of physiology,* 563**,** 393-408.

NAKAMURA, M., WATANABE, T., YONEKAWA, Y., KLEIHUES, P. & OHGAKI, H. 2001. Promoter methylation of the DNA repair gene MGMT in astrocytomas is frequently associated with G: C→ A: T mutations of the TP53 tumor suppressor gene. *Carcinogenesis,* 22**,** 1715-1719.

NAMBU, A., TOKUNO, H., HAMADA, I., KITA, H., IMANISHI, M., AKAZAWA, T., IKEUCHI, Y. & HASEGAWA, N. 2000. Excitatory cortical inputs to pallidal neurons via the subthalamic nucleus in the monkey. *Journal of neurophysiology,* 84**,** 289-300.

NAMBU, A., TOKUNO, H. & TAKADA, M. 2002. Functional significance of the cortico–subthalamo–pallidal 'hyperdirect'pathway. *Neuroscience research,* 43**,** 111-117.

NÉMETH, Z. H., DEITCH, E. A., DAVIDSON, M. T., SZABÓ, C., VIZI, E. S. & HASKÓ, G. 2004. Disruption of the actin cytoskeleton results in nuclear factor-κB activation and inflammatory mediator production in cultured human intestinal epithelial cells. *Journal of cellular physiology,* 200**,** 71-81.

NEUHAUS, E., ZIRJACKS, L., GANSER, K., KLUMPP, L., SCHÜLER, U., ZIPS, D., ECKERT, F. & HUBER, S. M. 2019. Alternating Electric Fields (TTFields) Activate Cav1. 2 Channels in Human Glioblastoma Cells. *Cancers,* 11**,** 110.

NIETO-SAMPEDRO, M., VALLE-ARGOS, B., GÓMEZ-NICOLA, D., FERNÁNDEZ-MAYORALAS, A. & NIETO-DÍAZ, M. 2011. Inhibitors of Glioma Growth that Reveal the Tumour to the Immune System. *Clin Med Insights Oncol,* 5**,** 265-314.

NONOGUCHI, N., OHTA, T., OH, J.-E., KIM, Y.-H., KLEIHUES, P. & OHGAKI, H. 2013. TERT promoter mutations in primary and secondary glioblastomas. *Acta neuropathologica,* 126**,** 931-937.

NORTHCOTT, P. A., SHIH, D. J., PEACOCK, J., GARZIA, L., MORRISSY, A. S., ZICHNER, T., STÜTZ, A. M., KORSHUNOV, A., REIMAND, J. & SCHUMACHER, S. E. 2012. Subgroup-specific structural variation across 1,000 medulloblastoma genomes. *Nature,* 488**,** 49.

OBEID, M., TESNIERE, A., GHIRINGHELLI, F., FIMIA, G. M., APETOH, L., PERFETTINI, J. L., CASTEDO, M., MIGNOT, G., PANARETAKIS, T., CASARES, N., MÉTIVIER, D., LAROCHETTE, N., VAN ENDERT, P., CICCOSANTI, F., PIACENTINI, M., ZITVOGEL, L. & KROEMER, G. 2007. Calreticulin exposure dictates the immunogenicity of cancer cell death. *Nat Med,* 13**,** 54-61.

OHGAKI, H. & KLEIHUES, P. 2013. The definition of primary and secondary glioblastoma. *Clin Cancer Res,* 19**,** 764-72.

OMAR, A. I. 2014. Tumor treating field therapy in combination with bevacizumab for the treatment of recurrent glioblastoma. *J Vis Exp***,** e51638.

ORR, C., YOSHIKAWA-FUKADA, M. & EBERT, J. 1972. Potassium: Effect on DNA synthesis and multiplication of baby-hamster kidney cells. *Proceedings of the National Academy of Sciences,* 69**,** 243-247.

OSTROM, Q. T., GITTLEMAN, H., LIAO, P., VECCHIONE-KOVAL, T., WOLINSKY, Y., KRUCHKO, C. & BARNHOLTZ-SLOAN, J. S. 2017. CBTRUS statistical report: primary brain and other central nervous system tumors diagnosed in the United States in 2010–2014. *Neuro-oncology,* 19**,** v1-v88.

PACKER, R. J., GAJJAR, A., VEZINA, G., RORKE-ADAMS, L., BURGER, P. C., ROBERTSON, P. L., BAYER, L., LAFOND, D., DONAHUE, B. R. & MARYMONT, M. H. 2006. Phase III study of craniospinal radiation therapy followed by adjuvant chemotherapy for newly diagnosed average-risk medulloblastoma. *Journal of clinical oncology,* 24**,** 4202-4208.

PACKER, R. J., SUTTON, L. N., GOLDWEIN, J. W., PERILONGO, G., BUNIN, G., RYAN, J., COHEN, B. H., D'ANGIO, G., KRAMER, E. D. & ZIMMERMAN, R. A. 1991. Improved survival with the use of adjuvant chemotherapy in the treatment of medulloblastoma. *Journal of neurosurgery,* 74**,** 433-440.

PAHWA, R., WILKINSON, S. B., OVERMAN, J. & LYONS, K. E. 2005. Preoperative clinical predictors of response to bilateral subthalamic stimulation in patients with Parkinson's disease. *Stereotactic and functional neurosurgery,* 83**,** 80-83.

PAJTLER, K. W., WITT, H., SILL, M., JONES, D. T., HOVESTADT, V., KRATOCHWIL, F., WANI, K., TATEVOSSIAN, R., PUNCHIHEWA, C. & JOHANN, P. 2015. Molecular classification of ependymal tumors across all CNS compartments, histopathological grades, and age groups. *Cancer cell,* 27**,** 728-743.

PARKER, N. R., KHONG, P., PARKINSON, J. F., HOWELL, V. M. & WHEELER, H. R. 2015. Molecular heterogeneity in glioblastoma: potential clinical implications. *Front Oncol,* 5**,** 55.

PARSA, A. T., WALDRON, J. S., PANNER, A., CRANE, C. A., PARNEY, I. F., BARRY, J. J., CACHOLA, K. E., MURRAY, J. C., TIHAN, T. & JENSEN, M. C. 2007. Loss of tumor suppressor PTEN function increases B7-H1 expression and immunoresistance in glioma. *Nature medicine,* 13**,** 84.

PARSONS, D. W., JONES, S., ZHANG, X., LIN, J. C., LEARY, R. J., ANGENENDT, P., MANKOO, P., CARTER, H., SIU, I. M., GALLIA, G. L., OLIVI, A., MCLENDON, R., RASHEED, B. A., KEIR, S., NIKOLSKAYA, T., NIKOLSKY, Y., BUSAM, D. A., TEKLEAB, H., DIAZ, L. A., HARTIGAN,

J., SMITH, D. R., STRAUSBERG, R. L., MARIE, S. K., SHINJO, S. M., YAN, H., RIGGINS, G. J., BIGNER, D. D., KARCHIN, R., PAPADOPOULOS, N., PARMIGIANI, G., VOGELSTEIN, B., VELCULESCU, V. E. & KINZLER, K. W. 2008. An integrated genomic analysis of human glioblastoma multiforme. *Science,* 321**,** 1807-12.

PASCHE, B., ERMAN, M., HAYDUK, R., MITLER, M. M., REITE, M., HIGGS, L., KUSTER, N., ROSSEL, C., DAFNI, U. & AMATO, D. 1996. Effects of low energy emission therapy in chronic psychophysiological insomnia. *Sleep,* 19**,** 327-336.

PATEL, A. P., TIROSH, I., TROMBETTA, J. J., SHALEK, A. K., GILLESPIE, S. M., WAKIMOTO, H., CAHILL, D. P., NAHED, B. V., CURRY, W. T. & MARTUZA, R. L. 2014. Single-cell RNA-seq highlights intratumoral heterogeneity in primary glioblastoma. *Science,* 344**,** 1396-1401.

PATEL, D., LAHIJI, A., PATEL, S., FRANKLIN, M., JIMENEZ, X., HICKLIN, D. J. & KANG, X. 2007. Monoclonal antibody cetuximab binds to and down-regulates constitutively activated epidermal growth factor receptor vIII on the cell surface. *Anticancer research,* 27**,** 3355-3366.

PAULINO, A. C., WEN, B.-C., BUATTI, J. M., HUSSEY, D. H., ZHEN, W. K., MAYR, N. A. & MENEZES, A. H. 2002. Intracranial ependymomas: an analysis of prognostic factors and patterns of failure. *American journal of clinical oncology,* 25**,** 117-122.

PERILONGO, G., MASSIMINO, M., SOTTI, G., BELFONTALI, T., MASIERO, L., RIGOBELLO, L., GARRÈ, L., CARLI, M., LOMBARDI, F. & SOLERO, C. 1997. Analyses of prognostic factors in a retrospective review of 92 children with ependymoma: Italian Pediatric Neuro-Oncology Group. *Medical and Pediatric Oncology: The Official Journal of SIOP—International Society of Pediatric Oncology (Societé Internationale d'Oncologie Pédiatrique,* 29**,** 79-85.

PERIS-BONET, R., MARTÍNEZ-GARCÍA, C., LACOUR, B., PETROVICH, S., GINER-RIPOLL, B., NAVAJAS, A. & STELIAROVA-FOUCHER, E. 2006. Childhood central nervous system tumours–incidence and survival in Europe (1978–1997): report from Automated Childhood Cancer Information System project. *European journal of cancer,* 42**,** 2064-2080.

PERLMUTTER, J. S. & MINK, J. W. 2006. Deep brain stimulation. *Annu. Rev. Neurosci.,* 29**,** 229-257.

PERRY, A. & WESSELING, P. 2016. Histologic classification of gliomas. *Handbook of clinical neurology.* Elsevier.

PERSSON, A. I., JONES, C., HAWKINS, C., HAAS-KOGAN, D. A., HARGRAVE, D., JONES, D. T. W., SIMONDS, E. F., STAFFORD, J. M., PHILLIPS, J. J., KIERAN, M. W., KARAJANNIS, M. A., MONJE, M., JABADO, N., GUPTA, N., BECHER, O. J., PACKER, R. J., MUELLER, S., PFISTER, S. M., BAKER, S. J., NICOLAIDES, T., WEISS, W. A., LI, X.-N., CHO, Y.-J. & TANG, Y. 2016. Pediatric high-grade glioma: biologically and clinically in need of new thinking. *Neuro-Oncology,* 19**,** 153-161.

PETRONCZKI, M., LÉNÁRT, P. & PETERS, J. M. 2008. Polo on the Rise-from Mitotic Entry to Cytokinesis with Plk1. *Dev Cell,* 14**,** 646-59.

PHILLIPS, H. S., KHARBANDA, S., CHEN, R., FORREST, W. F., SORIANO, R. H., WU, T. D., MISRA, A., NIGRO, J. M., COLMAN, H., SOROCEANU, L., WILLIAMS, P. M., MODRUSAN, Z., FEUERSTEIN, B. G. & ALDAPE, K. 2006. Molecular subclasses of high-grade glioma predict prognosis, delineate a pattern of disease progression, and resemble stages in neurogenesis. *Cancer Cell,* 9**,** 157-73.

PICHLMEIER, U., BINK, A., SCHACKERT, G. & STUMMER, W. 2008. Resection and survival in glioblastoma multiforme: an RTOG recursive partitioning analysis of ALA study patients. *Neuro-oncology,* 10**,** 1025-1034.

PIEKNY, A. J. & GLOTZER, M. 2008. Anillin is a scaffold protein that links RhoA, actin, and myosin during cytokinesis. *Curr Biol,* 18**,** 30-6.

PINES, J. 2011. Cubism and the cell cycle: the many faces of the APC/C. *Nat Rev Mol Cell Biol,* 12**,** 427-38.

PIRZKALL, A., MCGUE, C., SARASWATHY, S., CHA, S., LIU, R., VANDENBERG, S., LAMBORN, K. R., BERGER, M. S., CHANG, S. M. & NELSON, S. J. 2009. Tumor regrowth between surgery and initiation of adjuvant therapy in patients with newly diagnosed glioblastoma. *Neuro Oncol,* 11**,** 842-52.

PIZER, B. L. & CLIFFORD, S. C. 2009. The potential impact of tumour biology on improved clinical practice for medulloblastoma: progress towards biologically driven clinical trials. *British journal of neurosurgery,* 23**,** 364-375.

PLESS, M., DROEGE, C., VON MOOS, R., SALZBERG, M. & BETTICHER, D. 2013. A phase I/II trial of Tumor Treating Fields (TTFields) therapy in combination with pemetrexed for advanced non-small cell lung cancer. *Lung cancer,* 81**,** 445-450.

POLLAK, J., RAI, K. G., FUNK, C. C., ARORA, S., LEE, E., ZHU, J., PRICE, N. D., PADDISON, P. J., RAMIREZ, J.-M. & ROSTOMILY, R. C. 2017. Ion channel expression patterns in glioblastoma stem cells with functional and therapeutic implications for malignancy. *PloS one,* 12**,** e0172884.

POLLAK, P., FRAIX, V., KRACK, P., MORO, E., MENDES, A., CHABARDES, S., KOUDSIE, A. & BENABID, A. L. 2002. Treatment results: Parkinson's disease. *Movement disorders,* 17**,** S75-S83.

POLLARD, P. J. & RATCLIFFE, P. J. 2009. Puzzling patterns of predisposition. *Science***,** 192-194.

PORAT, Y., GILADI, M., SCHNEIDERMAN, R., MUNSTER, M., BLATT, R., WEINBERG, U., KIRSON, E. & PALTI, Y. 2014. ET-47TRIFLOUROPROMAZINE, AN APPROVED ANTIPSYCHOTIC DRUG, ENHANCES TUMOR TREATING FIELDS TREATMENT EFFICACY IN VITRO. *Neuro-oncology,* 16**,** v89-v89.

PORAT, Y., GILADI, M., SCHNEIDERMAN, R. S., BLAT, R., SHTEINGAUZ, A., ZEEVI, E., MUNSTER, M., VOLOSHIN, T., KAYNAN, N. & TAL, O. 2017. Determining the Optimal Inhibitory Frequency for Cancerous Cells Using Tumor Treating Fields (TTFields). *Journal of visualized experiments: JoVE*.

PRALONG, E., POLLO, C., BLOCH, J., VILLEMURE, J.-G., DANIEL, R. T., TÉTREAULT, M.-H. & DEBATISSE, D. 2004. Recording of ventral posterior lateral thalamus neuron response to contact heat evoked potential in patient with neurogenic pain. *Neuroscience letters,* 367**,** 332-335.

RANCK JR, J. B. 1975. Which elements are excited in electrical stimulation of mammalian central nervous system: a review. *Brain research,* 98**,** 417-440.

RASHEED, B. A., STENZEL, T. T., MCLENDON, R. E., PARSONS, R., FRIEDMAN, A. H., FRIEDMAN, H. S., BIGNER, D. D. & BIGNER, S. H. 1997. PTEN gene mutations are seen in high-grade but not in low-grade gliomas. *Cancer research,* 57**,** 4187-4190.

REGULA, J., MACROBERT, A., GORCHEIN, A., BUONACCORSI, G., THORPE, S., SPENCER, G., HATFIELD, A. & BOWN, S. 1995. Photosensitisation and photodynamic therapy of oesophageal, duodenal, and colorectal tumours using 5 aminolaevulinic acid induced protoporphyrin IX--a pilot study. *Gut,* 36**,** 67-75.

REHNCRONA, S., JOHNELS, B., WIDNER, H., TÖRNQVIST, A. L., HARIZ, M. & SYDOW, O. 2003. Long-term efficacy of thalamic deep brain stimulation for tremor: double-blind assessments. *Movement disorders: official journal of the Movement Disorder Society,* 18**,** 163-170.

REITE, M., HIGGS, L., LEBET, J. P., BARBAULT, A., ROSSEL, C., KUSTER, N., DAFNI, U., AMATO, D. & PASCHE, B. 1994. Sleep inducing effect of low energy emission therapy. *Bioelectromagnetics: Journal of the Bioelectromagnetics Society, The Society for Physical Regulation in Biology and Medicine, The European Bioelectromagnetics Association,* 15**,** 67-75.

RESTALL, I. J., PAROLIN, D. A., DANESHMAND, M., HANSON, J. E., SIMARD, M. A., FITZPATRICK, M. E., KUMAR, R., LAVICTOIRE, S. J. & LORIMER, I. A. 2015. PKCι depletion initiates mitotic slippage-induced senescence in glioblastoma. *Cell Cycle,* 14**,** 2938-48.

RICH, J. N., REARDON, D. A., PEERY, T., DOWELL, J. M., QUINN, J. A., PENNE, K. L., WIKSTRAND, C. J., VAN DUYN, L. B., DANCEY, J. E. & MCLENDON, R. E. 2004. Phase II trial of gefitinib in recurrent glioblastoma. *Journal of Clinical Oncology,* 22**,** 133-142.

RIEDER, C. L. & MAIATO, H. 2004. Stuck in division or passing through: what happens when cells cannot satisfy the spindle assembly checkpoint. *Dev Cell,* 7**,** 637-51.

RIFFELL, J. L., ZIMMERMAN, C., KHONG, A., MCHARDY, L. M. & ROBERGE, M. 2009. Effects of chemical manipulation of mitotic arrest and slippage on cancer cell survival and proliferation. *Cell Cycle,* 8**,** 3025-38.

RISINGER, A. L., PENG, J., ROHENA, C. C., AGUILAR, H. R., FRANTZ, D. E. & MOOBERRY, S. L. 2013. The bat flower: a source of microtubule-destabilizing and -stabilizing compounds with synergistic antiproliferative actions. *J Nat Prod,* 76**,** 1923-9.

ROA, W., BRASHER, P. M., BAUMAN, G., ANTHES, M., BRUERA, E., CHAN, A., FISHER, B., FULTON, D., GULAVITA, S., HAO, C., HUSAIN, S., MURTHA, A., PETRUK, K., STEWART, D., TAI, P., URTASUN, R., CAIRNCROSS, J. G. & FORSYTH, P. 2004. Abbreviated course of radiation therapy in older patients with glioblastoma multiforme: a prospective randomized clinical trial. *J Clin Oncol,* 22**,** 1583-8.

ROCK, K., MCARDLE, O., FORDE, P., DUNNE, M., FITZPATRICK, D., O'NEILL, B. & FAUL, C. 2012. A clinical review of treatment outcomes in glioblastoma multiforme—the validation in a non-trial population of the results of a randomised Phase III clinical trial: has a more radical approach improved survival? *The British journal of radiology,* 85**,** e729-e733.

ROMERO ACUÑA, L., LANGHI, M., PÉREZ, J., ROMERO ACUÑA, J., MACHIAVELLI, M., LACAVA, J., VALLEJO, C., ROMERO, A., FASCE, H., ORTIZ, E., GRASSO, S., AMATO, S., RODRÍGUEZ, R., BARBIERI, M. & LEONE, B. 1999. Vinorelbine and paclitaxel as first-line chemotherapy in metastatic breast cancer. *J Clin Oncol,* 17**,** 74-81.

RUDÀ, R., REIFENBERGER, G., FRAPPAZ, D., PFISTER, S. M., LAPRIE, A., SANTARIUS, T., ROTH, P., TONN, J. C., SOFFIETTI, R. & WELLER, M. 2017. EANO guidelines for the diagnosis and treatment of ependymal tumors. *Neuro-oncology,* 20**,** 445-456.

RUTKOWSKI, S., BODE, U., DEINLEIN, F., OTTENSMEIER, H., WARMUTH-METZ, M., SOERENSEN, N., GRAF, N., EMSER, A., PIETSCH, T. & WOLFF, J. E. 2005. Treatment of early childhood medulloblastoma by postoperative chemotherapy alone. *New England Journal of Medicine,* 352**,** 978-986.

SANAI, N., POLLEY, M.-Y., MCDERMOTT, M. W., PARSA, A. T. & BERGER, M. S. 2011. An extent of resection threshold for newly diagnosed glioblastomas. *Journal of neurosurgery,* 115**,** 3-8.

SANDERS, R. P., KOCAK, M., BURGER, P. C., MERCHANT, T. E., GAJJAR, A. & BRONISCER, A. 2007. High-grade astrocytoma in very young children. *Pediatr Blood Cancer,* 49**,** 888-93.

SCHNEIDERMAN, R. S., GILADI, M., PORAT, Y., MUNSTER, M., WEINBERG, U., KIRSON, E.D. AND PALTI, Y. 2013. Overcoming cell size escape from tumor treating fields using a varying frequency treatment paradigm in vitro. *In ASCO Annual Meeting Proceedings,* 31**,** e22134.

SCHNEIDERMAN, R. S., VOLOSHIN, T., GILADI, M., PORAT, Y., MUNSTER, M., BLAT, R., SHERBO, S., KIRSON, E. D., WEINBERG, U. & PALTI, Y. 2015. ATPS-25p53 STATUS DEPENDENCE OF TUMOR TREATING FIELDS (TTFIELDS) EFFICACY AGAINST GLIOMA CANCER CELLS. *Neuro-oncology,* 17**,** v23.

SCHUCHT, P., BECK, J., ABU-ISA, J., ANDEREGGEN, L., MUREK, M., SEIDEL, K., STIEGLITZ, L. & RAABE, A. 2012. Gross total resection rates in contemporary glioblastoma surgery: results of an institutional protocol combining 5-aminolevulinic acid intraoperative fluorescence imaging and brain mapping. *Neurosurgery,* 71**,** 927-936.

SCHULTZ, S., PINSKY, G. S., WU, N. C., CHAMBERLAIN, M. C., RODRIGO, A. S. & MARTIN, S. E. 2005. Fine needle aspiration diagnosis of extracranial glioblastoma multiforme: Case report and review of the literature. *Cytojournal,* 2**,** 19.

SCHWARTZBAUM, J. A., FISHER, J. L., ALDAPE, K. D. & WRENSCH, M. 2006. Epidemiology and molecular pathology of glioma. *Nature Reviews Neurology,* 2**,** 494.

SEBASTIANO, A. R., DEWEYERT, A., BENOIT, S., IREDALE, E., XU, H., OLIVEIRA, C., WONG, E., SCHMID, S. & HEBB, M. O. 2018. Preclinical outcomes of Intratumoral Modulation Therapy for glioblastoma. *Scientific reports,* 8**,** 7301.

SELLAL, F., HIRSCH, E., BARTH, P., BLOND, S. & MARESCAUX, C. 1993. A case of symptomatic hemidystonia improved by ventroposterolateral thalamic electrostimulation. *Movement disorders: official journal of the Movement Disorder Society,* 8**,** 515-518.

SENGUPTA, S., MARRINAN, J., FRISHMAN, C. & SAMPATH, P. 2012. Impact of temozolomide on immune response during malignant glioma chemotherapy. *Clin Dev Immunol,* 2012**,** 831090.

SEO, Y. J., CHO, W. H., KANG, D. W. & CHA, S. H. 2012. Extraneural metastasis of glioblastoma multiforme presenting as an unusual neck mass. *Journal of Korean Neurosurgical Society,* 51**,** 147.

SHTEINGAUZ, A., PORAT, Y., GILADI, M., SCHNEIDERMAN, R., VOLOSHIN, T., MUNSTER, M., KIRSON, E., WEINBERG, U. & PALTI, Y. 2018. Induction of autophagy following TTFields application serves as a survival mechanism mediated by AMPK activation. AACR.

SILGINER, M., WELLER, M., STUPP, R. & ROTH, P. 2017. Biological activity of tumor-treating fields in preclinical glioma models. *Cell Death & Disease,* 8**,** e2753.

SIM, E. H., YANG, I. A., WOOD-BAKER, R., BOWMAN, R. V. & FONG, K. M. 2018. Gefitinib for advanced non-small cell lung cancer. *Cochrane Database of Systematic Reviews*.

SMITH, S. J., RAHMAN, C. V., CLARKE, P., RITCHIE, A., GOULD, T., WARD, J. H., SHAKESHEFF, K. M., GRUNDY, R. G. & RAHMAN, R. 2014. Surgical delivery of drug releasing poly (lactic-co-glycolic acid)/poly (ethylene glycol) paste with in vivo effects against glioblastoma. *The Annals of The Royal College of Surgeons of England,* 96**,** 495-501.

SONODA, Y., WARITA, M., SUZUKI, T., OZAWA, H., FUKUDA, Y., FUNAKOSHI-TAGO, M. & KASAHARA, T. 2010. Proteolipid protein 2 is associated with melanoma metastasis. *Oncology reports,* 23**,** 371-376.

SORRELLS, S. F., PAREDES, M. F., CEBRIAN-SILLA, A., SANDOVAL, K., QI, D., KELLEY, K. W., JAMES, D., MAYER, S., CHANG, J. & AUGUSTE, K. I. 2018. Human hippocampal neurogenesis drops sharply in children to undetectable levels in adults. *Nature,* 555**,** 377.

SOTTORIVA, A., SPITERI, I., PICCIRILLO, S. G., TOULOUMIS, A., COLLINS, V. P., MARIONI, J. C., CURTIS, C., WATTS, C. & TAVARÉ, S. 2013. Intratumor heterogeneity in human glioblastoma reflects cancer evolutionary dynamics. *Proceedings of the National Academy of Sciences,* 110**,** 4009-4014.

SPOSTOL, R., ERTEL, I. J., JENKIN, R., BOESEL, C. P., VENES, J. L., ORTEGA, J. A., EVANS, A. E., WARAL, W. & HAMMOND, D. 1989. The effectiveness of chemotherapy for treatment of high grade astrocytoma in children: results of a randomized trial. *Journal of neuro-oncology,* 7**,** 165-177.

STEIGERWALD, F., MÜLLER, L., JOHANNES, S., MATTHIES, C. & VOLKMANN, J. 2016. Directional deep brain stimulation of the subthalamic nucleus: a pilot study using a novel neurostimulation device. *Movement Disorders,* 31**,** 1240-1243.

STEVE HALTIWANGER, M. The Electrical Properties of Cancer Cells.

STRAGLIOTTO, G., VEGA, F., STASIECKI, P., GROPP, P., POISSON, M. & DELATTRE, J.-Y. 1996. Multiple infusions of anti-epidermal growth factor receptor (EGFR) monoclonal antibody (EMD 55 900) in patients with recurrent malignant gliomas. *European Journal of Cancer,* 32**,** 636-640.

STRAIGHT, A. F., FIELD, C. M. & MITCHISON, T. J. 2005. Anillin binds nonmuscle myosin II and regulates the contractile ring. *Mol Biol Cell,* 16**,** 193-201.

STRÖBELE, S., SCHNEIDER, M., SCHNEELE, L., SIEGELIN, M. D., NONNENMACHER, L., ZHOU, S., KARPEL-MASSLE, G., WESTHOFF, M.-A., HALATSCH, M.-E. & DEBATIN, K.-M. 2015. A potential role for the inhibition of PI3K signaling in glioblastoma therapy. *PLoS One,* 10**,** e0131670.

STUMMER, W., NOVOTNY, A., STEPP, H., GOETZ, C., BISE, K. & REULEN, H. J. 2000. Fluorescence-guided resection of glioblastoma multiforme utilizing 5-ALA-induced porphyrins: a prospective study in 52 consecutive patients. *Journal of neurosurgery,* 93**,** 1003-1013.

STUMMER, W., PICHLMEIER, U., MEINEL, T., WIESTLER, O. D., ZANELLA, F., REULEN, H.-J. & GROUP, A.-G. S. 2006. Fluorescence-guided surgery with 5-aminolevulinic acid for resection of malignant glioma: a randomised controlled multicentre phase III trial. *The lancet oncology,* 7**,** 392-401.

STUPP, R., HEGI, M. E., MASON, W. P., VAN DEN BENT, M. J., TAPHOORN, M. J., JANZER, R. C., LUDWIN, S. K., ALLGEIER, A., FISHER, B., BELANGER, K., HAU, P., BRANDES, A. A., GIJTENBEEK, J., MAROSI, C., VECHT, C. J., MOKHTARI, K., WESSELING, P., VILLA, S., EISENHAUER, E., GORLIA, T., WELLER, M., LACOMBE, D., CAIRNCROSS, J. G., MIRIMANOFF, R. O., GROUPS, E. O. F. R. A. T. O. C. B. T. A. R. O. & GROUP, N. C. I. O. C. C. T. 2009. Effects of radiotherapy with concomitant and adjuvant temozolomide versus radiotherapy alone on survival in glioblastoma in a randomised phase III study: 5-year analysis of the EORTC-NCIC trial. *Lancet Oncol,* 10**,** 459-66.

STUPP, R., MASON, W. P., VAN DEN BENT, M. J., WELLER, M., FISHER, B., TAPHOORN, M. J., BELANGER, K., BRANDES, A. A., MAROSI, C., BOGDAHN, U., CURSCHMANN, J., JANZER, R. C., LUDWIN, S. K., GORLIA, T., ALLGEIER, A., LACOMBE, D., CAIRNCROSS, J. G., EISENHAUER, E., MIRIMANOFF, R. O., GROUPS, E. O. F. R. A. T. O. C. B. T. A. R. & GROUP, N. C. I. O. C. C. T. 2005. Radiotherapy plus concomitant and adjuvant temozolomide for glioblastoma. *N Engl J Med,* 352**,** 987-96.

STUPP, R., TAILLIBERT, S., KANNER, A. & ET AL. 2017a. Effect of tumor-treating fields plus maintenance temozolomide vs maintenance temozolomide alone on survival in patients with glioblastoma: A randomized clinical trial. *JAMA,* 318**,** 2306-2316.

STUPP, R., TAILLIBERT, S., KANNER, A., READ, W., STEINBERG, D. M., LHERMITTE, B., TOMS, S., IDBAIH, A., AHLUWALIA, M. S. & FINK, K. 2017b. Effect of tumor-treating fields plus maintenance temozolomide vs maintenance temozolomide alone on survival in patients with glioblastoma: a randomized clinical trial. *Jama,* 318**,** 2306-2316.

STUPP, R., TAILLIBERT, S., KANNER, A. A., KESARI, S., STEINBERG, D. M., TOMS, S. A., TAYLOR, L. P., LIEBERMAN, F., SILVANI, A. & FINK, K. L. 2015a. Maintenance therapy with tumor-treating fields plus temozolomide vs temozolomide alone for glioblastoma: a randomized clinical trial. *Jama,* 314**,** 2535-2543.

STUPP, R., TAILLIBERT, S., KANNER, A. A., KESARI, S., STEINBERG, D. M., TOMS, S. A., TAYLOR, L. P., LIEBERMAN, F., SILVANI, A., FINK, K. L., BARNETT, G. H., ZHU, J. J., HENSON, J. W., ENGELHARD, H. H., CHEN, T. C., TRAN, D. D., SROUBEK, J., TRAN, N. D., HOTTINGER, A. F., LANDOLFI, J., DESAI, R., CAROLI, M., KEW, Y., HONNORAT, J., IDBAIH, A., KIRSON, E. D., WEINBERG, U., PALTI, Y., HEGI, M. E. & RAM, Z. 2015b. Maintenance Therapy With Tumor-Treating Fields Plus Temozolomide vs

Temozolomide Alone for Glioblastoma: A Randomized Clinical Trial. *JAMA,* 314**,** 2535-43.

STUPP, R., WONG, E. T., KANNER, A. A., STEINBERG, D., ENGELHARD, H., HEIDECKE, V., KIRSON, E. D., TAILLIBERT, S., LIEBERMANN, F. & DBALÝ, V. 2012a. NovoTTF-100A versus physician's choice chemotherapy in recurrent glioblastoma: a randomised phase III trial of a novel treatment modality. *European journal of cancer,* 48**,** 2192-2202.

STUPP, R., WONG, E. T., KANNER, A. A., STEINBERG, D., ENGELHARD, H., HEIDECKE, V., KIRSON, E. D., TAILLIBERT, S., LIEBERMANN, F., DBALÝ, V., RAM, Z., VILLANO, J. L., RAINOV, N., WEINBERG, U., SCHIFF, D., KUNSCHNER, L., RAIZER, J., HONNORAT, J., SLOAN, A., MALKIN, M., LANDOLFI, J. C., PAYER, F., MEHDORN, M., WEIL, R. J., PANNULLO, S. C., WESTPHAL, M., SMRCKA, M., CHIN, L., KOSTRON, H., HOFER, S., BRUCE, J., COSGROVE, R., PALEOLOGOUS, N., PALTI, Y. & GUTIN, P. H. 2012b. NovoTTF-100A versus physician's choice chemotherapy in recurrent glioblastoma: a randomised phase III trial of a novel treatment modality. *Eur J Cancer,* 48**,** 2192-202.

STURM, D., BENDER, S., JONES, D. T., LICHTER, P., GRILL, J., BECHER, O., HAWKINS, C., MAJEWSKI, J., JONES, C., COSTELLO, J. F., IAVARONE, A., ALDAPE, K., BRENNAN, C. W., JABADO, N. & PFISTER, S. M. 2014. Paediatric and adult glioblastoma: multiform (epi)genomic culprits emerge. *Nat Rev Cancer,* 14**,** 92-107.

STURM, D., WITT, H., HOVESTADT, V., KHUONG-QUANG, D.-A., JONES, D. T., KONERMANN, C., PFAFF, E., TÖNJES, M., SILL, M. & BENDER, S. 2012. Hotspot mutations in H3F3A and IDH1 define distinct epigenetic and biological subgroups of glioblastoma. *Cancer cell,* 22**,** 425-437.

SURI, V., DAS, P., PATHAK, P., JAIN, A., SHARMA, M. C., BORKAR, S. A., SURI, A., GUPTA, D. & SARKAR, C. 2009. Pediatric glioblastomas: a histopathological and molecular genetic study. *Neuro Oncol,* 11**,** 274-80.

TAAL, W., OOSTERKAMP, H. M., WALENKAMP, A. M., DUBBINK, H. J., BEEREPOOT, L. V., HANSE, M. C., BUTER, J., HONKOOP, A. H., BOERMAN, D. & DE VOS, F. Y. 2014. Single-agent bevacizumab or lomustine versus a combination of bevacizumab plus lomustine in patients with recurrent glioblastoma (BELOB trial): a randomised controlled phase 2 trial. *The lancet oncology,* 15**,** 943-953.

TANAKA, M., UEDA, A., KANAMORI, H., IDEGUCHI, H., YANG, J., KITAJIMA, S. & ISHIGATSUBO, Y. 2002. Cell-cycle-dependent regulation of human aurora A transcription is mediated by periodic repression of E4TF1. *J Biol Chem,* 277**,** 10719-26.

TANDLE, A. T., KRAMP, T., KIL, W. J., HALTHORE, A., GEHLHAUS, K., SHANKAVARAM, U., TOFILON, P. J., CAPLEN, N. J. & CAMPHAUSEN, K. 2013. Inhibition of polo-like kinase 1 in glioblastoma multiforme induces mitotic catastrophe and enhances radiosensitisation. *Eur J Cancer,* 49**,** 3020-8.

TAYLOR, M. D., LIU, L., RAFFEL, C., HUI, C.-C., MAINPRIZE, T. G., ZHANG, X., AGATEP, R., CHIAPPA, S., GAO, L. & LOWRANCE, A. 2002. Mutations in SUFU predispose to medulloblastoma. *Nature genetics,* 31**,** 306.

TAYLOR, R. E., BAILEY, C. C., ROBINSON, K. J., WESTON, C. L., WALKER, D. A., ELLISON, D., IRONSIDE, J., PIZER, B. L. & LASHFORD, L. S. 2005. Outcome for patients with metastatic (M2–3) medulloblastoma treated with SIOP/UKCCSG PNET-3 chemotherapy. *European journal of cancer,* 41**,** 727-734.

TESCHENDORFF, A. E. & CALDAS, C. 2008. A robust classifier of high predictive value to identify good prognosis patients in ER-negative breast cancer. *Breast Cancer Research,* 10**,** R73.

THAKKAR, J. P., DOLECEK, T. A., HORBINSKI, C., OSTROM, Q. T., LIGHTNER, D. D., BARNHOLTZ-SLOAN, J. S. & VILLANO, J. L. 2014. Epidemiologic and molecular prognostic review of glioblastoma. *Cancer Epidemiology and Prevention Biomarkers,* 23**,** 1985-1996.

THIESSEN, B., STEWART, C., TSAO, M., KAMEL-REID, S., SCHAIQUEVICH, P., MASON, W., EASAW, J., BELANGER, K., FORSYTH, P. & MCINTOSH, L. 2010. A phase I/II trial of GW572016 (lapatinib) in recurrent glioblastoma multiforme: clinical outcomes, pharmacokinetics and molecular correlation. *Cancer chemotherapy and pharmacology,* 65**,** 353-361.

TIRAKOTAI, W., RIEGEL, T., SURE, U., ROHLFS, J., GHARABAGHI, A., BERTALANFFY, H. & HELLWIG, D. 2004. Image-guided motor cortex stimulation in patients with central pain. *min-Minimally Invasive Neurosurgery,* 47**,** 273-277.

TORRE, L. A., SIEGEL, R. L., WARD, E. M. & JEMAL, A. 2016. Global cancer incidence and mortality rates and trends—an update. *Cancer Epidemiology and Prevention Biomarkers,* 25**,** 16-27.

TOTH, A. B., SHUM, A. K. & PRAKRIYA, M. 2016. Regulation of neurogenesis by calcium signaling. *Cell Calcium,* 59**,** 124-134.

TSO, C. L., FREIJE, W. A., DAY, A., CHEN, Z., MERRIMAN, B., PERLINA, A., LEE, Y., DIA, E. Q., YOSHIMOTO, K., MISCHEL, P. S., LIAU, L. M., CLOUGHESY, T. F. & NELSON, S. F. 2006. Distinct transcription profiles of primary and secondary glioblastoma subgroups. *Cancer Res,* 66**,** 159-67.

TUSZYNSKI, J., WENGER, C., FRIESEN, D. & PRETO, J. 2016. An Overview of Sub-Cellular Mechanisms Involved in the Action of TTFields. *International Journal of Environmental Research and Public Health,* 13**,** 1128.

UHLMANN, K., ROHDE, K., ZELLER, C., SZYMAS, J., VOGEL, S., MARCZINEK, K., THIEL, G., NÜRNBERG, P. & LAIRD, P. W. 2003. Distinct methylation profiles of glioma subtypes. *International journal of cancer,* 106**,** 52-59.

ULASOV, I., GHOSH, D., BUTTERS, M., BUTTERS, J. & COBBS, C. SPECIFIC KNOCKDOWN OF EGFR AND PLK1 GENE EXPRESSION IN U87 GBM CELLS WITH RADIOFREQUENCY ENERGY (RFE) DEVICE. NEURO-ONCOLOGY, 2016. OXFORD UNIV PRESS INC JOURNALS DEPT, 2001 EVANS RD, CARY, NC 27513 USA, 70-70.

ULASOV, I. V., FOSTER, H., BUTTERS, M., YOON, J.-G., OZAWA, T., NICOLAIDES, T., FIGUEROA, X., HOTHI, P., PRADOS, M. & BUTTERS, J. 2017. Precision knockdown of EGFR gene expression using radio frequency electromagnetic energy. *Journal of neuro-oncology,* 133**,** 257-264.

URBAŃSKA, K., SOKOŁOWSKA, J., SZMIDT, M. & SYSA, P. 2014. Glioblastoma multiforme–an overview. *Contemporary oncology,* 18**,** 307.

VAKIFAHMETOGLU, H., OLSSON, M. & ZHIVOTOVSKY, B. 2008. Death through a tragedy: mitotic catastrophe. *Cell Death Differ,* 15**,** 1153-62.

VALTONEN, S., TIMONEN, U. L., TOIVANEN, P., KALIMO, H., KIVIPELTO, L., HEISKANEN, O., UNSGAARD, G. & KUURNE, T. 1997. Interstitial chemotherapy with carmustine-loaded polymers for high-grade gliomas: a randomized double-blind study. *Neurosurgery,* 41**,** 44-49.

VAN BROCKLYN, J. R., WOJTON, J., MEISEN, W. H., KELLOUGH, D. A., ECSEDY, J. A., KAUR, B. & LEHMAN, N. L. 2014. Aurora-A inhibition offers a novel therapy effective against intracranial glioblastoma. *Cancer Res,* 74**,** 5364-70.

VAN DEN BENT, M. J., BRANDES, A. A., TAPHOORN, M. J., KROS, J. M., KOUWENHOVEN, M. C., DELATTRE, J. Y., BERNSEN, H. J., FRENAY, M., TIJSSEN, C. C., GRISOLD, W., SIPOS, L., ENTING, R. H., FRENCH, P. J., DINJENS, W. N., VECHT, C. J., ALLGEIER, A., LACOMBE, D., GORLIA, T. & HOANG-XUAN, K. 2013. Adjuvant procarbazine, lomustine, and vincristine chemotherapy in newly diagnosed anaplastic oligodendroglioma: long-term follow-up of EORTC brain tumor group study 26951. *J Clin Oncol,* 31**,** 344-50.

VAN OMMEREN, R., STAUDT, M. D., XU, H. & HEBB, M. O. 2016. Advances in HSP27 and HSP90-targeting strategies for glioblastoma. *Journal of neuro-oncology,* 127**,** 209-219.

VERHAAK, R. G., HOADLEY, K. A., PURDOM, E., WANG, V., QI, Y., WILKERSON, M. D., MILLER, C. R., DING, L., GOLUB, T. & MESIROV, J. P. 2010a. Integrated genomic analysis identifies clinically relevant subtypes of glioblastoma characterized by abnormalities in PDGFRA, IDH1, EGFR, and NF1. *Cancer cell,* 17**,** 98-110.

VERHAAK, R. G., HOADLEY, K. A., PURDOM, E., WANG, V., QI, Y., WILKERSON, M. D., MILLER, C. R., DING, L., GOLUB, T., MESIROV, J. P., ALEXE, G., LAWRENCE, M., O'KELLY, M., TAMAYO, P., WEIR, B. A., GABRIEL, S., WINCKLER, W., GUPTA, S., JAKKULA, L., FEILER, H. S., HODGSON, J. G., JAMES, C. D., SARKARIA, J. N., BRENNAN, C., KAHN, A., SPELLMAN, P. T., WILSON, R. K., SPEED, T. P., GRAY, J. W., MEYERSON, M., GETZ, G., PEROU, C. M., HAYES, D. N. & NETWORK, C. G. A. R. 2010b. Integrated genomic analysis identifies clinically relevant subtypes of glioblastoma characterized by abnormalities in PDGFRA, IDH1, EGFR, and NF1. *Cancer Cell,* 17**,** 98-110.

VERHOEFF, J., LAVINI, C., VAN LINDE, M., STALPERS, L., MAJOIE, C., REIJNEVELD, J., VAN FURTH, W. & RICHEL, D. 2010. Bevacizumab and dose-intense temozolomide in recurrent high-grade glioma. *Annals of oncology,* 21**,** 1723-1727.

VIDAILHET, M., VERCUEIL, L., HOUETO, J.-L., KRYSTKOWIAK, P., BENABID, A.-L., CORNU, P., LAGRANGE, C., TÉZENAS DU MONTCEL, S., DORMONT, D. & GRAND, S. 2005. Bilateral deep-brain stimulation of the globus pallidus in primary generalized dystonia. *New England Journal of Medicine,* 352**,** 459-467.

VINAGRE, J., ALMEIDA, A., PÓPULO, H., BATISTA, R., LYRA, J., PINTO, V., COELHO, R., CELESTINO, R., PRAZERES, H. & LIMA, L. 2013. Frequency of TERT promoter mutations in human cancers. *Nature communications,* 4**,** 2185.

VIVANCO, I., ROBINS, H. I., ROHLE, D., CAMPOS, C., GROMMES, C., NGHIEMPHU, P. L., KUBEK, S., OLDRINI, B., CHHEDA, M. G. & YANNUZZI, N. 2012. Differential sensitivity of glioma-versus lung cancer–specific EGFR mutations to EGFR kinase inhibitors. *Cancer discovery*.

VOLOSHIN, T., MUNSTER, M., BLATT, R., SHTEINGAUZ, A., ROBERTS, P. C., SCHMELZ, E. M., GILADI, M., SCHNEIDERMAN, R. S., ZEEVI, E., PORAT, Y., BOMZON, Z., URMAN, N., ITZHAKI, A., CAHAL, S., KIRSON, E. D., WEINBERG, U. & PALTI, Y. 2016. Alternating electric fields (TTFields) in combination with paclitaxel are therapeutically effective against ovarian cancer cells in vitro and in vivo. *Int J Cancer,* 139**,** 2850-2858.

VON BARTHELD, C. S., BAHNEY, J. & HERCULANO-HOUZEL, S. 2016. The search for true numbers of neurons and glial cells in the human brain: a review of 150 years of cell counting. *Journal of Comparative Neurology,* 524**,** 3865-3895.

VON HOFF, K., HINKES, B., GERBER, N. U., DEINLEIN, F., MITTLER, U., URBAN, C., BENESCH, M., WARMUTH-METZ, M., SOERENSEN, N. & ZWIENER, I. 2009. Long-term outcome and clinical prognostic factors in children with medulloblastoma treated in the prospective randomised multicentre trial HIT '91. *European journal of cancer,* 45**,** 1209-1217.

VREDENBURGH, J. J., DESJARDINS, A., KIRKPATRICK, J. P., REARDON, D. A., PETERS, K. B., HERNDON II, J. E., MARCELLO, J., BAILEY, L., THREATT, S. & SAMPSON, J. 2012. Addition of bevacizumab to standard radiation therapy and daily temozolomide is associated with minimal toxicity in newly diagnosed glioblastoma multiforme. *International Journal of Radiation Oncology* Biology* Physics,* 82**,** 58-66.

VYMAZAL, J. & WONG, E. T. 2014. Response patterns of recurrent glioblastomas treated with tumor-treating fields. *Semin Oncol,* 41 Suppl 6**,** S14-24.

WAKSAL, H. W. 1999. Role of an anti-epidermal growth factor receptor in treating cancer. *Cancer and Metastasis Reviews,* 18**,** 427-436.

WANG, S. I., PUC, J., LI, J., BRUCE, J. N., CAIRNS, P., SIDRANSKY, D. & PARSONS, R. 1997. Somatic mutations of PTEN in glioblastoma multiforme. *Cancer research,* 57**,** 4183-4186.

WENGER, C., MIRANDA, P., SALVADOR, R., THIELSCHER, A., BOMZON, Z., GILADI, M., MRUGALA, M. M. & KORSHOEJ, A. R. 2018. A review on Tumor Treating Fields (TTFields): Clinical implications inferred from computational modeling. *IEEE Reviews in Biomedical Engineering*.

WENGER, C., SALVADOR, R., BASSER, P. J. & MIRANDA, P. C. 2015. The electric field distribution in the brain during TTFields therapy and its dependence on tissue dielectric properties and anatomy: a computational study. *Phys Med Biol,* 60**,** 7339-57.

WESTPHAL, M., HILT, D. C., BORTEY, E., DELAVAULT, P., OLIVARES, R., WARNKE, P. C., WHITTLE, I. R., JÄÄSKELÄINEN, J. & RAM, Z. 2003. A phase 3 trial of local chemotherapy with biodegradable carmustine (BCNU) wafers (Gliadel wafers) in patients with primary malignant glioma. *Neuro-oncology,* 5**,** 79-88.

WICK, W. 2016. TTFields: where does all the skepticism come from? : Society for Neuro-Oncology.

WICK, W., HARTMANN, C., ENGEL, C., STOFFELS, M., FELSBERG, J., STOCKHAMMER, F., SABEL, M. C., KOEPPEN, S., KETTER, R., MEYERMANN, R., RAPP, M., MEISNER, C., KORTMANN, R. D., PIETSCH, T., WIESTLER, O. D., ERNEMANN, U., BAMBERG, M., REIFENBERGER, G., VON DEIMLING, A. & WELLER, M. 2009. NOA-04 randomized phase III trial of sequential radiochemotherapy of anaplastic glioma with procarbazine, lomustine, and vincristine or temozolomide. *J Clin Oncol,* 27**,** 5874-80.

WICK, W., PLATTEN, M., MEISNER, C., FELSBERG, J., TABATABAI, G., SIMON, M., NIKKHAH, G., PAPSDORF, K., STEINBACH, J. P., SABEL, M., COMBS, S. E., VESPER, J., BRAUN, C., MEIXENSBERGER, J., KETTER, R., MAYER-STEINACKER, R., REIFENBERGER, G., WELLER, M. & SOCIETY, N.-S. G. O. N.-O. W. G. N. O. G. C. 2012. Temozolomide chemotherapy alone versus radiotherapy alone for malignant astrocytoma in the elderly: the NOA-08 randomised, phase 3 trial. *Lancet Oncol,* 13**,** 707-15.

WINTERS, J. L., WILSON, D. & DAVIS, D. G. 2001. Congenital glioblastoma multiforme: a report of three cases and a review of the literature. *Journal of the neurological sciences,* 188**,** 13-19.

WOLBERS, J. G. 2014. Novel strategies in glioblastoma surgery aim at safe, supra-maximum resection in conjunction with local therapies. *Chinese journal of cancer,* 33**,** 8.

WOLTER, M., REIFENBERGER, J., SOMMER, C., RUZICKA, T. & REIFENBERGER, G. 1997. Mutations in the human homologue of the Drosophila segment polarity gene patched (PTCH) in sporadic basal cell carcinomas of the skin and primitive neuroectodermal tumors of the central nervous system. *Cancer research,* 57**,** 2581-2585.

WONDERLIN, W. F., WOODFORK, K. A. & STROBL, J. S. 1995. Changes in membrane potential during the progression of MCF-7 human mammary tumor cells through the cell cycle. *Journal of cellular physiology,* 165**,** 177-185.

WONG, A. J., RUPPERT, J. M., BIGNER, S. H., GRZESCHIK, C. H., HUMPHREY, P. A., BIGNER, D. S. & VOGELSTEIN, B. 1992. Structural alterations of the epidermal growth factor receptor gene in human gliomas. *Proceedings of the National Academy of Sciences,* 89**,** 2965-2969.

WONG, E. T., LOK, E., GAUTAM, S. & SWANSON, K. D. 2015a. Dexamethasone exerts profound immunologic interference on treatment efficacy for recurrent glioblastoma. *Br J Cancer,* 113**,** 232-41.

WONG, E. T., LOK, E., SWANSON, K. D., GAUTAM, S., ENGELHARD, H. H., LIEBERMAN, F., TAILLIBERT, S., RAM, Z. & VILLANO, J. L. 2014. Response assessment of NovoTTF-100A versus best physician's choice chemotherapy in recurrent glioblastoma. *Cancer Med,* 3**,** 592-602.

WONG, E. T., TOMS, S. A. & AHLUWALIA, M. S. 2015b. Technological Advances in the Treatment of Cancer: Combining Modalities to Optimize Outcomes. *Clin Adv Hematol Oncol,* 13**,** 1-18.

WU, J., ARMSTRONG, T. S. & GILBERT, M. R. 2016. Biology and management of ependymomas. *Neuro-oncology,* 18**,** 902-913.

WU, S., KIM, C., BAER, L. & ZHU, X. 2010. Bevacizumab increases risk for severe proteinuria in cancer patients. *J Am Soc Nephrol,* 21**,** 1381-9.

WU, Y., LEVY, R., ASHBY, P., TASKER, R. & DOSTROVSKY, J. 2001. Does stimulation of the GPi control dyskinesia by activating inhibitory axons? *Movement disorders: official journal of the Movement Disorder Society,* 16**,** 208-216.

XING, W.-K., SHAO, C., QI, Z.-Y., YANG, C. & WANG, Z. 2015. The role of Gliadel wafers in the treatment of newly diagnosed GBM: a meta-analysis. *Drug design, development and therapy,* 9**,** 3341.

XU, H., BIHARI, F., WHITEHEAD, S., WONG, E., SCHMID, S. & HEBB, M. O. 2016. In Vitro Validation of Intratumoral Modulation Therapy for Glioblastoma. *Anticancer research,* 36**,** 71-80.

XU, T., KANG, X., YOU, X., DAI, L., TIAN, D., YAN, W., YANG, Y., XIONG, H., LIANG, Z. & ZHAO, G. Q. 2017. Cross-platform comparison of four leading technologies for detecting EGFR mutations in circulating tumor DNA from non-small cell lung carcinoma patient plasma. *Theranostics,* 7**,** 1437.

YADAV, R. K., CHAE, S.-W., KIM, H.-R. & CHAE, H. J. 2014. Endoplasmic reticulum stress and cancer. *Journal of cancer prevention,* 19**,** 75.

YAMADA, H. Y. & GORBSKY, G. J. 2006. Spindle checkpoint function and cellular sensitivity to antimitotic drugs. *Mol Cancer Ther,* 5**,** 2963-9.

YAMANAKA, R., HOMMA, J., YAJIMA, N., TSUCHIYA, N., SANO, M., KOBAYASHI, T., YOSHIDA, S., ABE, T., NARITA, M., TAKAHASHI, M. & TANAKA, R. 2005. Clinical evaluation of dendritic cell vaccination for patients with recurrent glioma: results of a clinical phase I/II trial. *Clin Cancer Res,* 11**,** 4160-7.

YANG, L., GUO, G., NIU, X. Y. & LIU, J. 2015. Dendritic Cell-Based Immunotherapy Treatment for Glioblastoma Multiforme. *Biomed Res Int,* 2015**,** 717530.

YANG, M. & BRACKENBURY, W. J. 2013. Membrane potential and cancer progression. *Frontiers in physiology,* 4**,** 185.

YANG, M., KOZMINSKI, D. J., WOLD, L. A., MODAK, R., CALHOUN, J. D., ISOM, L. L. & BRACKENBURY, W. J. 2012. Therapeutic potential for phenytoin: targeting Na v 1.5 sodium channels to reduce migration and invasion in metastatic breast cancer. *Breast cancer research and treatment,* 134**,** 603-615.

YOSHOR, D., HAMILTON, W. J., ONDO, W., JANKOVIC, J. & GROSSMAN, R. G. 2001. Comparison of thalamotomy and pallidotomy for the treatment of dystonia. *Neurosurgery,* 48**,** 818-826.

YUNG, W., ALBRIGHT, R., OLSON, J., FREDERICKS, R., FINK, K., PRADOS, M., BRADA, M., SPENCE, A., HOHL, R. & SHAPIRO, W. 2000. A phase II study of temozolomide vs. procarbazine in patients with glioblastoma multiforme at first relapse. *British journal of cancer,* 83**,** 588.

ZHANG, X., ZHANG, W., CAO, W. D., CHENG, G. & ZHANG, Y. Q. 2012. Glioblastoma multiforme: Molecular characterization and current treatment strategy (Review). *Exp Ther Med,* 3**,** 9-14.

ZHANG, Y., CRUICKSHANKS, N., YUAN, F., WANG, B., PAHUSKI, M., WULFKUHLE, J., GALLAGHER, I., KOEPPEL, A. F., HATEF, S. & PAPANICOLAS, C. 2017. Targetable T-type calcium channels drive glioblastoma. *Cancer research,* 77**,** 3479-3490.

ZIMMERMAN, J. W., JIMENEZ, H., PENNISON, M. J., BREZOVICH, I., MORGAN, D., MUDRY, A., COSTA, F. P., BARBAULT, A. & PASCHE, B. 2013. Targeted treatment of cancer with

radiofrequency electromagnetic fields amplitude-modulated at tumor-specific frequencies. *Chinese journal of cancer,* 32**,** 573.

ZONG, H., VERHAAK, R. G. & CANOLL, P. 2012. The cellular origin for malignant glioma and prospects for clinical advancements. *Expert Rev Mol Diagn,* 12**,** 383-94.